Chemical speciation of Rh^{III} complexes in acidic, halide-rich media by means of ^{103}Rh NMR spectroscopy: The importance of speciation in the selective separation and recovery of rhodium

by
Theodor Earl Geswindt

Dissertation presented for the degree of Doctor of Philosophy in the Faculty of Science at Stellenbosch University

Supervisor: Prof. Klaus Robert Koch

December 2013

Declaration

By submitting this thesis/dissertation electronically, I declare that the entirety of the work contained therein is my own, original work, that I am the sole author thereof (save to the extent explicitly otherwise stated), that reproduction and publication thereof by Stellenbosch University will not infringe any third party rights and that I have not previously in its entirety or in part submitted it for obtaining any qualification.

Date: March 2013

Acknowledgements

I would like to express my gratitude to

- My supervisor, Professor Klaus R. Koch, for all his support, motivation, enthusiasm and guidance throughout this project

- Dr. Wilhelmus J. Gerber for his friendship, time, fruitful discussions and proof-reading of this thesis

- Heraeus Chemicals GmbH, Anglo Platinum PLC and the University of Stellenbosch for funding

- The C.A.F. NMR lab staff, Dr. Jaco Brand and Mrs Elsa Malherbe

- Technical staff, Mr. Shafiek Mohammed, Mr. Roger Lawrence and Ms. Deidre Davids

- The Platinum Metals Research Group

Finally, a special dedication to my parents for their support throughout my studies…

"Once you decide on your occupation, you must immerse yourself in your work. You have to fall in love with your work, never complain about it. You have to dedicate your life to understanding, mastering and honing your skill – that's the secret to success and is the key to being regarded honourably"

- Jiro Ono

List of Abbreviations

PGM's	Platinum group metals
D_2O ($^1H_2O/^2H_2O$)	Deuterium oxide
v/v	volume/volume
UV-vis	Ultraviolet-Visible
K	Kelvin
M	molarity, $mol.L^{-1}$
mM	millimolar
ICP-OES	inductively coupled plasma optical emission spectrometry
ppm	parts per million (ICP-OES / NMR)
Deta	diethylenetriamine
Teta	triethylenetetramine
Tepa	tetraethylenepentamine
Tren	tris(2-aminoethyl)amine
RSD	relative standard deviation
Hz	Hertz, s^{-1}
$\delta(^{195}Pt)$	chemical shift of ^{195}Pt NMR signal
$\delta(^{103}Rh$	chemical shift of ^{103}Rh NMR signal
τ_c	rotational correlation time
ps	pico second
T_1	longitudinal (spin-lattice) relaxation time
T_2	transverse (spin-spin) relaxation time
T_2^*	effective transverse relaxation time
$P(n)$	binominal probability distribution function
$\alpha_{^{35}Cl}$	fractional natural abundance of ^{35}Cl
$\alpha_{^{37}Cl}$	fractional natural abundance of ^{37}Cl
$\Delta\nu_{1/2}$	peak width at half peak height
TBA^+Cl^-	tetrabutylammonium chloride
IP-RP-HPLC	ion-pair reversed-phase high-performance liquid chromatography

Abstract

In this thesis, the recovery of Rh^{III} from both synthetically prepared and authentic industrial PGM-containing solutions was systematically investigated *via* organic precipitation methods using several commercially available, *N*-containing organic receptors including (amongst others) diethylenetriamine (**Deta**), triethylenetetramine (**Teta**), tetraethylenepentamine (**Tepa**) and tris(2-aminoethyl)amine (**Tren**). These organic receptors act as precipitating agents in the presence of an appropriate protonating agent (HCl) by lowering the solubility of the PGM chlorido-anions through an ion-pairing mechanism. The recovery of Rh^{III} from synthetically prepared PGM (Rh^{III} and Pt^{IV}) containing solutions using these precipitants was excellent, while poor Rh recovery from authentic industrial process solutions was achieved. The poor Rh recovery from these process solutions was ascribed to the species distribution of the $[RhCl_n(H_2O)_{6-n}]^{3-n}$ complexes. In order to validate the proposition that Rh^{III} speciation effects are responsible for the poor Rh recovery observed during the precipitation studies, attempt were made to describe the species distribution of the $[RhCl_n(H_2O)_{6-n}]^{3-n}$ (n=3-6) by means of high-resolution ^{103}Rh NMR spectroscopy.

A detailed high-resolution ^{103}Rh NMR spectroscopic study of the series of $[RhCl_n(H_2O)_{6-n}]^{3-n}$ (n=3-6) complexes was conducted. During this study, all six Rh^{III} aqua chlorido-complexes have unambiguously been characterized by means of high-resolution ^{103}Rh NMR spectroscopy, proving the powerful analytical capability of this technique. Characterization of these complexes is based on the detailed analysis of the $^{35}Cl/^{37}Cl$ isotope effects which is observed in the 19.11 MHz ^{103}Rh NMR resonances of the $[RhCl_n(H_2O)_{6-n}]^{3-n}$ (n=3-6) complexes in aqueous HCl solutions at 292 K. These resonances show that the "fine-structure" of each of the ^{103}Rh resonances may be understood in terms of its unique isotopologue, and in certain cases, the isotopomer distribution of each complex, which manifests as a result of its statistically expected $^{35}Cl/^{37}Cl$ isotopologue and isotopomer distributions. As a result, the ^{103}Rh NMR resonance structure serves as a unique "NMR-fingerprint", which allows for the unambiguous assignment of $[RhCl_n(H_2O)_{6-n}]^{3-n}$ (n=3-6) complexes, without the reliance on accurate $\delta(^{103}Rh)$ chemical shifts.

Furthermore, this study reports the first *direct* species distribution diagram for the $[RhCl_n(H_2O)_{6-n}]^{3-n}$ (n=3-6) series of complexes (in aqueous HCl solutions at 292 K) as a

function of the "free" (unbound) chloride concentration, constructed from ^{103}Rh NMR measurements. The need for a revised speciation diagram of $[RhCl_n(H_2O)_{6-n}]^{3-n}$ (n=3-6) complexes is clearly reflected by the vast differences observed in the literature reported species distribution diagrams, which makes it difficult to decide which set of experimental conditions (if any) is required for the quantitative and "selective" recovery of Rh^{III} from aqueous HCl solutions containing associated PGMs (Pt, Pd, Ir, Ru) as well as other transition metals. The documented species distribution diagrams for Rh^{III} have been generally constructed *via* data from *indirect* (kinetic and spectrophotometric) measurements using *dilute* Rh^{III} solutions at relatively high HCl concentrations, which implies that the Rh^{III}:Cl^- mole ratio is higher than what may be expected in authentic process solutions – an important aspect to consider when optimizing Rh^{III} recovery methods. In addition, Rh^{III} kinetic investigations reported in this study shows that ionic strength and temperature effects are important factors that dramatically influences the rate of Rh^{III} ligand exchange (*i.e.* Rh^{III} aquation reactions) which, in turn, have contributing effects on the species distribution of $[RhCl_n(H_2O)_{6-n}]^{3-n}$ complexes. Notable differences exist between the speciation diagram reported in this study and those documented in literature, especially at a "free" chloride concentration of 1.0 M. At this "free" chloride concentration, the $[RhCl_5(H_2O)]^{2-}$ complex anion was found to have an abundance of 34%, while literature reports an abundance of 80%.

In order to ascertain its practical relevance, the proposed ^{103}Rh NMR speciation method was extended, for the first time, to authentic industrial Rh feed solutions (Anglo Platinum PLC). Each of the ^{103}Rh resonances was unambiguously assigned, and each species quantified. Moreover, the Rh^{III} species distribution of the industrial Rh feed solution was accurately predicted by the "*direct*" speciation diagram constructed form ^{103}Rh NMR measurements.

After careful optimization of the Heraeus industrial feed solutions (optimal chloride concentration followed by thermal treatment for enhancing Rh^{III} chloride anation reactions), the recovery of Rh *via* precipitation was repeated. In this instance, Rh recovery improved dramatically, with up to 95% of Rh removed from solution. This improvement is ascribed primarily to the increased "free" (unbound) chloride concentration. The presence of associated PGMs as well as other transition metals would lower the effective "free" chloride concentration, since these metals would act as "chloride binders". By adjusting the total chloride concentration, Rh^{III} chloride anation reactions is enhanced which leads to the

$[RhCl_n(H_2O)_{6-n}]^{3-n}$ (n=5,6) complex anions being the dominant species in solution, therefore leading to improved Rh recovery. Moreover, it was shown that, under carefully controlled conditions, "*selective*" recovery of Rh is achieved using tris(2-aminoethyl)amine (**Tren**). Considering the fact that Rh is the last precious metal recovered in all PGM refineries, this can possibly provide a cost-effective route for the "upfront" (early stage) recovery of Rh from industrial PGM feed solutions.

Keywords: Rh recovery, ^{103}Rh NMR spectroscopy, $^{35/37}$Cl isotope effects, isotopologue, isotopomer, $[RhCl_n(H_2O)_{6-n}]^{3-n}$ (n=3-6) complexes, direct ^{103}Rh NMR speciation

Uittreksel

In hierdie tesis word die herwinning van Rh^{III} uit laboratorium voorbereide sowel as ware industriële PGM-bevattende oplossings sistematies ondersoek deur middel van organiese neerslag metodes, deur gebruik te maak van verskeie kommersieël beskikbare, *N*-bevattende organiese reseptore insluitende dietileentriamien (**Deta**), tri-etileentetramien (**Teta**), tetra-etileenpentamien (**Tepa**) en tris(2-aminoetiel)amien (**Tren**). Hierdie organiese reseptore tree op as neerslag-agente in die teenwoordigheid van 'n geskikte protoneringsagent (in hierdie geval HCl) deur 'n verlaging van die oplosbaarheid van die PGM chloried-anione deur middel van 'n ioon parings meganisme. Die herwinning van Rh^{III} vanuit laboratorium voorbereide PGM (Rh^{III} en Pt^{IV}) oplossing met behulp van hierdie organiese neerslag-agente was uitstekend, terwyl Rh herwinning vanuit ware industriële oplossings swak was. Die onvolledige Rh herwinning uit hierdie industriële oplossings word toegeskryf aan die spesie-verspreiding van die $[RhCl_n(H_2O)_{6-n}]^{3-n}$ komplekse. Ten einde die effek van Rh^{III} spesie-verspreiding op die herwinning van Rh te bestudeer, is gepoog om die spesie-verspreiding van $[RhCl_n(H_2O)_{6-n}]^{3-n}$ (n=3-6) komplekse, deur middel van hoë resolusie ^{103}Rh KMR spektroskopie, te beskryf.

'n Gedetailleerde hoë resolusie ^{103}Rh KMR spektroskopiese studie van die reeks van $[RhCl_n(H_2O)_{6-n}]^{3-n}$ (n=3-6) komplekse was uitgevoer. Tydens hierdie studie was al ses Rh^{III} aqua chlorido-komplekse ondubbelsinnig gekarakteriseer deur middel van hoë resolusie ^{103}Rh KMR spektroskopie, wat bewys lewer van die kragtige analitiese vermoë van hierdie tegniek. Karakterisering van hierdie komplekse is gebaseer op die gedetailleerde analise van die $^{35}Cl/^{37}Cl$ isotoop effekte wat waargeneem word in die 19.11 MHz ^{103}Rh KMR resonansies van die $[RhCl_n(H_2O)_{6-n}]^{3-n}$ (n=3-6) komplekse in HCl oplossings by 292 K. Hierdie resonansies toon dat die "fyn struktuur" van elk van die ^{103}Rh resonansies verstaan kan word in terme van die unieke *isotopoloog*, en in sekere gevalle, die *isotopomeer* verspreiding van elke kompleks, wat manifesteer as 'n gevolg van die die statisties verwagte $^{35}Cl/^{37}Cl$ *isotopoloog* en *isotopomeer* verspreiding. Die ^{103}Rh KMR resonansie-struktuur kan sodoende dien as 'n unieke "KMR-vingerafdruk", wat voorsiening maak vir die ondubbelsinnige karakterisering van $[RhCl_n(H_2O)_{6-n}]^{3-n}$ (n=3-6) komplekse, sonder om vertroue op akkurate $\delta(^{103}Rh)$ chemiese verskuiwings te plaas.

Hierdie studie rapporteer verder die eerste *direkte* spesie-verspreiding-diagram vir die $[RhCl_n(H_2O)_{6-n}]^{3-n}$ (n=3-6) reeks komplekse (in HCl oplossings by 292 K) as 'n funksie van die "vrye"(ongebonde) chloried-konsentrasie, verkry van ^{103}Rh KMR metings. Die behoefte vir 'n aangepasde spesiasie-diagram vir die $[RhCl_n(H_2O)_{6-n}]^{3-n}$ (n=3-6) komplekse word duidelik weerspieël deur die groot verskille waargeneem in die literatuur gerapporteerde verspreidings diagramme, wat dit moeilik maak om te besluit watter stel eksperimentele toestande (indien enige) benodig word vir die kwantitatiewe en "selektiewe" herwinning van Rh^{III} in HCl oplossings in die teenwoordigheid van gepaardgaande PGM (Pt, Pd, Ir, Ru) sowel as ander oorgangsmetale. Die gedokumenteerde spesie-verspreiding-diagramme vir Rh^{III} is oor die algemeen verkry *via* data vanaf indirekte (kinetiese en spektrofotometriese metings) deur gebruik te maak van verdunde Rh^{III} oplossings in relatiewe hoë HCl konsentrasies, wat impliseer dat die Rh^{III}:Cl mol verhouding hoër is as wat verwag kan word in ware industriële proses oplossings - 'n belangrike aspek om te oorweeg gedurende die optimalisering van Rh^{III} herwinning-metodes. Verder, die Rh^{III} kinetiese ondersoeke gerapporteer in hierdie studie toon dat ioniese sterkte sowel as temperatuur effekte belangrike faktore is wat die tempo van Rh^{III} ligand uitruiling (*d.w.s.* Rh^{III} "aquation" reaksies), wat 'n betekenisvolle invloed hê op die spesie-verspreiding van $[RhCl_n(H_2O)_{6-n}]^{3-n}$ komplekse. Aansienlike verskille bestaan tussen die spesiasie-diagram gerapporteer in hierdie studie en dit gedokumenteer in die literatuur, veral by 'n "vrye" chloried-konsentrasie van 1.0 M. By hierdie "vrye" chloried-konsentrasie was die $[RhCl_5(H_2O)]^{2-}$ komplekse anioon gevind om in 34% teenwoordig te wees (hierdie studie), terwyl die publiseerde verslae 80% rapporteer.

Ten einde die praktiese toepaslikheid van die voorgestelde ^{103}Rh KMR spesiasie-metode te bepaal, was (vir die eerste keer) ware industriële Rh oplossings (Anglo Platinum PLC) gebruik. Elk van die ^{103}Rh resonansies was ondubbelsinnig gekarakteriseer, en elke Rh spesie teenwoordig gekwantifiseer. Daarbenewens is die Rh^{III} spesie-verspreiding van die industriële Rh oplossing deur die "direkte" spesiasie-diagram saamgestel vanuit ^{103}Rh KMR metings akkuraat voorspel. Die berekende Rh^{III} spesie-verspreiding van die industriële Rh oplossings was akkuraat voorspel deur die voorgestelde "direkte" spesiasie-diagram soos saamgestel vanuit die ^{103}Rh KMR metings.

Na deeglike optimalisering van Heraeus industriële oplossings (optimale chloried-konsentrasie gevolg deur termiese behandeling vir effektiewe Rh^{III} chloried anasie reaksies), is die herwinning van Rh *via* neerslag metodes herhaal. In hierdie geval, het die Rh

herwinning dramaties verbeter, met tot 95% van die Rh uit oplossing verwyder. Hierdie verbetering is hoofsaaklik toegeskryf aan die verhoogde "vry" (ongebonde) chloried-konsentrasie. Die teenwoordigheid van geassosieerde PGM's sowel as ander oorgangsmetale sal die effektiewe "vrye" chloried-konsentrasie verlaag, aangesien hierdie metale sou optree as "chloried-binders". Deur die aanpassing van die totale chloried-konsentrasie, word Rh^{III} chloried anasie reaksies verbeter, wat daartoe lei dat $[RhCl_n(H_2O)_{6-n}]^{3-n}$ (n = 5,6) komplekse anione die dominante spesies in oplossing word, en dus lei tot verbeterde Rh herwinning. Daarbenewens word verder aangetoon dat, onder noukeurig gekontroleerde voorwaardes, "selektiewe" herwinning van Rh bereik word deur gebruik te maak van tris(2-aminoetiel)amien (**Tren**). Met inagneming van die feit dat Rh die laaste edelmetaal is wat verhaal word in alle PGM-raffinaderye, kan dit 'n koste-effektiewe roete word vir die "vooraf" (vroeë-stadium) herwinning van Rh vanuit industriële PGM bevattende oplossings.

Trefwoorde: Rh herwinning, ^{103}Rh KMR spektroskopie, $^{35/37}$Cl isotoop effekte, *isotopoloog*, isotopomeer, $[RhCl_n(H_2O)_{6-n}]^{3-n}$ (n = 3-6) komplekse, direkte ^{103}Rh KMR spesiasie

Table of Contents

List of Figures

Figure 3.12: Residual [Rh^{III}] in the supernatant as a function of increasing [Precipitant]:[Metal chloride anion] ratio. [Rh] = 3.871 mM, [Cl^-] = 4.008 M. Typical RSD values was below 7%

Figure 3.13: Residual [Rh^{III}] in the supernatant as a function of increasing [Precipitant]:[Metal chloride anion] ratio. Precipitation was repeated after the industrial feed solution was heated for 3 days at 333.1 K. [Rh] = 3.871 mM, [Cl^-] = 4.008 M. Typical RSD values was below 7%

Figure 4.1: [a] Isotopologues associated with the *fac*-[$Rh^{35}Cl_2{}^{37}Cl(H_2O)_3$] species; [b] possible isotopomers associated with the isotopologue of the *mer*-[$Rh^{35}Cl_2{}^{37}Cl(H_2O)_3$] species where the $^{35}Cl/^{37}Cl$ is coordinated *trans* with respect to water in a 2:1 ratio. = ^{35}Cl; = ^{37}Cl; = H_2O

Figure 4.2: Experimental ^{103}Rh spectra of $[RhCl_n(H_2O)_{6-n}]^{3-n}$ (n = 3–6) species recorded at 292.1 K (symbols). The least-squares fits (solid lines) between experimental spectra of $[RhCl_6]^{3-}$ [a], *trans*-$[RhCl_4(H_2O)_2]^-$ [c] and *fac*-$[RhCl_3(H_2O)_3]$ [e] and the isotopologue model; the least-squares fits between the experimental spectra and the isotopologue model that includes isotopomers for the $[RhCl_5(H_2O)]^{2-}$, *cis*-$[RhCl_4(H_2O)_2]^-$ and *mer*-$[RhCl_3(H_2O)_3]$ species are denoted by [b], [d] and [f], respectively

Figure 5.1: Literature documented Rh^{III} species distribution diagrams illustrating the large discrepancies existing between proposed diagrams. The dashed blue lines indicate the Rh^{III} species distribution at 1.0 M free chloride concentration, while the dashed pink lines indicate the free chloride concentration at which a 1:1 ratio of $[RhCl_6]^{3-}$ and $[RhCl_5(H_2O)]^{2-}$ exists

Figure 5.2: The ratio of the integrated peak area A($[RhCl_6]^{3-}$)/A($[RhCl_5(H_2O)]^{2-}$) as a function of the relaxation time applied. The horizontal lines shows the 95% confidence interval (blue dashed lines) of the average peak area ratio (solid pink line)

Figure 5.3: Change in the ^{103}Rh NMR resonances of the $[RhCl_n(H_2O)_{6-n}]^{3-n}$ (n=3-6) complexes as a function of free chloride concentration. The assignment of the resonances is based on the $^{35}Cl/^{37}Cl$ isotope effects, as exhibited by the insert figures.

Figure 5.4: Partial species distribution diagram as a function of HCl concentration for all $[RhCl_n(H_2O)_{6-n}]^{3-n}$ (n=3-6) species, including stereoisomers. The open symbols represent data obtained directly after sample preparation; the closed (coloured) symbols represent data obtained after the samples have equilibrated at 298.1 K for a year.

Figure 5.5: The change in the UV-VIS spectrum as a function of time (90 minutes) upon dilution of a 0.1038 M Rh^{III} stock solution equilibrated in 10.18 M HCl to a 3.012 M HCl matrix (292.1 K)

Figure 5.6: Change in Rh^{III} UV-VIS spectrum as a function of time (90 minutes) upon dilution of a 0.1038 M Rh^{III} stock solution equilibrated in 10.181 M HCl to a 0.1018 HCl matrix. [a] Rh solution prepared in the absence of MeOH, sodium acetate buffer and TBA^+Cl^-; [b] Rh solution prepared in the presence of MeOH, Ac buffer and TBA^+Cl^-. [c] Kinetic traces illustrating the change in absorbance at 390 nm; symbols = Expt data, Lines = Simulated kinetic fits of the aquation model

Figure 5.7: Chromatographic traces obtained when injecting Rh^{III} stock samples, initially equilibrated in varying HCl (0.714 – 5.998 M) concentrations, immediately after the appropriate dilution to a 10 mM HCl matrix. Temp = 298.1 K. Several chromatograms were excluded for clarity.

Figure 5.8: Partial $[RhCl_n(H_2O)_{6-n}]^{3-n}$ species distribution diagram as a function of HCl concentration, derived from a modified RP-IP-HPLC-ICP-OES method. The total Rh^{III} concentration of each sample injected was 0.200 mM and the typical RSD for the mole fraction was below 5.5%

Figure 5.9: Partial $[RhCl_n(H_2O)_{6-n}]^{3-n}$ (n=4-6) species distribution diagram as a function of HCl concentration comparing the data obtained from HPLC-ICP-OES separations (dashed lines & open symbols) to that of the ^{103}Rh NMR spectroscopic data (solid lines & coloured symbols)

Figure 5.10: Visual illustration of 5.00 mM Rh^{III} solutions equilibrated at various HCl concentrations (0.00 – 5.00 M). [a] before addition of (poly)amines, [b] 2 hours after addition of the (poly)amines. The (poly)amine concentration added to each solution was always 5 times excess over the Rh concentration, which is sufficient to achieve quantitative precipitation of Rh.

Figure 5.11: Rh^{III} precipitation conducted as a function of chloride concentration. The organic (poly)amines used are denoted in the legend. [a] Precipitation studies conducted by "*in situ*" protonation of the (poly)amines, which typically occur at [HCl] > 0.100 M; [b] Precipitation studies conducted by protonating the (poly)amine, using a 3.0 M $HClO_4$ matrix, prior to addition of the (poly)amine stock solutions to the Rh^{III} containing solutions. [Rh] = 5.00 mM, [Amine] = 25.00 mM. All precipitation studies were conducted at 298.1 K and repeated in triplicate. Typical RSD values for the [Rh] were below 5%.

Figure 5.12: Partial $[RhCl_n(H_2O)_{6-n}]^{3-n}$ (n=5,6) species distribution diagram as a function of HCl concentration comparing the data obtained from precipitation titrations (dashed lines & open symbols) to that of the ^{103}Rh NMR experiments (solid lines and closed symbols)

Figure 5.13: ^{195}Pt NMR spectrum of an authentic industrial feed solution

Figure 5.14: ^{195}Pt NMR spectrum (enlarged), recorded at 293.1 K, of the co-axial reference insert, containing pure $[PtCl_6]^{2-}$, illustrating the $^{35/37}Cl$ isotopologue induced splitting of the ^{195}Pt resonance signal. The symbols illustrate the experimental data while the solid lines illustrate the isotopologue model fitted to the experimental data. ● = ^{35}Cl; ● = ^{37}Cl

Figure 5.15: Experimental ^{195}Pt NMR spectrum (enlarged) of an authentic industrial feed solution illustrating the "fine-structure" of the ^{195}Pt resonance. The solid lines represent the non-linear least-squares fits of the isotopologue model to the experimental ^{195}Pt NMR spectroscopic data. The symbols represent the experimental data while the solid lines represent the isotopologue model fits.

Figure 5.16: ^{103}Rh NMR spectrum of an authentic industrial rhodium feed solution recorded at 292.1 K. $[Rh]_{tot}$ = 0.2109 M; $[Cl^-]_{tot}$ = 2.121 M

Figure 5.17: Experimental ^{103}Rh NMR spectra of the $[RhCl_n(H_2O)_{6-n}]^{3-n}$ (n=4,5) complex anions recorded at 292.1 K (symbols). [a] $[Rh^{35/37}Cl_5(H_2O)]^{2-}$ complex anion; [b] *cis*-$[Rh^{35/37}Cl_4(H_2O)_2]^-$ complex anion. The non-linear least-squares fits between the experimental spectra and the isotopologue model that includes isotopomers is denoted by the solid lines.

Figure 3.16: Residual [Rh] in the supernatant as a function of increasing [Precipitant]:[Metal chloride anion] ratio. [Rh] = 3.871 mM, $[Cl^-]$ = 4.008 M

Figure 5.18: Residual [Rh] in the supernatant as a function of increasing [Precipitant]:[Metal chloride anion] ratio. The chloride concentration of the raw feed solution was adjusted to 8.01 M and the solution heated at 354.1 K for 2 weeks prior to performing precipitation titrations. [Rh] = 3.903 mM, $[Cl^-]$ = 8.01 M, Precipitation titrations were conducted at 298.1 K.

Figure 5.19: Residual [Pt] in the supernatant as a function of increasing [Precipitant]:[Metal chloride anion] ratio. [Rh] = 3.903 mM, $[Cl^-]$ = 8.01 M, Precipitation titrations were conducted at 298.1 K.

Figure 5.20: Comparison between the Pt- and Rh-precipitant titration curves for the organic precipitants used throughout this study. [Pt] = 18.79 mM; [Rh] = 3.903 mM, $[Cl^-]$ = 8.01 M

Figure A2.1: Change in UV-VIS spectra as a function of time upon diluting a 0.1021 M Rh^{III} solution initially equilibrated in 10.181 M HCl to a final HCl concentration of 0.1018 M. The ionic strength was varied from 0.301 M to 5.012 M, as denoted in the respective figures [a] – [f]. Spectra were recorded at 298 K

Figure A2.2: Change in UV-VIS spectra as a function of time upon diluting a 0.1021 M Rh^{III} solution initially equilibrated in 10.181 M HCl to a final HCl concentration of 0.1018 M. The temperature was varied from 303.1 K – 283.1 K, as denoted in the respective figures [a] – [e]. The denoted spectra were recorded at a constant ionic strength of 0.301 M $HClO_4$

List of Tables

Chapter 1

Introduction

1.1 The history and discovery of rhodium

Rhodium (derived from the Greek word *rhodon* – ″rose″) was first isolated by William Hyde Wollaston in 1804, of which he wrote:

> *"another metal, hitherto unknown, which may not be improperly distinguished by the name Rhodium, from the rose-red colour of a dilute solution of the metal containing it"* [1]

Wollaston aptly named this element after the rose colour of one of its chloride complexes, hexachlororhodate(III), which was produced after the dissolution of *platina* (a concentrated form of platinum ore) in *aqua regia* [1]. The bulk of the platinum was removed as $(NH_4)_2[PtCl_6]$ by the addition of ammonium chloride to this solution. Subsequently, zinc was added to the filtrate that resulted in the precipitation of residual platinum, palladium, rhodium, copper and lead; the latter two metals that were removed by dissolution in dilute nitric acid. The residue was subsequently dissolved by the addition of excess *aqua regia* and with the addition of sodium chloride, the solution was evaporated to near dryness to yield $Na_3[RhCl_6]\cdot nH_2O$. Rhodium metal was produced after extraction of hexachlororhodate(III) with hot ethanol to which zinc was added. [1,2]

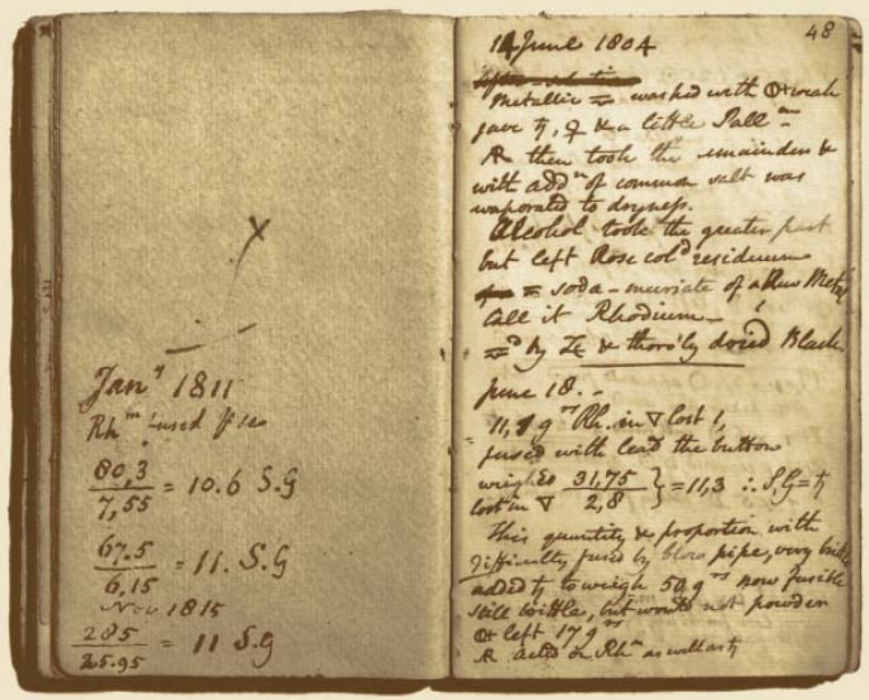

Figure 1.1: An excerpt of one of Wollaston's notebooks showing the page for 14 June 1804, which details the discovery of the new metal rhodium[2]

1.2 Occurrence and natural distribution of rhodium

Rhodium is a member of the platinum group metals (PGMs – Ir, Pt, Pd, Os, Ru) and as befits an element of the platinum metal sextet, it occurs mainly as a minor constituent of platinum group metal ores. These metals are occasionally referred to as precious metals due to their high economic value and scarcity with respect to worldwide deposits and abundances in the earth's crust (0.001 g/ton) [3]. The major PGM deposits worldwide are located in South Africa (Gauteng and North West Province), the Ural range in Russia and in Ontario, Canada, Figure 1.2 [4].

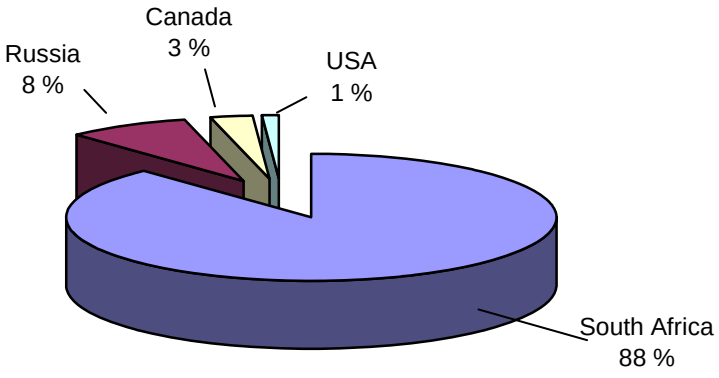

Figure 1.2: Percentage global production of PGM in 2004 [4]

In South Africa, rhodium ore deposits are found mainly in the three-layered intrusion of the Bushveld Igneous Complex (BIC). The Bushveld complex is the world's largest intrusion and encompasses the Limpopo and part of the North West Province [5], Figure 1.3. The three layers of the intrusion are the Merensky reef (0.3 – 0.9 m in thickness), the Upper Ground 2 reef (UG2: 18 – 36 m) and the Plat reef (275 m). The Merensky and UG2 reefs collectively contain approximately 90% of the world's PGM reserves [5].

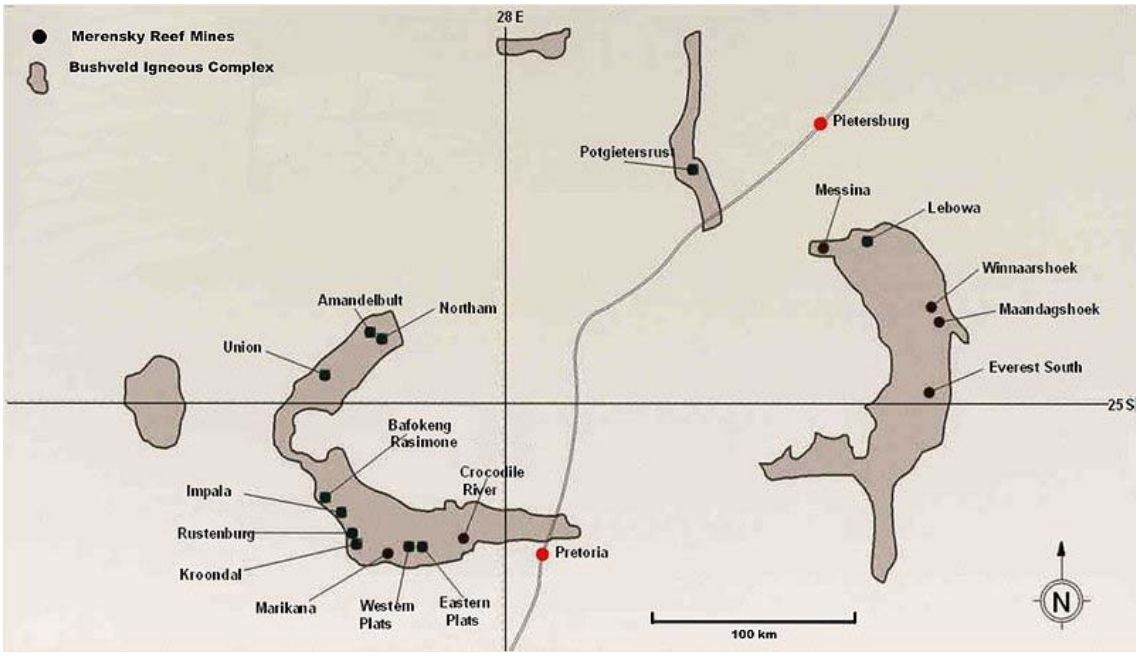

Figure 1.3: The Bushveld Igneous Complex illustrating the Merensky reef [5]

South Africa contains the world's largest known PGM deposits and is the principal exporter of precious metals, exporting approximately 75% of the world's supply in 2010[6]. The annual world production of rhodium is estimated between 19 000 and 25 000 kg [6].

Rhodium is relatively expensive due to the demand and supply constraint in the world's market. Figure 1.4 shows the average annual Rh price over the last twelve years. Since 2003, the average price of Rh has steadily been increasing, Figure 1.4, and in a five-year span it attained an average price of US$ 3,224.51 per troy ounce, climbing higher than US$ 9000 per troy ounce during 2008. This trend is especially important in terms of the South African economy, which benefits from increasing Rh prices because of the supply shortages and the increasing demand of this commodity.

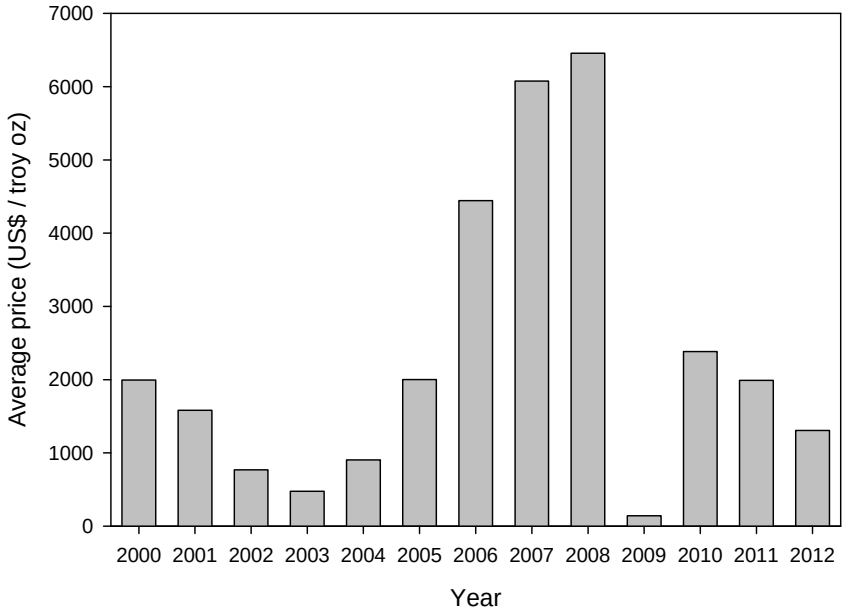

Figure 1.4: Average annual rhodium price for the last 12 years [7]

1.3 Industrial applications of rhodium

Rh has a number of industrial applications, including its use in homogeneous / heterogeneous catalysis in numerous industrial processes, the manufacturing of jewellery (Rh plating of Pt or Au in order to improve corrosion resistance), the use in electronic and electrical devices and dental applications [8]. However, the most important application of Rh is in the emission exhaust control systems of automobiles as a catalytic converter which effectively transforms NO_x emissions (predominantly NO and NO_2) from the engine into harmless N_2 (g) with little to no ammonia formation [9]. Approximately 83% of the Rh consumed worldwide during 2010 (~27,200 kg) was used in the production of catalytic converters – *paradoxically, only 7.300 kg was recovered from this application* [10]. Other large consumers of Rh include the chemical industry (7.8%) and the glass industry (6.5%), which integrates Rh predominantly for the production of fibreglass and flat-panel glass [10]. Furthermore, in the chemical industry, Rh-based catalysts are used for the catalytic carbonylation of methanol to form acetic acid, by the Monsanto process [11,12]. Among the miscellaneous Rh-catalysed reactions that have received considerable attention are the following examples: (*i*) the hydrogenation of olefins [13] which includes the first commercial asymmetric catalytic process for the synthesis of L-3,4-dihydroxyphenylalanine (L-DOPA) – a precursor to various physiological neurotransmitters which is also used as part of a treatment regimen for Parkinson's disease [14,15]; (*ii*) hydrogenation of arenes [16]; (*iii*)

hydroformylation of olefins [17]; (*iv*) Wilkinson's catalyst for the hydrogenation of alkenes [18] and (*v*) the hydrogenation of enamides [19].

1.4 The industrial refining of PGMs

In the previous section the wide range of applications of Rh was highlighted, from which it can be seen that the most important application is its use as a catalyst in catalytic converters in automobile exhaust emission control systems. In this regard, there is ever increasing evidence that small amounts of Rh (as well as Pd and Pt) used in these exhaust systems are being emitted (possibly as metal oxides) at the high temperature at which these catalysts work. The discharge of these PGMs into the environment could lead to environmental as well as potential health hazards [20,21]. From this perspective, there has been increased research specifically focussing on the recovery of Rh as a secondary metal, *i.e.* after its use. However, Rh is still predominantly recovered directly from PGM containing ores and hence the remainder of this review will focus on the general refining scheme of PGMs from precious metal ore concentrates, as it transpire in the PGM refining industry.

On average, the feed supplied to a precious metal refinery is a concentrate containing 50 – 70 % of the precious metals, *i.e.* Pt, Pd, Rh, Ir, Ru, Os, Au and Ag; from which the refining of PGMs would proceed according to the following three stages:
(i) Primary separation – refers to the first instance in which a particular PGM is separated from impurities as well as other PGMs. This method of separation seldom produces metal of suitable purity.
(ii) Secondary purification – The stage of refining where the product of the primary separation step is processed via a series of techniques, *vide infra.*
(iii) Reduction to metal – The stage during which the products of the secondary purification (often a metal salt) are reduced to the metal of suitable purity for commercial sale.

The entire separation and purification stages/techniques typically employed in industry can be summarized as follow [22]:

- *Dissolution*: The stage during which the precious metal ore concentrate is brought into solution. Traditionally this was done by means of an oxidizing acid, such as aqua regia, and would provide a crude form of separation between the primary (Pt, Pd, Au) and

secondary (Rh, Ir, Ru, Os, Ag) precious metals. However, contemporary refining methodology does not use dissolution as a separation technique; rather it is preferred to dissolve all PGMs in HCl using chlorine gas. This is the most cost-effective manner in which all precious metals are simultaneously brought into solution

- *Crystallization and precipitation*: This method of separation exploits the difference in solubility of the PGM (aqua) chlorido complexes during the primary and secondary stages. Amine-based precipitants (*e.g.* ammonium chloride) are typically used during this process. The solubility of the metal is strongly dependent on the particular PGM chlorido complex that is formed as well as the oxidation state of the metal centre. In this respect, factors such as pH, redox potential and the free chloride concentration play an important role.
- *Hydrolysis*: A method principally used for the removal of base metals (*e.g.* Cu, Ni, Fe). The pH of the solution is raised, which facilitates the formation of insoluble metal hydroxido complexes.
- *Distillation (oxidative distillation)*: This is a process designed for the selective removal of Ru and Os as their volatile tetroxides, RuO_4 and OsO_4. The process involves the use of strong oxidants such as sodium chlorate or sodium bromate at an elevated temperature. Ru and Os are consequently oxidized to the +8 oxidation state, allowing for the selective removal of gaseous RuO_4 and OsO_4 from the other PGMs. In order to separate Ru and Os from each other, the volatile tetroxides are scrubbed into a solution containing potassium hydroxide and ethanol, facilitating the reduction of Ru to oxidation state +4 and Os to oxidation state +6. Under these conditions, Os forms the soluble osmate, $[Os^{VI}O_2(OH)_4]^{2-}$ while Ru forms the insoluble ruthenium dioxide, RuO_2, commonly known as "ruthenium black". Os is subsequently precipitated as the $K_2[Os^{VI}O_2(OH)_4]$ salt by the addition of excess potassium hydroxide. In this manner, a highly efficient, if somewhat hazardous [RuO_4 (s) is highly explosive, while OsO_4 is highly toxic], separation process is achieved for Ru and Os.
- *Organic precipitation*: Various organic compounds are typically used for the selective precipitation of PGMs. As an example, Pd is routinely selectively precipitated with dimethylglyoxime, effectively removing all Pd during the final Pt purification step.

  Ir and Rh are generally precipitated with diethylenetriamine [22]. Under the appropriate conditions (*i.e.* Ir being present as Ir^{IV} and Rh as Rh^{III}) this type of precipitation can be used to separate Ir and Rh from each other.

- *Liquid-Liquid (Solvent) extraction*: Au, Pd, Pt and Ir can be separated with great efficacy using a range of solvent extraction methodologies. Various high molecular weight organic compounds have been successfully used for the solvent extraction of these metals. These organic compounds include the Cyanex range (Cyanex 921, 923 and 925) [23], Kelex 100 [24] and trioctylamine [25] to mention but a few.
- *Ion-exchange separation*: Ion-exchange resins are routinely used for the selective removal of Au (e.g. Amberlite IRA35 [26]) and Pd (e.g. Amberlite XAd-7 coated with dithiocarbamate [27]).

Figure 1.5 provides an overview the processing of PGMs by utilizing a combination of the abovementioned technologies. The refining scheme depicted in Figure 1.5 is adopted from that used by Anglo Platinum and does not reflect the schemes used by other refineries.

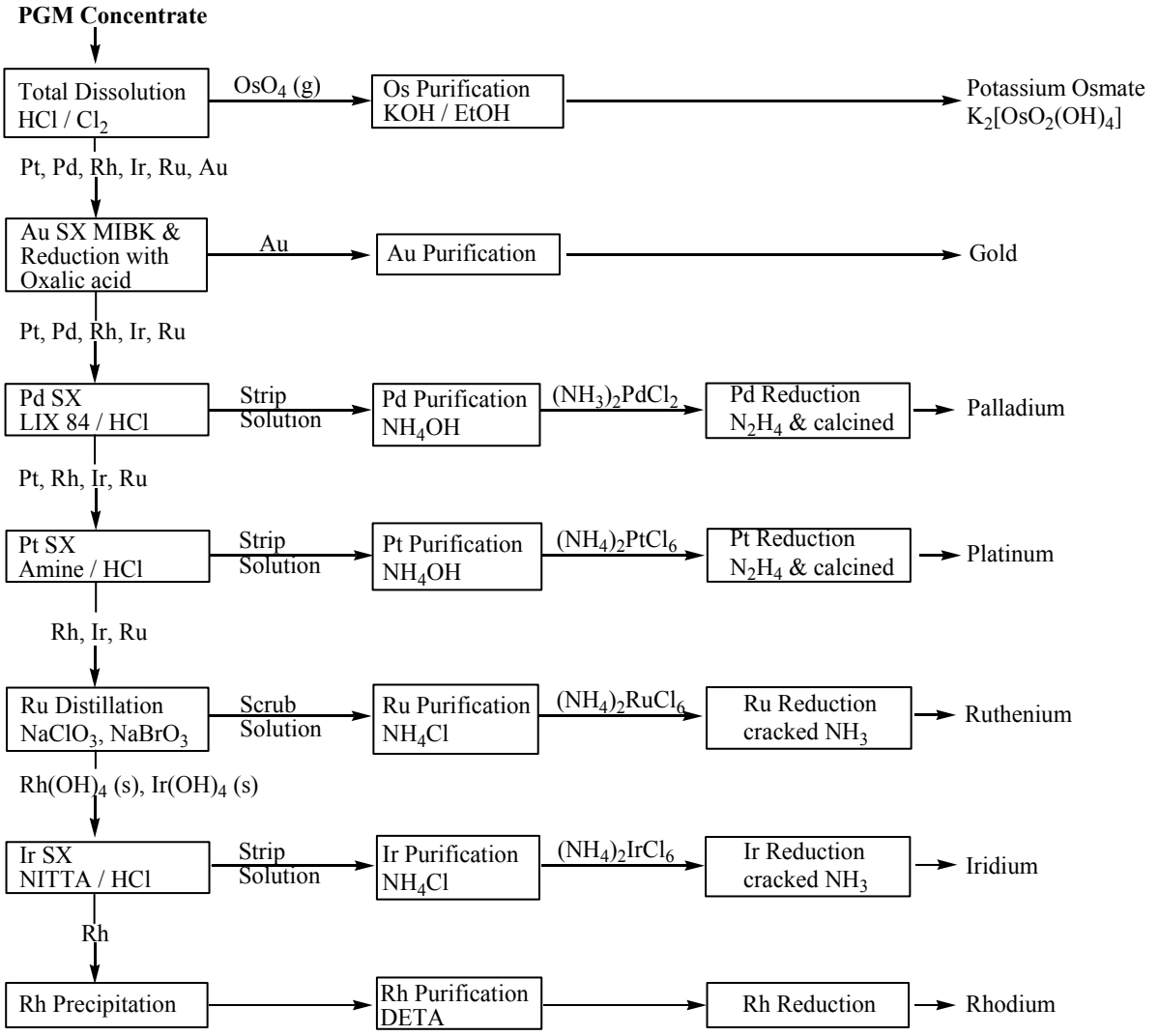

Figure 1.5: A detailed overview of the processes involved in the refining of PGMs at Anglo Platinum's refinery in Rustenburg, South Africa [22]

Due to its expense and chemical/industrial relevance, it would be highly beneficial to any refinery if Rh could be separated and refined at an early stage of the industrial refining process. However, the separation and purification of Rh from the other precious metals continue to pose the most difficult aspect of PGM refining. This is chiefly due to the poor extractability of Rh, which could be attributed to the inert nature of its chlorido-species toward ligand substitution reactions , in addition to their labile character toward aquation reactions [28]. Because of the difficulties encountered in the separation of Rh, mainly as its halide complexes, it is often the last metal recovered and refined in most separation schemes, Figure 1.5.

1.5 General coordination chemistry of rhodium

The platinum group metals can be classified as metals with "soft" to "hard" character, depending on the oxidation state of the element [29]. Accordingly, Rh^{3+} ions can be considered as being "harder" than Rh^{+} ions. In view of the fact that rhodium can adopt various oxidation states from -1 to +6, numerous rhodium complexes with various ligands have been documented [30]. Table 1.1 provides an overview of some rhodium compounds in various oxidation states that have been reported over the last five decades.

Rhodium in oxidation state -1 is typically stabilized by ligands having "B-type" or "soft" character, such as carbonyl ligands, while the only non-carbonyl complexes in this oxidation state are those of the $[Rh(PF_3)_4]^-$ complex anion [30]. The oxidation state 0 Rh species are often dimeric, with the only monomeric species documented being the highly reactive $[Rh(diphos)_2]$ complex [30].

The +1 and +3 oxidation states are considered the most common and important oxidation states of Rh. In its lower (+1) oxidation state, Rh does not readily form anionic complexes; presumably due to the fact that π-acid ligands are usually required to disperse the electron density from the metal in neutral or even cationic complexes [30]. Hence, it is not unexpected that the few examples of Rh^{I} complex anions contain potent π-acid ligands, such as $[SnCl_3]^-$, which reduces and coordinates to $RhCl_3$ to form the $[RhCl(SnCl_3)_2]_2^{4-}$ complex anion [30]. Moreover, the d^8 (t_{2g}^6 e_g^2) electronic configuration favours a 4-coordinate square-planar geometry [30]. A large amount of Rh-containing catalysts contain Rh in the +1

oxidation state (*e.g.* Wilkinson's catalyst – $[RhCl(PPh_3)_3]$), which owes its catalytic activity to the fact that it readily undergoes changes in coordination number and oxidation state [31,32].

Despite the existence of a vast number of Co^{II} complexes, the dipositive oxidation state is atypical for Rh. All Rh^{II} complexes are low-spin species, and the lack of spin reorientation required in forming a low-spin Rh^{II} complex implies that these are excellent reducing agents. A large number of the Rh^{II} complexes that have been documented [30] are dimeric, with the presence of an Rh-Rh bond. The stability of the Rh-Rh bond in these dimers prevents their facile oxidation [30]. To date, the only stable isolatable monomeric Rh^{II} complexes reported are those containing tertiary phosphines and related group VB ligands [30].

The tripositive oxidation state of Rh is considered the most common and its coordination chemistry is extensive. Virtually all of the complexes in this oxidation state are low-spin, diamagnetic, having an octahedral symmetry and obtaining a t_{2g}^6 electronic configuration. Rh complexes in the tripositive oxidation state exemplify high stability since the low-spin form of Rh implies a very high ligand field stabilization energy ($-2.4\Delta_0$) [30].This high energy is due to the fact that all the electrons are paired in the lowest *d*-orbital [33]. In the trivalent state, Rh forms octahedral anionic, neutral and cationic complexes with oxygen donor ligands (*e.g.* sulfates, nitrates and carboxylic acids), nitrogen donor ligands (e.g. ammonia, amines) and sulfur donor ligands (e.g. sulfites, sulfates, thiosulfates) [30]. Depending on the nature of the ligand, it may coordinate in either a monodentate or a chelate manner [30].

Beyond the tripositive oxidation state, Rh forms a limited number of complexes in the +4, +5 and +6 oxidation states, all of which are presumably octahedral [30]. The +5 and +6 oxidation states are exclusively stabilized by fluoride anions [30], although there have also been reports of less thoroughly characterized oxide complexes [30].

Table 1.1: Oxidation states and geometries of common rhodium complexes

Oxidation State	Coordination number	Geometry	Example of complexes
-1 (d^{10})	4	Tetrahedral	$K[Rh(PF_3)_4]$
0 (d^9)	5	Trigonal bipyramidal	$[Rh_2(PF_3)_8]$
	3	Planar	$[RhX(PCy_3)_2]$, $[RhH(PBu^t_3)_2]$
1 (d^8)	4	Square planar	$[RhCl(PPh_3)_3]$
	5	Trigonal bipyramidal	$[RhH(PPh_3)_4]$
2 (d^7)	4	Square planar	$[Rh(X')_2(PCy_3)_2]$
	6	Octahedral	$[Rh_2(O_2CMe_4)L_2]$
	5	Square pyramidal	$[RhHCl_2(PPh_3)_2]$
3 (d^6)	5	Trigonal bipyramidal	$[RhH_2Cl(PPh_3)_2]$
	6	Octahedral	$[Rh(acac)_3]$, $[RhX'_6]Y_3$, $[Rh(en)_3]Cl_3$
4 (d^5)	6	Octahedral	$M_2[RhF_6]$; $M_2[RhCl_6]$
5 (d^4)	6	Octahedral	$M[RhF_6]$
6 (d^3)	6	Octahedral	$[RhF_6]$

X = F, Cl, Br, I; **X′** = Cl, Br; **Y** = K, Na, NH_4; **L** = MeOH, MeCN, H_2O, Cl, CO, PF_3, PPh_3; **M** = Na, K, Rb, Cs

1.6 Rh^{III} aqua chlorido equilibria and ligand exchange kinetics

It has been previously highlighted that the separation and purification of Rh remains one of the most difficult processes in precious metal refining. This is ascribed mainly to the complex solution chemistry of Rh in chloride solutions. The Rh species formed in these solutions are of such a nature that liquid-liquid extraction (solvent extraction, SX), which has successfully been applied to the recovery of other PGMs (Figure 1.5), cannot easily be applied to the recovery of Rh. For this reason, a vast amount of research has been conducted on the solution chemistry of Rh^{III} in chloride-rich solutions, with the aim of assessing the thermodynamic and kinetic parameters of Rh^{III} chloro-complexes

The existence of hexachlororhodate(III), $[RhCl_6]^{3-}$, was first documented in 1951 [34] and was prepared by mixing finely divided Rh metal with "ignited NaCl" in a combustion furnace (700°C) under Cl_2 (g) atmosphere. This octahedral anion is generally known to undergo a series of consecutive stereochemical aquation reactions in acidic solutions, *vide infra*, but is considered to be unusually photoinert for a Rh^{III} complex [35]; with quantum yields for aquation of the low-energy ligand field being an order of magnitude less than the higher ligand field strength amine complexes [35]. Hydration of the $[RhCl_6]^{3-}$ complex anion leads to the formation of an array of aquachlorido complexes, $[RhCl_n(H_2O)_{6-n}]^{3-n}$ (n=0-6).

Generally, the stereochemical course of successive substitution reactions occurs according to the reaction scheme, Figure 1.6. It is interesting to note that the stereochemical course of the reactions depicted in Figure 1.6 is dictated almost exclusively by the *trans* effect of the chloride ligands on each reactant species.

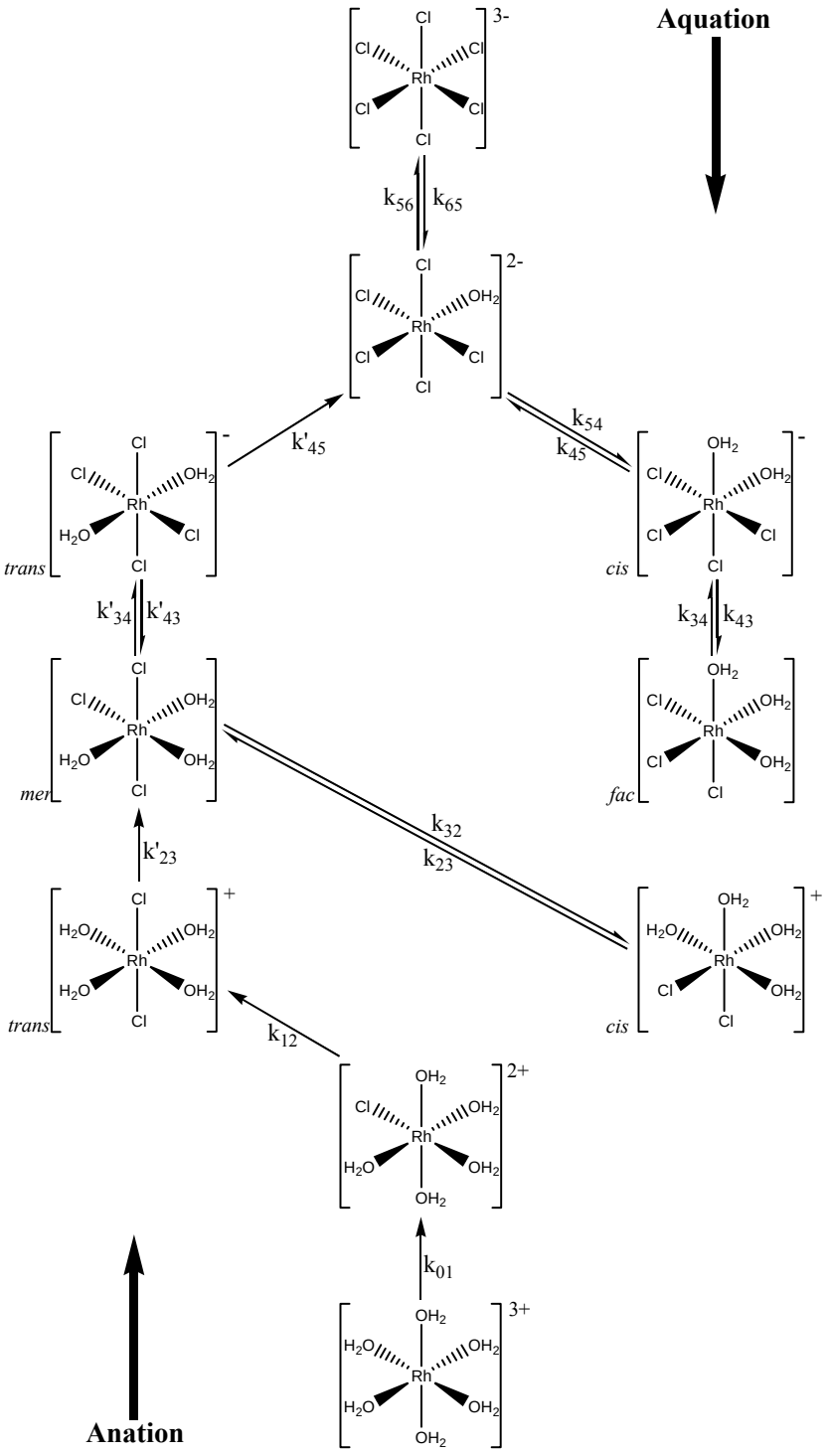

Figure 1.6: Reaction scheme illustrating the stereochemical course of successive aquation/chloride anation reactions, adapted from Palmer and Harris [36]

Due to the fact that the $[RhCl_6]^{3-}$ complex is considered to be both thermodynamically and kinetically unstable, being especially susceptible to aquation reactions, a number of researchers [36,11,14-23] have documented the aquation of Rh chloro-complexes in chloride-containing matrices. The most prevalent Rh species present in chloride-rich (> 5.0 M) media are the $[RhCl_6]^{3-}$ and $[RhCl_5(H_2O)]^{2-}$ complex anions, although the $[RhCl_4(H_2O)_2]^{-}$ species is also known to exist as a minor component [36]. A decrease in the chloride concentration readily leads to an increase in the extent to which aquation takes place. Furthermore, an increase in the rate of aquation was also observed upon increasing temperature [37,46].

1.7 High-resolution ^{103}Rh NMR spectroscopy as a tool to study Rh^{III} aqua-chlorido complexes

In recent years, transition metal nuclear magnetic resonance spectroscopy (TM NMR) has become a tool of substantial importance for modern-day research in the areas of coordination and organometallic chemistry, as well as catalysis. The chemical shift of metal nuclei may present constructive information relating to the electron density and the ligand in the primary coordination sphere of the metal centre. TM NMR can be considered as having several advantages over conventional / routine NMR, for example ^{1}H NMR, due to the fact that hydrogen atoms are often located at the periphery of coordination compounds whereas the metal atom constitutes the centre of most studies. Moreover, the range of chemical shifts is several orders of magnitude larger for TM NMR compared to the scale for ^{1}H or ^{13}C (≈12000 ppm for ^{103}Rh) [47]. Furthermore, the sensitivity of the transition metal chemical shift toward small disparities in the primary coordination sphere (generally due to minor steric and electronic perturbations) is more often than not extremely large, thus rendering TM NMR a sensitive tool for the observation of these changes [47].

Rhodium consists of a single naturally abundant isotope (100%), with the ^{103}Rh nuclide having a spin of I = ½. This is a very desirable feature in NMR spectroscopy, which is unfortunately counterbalanced by the low, negative gyromagnetic ratio, which is a factor of 31.8 smaller than that of ^{1}H [47]. The low frequency (Ξ = 3.16 MHz) often requires the use of a special probe, rendering the technique particularly expensive. Generally, the major problems encountered in TM NMR for nuclei with nuclear spin I = ½ are ascribed to long T_1 relaxation times and a low sensitivity; the latter which is due to a low natural abundance or a

low gyromagnetic ratio for the magnetically active nuclide of interest, or a combination of both these factors. Table 1.2 illustrates the classification of several $I = ½$ nuclei according to their respective elementary magnetic strength, $\gamma(X)/\gamma(^1H)$ [where $\gamma(^1H) = 26.7 \times 10^7$ $rad.T^{-1}.s^{-1}$] [47]. According to Table 1.2, ^{103}Rh would not necessarily be the most difficult nucleus to investigate via NMR spectroscopy, compared to *e.g.* ^{187}Os, because the natural abundance of the ^{103}Rh isotope is 100%.

Table 1.2: Classification of various $I = ½$ nuclei according to their respective elementary magnetic strength, $\gamma(X)/\gamma(^1H)$ [47]

Elementary magnetic strength [$\gamma(X)/\gamma(^1H)$]	Natural Abundance (%)		
	> 90	10 – 90	< 10
Strong	^1H, ^{19}F	^{205}Tl	
Medium	^{31}P	^{195}Pt, ^{207}Pb	^{13}C, ^{119}Sn
Weak	^{89}Y, ^{103}Rh	^{108}Ag, ^{183}W	^{57}Fe, ^{187}Os

One of the major debates pertaining to ^{103}Rh NMR spectroscopy is the use of a reliable referencing method for ^{103}Rh resonance signals. Traditionally, various substances were used as referencing compounds. These include the use of Rh metal (this has the disadvantage of producing a broad signal which is highly susceptible to small temperature variations) as well as $[Rh(acac)_3]$ (which has a long T_1 relaxation time) [48,49]. Furthermore, the set reference frequencies, Ξ, of the reference materials must be rescaled to the $SiMe_4$ (TMS) reference frequency. Therefore, the use of various reference materials generally leads to confusion. In this regard, the use of the calculated accurate frequency, $\Xi(^{103}Rh)$ = 3.16 MHz, relative to the TMS scale at 100.000 MHz, has been generally accepted [47]. However, care should be taken when using / reporting an accurate chemical shift (δ), since various chemical shifts have been reported for the simple [RhCln(H2O)6-n]3-n (n=0-6) complexes, Table 1.3.

Table 1.3: Comparison of reported chemical shifts, $\delta(^{103}Rh)$, for various $[RhCl_n(H_2O)_{6-n}]^{3-n}$ (n=0-6) species. For convenience, the chemical shifts were recalculated relative to the $[RhCl_6]^{3-}$ resonance

Rh^{III} species	Reference [50] (35°C)	Reference [51] (3°C)	Reference [51] (35°C)	Reference [52]
$[RhCl_6]^{3-}$	0	0	0	0
$[RhCl_5(H_2O)]^{2-}$	232.0	233.7	222.8	258
cis-$[RhCl_4(H_2O)_2]^{-}$	486.7	484.9	466.6	320
trans-$[RhCl_4(H_2O)_2]^{-}$	551.3	559.7	545.1	630
fac-$[RhCl_3(H_2O)_3]$	815.3	751.5	-	570
mer-$[RhCl_3(H_2O)_3]$	880.9	815.4	795.5	883
cis-$[RhCl_2(H_2O)_4]^{+}$	1154.7	1086.4	1066.9	819
trans-$[RhCl_2(H_2O)_4]^{+}$	-	1151.9	1133.3	1140
$[RhCl(H_2O)_5]^{2+}$	-	1443.2	1428.6	1504
$[Rh(H_2O)_6]^{3+}$	-	1964.4	1856.2	2017

Table 1.3 shows that the chemical shifts for these complexes are not entirely acceptable for the assignment of the ^{103}Rh resonances of these Rh^{III} complexes. This is primarily due to the extreme sensitivity of the ^{103}Rh nuclear shielding to numerous effects such as solvent, analyte concentration, temperature, pressure as well as other effects [53]. By way of example, it is documented that ^{103}Rh chemical shifts can vary between 0.5 – 3.0 ppm K^{-1}, illustrating a considerable temperature dependence. This makes comparison of ^{103}Rh chemical shifts somewhat uncertain – a subject which will be addressed during the course of this study.

Despite these difficulties, and the low sensitivity of ^{103}Rh NMR spectroscopy, this method has numerous advantages for the study, characterisation and speciation of various Rh complexes. The advent of reliable and validated computational approaches such as density functional theory (DFT) [54-56], in conjunction with NMR spectroscopic data, can result in new insights in relation to structural data and other physical / thermodynamic phenomena.

1.8 Research objectives and thesis outline

The selective separation and recovery of PGMs (Pd^{II}, Rh^{III}, $Ir^{III/IV}$, Pt^{IV}) in acidic, chloride-rich solutions has been the subject of numerous studies, with most focussing on solvent-extraction [23-27] and solid–phase extraction [57-59]. In general, the modern separation and recovery techniques of PGMs, on an industrial scale, predominantly depends

on the selective distribution of the stable, kinetically inert, anionic chlorido-complexes of these elements between the acidic, chloride rich aqueous phase and the organic receptor phase; with the general notion that the distribution mechanism involves either an ion-exchange or ion-association mechanism, or a combination of both. The selectivity of recovery of the metal chlorido-anion complexes, in turn, depends on several factors, most importantly the chemical speciation of the PGM complexes in solution.

Over the last five decades, several speciation diagrams for the Rh^{III} aqua chlorido-complexes, $[RhCl_n(H_2O)_{6-n}]^{3-n}$ (n=3-6), in HCl media have been reported [28,37,39,40,42,60]. The published Rh^{III} species distribution diagrams have generally been constructed using data from indirect (kinetic and spectrophotometric) measurements. Furthermore, these investigations were conducted using rather dilute Rh^{III} solutions at high HCl concentrations, in which the Rh^{III}:Cl^- mole ratio is relatively higher when compared to industrial feed solutions. Moreover, there is vast differences between the documented Rh^{III} speciation diagram, which makes it difficult to establish which set of experimental conditions should be used in developing novel extraction protocols for the selective recovery of Rh.

The overarching objectives of the research described in this thesis is the screening and application of commercially available *N*-containing organic receptors as selective precipitants in the recovery of Rh from laboratory prepared PGM-containing solutions as well as authentic industrial PGM feed solutions. In this regard, the complexities involved in the quantitative recovery of Rh from industrial feed solutions is described, with particular emphasis on the species distribution of the Rh^{III} aqua chlorido-complexes, $[RhCl_n(H_2O)_{6-n}]^{3-n}$ (n=3-6), and its influence on the recovery of Rh from acidic chloride-rich solutions.

In order to fully comprehend all the factors that may influence the separation and recovery of Rh from acidic chloride solutions, the kinetic and thermodynamic properties related to Rh^{III} ligand exchange reactions, particularly aquation and chloride anation reactions, has to be considered. ***Chapter 2*** provides a detailed account of the kinetics of interconversion of Rh^{III} aqua-chlorido complexes. Important factors influencing the rate at which aquation/anation reactions occur (*e.g.* temperature and ionic strength) are discussed. The factors which influence the rate at which Rh^{III} aquation reactions occur generally has an overbearing effect on the selectivity of a particular extraction/separation technique, which is

the rationale for this investigation. Furthermore, a simplistic method for the calculation of molar extinction coefficient spectra of several $[RhCl_n(H_2O)_{6-n}]^{3-n}$ species is presented.

Although methods such as solvent extraction and solid-phase extraction have been well documented, a review of available literature reveals that only a few publications deal with the "selective" recovery of Rh by means of organic precipitation. The premise of ***Chapter 3*** is based on the "upfront" separation of Rh^{III} (*i.e.* Rh being separated and refined *before* any other PGMs) using organic precipitants. The chapter details the screening of various commercially available *N*-containing organic precipitants for the selective and quantitative precipitation of Rh^{III} as its chloro-anionic complexes, from laboratory prepared PGM solutions as well as authentic industrial PGM feed solutions. Selective and quantitative recovery of Rh is achieved when this separation technique is applied to laboratory prepared PGM solutions; however, this is not the case when applied to authentic industrial feed solutions. Possible explanations for this phenomenon are provided, with the aim of utilising ^{103}Rh NMR spectroscopy for the ***direct*** speciation of Rh^{III} aqua chlorido-complexes.

In order to utilize ^{103}Rh NMR spectroscopy as a tool for the ***direct*** speciation of Rh^{III} aqua chlorido-complexes, all the ^{103}Rh resonances observed in a spectrum needs to be accurately assigned. ***Chapter 4*** details the use of $^{35}Cl/^{37}Cl$ isotope effects in the observed 19.11 MHz ^{103}Rh NMR resonances of $[RhCl_n(H_2O)_{6-n}]^{3-n}$ (n=3-6) complexes in acidic chloride solutions (at 292 K), which shows that the "fine-structure" observed in the ^{103}Rh resonances can be understood in terms of the unique *isotopologue*, and in certain cases the isotopomer distribution within each complex. The ^{103}Rh NMR resonance structure thus served as a novel NMR-fingerprint, which can be used for the unambiguous assignment of $[RhCl_n(H_2O)_{6-n}]^{3-n}$ (n=3-6) complexes, without the reliance on accurate $\delta(^{103}Rh)$ chemical shifts.

Chapter 5 describes the use of ^{103}Rh NMR spectroscopy as a powerful analytical tool for the detection, unambiguous characterisation and ***direct*** chemical speciation of $[RhCl_n(H_2O)_{6-n}]^{3-n}$ (n=3-6) complexes present in acidic chloride-rich media, without altering the chemical composition (and thereby the chemical speciation) of a solution. Using this method, a revised ***direct*** species distribution diagram, as a function of the free chloride concentration, has been established for the $[RhCl_n(H_2O)_{6-n}]^{3-n}$ (n=3-6) complexes using this method. The proposed speciation diagram have been compared to that determined through

conventional analytical methods, such as reversed-phase ion-pair HPLC-ICP-OES techniques, and good correlation between the two methods were established. Furthermore, the precipitation of Rh^{III} aqua chlorido-complexes was performed as a function of HCl concentration, from which the Rh^{III} species distribution was directly correlated to the proposed speciation diagram. Subsequently, the developed ^{103}Rh NMR speciation method was extended to authentic industrial PGM feed solutions, and it was observed that the proposed speciation diagram accurately predicts the $[RhCl_n(H_2O)_{6-n}]^{3-n}$ (n=3-6) species distribution of these industrial PGM solutions. Using the knowledge obtained from the Rh speciation studies, revised experimental conditions were developed for the precipitation of Rh from industrial feed solutions from which the Rh was "selectively" and quantitatively recovered.

Chapter 6 summarizes the findings presented in the preceding chapters, evaluating the proposed speciation techniques and its relevance to industry.

1.9 References

1. W. H. Wollaston, *Phil. Trans. Roy. Soc.* **94** (1804) 419
2. W. P. Griffith, *Platinum Metals Rev.*, **47** (4) (2003) 175-183
3. W. P. Griffith, *The Chemistry of the Rare Platinum Metals (Os, Ru, Ir and Rh)*, Interscience, London (1967)
4. D. R. Wilburn, D. I. Bleiwas, *Platinum-Group Metals-World Supply and Demand*, U.S. Geological Survey Open-File Report (2004)
5. http://en.wikipedia.org/wiki/Bushveld_Igneous_Complex
6. J. Butler, *Platinum 2011*, Johnson Matthey PLC, England, United Kingdom (2011)
7. *Platinum 2000 – 2012*, Johnson Matthey PLC, England, United Kingdom
8. A. M. Weisberg, "Rhodium plating". *Metal Finishing* **97** (1) (1999) 296–299
9. M. Shelef, G. W. Graham, *Catalysis Reviews*, **36** (3) (1994) 433–457
10. P. J. Loferski, *Commodity Report: Platinum-Group Metals*, United States Geological Survey USGS (2011)
11. P. Powel, *Principles of organometallic chemistry*, 2nd Ed., Chapman and Hall, London (1988)

12. M. Gauss, A. Seidel, P. Torrence and P. Heymanns, in *Applied Homogeneous Catalysis with Organometallic Compounds*; Eds. B. Cornils and W. A. Herrmann, VCH Publishers, N.Y. (1996)
13. J. F. Young, J. A. Osborn, F. H. Jaidine and G. Wilkinson, *J. Chem. Comm*. **7** (1965) 131
14. W. S. Knowles and M. J. Sabacky, *J. Chem. Comm.* (1968) 1445
15. W. S. Knowles, *J. Chem. Ed*. 63 (1986) 222
16. H. Y. H. Gao and J. R. Angelici, *Organometallics*. **19** (4) (2000), 622 – 629
17. R. Cramer, *J. Am. Chem. Soc.*, **7** (1967), 1633 – 1639
18. J. A. Osbom, F. H. Jardine, J. F. Young and G. Wilkinson, *J. Chem. Soc. A.* **526** (1966), 175 -183
19. X. Y. Huang, R. X. Li, H.Chen and X. J. Li, *Chinese Chemical Letters.,* **14** (2003), 623 – 626
20. S. Artelt, H. Kock, H. P. König, K. Levsen and G. Rosner, Atmos. Environ., **33** (1999) 3559
21. K. Pyrzynska, *J. Eviron. Monit.* **2** (2000), 99N
22. F. Crundwell, M. Moats, V. Ramachandran, T. Robinson, W. G. Davenport, *Refining of the Platinum-Group Metals*, in: Extractive Metallurgy of Nickel, Cobalt and Platinum Group Metals, Elsevier, United Kingdom (2011) *and references therein*
23. A. A. Mhaske and P. M. Dhadke, *Hydrometallurgy*, **61** (2001) 143-150
24. M. S. Alam and K. Inoue, *Hydrometallurgy*, **46** (1997) 373-382
25. P.P. Sun and M. S. Lee, *Hydrometallurgy*, **105** (2011) 334-340
26. I. Matsubara, Y. Takeda and K. Ishida, *Fresenius J. Anal. Chem*. **366** (2000) 213-217
27. W. Chwastowska, E. Skwara, E. Sterlinska, L. Pszonicki, *Talanta* **64** (2004) 224-229
28. E. Benguerel, G. P. Demopoulos and G. B. Harris, *Hydrometallurgy,* **40** (1996) 135 – 152
29. R. G. Pearson, *J. Am. Chem. Soc.*, **85** (1963) 3533
30. F. H. Jardine, P. S. Sheridan, in *Comprehensive Coordination Chemistry. The Synthesis, Reactions, Properties and Applications of Coordination Compounds* (Vol. 4) Eds. G. Wilkinson, R. D. Gillard and J. A. McCleverty, Pergamon Press, Oxford (1987)
31. J. F. Nixon, *Adv. Inorg. Chem. Radiochem.* **13** (1970) 363.
32. T. Kruck, W. Lang, N. Derner and M. Stadler, *Chem. Ber.*, **101 (**1968) 3816.
33. N. N. Greenwood and A. Earnshaw, *Chemistry of the Elements*, Pergamon Press, Oxford (1984)
34. G. H. Ayres and F. Young, *Anal. Chem.* **24** (1952) 165
35. N. A. P. Kane-Maguire and C. H. Langford, *Inorg. Chim. Acta,* **17** (1976) L29

36. D.A. Palmer, G.M. Harris, Inorg. Chem. **14** (1975) 1316
37. D. Cozzi, F. Pantani, *J. Inorg. Nucl. Chem.* **8** (1958) 385-398
38. M.H. Mihailov, V.T.S. Mihailova, V.A. Khalkin, *J. Inorg. Nucl. Chem*. **36** (1974) 115-122
39. W. Robb, G.M. Harris, *J. Am. Chem. Soc*. **87** (1965) 4472-4476
40. W. Robb, M.M. de V. Steyn, *lnorg. Chem*. **6** (1967) 616-619
41. M.J. Pavelich, G.M. Harris, *lnorg. Chem*. **12** (1973) 423-431
42. D. Robb, M.M. de V. Steyn, H. Kruger, *lnorg. Chim. Acta*, **3** (1969) 3873-387
43. G.M. Harris, K. Swaminathan, *J. Am. Chem. Soc*. **88** (1966) 4411-4414
44. A.V. Belyaev, A.B. Venediktov, *Koord. Khim*. **8** (1982) 443
45. K. Swaminathan, G.M. Harris, *J. Am. Chem. Soc*. **88** (1966) 4411
46. S.J. Al-Bazi, A. Chow, *Talanta*, **31** (1984) 815-836
47. J. M. Ernsting, S. Gaemers, C. J. Elsevier, *Magn. Reson. Chem*. **42** (2004) 721 – 736
48. R.K. Harris, E. D. Becker, S. M. Cabral de Menezes, R. J. Goodfellow, P. Granger, *Pure Appl. Chem.* **73** (2001) 1795
49. R. Benn and A. Rufinska, *Angew. Chem., Int. Ed. Engl*. **25** (1986) 861
50. T. S. Slotte, *Adsorption of Platinum and Rhodium Complexes on Modified γ-Al_2O_3 surfaces*, Ph.D. Thesis, University of Oulu (2000)
51. C. Carr, J. Glaser, M. Sandström, *Inorg. Chimica. Acta*. **131** (1987) 153-156
52. B. E. Mann, C. Spencer, *Inorg. Chim. Acta*. **65** (1982), L52-L58
53. T. E. Geswindt, W. J. Gerber, D. J. Brand, K. R. Koch, *Anal. Chim. Acta*. **730** (2012) 93-98
54. G. Schreckenbach, T. Ziegler, *J. Chem. Phys.* **99** (1995) 606
55. M. Bühl, *Chem. Phys. Lett.* **267** (1997) 251
56. C. Fonseca Guerra, J. G. Snijders, G. Te Velde, E. J. Baerends. *Theor. Chem. Acc.* **99** (1998) 391
57. J. G. H. Du Preez and U. Naidoo*, Solvent Extraction and Ion Exchange*, **23** (2005) 439-447
58. L.G. Floyd, in: *2nd International Conference on New Process for Ruthenium, Rhodium and Iridium*, Int. Precious Metals Institute Inc. New York (1978)
59. R.M. Izatt, J.S. Bradshaw, R.L. Bruening, N.E. Izatt, K.E. Krakowiak, in: K.C. Liddell, D.J. Chaiko (Eds.), *Metal Separation Technologies beyond 2000: Integrating Novel Chemistry with Processing*, Symposium Proceeding, Hawaii, June 13–18, TMS (1999) 357–370.

60. W. J. Gerber, K. R. Koch, H. E. Rohwer, E. C. Hosten, T. E. Geswindt, *Talanta*, **82** (2010) 348–358.

Chapter 2

The aquation kinetics of Rh^{III} aqua chlorido complexes†

2.1 Introduction

2.1.1 Aquation of $[RhCl_6]^{3-}$ and $[RhCl_5(H_2O)]^{2-}$ complex anions

The colour of Rh^{III} aqua chlorido-complexes in aqueous HCl solutions varies from yellow to various shades of red, depending on the nature and history of the solution, illustrated in Figure 2.1. The gradual change in colour upon varying HCl concentration is indicative of the presence of various Rh^{III} species. These colour changes prompted the extensive study of the aqua chlorido ligand exchange kinetics of Rh^{III} complexes by various authors [1-6]. An overview of the documented reactions is outlined in Figure 2.2.

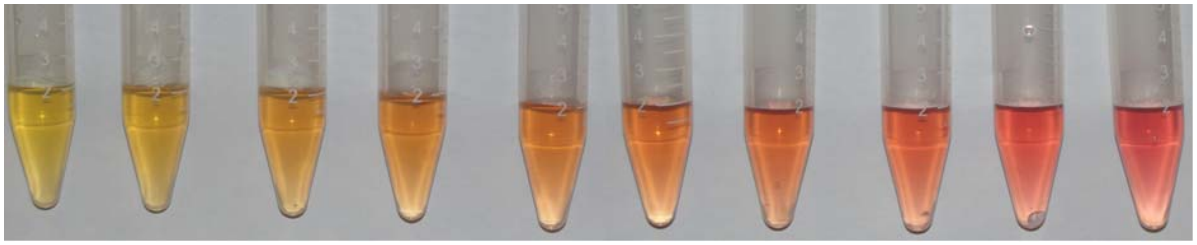

Increasing [HCl] from 0 - 6.0 M

Figure 2.1: Rh^{III} containing solutions as a function of HCl concentration. All solutions contain identical Rh^{III} concentrations while the HCl concentration of the solutions were increased from 0 – 6.0 M in the direction illustrated

† This Chapter is partially based on the publication: W. J. Gerber, K. R. Koch, H. E. Rohwer, E. C. Hosten and T.E. Geswindt, The separation and quantification of $[RhCl_n(H_2O)_{6-n}]^{3-n}$ complexes, including stereoisomers, by means of ion-pair HPLC-ICP-MS. *Talanta* **82** (2010) 348-358

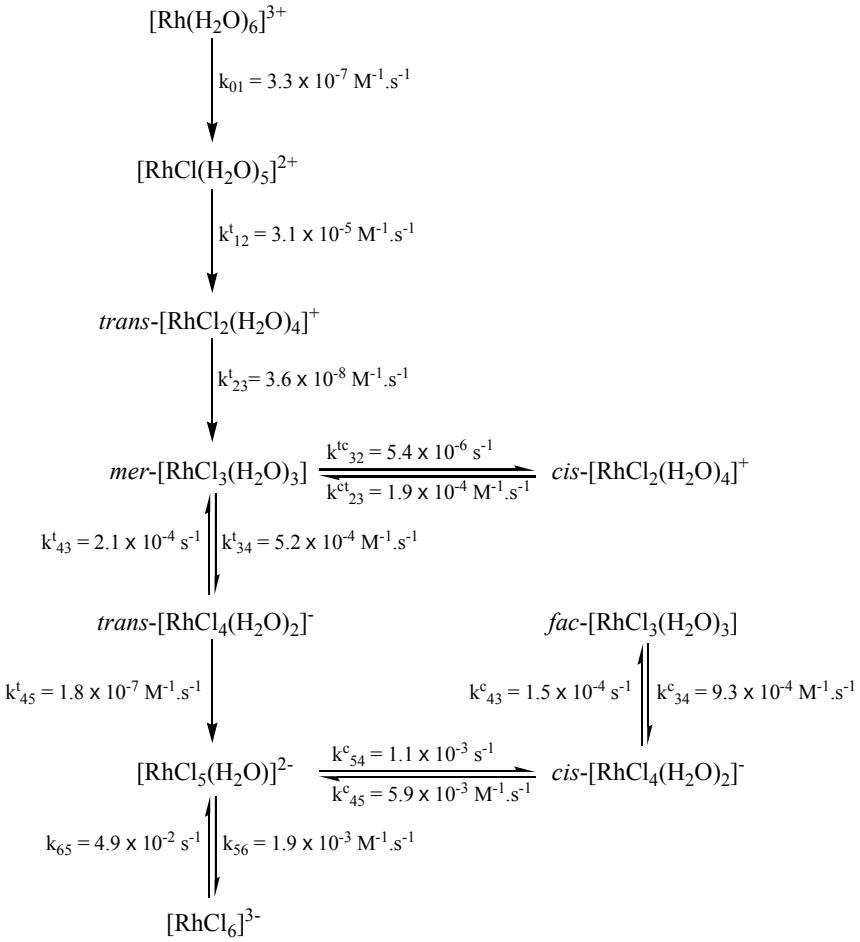

Figure 2.2: Kinetic data for the aquation / anation reactions of $[RhCl_n(H_2O)_{6-n}]^{3-n}$ species illustrating the stereochemical course of successive ligand substitution reactions, adapted from Palmer and Harris [5]

The stereochemical course of these reactions is dominated by the *trans*-labilizing effect of chloride ligands, Figure 2.2. As an example, the aquation of $[RhCl_5(H_2O)]^{2-}$ complex anion leads to the formation of *only* the *cis*-$[RhCl_4(H_2O)_2]^-$ complex anion; the latter subsequently undergoes aquation yielding *only* the *fac*-$[RhCl_3(H_2O)_3]$ species. The *fac*-$[RhCl_3(H_2O)_3]$ species is considered to be resistant to further chloride-induced hydrolysis in the absence of chloride ligands being *trans* to each other. In a similar manner, chloride anation reactions, when the *fac*-$[RhCl_3(H_2O)_3]$ species, occur more readily at a site *trans* to a coordinated chloride ligand. These types of regiospecific substitution reactions only occur in strongly acidic media where every coordinated aqua ligand is fully protonated [1-6].

Although the Rh^{III} aqua chlorido system has been studied extensively, there is a general shortage of *reliable* speciation, rate and equilibrium data [1-6]. The reliability of the

aforementioned data is clearly reflected by the discrepancies observed in the reported Rh^{III} aqua/chlorido speciation diagrams, Figure 2.3 [1-7].

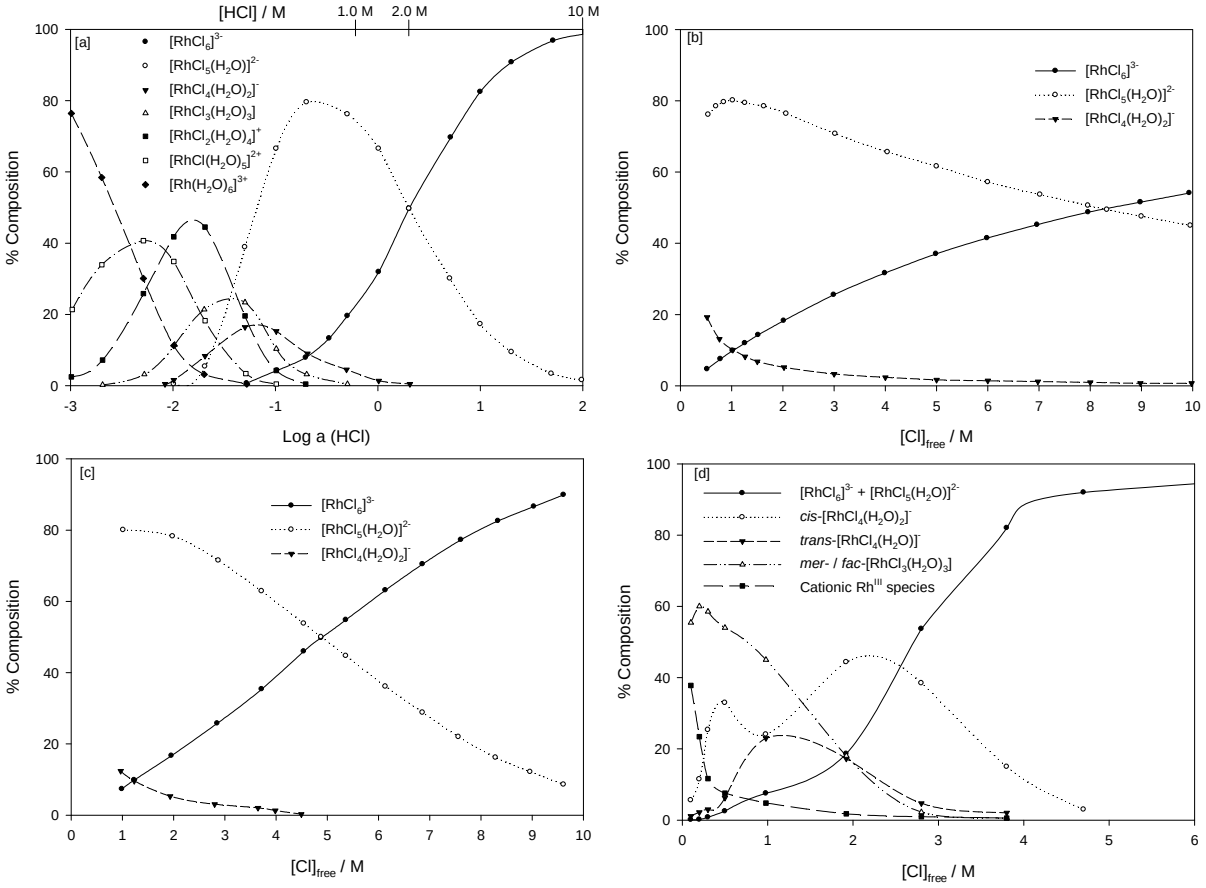

Figure 2.3: Literature documented Rh^{III} species distribution diagrams illustrating the large discrepancies existing between proposed speciation diagrams [1-7]

The large inconsistencies in the documented Rh^{III} speciation diagrams, shown in Figure 2.3, could originate from various factors and inaccuracies; one of these being (in the case of UV-vis based speciation diagrams) the discrepancies between the molar extinction coefficient spectra for individual Rh^{III} aqua chlorido-complexes reported in literature [5,8], Figure 2.4 and Table 2.1. Conventionally, the molar extinction coefficient spectra of the Rh^{III} aqua chlorido-complexes were determined by preparing crystals of the desired complex and, directly following dissolution of these crystals, recording the absorbance spectrum [8]. The isolation of the desired Rh^{III} aqua chlorido-complex by means of resin-based ion-exchange columns has also been reported [8]. Directly after isolation of the desired species, the absorbance spectrum was recorded. However, Wolsey *et al* [8] acknowledged that when four or more chloride ligands are coordinated to the Rh metal centre, a considerable error transpires because of reasonably fast ligand exchange kinetics [8].

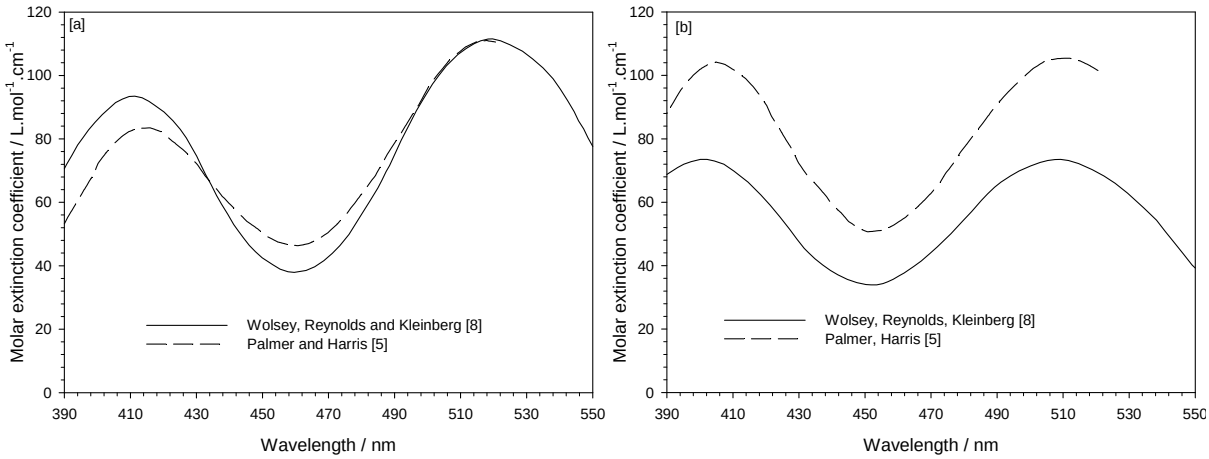

Figure 2.4: Comparison of the literature documented molar extinction coefficient spectra for [a] $[RhCl_6]^{3-}$ and [b] $RhCl_5(H_2O)]^{2-}$, adapted from references [5,8]

Table 2.1: Comparison of literature reported molar extinction coefficients at selected wavelengths [5,8]

Wavelength / nm	Molar extinction coefficient / $L.mol^{-1}.cm^{-1}$			
	$[RhCl_6]^{3-}$		$[RhCl_5(H_2O)]^{2-}$	
	Reference [5]	Reference [8]	Reference [5]	Reference [8]
390	52.8	71.5	89.5	69.0
400	72.9	85.5	102.9	73.7
410	81.7	92.7	101.7	69.0
420	81.0	86.7	90.5	59.7
430	69.4	73.1	71.8	48.5
440	56.9	54.5	60.0	37.0
450	49.6	42.6	50.7	34.2
460	46.5	38.6	52.5	36.7
470	50.9	42.6	62.5	45.1
480	64.4	54.2	79.6	54.1
490	79.5	76.3	91.7	65.3
500	95.8	95.1	101.3	72.1

In terms of developing targeted liquid-liquid extraction [1,9-11], solid-phase extraction [12] or organic precipitation [13] methods for the selective and quantitative separation of Rh, it is thus necessary to identify both the specific Rh species present in such halide-rich solutions as well as their relative abundances. This is because cationic, anionic and neutral Rh species are separated through different mechanisms and with different types of extractants. In this respect, an accurate and thus *reliable* Rh^{III} aqua / chlorido speciation diagram would provide this information. Furthermore, the ligand exchange kinetics between H_2O and Cl^- ligands must be considered equally (if not more) important since an equilibrium distribution of species is essential for reliable Rh recovery. The data obtained from the kinetic studies typically provide information regarding how fast a solution reaches an equilibrium

state, which is directly related to whether or not the postulated equilibrium distribution diagram will be of use in determining an industrial processing scheme.

2.1.2 Isosbestic points

Isosbestic points arise when two or more absorbing species have equal molar extinction coefficients at the same wavelength when the total concentration of said species is constant. The presence of an isosbestic point is usually ascribed to the presence of only two absorbing species, because the probability of more than two species having equal molar extinction coefficients at the same wavelength is very small. This is not to say that other species are completely absent, but these species might be present in low concentrations such that it does not interfere with the absorbance measured at that wavelength. In other instances it is possible that multiple species could be present at appreciable concentrations with molar extinction coefficients that are similar in magnitude to that occurring at the isosbestic wavelength, or the molar extinction coefficients are multiples of each other, or that some species have comparatively low molar extinction coefficients. In these cases, isosbestic points would not be very useful, and the assumption that only two absorbing species are present in appreciable concentrations during the formation of an isosbestic point would be incorrect. These cases are normally difficult to evaluate; however, careful experimental and data analysis could reveal such anomalies. Throughout this study, it is assumed that only two light absorbing species are present in appreciable concentrations when reference is made to an isosbestic point.

2.1.3 Mauser diagrams

In virtually all aspects of physical chemistry, the kinetics of chemical reactions is treated only on the level of concentration equations. Furthermore, most of these chemical reactions in liquid phase are investigated via UV-Vis spectrophotometry, where the measured output used is absorbance data, which generally obey the Beer-Lambert law. In contrast to concentration determinations, absorbance data leads to a loss of kinetic information due to its inherent limited sensitivity [14].

A Mauser diagram is a powerful tool used for the evaluation of absorbance data. These diagrams are the collective name given to the absorbance (A), absorbance difference (AD) and absorbance difference quotient (ADQ) diagrams. These are typically two-

dimensional diagrams, with the so-called Mauser space being multidimensional ($n \geq 2$) [14], which allows for the determination of the number (s) of linearly independent reaction steps of a chemical reaction. By definition, a linear reaction system consists of first-order reaction steps; while linearly independent reactions are those reactions that are independent of the reaction order. Each reaction mechanism consists of a distinct number (s) of linearly independent reaction steps that can be determined through Mauser diagrams. Recently it has been established that, in addition to obtaining the number of linearly independent reaction steps, the geometric analysis of the "Mauser space" (or absorbance space) could provide new routes for the kinetic evaluation of chemical reactions.

The absorbance (or absorbance differences) of n wavelengths establishes the axes of the absorbance space. A straight line in this space is obtained when the reaction system consists of a single linearly independent reaction step ($s = 1$). A reaction system being described by two linearly independent steps ($s = 2$) would lead to a bent curve in the Mauser space, which lies on a single plane. Since the curve lies on a single plane, a two-dimensional coordinate system can be introduced which lies in this plane. The coordinates of the Mauser curve with regard to the established two-dimensional coordinate system can thus be evaluated [14-19].

The reaction systems described by three linearly independent reaction steps ($s = 3$) also lead to a bent curve in the Mauser space. However, these systems differ from reaction systems with two linearly independent reaction steps in that the absorbance curve obtained does not lie on a single plane, and thus a two-dimensional coordinate system cannot be introduced. These reaction systems are evaluated on the basis of three-dimensional absorbance diagrams (*i.e.* A_i versus A_j versus A_k, where the subscripts refer to the respective wavelengths), using the concept of parallel projection [18], during which the three-dimensional absorbance diagram is geometrically projected onto a two-dimensional coordinate system. In this manner, the eigenvalues describing the reaction mechanism can be determined. Furthermore, the reaction system $s = 3$ is reduced to a system which is described by only two linearly independent concentration variables [18].

The principles for the evaluation of the n-dimensional Mauser space is generally applicable to reactions where $s = 1$, $s = 2$ and $s = 3$ for linear and non-linear reaction systems.

The following equations illustrate examples of the reaction systems which could be evaluated through geometric analysis of the absorbance space [15-18]:

for $s = 1$

$$A \rightleftharpoons B$$

$$A \longrightarrow B \quad ; \quad A \longrightarrow C$$

$$A + B \longrightarrow C$$

for $s = 2$

$$A \rightleftharpoons B \rightleftharpoons C$$

$$A \longrightarrow B \; ; \; C \rightleftharpoons D$$

$$A + B \rightleftharpoons C + D \; ; \; E \longrightarrow F + D$$

$$A \rightleftharpoons B \; ; \; B + C \rightleftharpoons D$$

for $s = 3$

$$A \longrightarrow B \longrightarrow C \longrightarrow D$$

$$A \rightleftharpoons B \rightleftharpoons C \rightleftharpoons D$$

$$A \longrightarrow B; \; C \longrightarrow D; \; E \longrightarrow F$$

$$A \rightleftharpoons B; \; C \rightleftharpoons D; \; E \rightleftharpoons F$$

$$A \longrightarrow B + C; \; D \rightleftharpoons E; \; F \longrightarrow G$$

$$A \rightleftharpoons B; \; C \longrightarrow D \begin{cases} \longrightarrow E \\ \longrightarrow F \end{cases}$$

Mauser diagrams provide particularly attractive routes for the elucidation of reaction models, and consequently reduce the number of unknown parameters associated with the reaction. This is because knowledge of the molar extinction coefficients of the absorbing species is not a prerequisite for the application of the theory. The only requirement for this type of evaluation is that a sufficient number of species absorb in the region of interest, *i.e.* that the single reactions of the system are individually registered spectrophotometrically. It should be noted that reaction models defined by a specific number of linearly independent steps cannot be distinguished from one another by purely spectroscopic means; *e.g.* for the system s = 3 the reaction model A → B → C → D cannot be distinguished from the reaction model A → B; C → D; E → F.

To elaborate on the evaluation of Mauser diagrams, consider the following general consecutive reactions that are described by two linearly independent reaction steps:

$$A \underset{k_{-1}}{\overset{k_1}{\rightleftharpoons}} B \underset{k_{-2}}{\overset{k_2}{\rightleftharpoons}} C \qquad \text{Model A1}$$

From Model A1 it could be assumed that, at any given time, only two absorbing species are present in appreciable concentrations. Figure 2.5 depicts a general Mauser diagram for a

reaction system consisting of two linearly independent steps, such as the reaction represented by Model A1. The bent curve illustrated in Figure 2.5, consists of two linear regions, denoted by regressions [1] and [2]. By taking the aforementioned assumption (i.e. that only two absorbing species are present in appreciable concentrations at any given time) into consideration, two important conclusions can be derived from Figure 2.5 [20], namely:

- the linear region denoted by the regression line denoted [1] represents the reaction A ↔ B
- the linear region denoted by the regression line denoted [2] represents the reaction B ↔ C

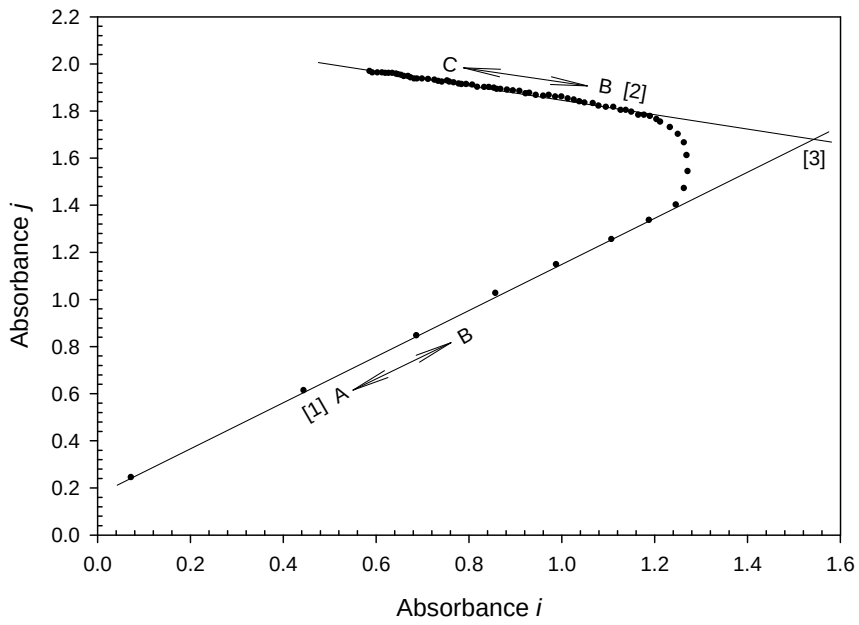

Figure 2.5: Typical 2-dimensional Mauser diagram for the general reaction A ↔ B ↔ C

Extrapolation of the regression lines [1] and [2] results in a point where the two regression lines intersect, which is denoted as [3] in Figure 2.5. Effectively, this point represents the absorbance of purely species B, at the respective wavelengths, *i* and *j*. At this point the species in solution exists solely as species B, which implies that the concentration of species B at this point would equal the concentration of species A at the start of the reaction [20]. Since the concentration of species A at the start of the reaction is usually known, the molar extinction coefficient of species B can be calculated (at various wavelengths) using the Beer-Lambert law.

2.2 Experimental

2.2.1 Reagents and preparation of Rh^{III} aqua chlorido-complexes

A 0.1021 M Rh^{III} stock solution was prepared by dissolving 0.2825 g of $RhCl_3 \cdot nH_2O$ (Alfa Aesar, Rh 38.5-45.5%) in 10 mL 32% ($^{v}/_{v}$) hydrochloric acid (Merck chemicals). After dissolution, the solution was heated at 60°C for five days. This stock solution was subsequently kept at 25°C for three days prior to its use. A 7.012 M stock perchloric acid (Saarchem – 72% $^{v}/_{v}$) solution was prepared in MilliQ water. This solution was used to keep the total ionic strength constant for each kinetic experiment.

2.2.2 pH Measurements

The pH of solutions was measured with a Metrohm 780 pH meter using a Metrohm 6.0232.100 combined pH glass electrode. The electrode was calibrated with pH 4.00 (Metrohm 6.2307.100) and pH 7.00 (Metrohm 6.2307.110) buffer solutions.

2.2.3 Standardization of acids

Acid solutions were standardized with freshly prepared borax solutions (borax was used as a primary standard). The precise concentration of the acid and base solutions was in the order of 1.0×10^{-3} M. Titrations were performed in triplicate until concordant results were attained.

2.2.4 ICP-OES quantification of metal and chloride concentrations

The total rhodium and chloride concentrations were determined by means of ICP-OES (SPECTRO *Arcos*), equipped with a Schott spray chamber and a cross-flow nebulizer. The optimal ICP-OES spectrometer settings used were: RF power = 1400 W, Argon coolant flow = 13.0 $L.min^{-1}$, auxiliary flow = 1.0 $L.min^{-1}$, nebulizer flow = 0.80 $L.min^{-1}$.

A rhodium elemental standard (De Bruyn Spectroscopy - 1000 ± 3ppm, 99.99% purity) was used for rhodium determination while dried NaCl (Sigma Aldrich; 99.5% UltraPure) was used for total chloride determination. The 343.489 nm and 134.724 nm emission lines were used for the detection of Rh and Cl, respectively. Although unconventional, ICP-OES was used for quantification of the total chloride concentration. To

date, there have been few reports in literature documenting the use of ICP-OES in the quantification of halogens [21,22]. This is probably due to the relatively low emissivity of the halogen atoms. In addition, the halogen atoms/ions emit well below 160 nm [21], with most modern ICP-OES spectrometers not being able to detect elements in these low ultraviolet ranges. Nonetheless, it has been shown that Cl, Br and I can satisfactorily be quantified in waste oils [21], and more recently in acidic halide-rich aqueous solutions containing PGM [23].

2.2.5 UV-vis Spectrophotometric recording

UV- Vis spectra were recorded using a Perkin-Elmer Lambda 12, double beam UV-vis spectrophotometer, interfaced with the UV WinLab (Version 1.22) software package. The spectra were recorded using the following settings:

- cycle time (where applicable): 55 seconds
- scan rate: 240 nm/min
- slit width: 1 nm

A Grant KD100 circulating thermostat controller, mounted onto a Grant W6 water bath equipped with a cooling coil, was used to maintain the desired temperature of the spectrophotometer sample chamber (± 0.1°C). A pump, attached to the thermostatic water bath, was used to circulate water through the rubber tubing, as illustrated in Figure 2.1. The tubing extends through the cuvette-containing chamber of the spectrophotometer, and is attached to a thermostatic vessel containing the sample solutions. This ensures that the contents of the reaction vessel and the cuvettes are maintained at the same temperature.

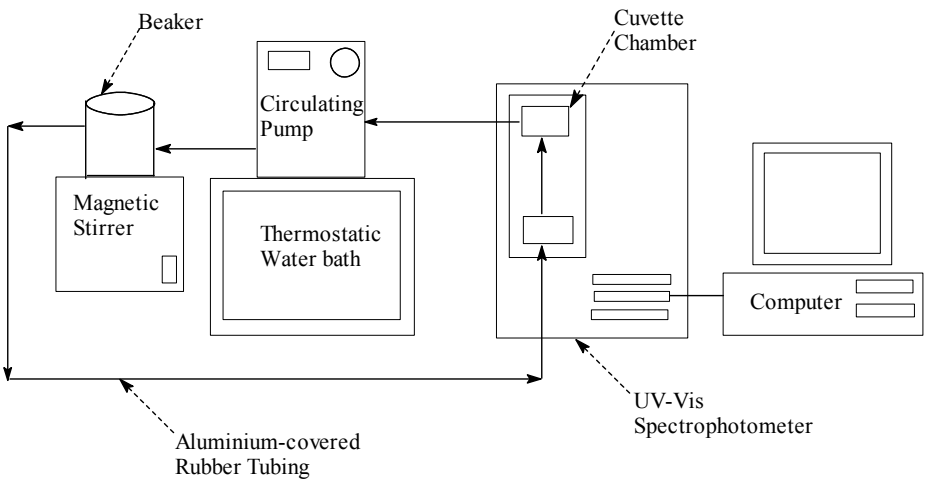

Figure 2.6: The experimental setup used to record UV-vis spectra at constant temperatures

For the spectrophotometric measurements, the 0.1021 M Rh^{III} stock solution prepared in 10.181 M HCl was diluted 100 times, such that the final HCl concentration was 0.1018 M. To each of these solutions, the appropriate amount of a 7.012 M $HClO_4$ stock solution was added, such that the molarity of the $HClO_4$ varied from 0.3011 M to 5.993 M. The kinetic measurements for the ionic strengths investigated were repeated at the following temperatures: 10, 15, 20, 25 and 30ºC (± 0.1ºC). These experiments were designed to investigate the effects of ionic strength and temperature on the aquation rate of $[RhCl_n(H_2O)_{6-n}]^{3-n}$ (n=5,6) complex anions.

Approximately 40 s was required from the dilution of the Rh^{III} stock solution until the first spectrum was recorded. Moreover, the pH of each solution was always < 1.00 in order to prevent possible hydrolysis reactions.

2.3 Results and Discussion

2.3.1 The aquation of $[RhCl_n(H_2O)_{6-n}]^{3-n}$ (n=5,6) complex anions in a 0.1018 M HCl matrix

Figure 2.7 illustrates the typical change in the Rh^{III} UV-vis spectrum as a function of time upon dilution of a 0.1012 M Rh^{III} solution, equilibrated in a 10.181 M HCl matrix, to a 0.1018 M HCl matrix. Figure 2.7a illustrates the UV-vis spectral changes over the first 90 minutes, while Figure 2.7b illustrates the spectral changes over a period of 3 days. It is evident that the aquation reactions progress with the formation of several isosbestic points, indicated by the vertical solid and dashed lines. The first set of isosbestic points occur within 6 minutes after dilution of the Rh^{III} stock solution, Figure 2.7a (solid vertical lines), which is followed by the formation of a second set of isosbestic points (dashed vertical lines). These sets of isosbestic points indicate that only two Rh^{III} species exist in predominant concentration at any given time during the consecutive aquation reactions denoted by equations (2.1) and (2.2). The wavelengths at which these isosbestic points occur are given in Table 2.2.

$$[RhCl_6]^{3-} + H_2O \underset{k_{56}}{\overset{k_{65}}{\rightleftharpoons}} [RhCl_5(H_2O)]^{2-} + Cl^- \qquad (2.1)$$

$$[RhCl_5(H_2O)]^{2-} + H_2O \underset{k_{45}}{\overset{k_{54}}{\rightleftharpoons}} \textit{cis}\text{-}[RhCl_4(H_2O)_2]^- + Cl^- \qquad (2.2)$$

$$\textit{cis}\text{-}[RhCl_4(H_2O)_2]^- + H_2O \underset{k_{34}}{\overset{k_{43}}{\rightleftharpoons}} \textit{fac}\text{-}[RhCl_3(H_2O)_3] + Cl^- \qquad (2.3)$$

Table 2.2: Wavelengths at which the isosbestic points of the respective aquation reactions occur

Time interval	Wavelength / nm	Associated aquation reaction
10 min	422, 451, 513	$[RhCl_6]^{3-} + H_2O \rightleftharpoons [RhCl_5(H_2O)]^{2-} + Cl^-$
90 min	399, 448. 496	$[RhCl_5(H_2O)]^{2-} + H_2O \rightleftharpoons$ *cis*-$[RhCl_4(H_2O)_2]^- + Cl^-$
4329 min (3 days)	431, 473	*cis*-$[RhCl_4(H_2O)_2]^- + H_2O \rightleftharpoons$ *fac*-$[RhCl_3(H_2O)_3] + Cl^-$

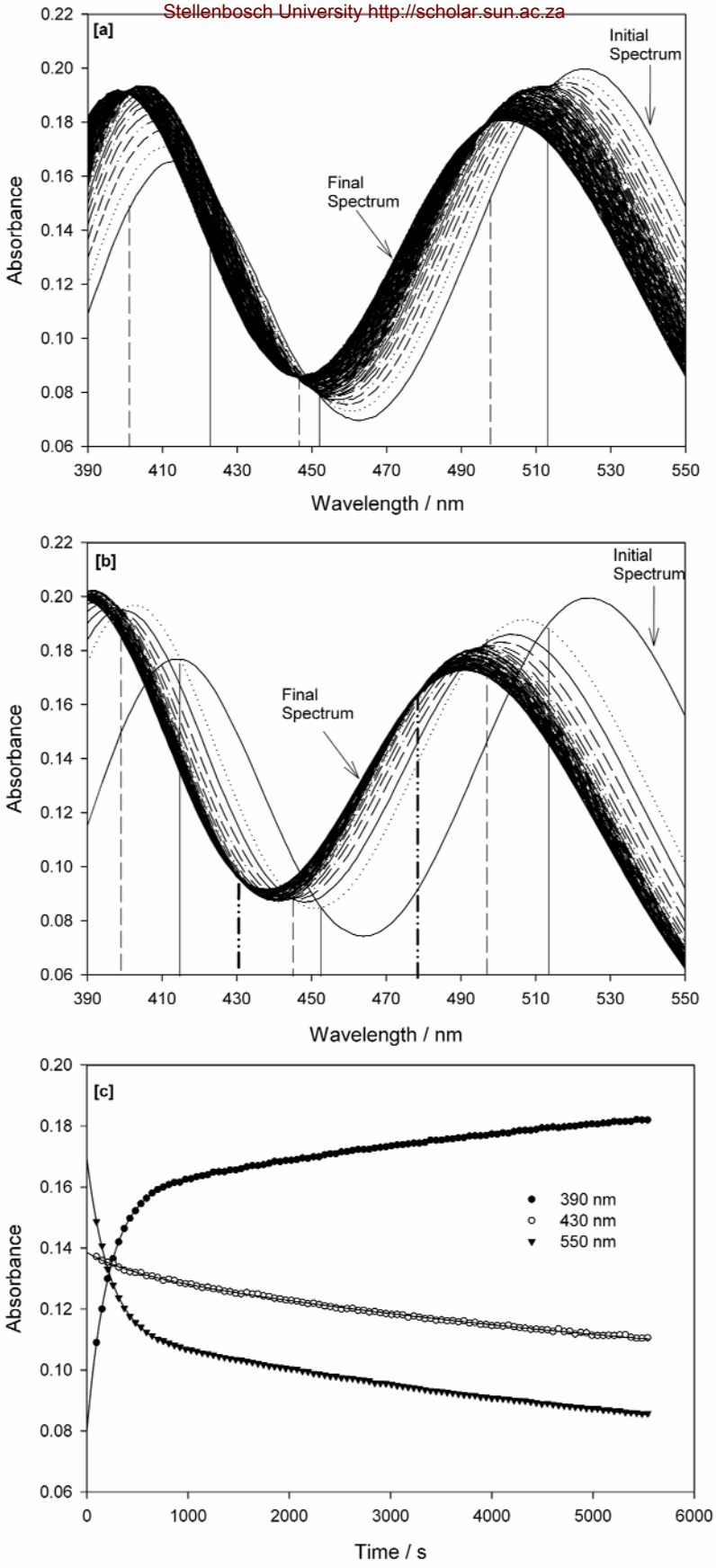

Figure 2.7: Change in the UV-vis spectrum as a function of time upon dilution of a 0.1021 M Rh^{III} stock solution equilibrated in 10.18 M HCl 100 times, to a 0.1018 M HCl matrix. (a) the spectral change over 90 min (b) the spectral change over 3 days (c) a typical kinetic trace at several wavelengths obtained from (a), the symbols are the experimental data and the lines are the least-squares fit of reaction models (2.4)-(2.6). The final [Rh] = 1.021 mM

It is observed that after 90 minutes following the dilution of the Rh^{III} stock solution, the rate at which the UV-vis spectrum changes decreases dramatically, Figure 2.7a. This phenomenon is associated with the relatively slower rate of aquation of the *cis*-$[RhCl_4(H_2O)_2]^-$ complex anion. This necessitates that the UV-vis spectrum of the diluted sample should be recorded over a period of at least four days, in order to observe the formation of the third set of isosbestic points at 431 and 473 nm, Figure 2b and Table 2.2. The formation of a third set of isosbestic points is indicative of the fact that aquation of the *cis*-$[RhCl_4(H_2O)_2]^-$ complex anion leads to the formation of the *fac*-$[RhCl_3(H_2O)_3]$ stereoisomer (equation 2.3), as expected from the dominant *trans*-labilizing effect induced by chloride ligands. The rate laws of equations (2.1) – (2.3) are given by:

$$\frac{d[A]}{dt} = -k_{65}[A] + k_{56}[B][Cl^-] \qquad (2.4)$$

$$\frac{d[B]}{dt} = k_{65}[A] - k_{56}[B][Cl^-] - k_{54}[B] + k_{45}[C][Cl^-] \qquad (2.5)$$

$$\frac{d[C]}{dt} = k_{54}[B] - k_{45}[C][Cl^-] \qquad (2.6)$$

where: $A = [RhCl_6]^{3-}$; $B = [RhCl_5(H_2O)]^{2-}$; $C = cis\text{-}[RhCl_4(H_2O)_2]^-$

The rate laws denoted by equations (2.4) – (2.6) were simulated using custom-developed software ($Kinetic_5Ver$[1]) and the non-linear least-squares regression fits was performed at several wavelengths, Figure 2.7c. Due to the slow rate of aquation of the cis-$[RhCl_4(H_2O)_2]^-$ complex anion compared to the $[RhCl_5(H_2O)]^{2-}$ complex anion, the stereo-specific aquation of the *cis*-$[RhCl_4(H_2O)_2]^-$ species to yield the *fac*-$[RhCl_3(H_2O)_3]$ stereoisomer was not taken into consideration in the reaction model fitted. There is excellent agreement between the experimental and simulated data, Figure 2.7c, which confirms the proposed rate laws. The calculated rate constants, an average of at least three repeated experiments, are listed in Table 2.3.

[1] This program was developed by Dr. W. J. Gerber using the Visual Basic 6 software package. Further information regarding the program can be supplied upon request.

Table 2.3: Calculated Rh^{III} aqua chlorido-complexes' pseudo first-order aquation/anation rate constant. The rate constants documented in literature [1,2,24] is included for comparison.

Experimental technique	Aquation / anation rate constants	
	k_{65} / s^{-1}	k_{54} / $M^{-1}.s^{-1}$
UV-vis	$8.79 (\pm 0.38) \times 10^{-3}$	$2.41 (\pm 0.12) \times 10^{-4}$
HPLC-ICP-MS [24]	-[a]	$2.46 (\pm 0.10) \times 10^{-4}$
UV-vis [1,2]	$1.83 (\pm 0.38) \times 10^{-3}$[b]	$3.72 (\pm 0.38) \times 10^{-5}$[b]

The corresponding chloride anation reactions are considered to be negligibly small at an ionic strength of 0.1018 M HCl

[a] The HPLC-ICP-MS study cannot separate $[RhCl_6]^{3-}$ and $[RhCl_5(H_2O)]^{2-}$ complex anions since these species elute as a single peak

[b] These rate constants were determined at an ionic strength of 4.0 M, a possible reason for the observed discrepancy

The non-linear least-squares fits of the kinetic data discussed thus far not only allows for the determination of the pertinent aquation/anation rate constants, but the $Kinetic_5Ver$ software also allows for the calculation of the molar extinction coefficients of the $[RhCl_n(H_2O)_{6-n}]^{3-n}$ (n=4-6) complexes. In order to supplement the kinetic analyses, the molar extinction coefficients of the $[RhCl_5(H_2O)]^{2-}$, *cis*-$[RhCl_4(H_2O)_2]^-$ and *fac*-$[RhCl_3(H_2O)_2]$ species were independently verified using the principle of Mauser diagrams [14-19]. The program Mauser1Ver[2] [25] was developed specifically for the geometrical analysis of the Mauser diagrams since calculation of all the molar extinction coefficients in the 390-550 nm region would require, quite literally, 25600 absorbance (λ_y) versus absorbance (λ_x) plots, which originate from plotting all the wavelengths against each other. A typical Mauser diagram obtained with the program $Mauser_1Ver$ is shown in Figure 2.8 and the analysis of these diagrams were performed as outlined in section 2.1.3. The molar extinction coefficient spectra of the $[RhCl_n(H_2O)_{6-n}]^{3-n}$ (n=3-5) species are illustrated in Figure 2.9. The agreement between the molar extinction coefficients calculated for the Rh^{III} species with the two different computational methods is excellent and validate the results of the kinetic analyses. Furthermore, the calculated molar extinction coefficient spectra of the $[RhCl_n(H_2O)_{6-n}]^{3-n}$ (n=3-5) species overlap at all the experimentally obtained isosbestic points which is indicative of the internal consistency of the aquation / anation reaction models fitted, Figure 2.9. Regrettably, the molar extinction coefficient spectrum of the $[RhCl_6]^{3-}$ complex anion could not be determined from Mauser diagrams. In this instance it was assumed, as documented in the reviewed literature [5,8], that the $[RhCl_6]^{3-}$ species is the only predominant species present in concentrated (> 9.0 M) HCl. It is interesting to note that although the

[2] This program was developed by T. E. Geswindt using the Visual Basic.Net software package. Further information regarding this program can be supplied upon request.

literature reported [5,8] molar extinction coefficient spectra of the $[RhCl_n(H_2O)_{6-n}]^{3-n}$ (n=3-6) species differ substantially, the molar extinction coefficient spectra calculated in this study is consistent with that reported by Harris *et al* [5].

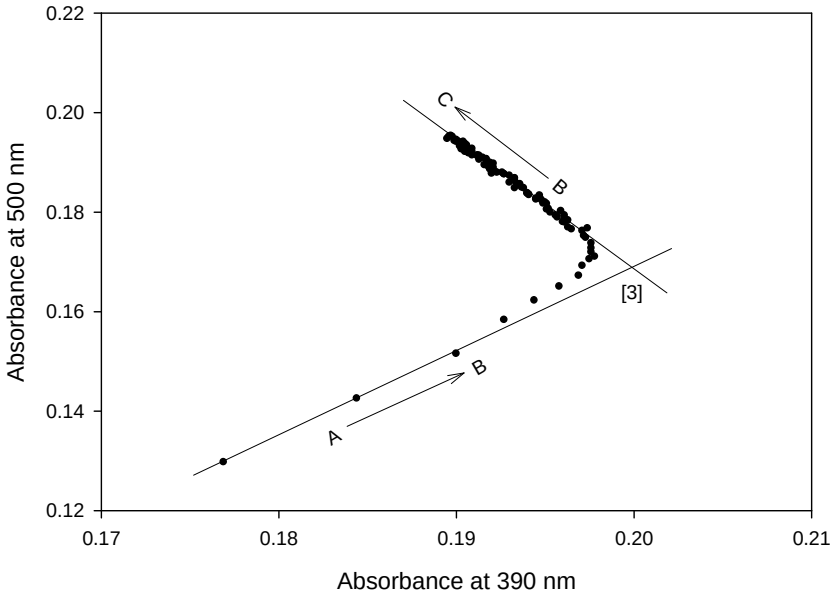

Figure 2.8: A typical example of a Mauser plot obtained in this study for the determination of molar extinction coefficients for the $[RhCl_5(H_2O)]^{2-}$, *cis*-$[RhCl_4(H_2O)_2]^-$ and *fac*-$[RhCl_3(H_2O)_3]$ species

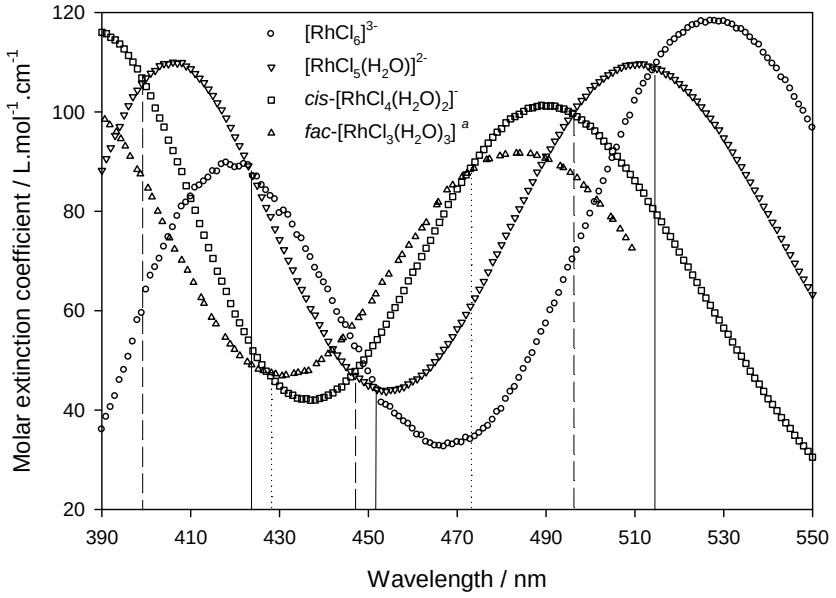

Figure 2.9: Molar extinction coefficient spectra of the $[RhCl_n(H_2O)_{6-n}]^{3-n}$ (n=3-6) aqua chlorido-complexes calculated with the program Mauser1Ver. [a] Reproduced with permission from Gerber *et al* [24]

2.3.2 Effect of ionic strength on the aquation kinetics of $[RhCl_n(H_2O)_{6-n}]^{3-n}$ (n=5,6) complex anions

In the previous section, the pseudo first-order aquation rate constants calculated were found to be considerably larger than that reported in literature [1-6]. This is presumably due to the difference in ionic strength between the experiments highlighted in the previous section and those reported in literature. As such, the effect of ionic strength on the aquation kinetics of $[RhCl_n(H_2O)_{6-n}]^{3-n}$ (n=5,6) complexes was investigated at a constant chloride concentration (0.1018 M), while $HClO_4$ was used to adjust the total ionic strength. The ionic strength is generally known to have a profound influence on the activity (*or* the effective concentration) of reacting species in solution. An example of this effect is illustrated in Figure 2.10, which exemplifies how the activity of water changes as a function of the $HClO_4$ molality. This figure shows that as the $HClO_4$ molality is increased, there is a corresponding decrease in the activity of water. It therefore makes sense that a decrease in the activity of water with increasing $HClO_4$ concentration would lead to a decrease in the rate at which aquation of Rh^{III} aqua chlorido-complexes occur.

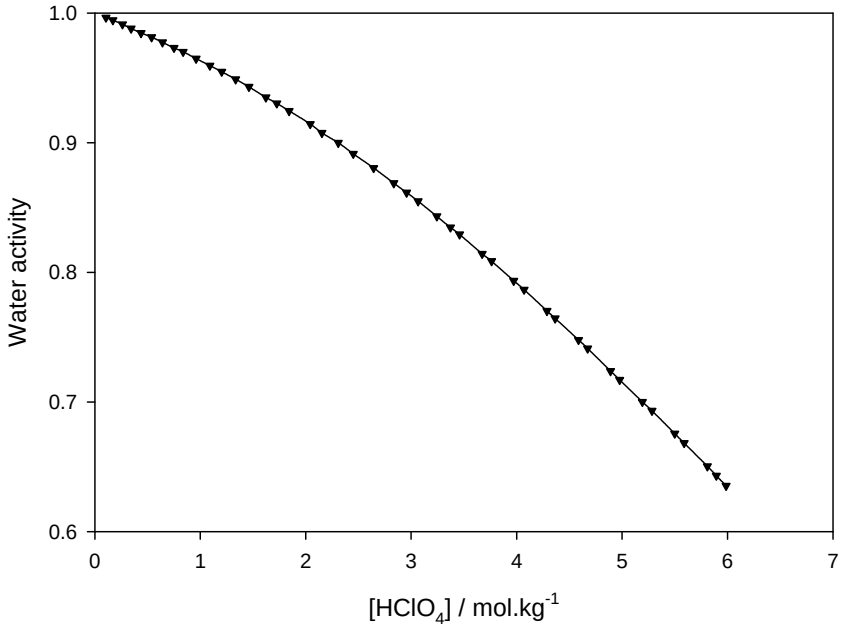

Figure 2.10: The activity of water as a function of $HClO_4$ molality. Water activities were determined by Wai and Yates [26] using a modified isopiestic method.

Figure A2.1 [a] – [f] illustrates the experimental results acquired when the concentration of $HClO_4$ was increased from 0.301 M to 5.012 M. These figures demonstrate

that an increase in the $HClO_4$ concentration leads to a decrease in the rate of change of the UV-vis spectra. This implies that the rate of aquation of Rh^{III} aqua chlorido-complexes has decreased, since the effective concentration of water is lowered. The formation of two sets of isosbestic points is evident from Figure A2.1 [a] – [c]. However, at ionic strengths > 3.0 M, the formation of the second set of isosbestic points becomes progressively less apparent, Figure A2.1 [d] – [f]. The absence of the second set of isosbestic points may either imply that (i) more than two Rh^{III} species are present in significant concentrations, or (ii) the $[RhCl_5(H_2O)]^{2-}$ complex anion has not undergone aquation, to any significant extent. Non-linear least-squares simulations (*vide infra*) was used to resolve this problem.

Although the $HClO_4$ concentration was varied from 0.301 M to 5.012 M, the chloride concentration was 0.1018 M, and therefore the aquation model previously proposed by equations (2.1) – (2.3) can be used to simulate the experimental results. Due to the low chloride concentration, the chloride anation reactions are considered to occur to a negligible extent.

$$[RhCl_6]^{3-} + H_2O \underset{k_{56}}{\overset{k_{65}}{\rightleftharpoons}} [RhCl_5(H_2O)]^{2-} + Cl^- \qquad (2.1)$$

$$[RhCl_5(H_2O)]^{2-} + H_2O \underset{k_{45}}{\overset{k_{54}}{\rightleftharpoons}} \textit{cis}\text{-}[RhCl_4(H_2O)_2]^- + Cl^- \qquad (2.2)$$

$$\textit{cis}\text{-}[RhCl_4(H_2O)_2]^- + H_2O \underset{k_{34}}{\overset{k_{43}}{\rightleftharpoons}} \textit{fac}\text{-}[RhCl_3(H_2O)_3] + Cl^- \qquad (2.3)$$

The experimental kinetic traces, Figure 2.11, demonstrate that increasing ionic strength leads to a decrease in the rate at which aquation occurs. Furthermore, the simulated pseudo first-order aquation model resulted in exceptional fits to the experimental data, Figure 2.11, thus validating the proposed model. The calculated rate constants, k_{65} and k_{54}, as a function of the ionic strengths investigated are shown in Table 2.4; highlighting the profound effect of ionic strength on the aquation of Rh^{III} aqua chlorido-complexes. Additionally, the calculated rate constants are consistent with that reported in literature [1, 2], Table 2.4. In a similar manner as the previous kinetic analyses, the molar extinction coefficient spectra were determined by two independent methods, *i.e.* via kinetic simulation of the applicable rate laws and the geometrical analysis of Mauser diagrams. These values are consistent with that highlighted in section 2.3.1 thus validating the kinetic analyses.

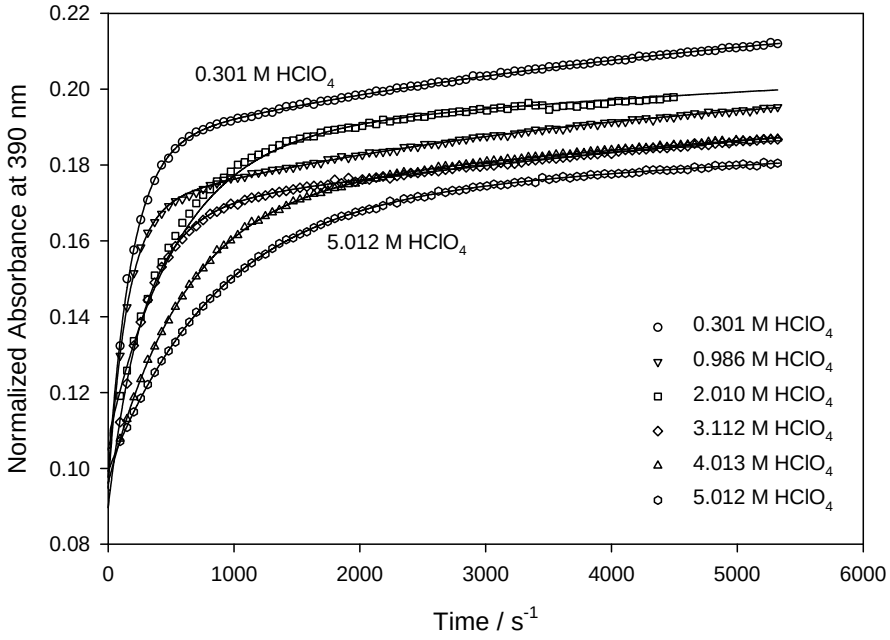

Figure 2.11: Kinetic traces illustrating the change in absorbance as a function of time upon dilution of a 0.1021 M Rh^{III} solution equilibrated in 10.18 M HCl to a final HCl concentration of 0.1018 M and specified $HClO_4$ concentration. The symbols indicate the experimental data while the lines illustrate the exceptional non-linear least-squares fits of the aquation model denoted by (2.1) – (2.3). $[Rh]_{final}$ = 1.021 mM

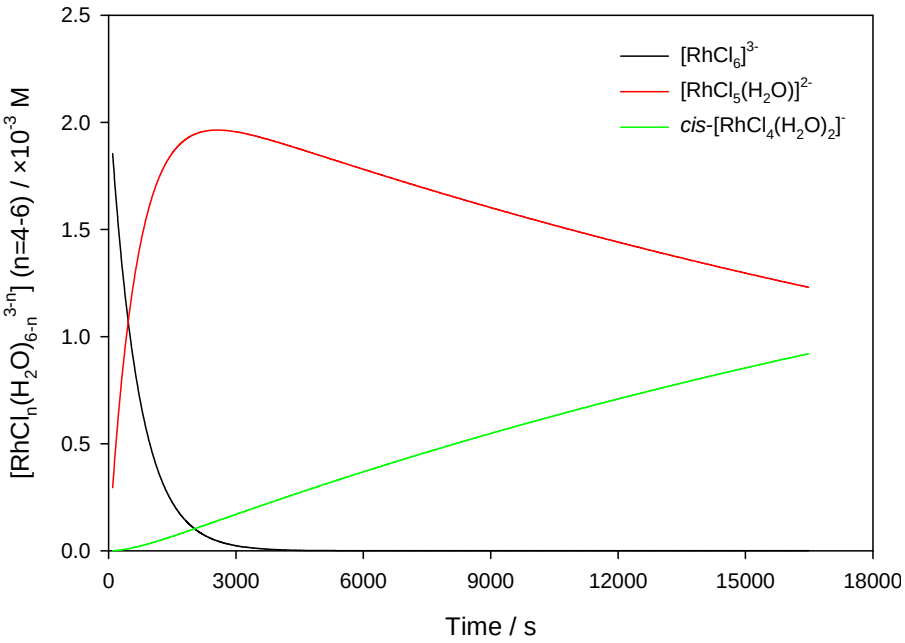

Figure 2.12: An example of the calculated species concentration profile as a function of time obtained from the non-linear least-squares model fits.

Table 2.4: Comparison of the aquation rate constants of $[RhCl_n(H_2O)_{6-n}]^{3-n}$ (n=5,6) complex anions as a function of ionic strength at 298.1 K calculated during this study and that documented in literature[24]

Ionic strength / M	Aquation rate constants			
	This study		Literature [24]	
	k_{65} / $\times 10^{-3}$ s^{-1}	k_{56} / $\times 10^{-4}$ s^{-1}	k_{65} / $\times 10^{-3}$ s^{-1}	k_{56} / $\times 10^{-4}$ s^{-1}
0.301	6.60 ± 0.11	2.56 ± 0.08	-	-
0.986	5.36 ± 0.14	1.96 ± 0.04	5.25 ± 0.28	2.10 ± 0.07
2.011	3.57 ± 0.21	1.01 ± 0.04	3.38 ± 0.22	1.13 ± 0.06
3.112	2.49 ± 0.10	0.56 ± 0.01	2.02 ± 0.13	0.40 ± 0.03
4.013	1.63 ± 0.03	0.38 ± 0.006	1.03 ± 0.05	0.27 ± 0.008
5.012	1.07 ± 0.01	0.36 ± 0.002	-	-
5.993	0.79 ± 0.02	-	0.77 ± 0.04	-

In conclusion, the aquation rate constants for the $[RhCl_n(H_2O)_{6-n}]^{3-n}$ (n=5,6) complex anions have been calculated as a function of ionic strength. It was observed that the ionic strength has a profound effect on the rate at which these species undergo aquation. Furthermore, the calculated molar extinction coefficient spectra are consistent with that depicted in Figure 2.9. The lack of significant UV-vis spectral changes for the subsequent aquation reactions (i.e. for the formation of higher aquated Rh^{III} species) combined with the large period of time required for these aquation reactions to take place, render UV-vis spectrophotometry unsuitable to study the kinetics of the neutral and cationic Rh^{III} aqua chlorido-complexes.

2.3.3 The effect of temperature on the aquation kinetics of $[RhCl_n(H_2O)_{6-n}]^{3-n}$ (n=5,6) complex anions

The kinetics of the aquation and chloride anation reactions of Rh^{III} aqua chlorido-complexes have been a subject of a number of studies [1-6, 24]. To date, however, very few studies investigated the effect of temperature on the aquation reactions of Rh^{III} aqua chlorido-complexes, with Harris *et al* [2] only investigating the effects of temperature on the chloride anation kinetics of the chloropentaaquarhodium(III) cation in aqueous solution. Therefore, it was of significant interest to investigate the effects of temperature on the kinetics of the aquation of the $[RhCl_n(H_2O)_{6-n}]^{3-n}$ (n=5,6) complex anions.

Temperature is known to influence the rates at which chemical reactions occur, by either enhancing or impeding the reactions. Generally, an increase in temperature would lead

to a corresponding increase in the rate of the reaction. This is attributed to the fact that increasing temperature leads to an increase in the kinetic energy of reacting molecules, which provides the colliding molecules sufficient energy to overcome the energy barrier of a reaction. A decrease in temperature generally has an opposing effect.

Figures A2.2 [a] – [e] illustrates the experimental UV-vis spectral profiles obtained upon decreasing the reaction temperature from 303.1 K to 283.1 K. All the spectra depicted in Figure A2.2 were obtained at a constant ionic strength of 0.301 M. The formation of two sets of isosbestic points at high temperatures is evident in Figures A2.2 [a] – [c]. However, at temperatures < 20.0°C (293.1 K) the formation of the second set of isosbestic points becomes less apparent, Figure A2.2 [d] - [e]. The absence of the second set of isosbestic points implies that aquation of the $[RhCl_5(H_2O)]^{2-}$ complex anion has not taken place to a considerable extent. It is thus evident that a decrease in temperature leads to a decrease in the rate of aquation of $[RhCl_n(H_2O)_{6-n}]^{3-n}$ (n=5,6) complex anions.

As in the previous sections, the aquation rate constants of the reactions denoted by equations (2.1) – (2.3) were calculated using the program $Kinetic_5Ver$. The non-linear least-squares fits of the simulated pseudo first-order rate laws, equations (2.4) – (2.6), are shown in Figure 2.13 [a] and [b]. The aquation model least-squares fits (solid lines) are excellent, and the calculated aquation rate constants at each of the temperatures (and ionic strengths) are illustrated in Figures 2.14 - 2.15. A summary of the effects of ionic strength and temperature on the aquation rate constants, k_{65} and k_{54}, are provided in Table 2.5.

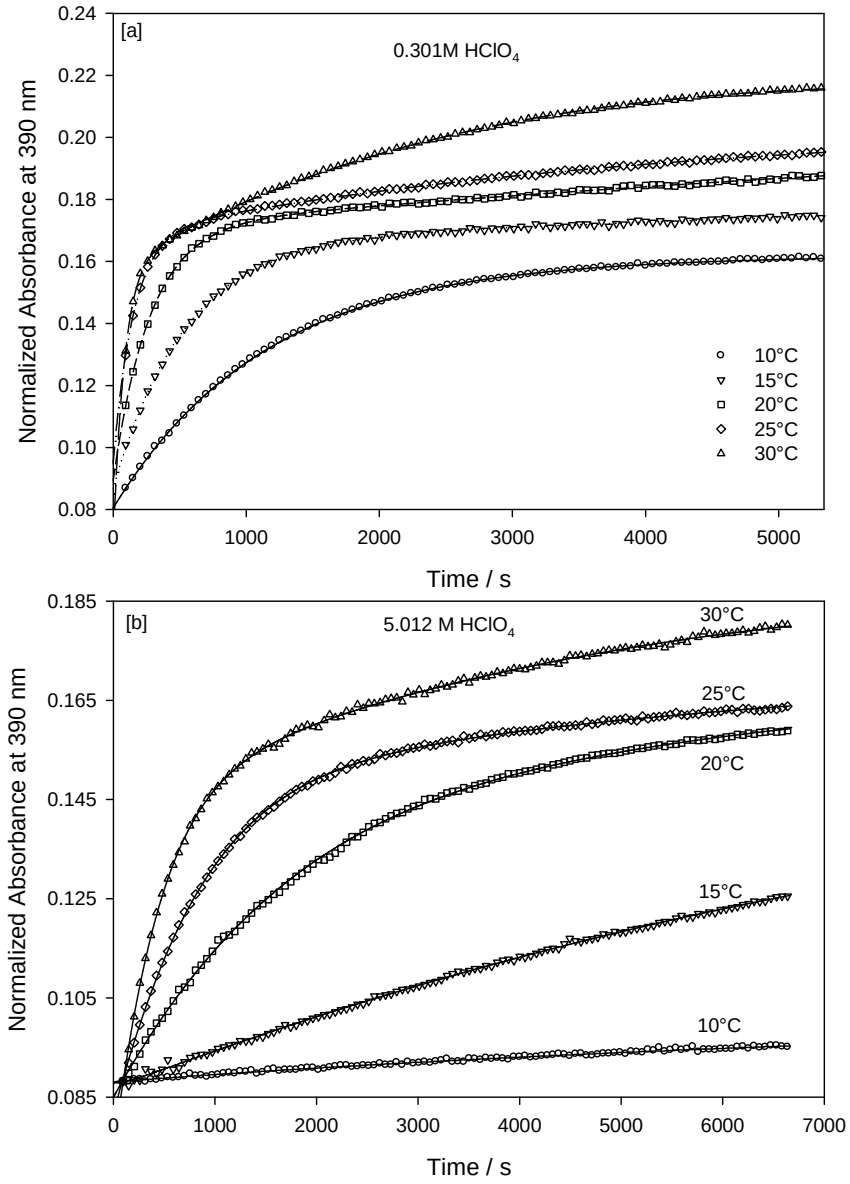

Figure 2.13: Kinetic traces illustrating the change in absorbance upon dilution of a 0.1021 M Rh^{III} solution equilibrated in 10.18 M HCl to a final HCl concentration of 0.1018 M. Reactions were conducted at several temperatures as denoted in the figures. [a] Reactions conducted at an ionic strength of 0.3011 M $HClO_4$; [b] Reactions conducted at an ionic strength of 5.012 M $HClO_4$. The symbols indicate the experimental data while the lines illustrate the exceptional non-linear least squares fits of the aquation model denoted by (2.1) – (2.3) $[Rh]_{final}$ = 1.021 mM

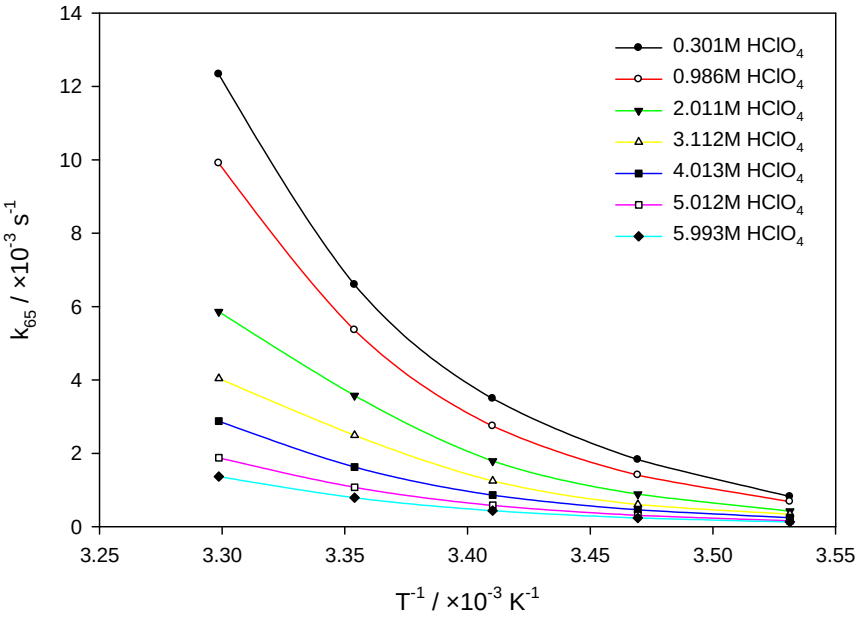

Figure 2.14: The calculated rate constants (k_{65}) for the aquation of $[RhCl_6]^{3-}$ as a function of temperature and ionic strength

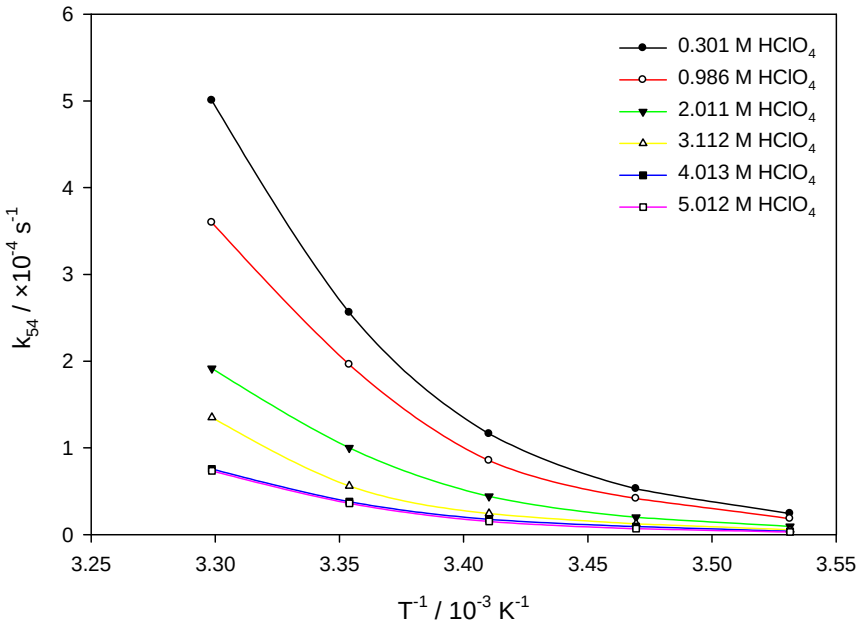

Figure 2.15: The calculated rate constants (k_{54}) for the aquation of $[RhCl_5(H_2O)]^{2-}$ as a function of temperature and ionic strength

Table 2.5: Summary of the calculated Rh^{III} aquation rate constants, k_{65} and k_{54}, as a function of ionic strength and temperature

Ionic Strength / M	Aquation rate constant k_{65} / $\times 10^{-3}$ s^{-1}				
	283.1 K	288.1 K	293.1 K	298.1 K	303.1 K
0.301	0.81 ± 0.09	1.83 ± 0.13	3.49 ± 0.09	6.60 ± 0.11	12.33 ± 0.16
0.986	0.68 ± 0.06	1.40 ± 0.04	2.74 ± 0.08	5.36 ± 0.14	9.91 ± 0.11
2.010	0.43 ± 0.04	0.89 ± 0.02	1.79 ± 0.08	3.57 ± 0.21	5.86 ± 0.13
3.112	0.34 ± 0.03	0.60 ± 0.02	1.25 ± 0.04	2.49 ± 0.10	4.04 ± 0.11
4.013	0.25 ± 0.01	0.46 ± 0.03	0.86 ± 0.03	1.63 ± 0.03	2.88 ± 0.06
5.012	0.16 ± 0.01	0.31 ± 0.01	0.58 ± 0.03	1.07 ± 0.01	1.88 ± 0.04
5.993	0.13 ± 0.01	0.24 ± 0.01	0.44 ± 0.02	0.79 ± 0.02	1.37 ± 0.01

Ionic Strength / M	Aquation rate constant k_{54} / $\times 10^{-5}$ s^{-1}				
	283.1 K	288.1 K	293.1 K	298.1 K	303.1 K
0.301	2.42 ± 0.02	5.27 ± 0.61	11.62 ± 0.54	25.62 ± 0.81	50.05 ± 1.02
0.986	1.83 ± 0.01	4.15 ± 0.16	8.52 ± 0.61	19.63 ± 0.43	35.98 ± 1.10
2.010	0.94 ± 0.01	2.01 ± 0.06	4.41 ± 0.40	10.01 ± 0.44	16.16 ± 0.61
3.112	0.54 ± 0.01	1.24 ± 0.04	2.42 ± 0.13	5.62 ± 0.11	13.50 ± 0.57
4.013	0.37 ± 0.01	0.92 ± 0.03	1.76 ± 0.09	3.80 ± 0.06	7.56 ± 0.10
5.012	0.29 ± 0.01	0.68 ± 0.01	1.51 ± 0.09	3.61 ± 0.02	7.34 ± 0.41

It is interesting to note that, according to Figures 2.14 and 2.15, the rate constants k_{65} and k_{54} are not linearly dependent on the reaction temperature. This type of behaviour could be explained by the Arrhenius equation, which enables the description of rate constants as a function of temperature:

$$k = A\, e^{-E_a/RT} \qquad (2.7)$$

where **k** = the relevant reaction rate constant; **A** = pre-exponential factor (*or* frequency factor); **R** = the gas constant in $J.K^{-1}.mol^{-1}$; **T** = temperature in Kelvin; $\mathbf{E_a}$ = the reaction activation energy

In order to understand the empirical term activation energy, it would be useful to consider how energy changes occur in the course of a chemical reaction beginning with a collision between two molecules. As a reaction ensues, two molecules come into contact, undergo distortion and start to exchange or discard atoms. During this process, the "potential energy" reaches a maximum, the cluster of atoms that correspond to the region "close" to this maximum being known as the activated complex. Once the energy maximum has been reached, the potential energy decreases exponentially as the atoms in the cluster rearranges, and the energy reaches a value characteristic of the products. The maximum reaction potential energy corresponds to the activation energy, E_a. At this stage, the two reacting species reached such a close proximity and degree of distortion, that any additional distortion will result in the formation of the products. Thus, we can define the activation energy as the minimum amount of energy required by reacting species in order to form products.

By taking the natural logarithm of Equation 2.7, the Arrhenius equation can be re-written as:

$$\ln(k) = \ln(A) - \frac{E_a}{RT} \qquad (2.8)$$

Thus, a plot of ln(k) versus $^1/_T$ would yield a linear trend, with the slope of the regression being given by $-E_a/R$, and the intercept of the y-ordinate yielding the value of ln(A), Figures 2.16 and 2.17. The magnitude of E_a for the aquation of $[RhCl_6]^{3-}$ was calculated as 89.29 (± 3.29) $J.mol^{-1}$, while that for the aquation of $[RhCl_5(H_2O)]^{2-}$ was found to be 108.15 (± 2.65) $J.mol^{-1}$. The fact that the rate of the aquation of $[RhCl_6]^{3-}$ is always faster than that of the aquation of $[RhCl_5(H_2O)]^{2-}$ can thus be understood in terms of the activation energy; with the activation energy of the aquation of $[RhCl_6]^{3-}$ being significantly lower than that corresponding to the aquation of the $[RhCl_5(H_2O)]^{2-}$ complex anion. Furthermore, it is

interesting to note that the activation energy of the aquation reactions investigated is independent of ionic strength, Figures 2.16 and 2.17.

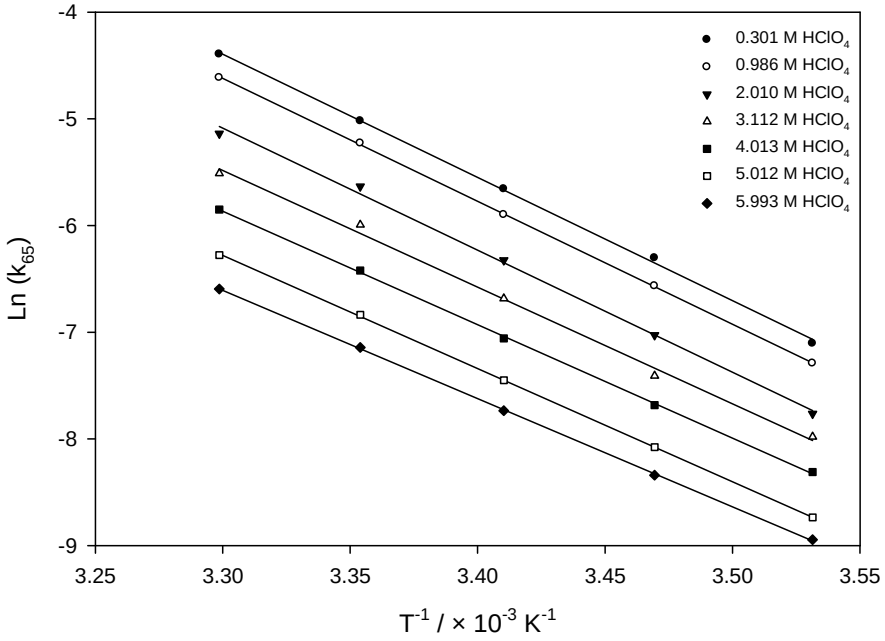

Figure 2.16: Arrhenius plot of $\ln(k_{65})$ as a function of temperature and ionic strength, indicating the temperature dependence of the aquation of the $[RhCl_6]^{3-}$ complex anion

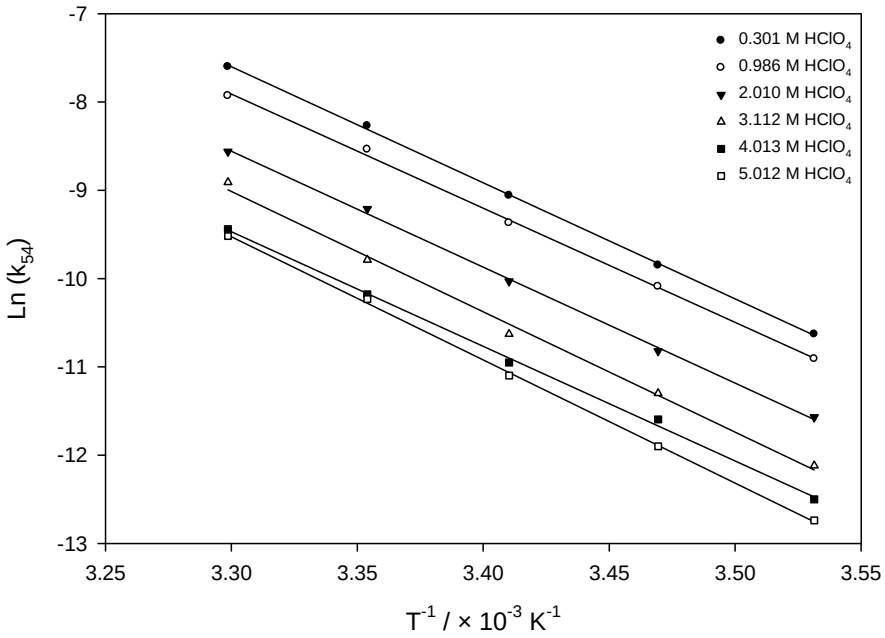

Figure 2.17: Arrhenius plot of $\ln(k_{54})$ as a function of temperature and ionic strength, indicating the temperature dependence of the aquation of the $[RhCl_5(H_2O)]^{2-}$ complex anion

2.4 Concluding remarks

The rate constants, k_{65} and k_{54}, for the aquation of the $[RhCl_6]^{3-}$ and $[RhCl_5(H_2O)]^{2-}$ complex anions were calculated from UV-vis kinetic data. Simulation of the kinetic traces, using the custom developed software Kinetic$_5$Ver, allowed the determination of the molar extinction coefficient spectra of the $[RhCl_5(H_2O)]^{2-}$ and *cis*-$[RhCl_4(H_2O)_2]^{2-}$ complex anions. This was possible since aquation of the $[RhCl_6]^{3-}$ complex anion is faster than that of the $[RhCl_5(H_2O)]^{2-}$ complex anion which allows for the accurate assessment of the $[RhCl_5(H_2O)]^{2-}$ species' concentration approximately 8-10 minutes after dilution. Furthermore, the program Mauser$_1$Ver, developed for the geometrical analysis of Mauser diagrams, was used for the calculation of the molar extinction coefficient spectra of the $[RhCl_5(H_2O)]^{2-}$ and *cis*-$[RhCl_4(H_2O)_2]^{-}$ complex anions. It was found that the agreement between the two differing computational methods for the calculation of molar extinction coefficient spectra was exceptional. Moreover, the calculated molar extinction coefficient spectra overlap at all the experimentally observed isosbestic points that are indicative of the internal consistency of the aquation/anation models fitted to the kinetic data.

The effect of ionic strength on the aquation rate of the $[RhCl_6]^{3-}$ and $[RhCl_5(H_2O)]^{2-}$ complex anions was investigated, from which the rate constants k_{65} and k_{54} were determined as a function of ionic strength. The ionic strength at which the reactions were conducted was found to influence the rate of ligand substitution dramatically. Typically, an increase in ionic strength led to a decrease in the rate of aquation. This is attributed to the lowered water activity upon increasing the ionic strength.

Finally, it was shown that temperature has a profound effect on the rate of ligand substitution. The transition state activation energy (E_a) for the aquation of the $[RhCl_6]^{3-}$ species was calculated as 89.29 ± 3.29 J.mol^{-1}, while that of the $[RhCl_5(H_2O)]^{2-}$ species was calculated as 108.15 ± 3.29 J.mol^{-1}. Furthermore, the activation energies for the aquation of both the $[RhCl_6]^{3-}$ and $[RhCl_5(H_2O)]^{2-}$ complex anions were found to be independent of ionic strength

2.5 References

[1] E. Benguerel, G.P. Demopoulos, G.B. Harris, *Hydrometallurgy*. **40** (1996) 135

[2] W. Robb, G.M. Harris, *J. Am. Chem. Soc*. **87** (1965) 4472

[3] W. Robb, M.M. de V. Steyn, *Inorg. Chem*. **6** (1966) 616

[4] W. Robb, M.M. de V. Steyn, H. Kruger, *Inorg. Chim. Acta*. **3** (1969) 383

[5] D.A. Palmer, G.M. Harris, *Inorg. Chem*. **14** (1975) 1316

[6] M. J. Pavelich and G. M. Harris, *Inorg. Chem.* **12** (1973) 423

[7] D. Cozzi, F. Pantani, *J. Inorg. Nucl. Chem.*, **8** (1958): 385

[8] W.C. Wolsey, C.A. Reynolds, J. Kleinberg, *Inorg. Chem*. **2** (1963) 463

[9] L. Zou, J. Chen, X. Pan, *Hydrometallurgy*. **50** (1998) 193

[10] M.T. Kostanski, H. Freiser, *Anal. Chim. Acta*. **242** (1991) 191

[11] E. Benguerel, G.P. Demopoulos, G. Cote, D. Bauer, *Solvent Extraction and Ion Exchange.* **12** (3) (1994) 497

[12] M.S. Alam, K. Inoue, K. Yoshizuka, *Hydrometallurgy*. **49** (1998) 213

[13] G. Schmuckler, *US patent 4 885 143*, United States of America (1989)

[14] J. Polster, H. Mauser, *Talanta*, **39** (10) (1992) 1355

[15] J. Polster, H. Dithmar, *Phys. Chem. Chem. Phys*. **3 (**2001) 993

[16] J. Polster, *Chemical Physics*, **240** (1999) 331

[17] J. Polster, *Phys. Chem. Chem. Phys*. **1 (**1999) 4791

[18] J. Polster, *Chemical Physics*. **263** (2001) 69

[19] J. Polster, H. Dithmar, *Chemical Physics*, **283 (**2002) 473

[20] T.E. Geswindt, W.J. Gerber, H.E. Rohwer, E.C. Hosten,. *A kinetic approach to determine the activity coefficients of Rhodium(III) species in an HCl matrix*, Unpublished work presented at the SACI convention, Durban, South Africa (2006)

[21] K. Krengel-Rothensee, U. Richter and P. Heitland, *J. Anal. At. Spectrom.*, **14** (1999) 699–702.

[22] J. Naozuka, M. A. Mesquita Silva da Veiga, P. V. Oliveira and E. de Oliveira, *J. Anal. At. Spectrom.*, **18** (2003) 917–921.

[23] P-H. van Wyk, W. J. Gerber and K. R. Koch, *J. Anal. At. Spectrom.*, **27** (2012) 577

[24] W. J. Gerber, K. R. Koch, E. C. Hosten and T. E. Geswindt, *Talanta*, **82** (2010) 348–358.

[25] T. E. Geswindt, *M.Sc. Dissertation*, Nelson Mandela Metropolitan University (2009)

[26] H. Wai and K. Yates, *Canadian J. Chem.*, **47** (1969) 2326-2328

Chapter 3

Screening of commercially available organic compounds for the selective precipitation of Rh^{III} aqua chlorido-complexes present in chloride-rich media

3.1 Introduction

The results described in the previous chapter highlight the important parameters related to the successive aquation reactions of the $[RhCl_6]^{3-}$ complex anion. These parameters allow for the preparation of solutions in which the Rh^{III} aqua chlorido-complexes are well defined - an important aspect for the recovery of Rh by methods such as solvent extraction, ion exchange or organic precipitation.

The separation of Rh from other transition metals has been the subject of numerous investigations, with most focussing on liquid-liquid [1-7] and solid-phase extraction techniques [8-10]. Owing to its expense and chemical/industrial relevance, it is highly beneficial to any refinery if Rh is separated and refined at an early stage of the PGM refining process, *i.e.* the recovery of Rh before other associated PGMs (Pt, Pd, Ir and Ru). However, very few publications document the recovery of Rh from an ore concentrate containing associated PGMs as well as other transition metals by means of selective precipitation using organic (typically *N*-containing) compounds. A 1992 patent by Crozier and Grant [11] describes the use of the (poly)amine diethylenetriamine (**Deta**) as an organic precipitant, in the presence of an appropriate protonating agent (HCl, H_3PO_4, HNO_3 or H_2SO_4) for the selective precipitation of Rh from an industrial, chloride-rich, ore concentrate. Furthermore, these authors documented a dramatic increase in the selectivity toward the removal of Rh when using **Deta** when compared to ethylenediamine (en), with an Rh recovery efficacy > 98% reported when using **Deta**. It should be highlighted, however, that the concentration of other associated transition metals was *relatively* low compared to the Rh concentration, suggesting that this method was applied on Rh feed solutions prepared for the final Rh purification stage, *i.e.* the bulk of the associated transition metals had been removed prior to

the precipitation stage. However, the separation of Rh from other precious metals continues to pose the most difficult aspect of PGM refining. The poor separation of Rh is chiefly attributed to the presence of the aquated Rh^{III} species, $[RhCl_n(H_2O)_{6-n}]^{3-n}$ (n=3-5), combined with the labile character of the $[RhCl_6]^{3-}$ complex anion toward aquation reactions, as was seen in the previous chapter

From the trends observed by Crozier and Grant [11], it is evident that an increase in the chain-length of the aliphatic, *N*-containing organic precipitant could lead to an increase in selectivity of the precipitant toward Rh precipitation. Possible reasons for the increased selectivity may include: (*i*) differing modes of binding of the protonated organic receptor (precipitant) to different anionic metal chlorido-complexes, *e.g.* binding of the organic receptor through hydrogen-bonding interactions with either the *faces* or the *edges* of the hexachlorido octahedron of $[RhCl_6]^{3-}$ or $[PtCl_6]^{2-}$; (*ii*) lower solubility of the (**DetaH$_3$**)[$RhCl_6$] (*s*) precipitate compared to the analogous (**DetaH$_3$**)[$PtCl_6$]Cl (*s*) precipitate, which may originate from the charge differences between the triply charged cation (**DetaH$_3^{3+}$**) and the anionic metal chlorido-complex, or the bulky nature of **Deta** compared to ethylenediamine. Therefore, factors that can be exploited to affect the selectivity of the precipitation of a single metal chlorido-complex include:

(*a*) the charge difference between various anionic metal chlorido-complexes, *e.g.* $[PdCl_4]^{2-}$, $[RhCl_6]^{3-}$, $[IrCl_6]^{2/3-}$ and $[PtCl_6]^{2-}$, and the cationic precipitants

(*b*) solvation/desolvation energy differences of the anionic metal chlorido-complexes as well as the protonated organic precipitants

(*c*) lattice energy differences of the precipitates, which is reflected by the efficacy of the packing arrangement between anionic and cationic molecules in the solid state.

Considering these factors, several commercially available *N*-containing organic compounds were screened for its efficacy in the preferential and quantitative precipitation of Rh from an industrial PGM ore concentrate, with the overarching objective being the "upfront" (early) recovery of Rh from the ore concentrate. The criteria for selecting appropriate agents as precipitants were reasonably straightforward: (*i*) the precipitating agent should react with the analyte (*ii*) be unreactive towards atmospheric conditions (*iii*) the compound must be soluble and stable in concentrated acidic media (*iv*) the reagent should be relatively cost-effective; thus synthesis of novel organic compounds was not considered as this is often an expensive route which does not necessarily yield improved precipitation results compared to relatively inexpensive commercially available compounds (*v*) it should be able to precipitate Rh^{III}, as its

chlorido anion(s), *quantitatively* (*i.e.* with > 90% efficiency) and preferably selectively from acidic aqueous solutions containing Rh^{III} and other PGMs. Table 3.1 lists the commercially available precipitants used throughout this study.

Table 3.1: Commercially available, *N*-containing precipitants used throughout this study

	Compound name	Structure
Linear Motif	diethylenetriamine [**Deta**]	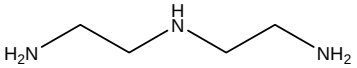
	triethylenetetramine [**Teta**]	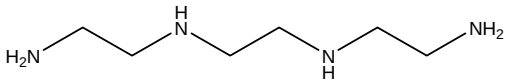
	tetraethylenepentamine [**Tepa**]	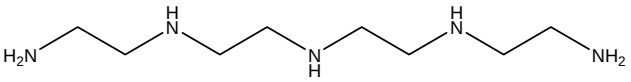
	ethylenimine oligomer mixture (Avg. MW = 423 g.mol^{-1})	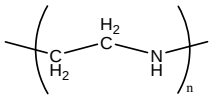
	Lupamin® 1595 (Avg. MW = <10 000 g.mol^{-1})	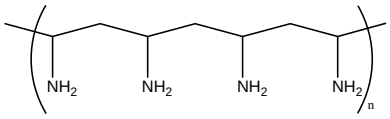
	Lupamin® 9030 (Avg. MW = 340 000 g.mol^{-1})	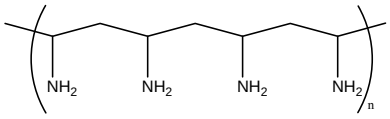
Branched Motif	tris(2-aminoethyl)amine [**Tren**]	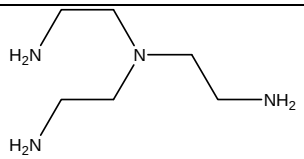
	tris[(2-isopropylamino)-ethyl]amine [Trien]	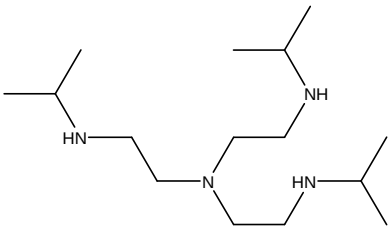
	1,4,7-triazonane	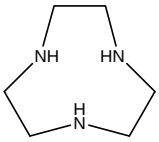

3.2 Experimental

3.2.1 Preparation of PGM containing stock solutions

3.2.1.1 Preparation of Rh^{III} and Pt^{IV} stock solutions

A 0.2011 M stock solutions of $[RhCl_n(H_2O)_{6-n}]^{3-n}$ (n=5,6) complex anions were prepared by dissolving *ca* 1.06 g of commercially available $RhCl_3 \cdot nH_2O$ (Heraeus chemicals GmbH) in 20 mL 32% ($^{v}/_{v}$) HCl (Merck chemicals). This solution was sealed and kept at 333 K for a week and thereafter allowed to equilibrate at 292 K for a further 5 days. UV-vis spectrophotometry conducted on the prepared stock solution (after appropriate dilution with 32% HCl) yielded a spectrum characteristic to that of (*predominantly*) $[RhCl_6]^{3-}$ with the presence of two maxima, *i.e.* at 523 nm and 415 nm. The total chloride concentration was 10.101 M.

A 0.2118 M $[PtCl_6]^{2-}$ stock solution was prepared by dissolving ca 1.74 g of commercially available platinic acid ($H_2[PtCl_6]$ – Heraeus chemicals GmbH) in 20 mL 32% ($^{v}/_{v}$) HCl. UV-vis spectrophotometry conducted on the stock solution after appropriate dilution revealed a spectrum characteristic of $[PtCl_6]^{2-}$ with a single peak maximum at 261 nm. The total chloride concentration was 10.011 M

The total Rh, Pt and chloride concentrations of these stock solutions were determined by means of ICP-OES (SPECTRO Arcos); equipped with a Schott spray chamber and cross-flow nebulizer. The general ICP-OES conditions were: ICP RF power = 1400 W, coolant gas flow = 13.00 $L.min^{-1}$, auxiliary gas flow = 1.00 $L.min^{-1}$, nebulizer gas flow = 0.80 $L.min^{-1}$. The most sensitive Rh (343.489 nm), Pt (265.945 nm) and chloride (134.742 nm) wavelengths were used for these determinations. ULTRASPEC single element Rh and Pt standard solutions (De Bruyn Spectroscopic Solutions; 99.998% purity, 10% $^{v}/_{v}$ HCl) were used for Rh and Pt standardisation. Dried sodium chloride (Sigma-Aldrich; 99.95% purity) was used for chloride standardisation.

3.2.1.2 Preparation of synthetic mixed metal (Rh^{III} and Pt^{IV}) stock solution

The single element stock solutions, prepared as outlined in Section 3.2.1.1, were mixed in an equimolar ratio and diluted to a final metal concentration of *ca* 0.1 M with 32% $^{v}/_{v}$ HCl. The total metal and chloride concentration, determined by means of ICP-OES (Section 3.2.1.1) was: [Rh] = 0.101 M, [Pt] = 0.100 M and [Cl^-] = 10.1 M

3.2.1.3 Authentic industrial feed solutions

Several industrial PGM process solutions, supplied by Heraeus chemicals GmbH, were used to test the efficacy of the screened organic compounds (*vide infra*) as possible "selective" precipitants for the quantitative "upfront" removal of Rh from an ore concentrate containing various associated PGMs as well as other transition metals. Table 3.2 shows the elements present in a typical industrial feed solution (determined by ICP-OES) and the concentration of each element in such a solution. The total chloride concentration of the feed solution was at 4.008 M, determined by means of ICP-OES. During the precipitation titration experiments, the total chloride concentration of the feed solution was adjusted to 6.0 M by the addition of the required volume of 32% $^{v}/_{v}$ HCl. This was done in order to compare the results of the process solutions to that of the laboratory prepared Rh^{III} and Pt^{IV} containing solutions.

Table 3.2: Elemental composition and concentration of the industrial feed solution used throughout this study. The highlighted elements are those with the highest concentrations

Element	mg/L	M
Au	1	5×10^{-6}
Ag	95	8.8×10^{-4}
Pt	**30646**	**1.5712×10^{-1}**
Pd	**12827**	**1.2054×10^{-1}**
Ir	997	5.18×10^{-3}
Rh	**3435**	**3.338×10^{-2}**
Ru	273	2.70×10^{-3}
Re	< 1	-
Al	164	6.08×10^{-3}
As	7	9×10^{-5}
Co	203	3.44×10^{-3}
Cr	24	4.6×10^{-4}
Cu	**2051**	**3.228×10^{-2}**
Fe	**21271**	**3.8091×10^{-1}**
Ni	**3514**	**5.987×10^{-2}**
Pb	**4235**	**2.044×10^{-2}**
Se	< 1	-
Si	318	1.13×10^{-2}
Te	1468	1.150×10^{-2}
Zn	8	1×10^{-4}

3.2.2 Preparation of stock precipitant solutions

All the organic compounds (hereafter called precipitants) listed in Table 3.3 are fully miscible with water. Stock solutions of these reagents were prepared in 6.0 M HCl (unless otherwise stated), by *slow* addition of the precipitant to the acid (all of the compounds, excluding 1,4,7-triazonane - which is a white chloride salt, react violently upon contact with acidic media). Tetraethylenepentamine (0.501 M) stock solutions were prepared in 3.0 M HCl due to the precipitation of the amine, as its chloride salt, at high (> 3.5 M) HCl concentrations. With the exception of ethylenimine oligomer and Lupamin® polymeric solutions, the molar concentration of the prepared stock solutions was *ca* 0.5 M with respect to the precipitant. Stock ethylenimine oligomer (2.16% $^{v}/_{v}$) and Lupamin® (7.31% $^{v}/_{v}$) solutions were prepared by pipetting the required volume of the reagent into a volumetric flask containing the necessary volume of HCl, such that the final HCl concentration upon dilution was 6.0 M. The prepared stock solutions were further diluted, with 6.0 M HCl, as required for a particular experiment. According to the protonation constants documented in literature [12,13], the precipitants are considered to be fully protonated under the conditions at which the solutions were prepared. It is essential that the precipitants are fully protonated since (poly)amines are known to coordinate to the metal centre, especially in the case of Rh^{III}, $Pt^{II/IV}$ and $Ir^{III/IV}$, under neutral – basic conditions [14-17].

Table 3.3: The amine-based organic compounds screened as possible selective precipitants for Rh^{III}

Reagent	Chemical structure	% Composition	Supplier
diethylenetriamine [**Deta**]	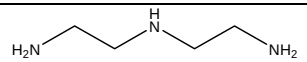	99	Riedel de Haën
triethylenetetramine [**Teta**]	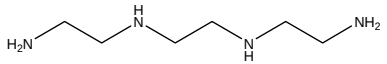	98	Fluka
tetraethylenepentamine [**Tepa**]	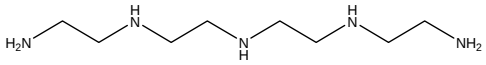	98	Fluka
tris(2-aminoethyl)amine [**Tren**]	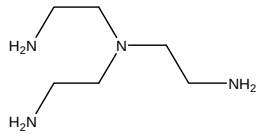	98	Fluka
tris[(2-isopropylamino)-ethyl]amine [Trien]	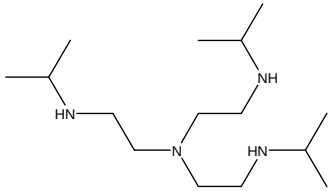	98	Sigma-Aldrich
1,4,7-triazonane	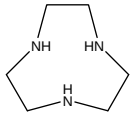	95	Sigma-Aldrich
ethylenimine oligomer mixture (Avg. MW = 423 $g.mol^{-1}$)	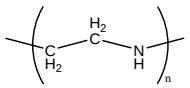	91	Sigma-Aldrich
Lupamin® 1595 (Avg. MW = <10 000 $g.mol^{-1}$)	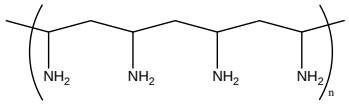	-[a]	BASF Corporation
Lupamin® 9030 (Avg. MW = 340 000 $g.mol^{-1}$)	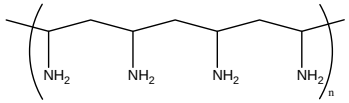	-[a]	BASF Corporation

[a] Information not available

3.2.3 Mole ratio precipitation titrations of precious metal (Rh and Pt) chloride anions with several commercially available organic precipitants

Generally, the screening of possible precipitants involves the titration of a solution containing the metal of interest against the precipitant. However, the conventional method of precipitation titrimetry is not feasible, since the precipitate formation is not instantaneous. Therefore, a typical titration consisted of a series of 25-30 samples in which the total metal content of each solution was kept constant while the concentration of the precipitant was gradually increased along the series. The precipitation titrations were conducted at a total HCl concentration of 6.0 M. A typical precipitant – metal chloride anion titration for a single organic compound is shown in Table 3.4.

Table 3.4: An example of a typical Rh^{III} chloride anion *versus* precipitant titration, conducted at 298.1 K

Sample Number	$[\mathbf{L}]_{stock}$ / M	$[\mathbf{L}]_{final}$ / mM	[**M**] / mM	[**L**] / [**M**] Ratio
1	-	-	7.011	0.00
2	0.0100	0.0351	7.011	0.005
⋮	⋮	⋮	⋮	⋮
10	0.0500	7.010	7.011	1.00
⋮	⋮	⋮	⋮	⋮
20	0.100	35.01	7.011	4.99
⋮	⋮	⋮	⋮	⋮
30	0.500	210.1	7.011	29.97

[**L**] = Precipitant concentration; [**M**] = Rh^{III} chloride anion concentration

Titrations were allowed to proceed for 3 days at 298.1 K. Once equilibration was attained, each solution was centrifuged at 6500 rpm, the supernatant of each solution removed and analysed for its metal content by ICP-OES spectroscopy. All the titrations performed were repeated in triplicate to attain concordant results and results presented are an average of these repeats. Titrations were performed on HCl solutions containing the single metal chloride anions (*i.e.* Rh^{III} or Pt^{IV}), laboratory prepared solutions containing mixed metal chloride anions (Rh^{III} and Pt^{IV}) and an authentic industrial process solution containing all the metals outlined in Table 3.2.

Generally, the metal concentration in the solid phase was calculated by means of mass balance of the metal content in the aqueous phase before and after precipitation. In order to validate this method, total metal mass balance experiments were conducted. After the precipitation stage, the salt was washed with aliquots of cold water/HCl mixture and dried under vacuum. Dissolution was achieved by slow addition of *aqua regia* to the dried precipitate at 333.1 K, with constant stirring. It is essential that *aqua regia* is added very slowly to the precipitate in order to prevent the possible formation of nitrosamines in the presence of concentrated nitric acid. Following complete dissolution of the precipitate, the metal containing solution was made up to volume (50 mL) with 3.0 M HCl.

3.2.4 Crystal structure of isolated (**TepaH$_5$**)[RhCl$_6$]Cl$_2$·2H$_2$O

As part of this work, suitable crystals of Tetraethylenepentammonium diaqua hexachlororhodate(III) dichloride, (**TepaH$_5$**)[RhCl$_6$]Cl$_2$·2H$_2$O, were isolated by the drop-wise addition of 20 mL tetraethylenepentamine (**Tepa** – 7.011 mM in 3.0 M HCl) to an aqueous solution containing $[RhCl_6]^{3-}$ (20 mL, [Rh] = 7.103 mM in 6.0 M HCl). The solution temperature was maintained at 313 K, under constant stirring, in order to prevent rapid precipitation of Rh^{III} as the tetraethylenepentammonium salt. Following **Tepa** addition, the solution was slowly cooled to ambient temperature and crystallization allowed to proceed by slow evaporation of the solvent (± 3-4 weeks). The resulting crystalline material was washed with aliquots of cold ethanol. Light microscopy revealed small red single-crystals that illustrated hexagonal, plate-like morphology.

Single crystal X-ray diffraction data were recorded using a Bruker SMART APEX diffractometer equipped with a graphite monochromated Mo Kα radiation (λ = 0.71073 Å), at 105 K. Empirical absorption corrections were applied using SADBS [19]. Crystal structures were solved using SHELXS 97 [20] and all ordered non-hydrogen atoms were refined anisotropically by full-matrix least-squares of F^2 using SHELXL-97 [21] within the X-SEED environment [22]. All hydrogen atoms were placed in calculated positions. Hydrogen bond and coordination sphere geometric parameters are available in the supplementary section.

Table 3.5: Data collection and final refinement parameters for (**TepaH$_5$**)[RhCl$_6$]Cl$_2$·2H$_2$O

	(**TepaH$_5$**)[RhCl$_6$]Cl$_2$
Empirical formula	C8 H29 N5 Cl6 Rh, 2(H$_2$O), 2(Cl),
Formula weight	617.906
Temperature / K	105
Crystal system	Monoclinic
Space group	$P2_1/n$
a (Å)	7.1601(4)
b (Å)	31.9491(17)
c (Å)	9.8711(5)
α°	90
β°	91.057(1)
γ°	90
Cell volume (Å^3)	2257.7(2)
ρ (g.cm^{-3})	1.812
Absorption coefficient (mm^{-1})	0.776
Final R indices [I > 2σ(I)]	0.0365
R indices (all data): R$_1$, *w*R$_2$	0.0921 0.1602
Goodness-of-fit on F^2	1.040
$\Delta\rho_{max}$ / $\Delta\rho_{min}$ [e / Å^3]	0.368 / -0.416

3.2.5 High-resolution ^{195}Pt NMR spectroscopic study of an authentic industrial feed solution

400 μL (Pt content = 98.867 mM in 4.008 M HCl) of an industrial PGM feed solution (Heraeus chemicals GmbH) in 30% ($^v/_v$) $^2H_2O/^1H_2O$ was used for the recording of ^{195}Pt NMR spectra.

128.8 MHz ^{195}Pt NMR spectra were recorded (at 293 K ± 0.1 K) using a Varian INOVA 600 MHz spectrometer, with a 5 mm broad-band probe. Particular attention to temperature equilibration of the sample and optimal shimming is necessary. Although no absolute referencing was required, chemical shifts (ppm) are reported relative to the widely used external $[PtCl_6]^{2-}$ as reference solution (δ^{195}Pt = 0.0 ppm at 500 mg.ml^{-1} $H_2PtCl_6·2H_2O$ in 30% $^v/_v$ $^2H_2O/^1H_2O$ – 1 M HCl) at 303 K, without attempting to adjust for small temperature induced changes in δ ^{195}Pt shifts [23]. Spectra were recorded under conditions of

optimal resolution using a 2.0 μs excitation pulse (corresponding to a ~20° pulse) at maximum practical power, an acquisition time of *ca.* 1.1 s with no relaxation delay, in an attempt to ensure homogeneous and complete excitation over the spectral width. Typical resonance line-widths ($\nu_{1/2}$) ranged from 9–12 Hz, and spectra were processed to ensure optimal resolution. The measured T_1 relaxation times of these platinum complexes ranged from 1–1.5 s for the solution, in effect ensuring complete relaxation of all complex species in solution.

3.3 Results and discussion

3.3.1 Description of organic compounds not used as precipitants

3.3.1.1 tris[(2-isopropylamino)-ethyl]amine

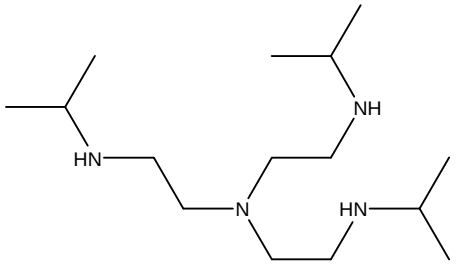

Chemical structure of tris[(2-isopropylamino)-ethyl]amine

This amine, at first glance, appears to be a perfect candidate for the precipitation of metal chlorido anions from acidic solution. However, no precipitation was observed for any of the metals (Rh^{III}, Pt^{IV} and Ir^{IV}) investigated. The reason for this could be that the bulky isopropyl groups coordinated to the nitrogen atoms sterically hinder interaction between the protonated nitrogen atoms and the metal chlorido anion, thus impeding the precipitation. It could also be that the isopropyl groups improve the solubility of the resulting ion-pair between the "precipitant" and the metal complex anion[3]. Further investigations relating to this compound were therefore discontinued.

[3] The author thanks one of the thesis reviewers for this comment.

3.3.1.2 1,4,7-triazonane

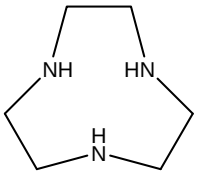

Chemical structure of 1,4,7-triazonane

This organic precipitant can be considered a cyclic "analogue" of diethylenetriamine, and thus it is not surprising that it is highly efficient in precipitating both $[RhCl_6]^{3-}$ as well as $[PtCl_6]^{2-}$ complex anions from aqueous acidic solution, as preliminary observations had shown. However, at a price of US$ 88.99 (R 711.99) per 100 mg compared to US$ 23.80 (R 190.40) per 250 mL for diethylenetriamine, it is too expensive to be regarded as a viable precipitating agent, especially considering that the precipitating agents would not necessarily be recycled. Further investigations related to this compound were therefore discontinued.

3.3.1.3 ethylenimine oligomer mixture

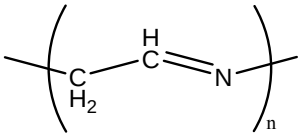

Repeating unit of the ethylenimine oligomer mixture

Preparation of this precipitant in acidic matrices (> 1.0 M HCl or $HClO_4$) leads to the formation of a grey precipitate, albeit approximately four hours after preparation. Furthermore, addition of excess ethylenimine oligomer, freshly prepared in 6.0 M HCl, to an aqueous solution predominantly containing the $[RhCl_6]^{3-}$ complex anion led to the formation of a pink colloidal suspension. Similarly, addition of this compound to an HCl solution containing $[PtCl_6]^{2-}$ led to the formation of a yellow colloidal suspension. The formation of a colloidal suspension makes the separation of the solid "precipitate" *via* centrifugation and filtration complicated. This, in turn, leads to inconsistent results when analyzing the supernatant for its metal content. Hence, due to its instability in acidic solutions combined with the formation of a colloidal suspension instead of a precipitate upon addition to PGM containing solutions, further investigations were discontinued.

3.3.1.4 Lupamin® 1595 and 9030

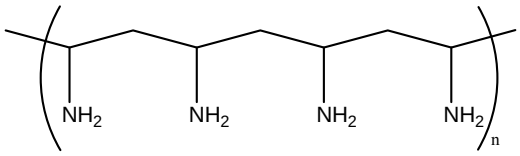

Repeating unit of Lupamin® 1595 and 9030 polymers

The Lupamin® range is tailor-made polymeric compounds prepared by the polymerization of the monomer vinylformamide, to produce a linear high molecular weight polyvinylamine that is a colourless to yellow solution [18]. According to available literature [18], Lupamin® 1595 is greater than 90% hydrolysed, while Lupamin® 9030 is only 30% hydrolysed. These polymers are fully miscible in water and acidic media, with no salting observed during its preparation in 6.0 M HCl.

Addition of excess Lupamin® 1595 (freshly prepared in 6.0 M HCl) to an aqueous solution containing predominantly the $[RhCl_6]^{3-}$ complex anion led to the formation of a pink colloidal suspension. Correspondingly, addition of this polymer to an aqueous HCl solution containing the $[PtCl_6]^{2-}$ complex anion led to the formation of a yellow colloidal suspension. Furthermore, Lupamin® 9030 polymer did not yield any precipitate or colloid formation when added to aqueous HCl solutions containing either the $[RhCl_6]^{3-}$ or $[PtCl_6]^{2-}$ complex anions. Consequently, due to the formation of a colloidal suspension (in the case of Lupamin® 1595) and the total lack of precipitate formation (in the case of Lupamin® 9030) upon its addition to a PGM containing solution, detailed investigations of these compounds were discontinued.

The precipitants that were subsequently used for comprehensive investigations included diethylenetriamine (**Deta**), triethylenetetramine (**Teta**), tetraethylenepentamine (**Tepa**) and tris(2-aminoethyl)amine (**Tren**); since these (poly)amines produced precipitates relatively rapid upon addition to aqueous HCl solutions containing PGMs. Nevertheless, reference would be made to a few of the results obtained from the ethylenimine oligomer and Lupamin® 1595 studies.

3.3.2 Precipitation of Pt^{IV} and Rh^{III} chlorido-complexes from laboratory prepared solutions

Various organic compounds are used industrially for the "selective" precipitation of PGMs, with **Deta** routinely used for the precipitation of $Ir^{III/IV}$ and Rh^{III} during the final purification steps of these metals. The addition of excess diethylenetriamine (**Deta**), in the presence of an appropriate protonating agent (*e.g.* HCl or $HClO_4$) to an aqueous chloride-rich solution containing $[PtCl_6]^{2-}$ leads to the formation of a fine, yellow crystalline precipitate that is stable in air and insoluble in water and ethanol. Comparable observations were made upon the addition of protonated triethylenetetramine (**Teta**), tetraethylenepentamine (**Tepa**) and tris(2-aminoethyl)amine (**Tren**) to acidic solutions containing $[PtCl_6]^{2-}$. The precipitate formed upon addition of protonated diethylenetriamine has been described by Makotchenko *et al* [24] as the diethylenetriammonium hexachloroplatinate(IV) chloride salt, (**Deta**H_3)$[PtCl_6]Cl$. These precipitation reactions are typically (*but not wholly*) described as:

$$[PtCl_6]^{2-}_{(aq)} + Cl^- + (\mathbf{Deta}H_3)^{3+}_{(aq)} \rightarrow (\mathbf{Deta}H_3)[PtCl_6]Cl_{(s)} \quad (3.1)$$

$$[PtCl_6]^{2-}_{(aq)} + 2Cl^- + (\mathbf{Teta}H_4)^{4+}_{(aq)} \rightarrow (\mathbf{Teta}H_4)[PtCl_6]Cl_{2\,(s)} \quad (3.2)$$

$$[PtCl_6]^{2-}_{(aq)} + 3Cl^- + (\mathbf{Tepa}H_5)^{5+}_{(aq)} \rightarrow (\mathbf{Tepa}H_5)[PtCl_6]Cl_{3\,(s)} \quad (3.3)$$

$$[PtCl_6]^{2-}_{(aq)} + 2Cl^- + (\mathbf{Tren}H_4)^{4+}_{(aq)} \rightarrow (\mathbf{Tren}H_4)[PtCl_6]Cl_{2\,(s)} \quad (3.4)$$

However, other reactions are certainly possible, by way of example:

$$[PtCl_6]^{2-}_{(aq)} + 3Cl^- + (\mathbf{Tepa}H_5)^{5+}_{(aq)} \rightarrow (\mathbf{Tepa}H_5)[PtCl_6]Cl_{3\,(s)} \quad (3.3)$$

$$2[PtCl_6]^{2-}_{(aq)} + Cl^- + (\mathbf{Tepa}H_5)^{5+}_{(aq)} \rightarrow (\mathbf{Tepa}H_5)[PtCl_6]_2Cl_{(s)} \quad (3.5)$$

$$3[PtCl_6]^{2-}_{(aq)} + H_3O^+ + (\mathbf{Tepa}H_5)^{5+}_{(aq)} \rightarrow (\mathbf{Tepa}H_5)[PtCl_6]_3H_{(s)} \quad (3.6)$$

$$3[PtCl_6]^{2-}_{(aq)} + 4Cl^- + 2(\mathbf{Tepa}H_5)^{5+}_{(aq)} \rightarrow (\mathbf{Tepa}H_5)_2[PtCl_6]_3Cl_{4\,(s)} \quad (3.7)$$

Due to existence of these multiple reactions, no attempt was made to calculate the solubility product constants of the reactions depicted by Equations 3.1 – 3.4.

The mole ratio precipitation curves of $[PtCl_6]^{2-}$ as a function of increasing precipitant concentration are shown in Figure 3.1. From this figure it can be concluded that $[PtCl_6]^{2-}$ is precipitated quantitatively from aqueous chloride-rich solutions with **Teta** and **Tren** when in > 15× excess. However, **Deta** and **Tepa** does not seem to remove Pt^{IV} quantitatively from solution in the tested precipitant concentration range. The $[PtCl_6^{2-}]$ – **Teta** titration curve

appears very interesting in the sense that it demonstrates two end-points, Figure 3.1. This could be explained by considering that upon the addition of **Teta** to a $[PtCl_6]^{2-}$ containing solution, **Teta** (with four protonated nitrogen atoms) could coordinate with two $[PtCl_6]^{2-}$ complex anions. However, as the $[PtCl_6]^{2-}$ complex anions remaining in the supernatant is depleted, **Teta** would instead coordinate with a single $[PtCl_6]^{2-}$ complex anion and two chloride ions in order to maintain charge balance.

$$2[PtCl_6]^{2-}_{(aq)} + C_6H_{22}N_4{}^{4+}_{(aq)} \rightarrow [C_6H_{22}N_4][PtCl_6{}^{2-}]_{2\,(s)} \qquad :K_{sp} = [PtCl_6{}^{2-}]^2 \times [C_6H_{22}N_4]$$

$$[PtCl_6]^{2-}_{(aq)} + C_6H_{22}N_4{}^{4+}_{(aq)} + 2Cl^-_{(aq)} \rightarrow [C_6H_{22}N_4][PtCl_6{}^{2-}][Cl^-]_{2\,(s)} \qquad :K_{sp} = [PtCl_6{}^{2-}] \times [C_6H_{22}N_4] \times [Cl^-]^2$$

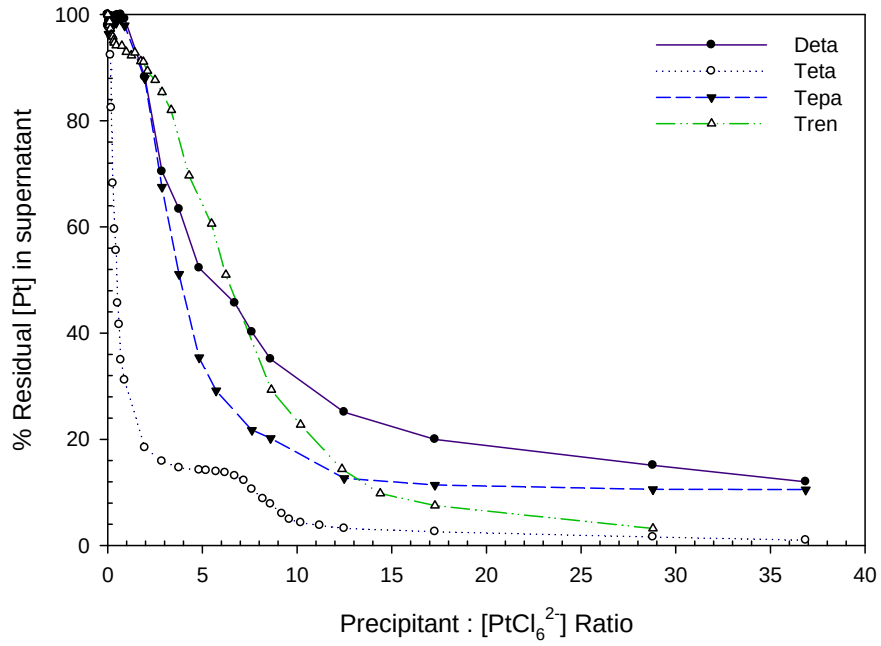

Figure 3.1: Residual $[PtCl_6^{2-}]$ in the supernatant as a function of increasing [Precipitant]:$[PtCl_6^{2-}]$ ratio. [Pt] = 7.011 mM; [HCl] = 6.0 M. The precipitants used are denoted in the legend. Typical RSD values was below 7%.

The addition of the (poly)amines utilized during this study (**Deta**, **Teta**, **Tepa** and **Tren**) to an acidic chloride-rich solution (6.0 M HCl) containing Rh^{III}, predominantly in the form of the $[RhCl_6]^{3-}$ complex anion, results in the formation of a deep, rose-red, crystalline precipitate, that is stable under atmospheric conditions and insoluble in water. The precipitate formed upon addition of diethylenetriamine to a Rh^{III} containing solution (6.0 M HCl) was formally identified by Frank *et al* [24] as the diethylenetriammonium hexachlororhodate(III) salt, (**Deta**H_3)$[RhCl_6]$, while Mandan *et al* [17] characterized the analogous tris(2-aminoethyl)ammonium hexachlororhodate(III) salt, (**Tren**H_3)$[RhCl_6]$. In a similar manner to

the Pt^{IV} precipitation studies, equations 3.10 – 3.13 can be used to describe the general precipitation of Rh^{III} by the (poly)amines utilised throughout this study:

$$[RhCl_6]^{3-}_{(aq)} + (\mathbf{Deta}H_3)^{3+}_{(aq)} \rightarrow (\mathbf{Deta}H_3)[RhCl_6]_{(s)} \quad (3.10)$$

$$[RhCl_6]^{3-}_{(aq)} + Cl^- + (\mathbf{Teta}H_4)^{4+}_{(aq)} \rightarrow (\mathbf{Teta}H_4)[RhCl_6]Cl_{(s)} \quad (3.11)$$

$$[RhCl_6]^{3-}_{(aq)} + 2Cl^- + (\mathbf{Tepa}H_5)^{5+}_{(aq)} \rightarrow (\mathbf{Tepa}H_5)[RhCl_6]Cl_{2\,(s)} \quad (3.12)$$

$$[RhCl_6]^{3-}_{(aq)} + Cl^- + (\mathbf{Tren}H_4)^{4+}_{(aq)} \rightarrow (\mathbf{Tren}H_4)[RhCl_6]Cl_{(s)} \quad (3.13)$$

It is pertinent to mention that, as seen in Chapter 2, in a 6.0 M HCl matrix both $[RhCl_6]^{3-}$ and $[RhCl_5(H_2O)]^{2-}$ complex anions are present. Therefore, precipitation may proceed *via* an array of mechanisms, including:

(*i*) The exclusive precipitation of the $[RhCl_6]^{3-}$ complex anion. Precipitation of the $[RhCl_6]^{3-}$ complex anion leads to a disturbance in the chemical equilibrium depicted by Equation 2.1 and, according to Le Châtelier's principle, the reactants and products of the reaction would shift to partially undo the effects of the disturbance. This implies that the mono-aquated Rh^{III} complex anion would undergo chloride anation as more $[RhCl_6]^{3-}$ is precipitated in order to re-establish chemical equilibrium.

$$[RhCl_6]^{3-} + H_2O \underset{k_{56}}{\overset{k_{65}}{\rightleftharpoons}} [RhCl_5(H_2O)]^{2-} + Cl^- \quad (2.1)$$

(*ii*) The precipitation of both the $[RhCl_6]^{3-}$ and $[RhCl_5(H_2O)]^{2-}$ complex anions. There is crystallographic evidence documented in literature [26,27] that both these anions can be precipitated using ammonium chloride.

Therefore, it is evident that the precipitation of Rh^{III} is much more complicated than that of the analogous Pt^{IV} and thus no attempt was made to calculate the relevant solubility product constants of the respective reactions.

The titration curves for the precipitation of Rh^{III} as a function of increasing precipitant concentration are illustrated in Figure 3.2. This figure shows that a 1:1 stoichiometric [precipitant]:[Rh^{III} chloride anion] is required to achieve > 90% precipitation of Rh from solution. At a stoichiometric ratio of 3.5:1, Rh is quantitatively (> 98%) removed from solution, for all the precipitants investigated. Compared to the Pt^{IV} titration curves, Figure 3.1, it is evident that selective removal of Rh^{III} from a solution containing Pt^{IV} might be plausible using the selected precipitants.

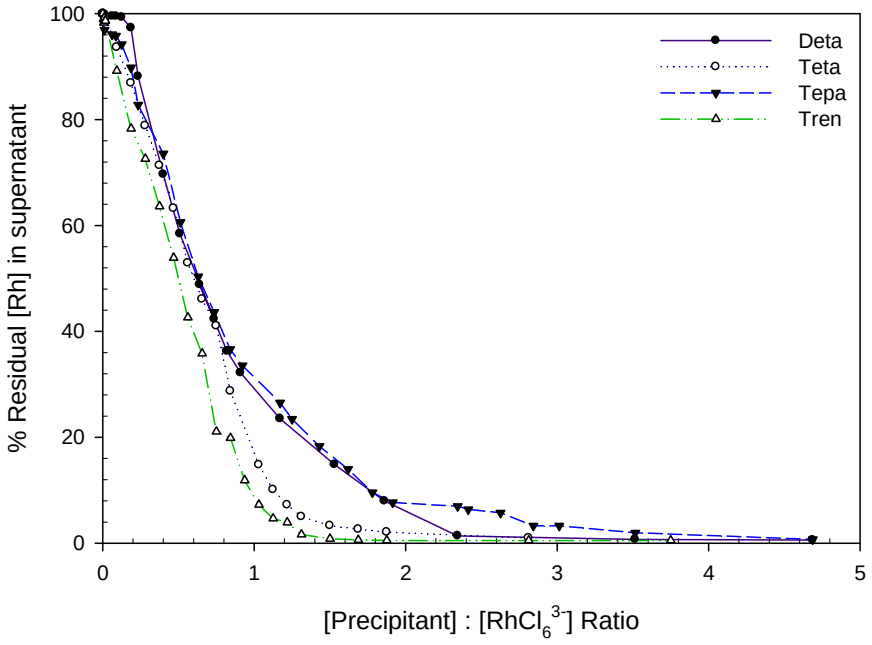

Figure 3.2: Residual [Rh^{III}] in the supernatant as a function of increasing [Precipitant]:[$RhCl_6^{3-}$] ratio. [Rh] = 7.134 mM; [HCl] = 6.0 M. The precipitants used are denoted in the legend. Typical RSD values was below 7%.

Figure 3.3 [a] – [f] compares the results obtained for the Pt^{IV}- and Rh^{III}-precipitant titrations. The results of the Lupamin® 1595 and ethylenimine oligomer precipitation studies are also included, although these results showed poor reproducibility due to the formation of a colloidal suspension instead of a precipitate. It is evident from Figure 3.3 that **Deta**, **Tepa** and **Tren** shows the greatest selectivity toward the precipitation of Rh^{III} above Pt^{IV}. **Teta** shows the poorest selectivity, as can be seen in Figure 3.3[b]. At a stoichiometric [**Teta**]:[metal chloride anion] ratio of 1, 85.4% of Rh^{III} was removed, while 71.2% of Pt^{IV} was removed at the corresponding ratio. Preliminary evaluation of the comparative figures, Figure 3.3 [a]-[f], show that **Tren** illustrates the greatest selectivity toward Rh precipitation, with 93.2% of the Rh removed at a [**Tren**]:[metal chloride anion] ratio of 1, while only 6.6% of Pt was removed at a corresponding ratio. The selectivity of **Deta** and **Tren** toward the precipitation of Rh^{III} aqua chlorido-complexes is mainly attributed to the charge balance between the triply charged cation (amine) and the triply charged anion ($[RhCl_6]^{3-}$). This is also the reason why **Teta** is more selective toward the $[PtCl_6]^{2-}$ complex anion rather than the $[RhCl_6]^{3-}$ complex anion.

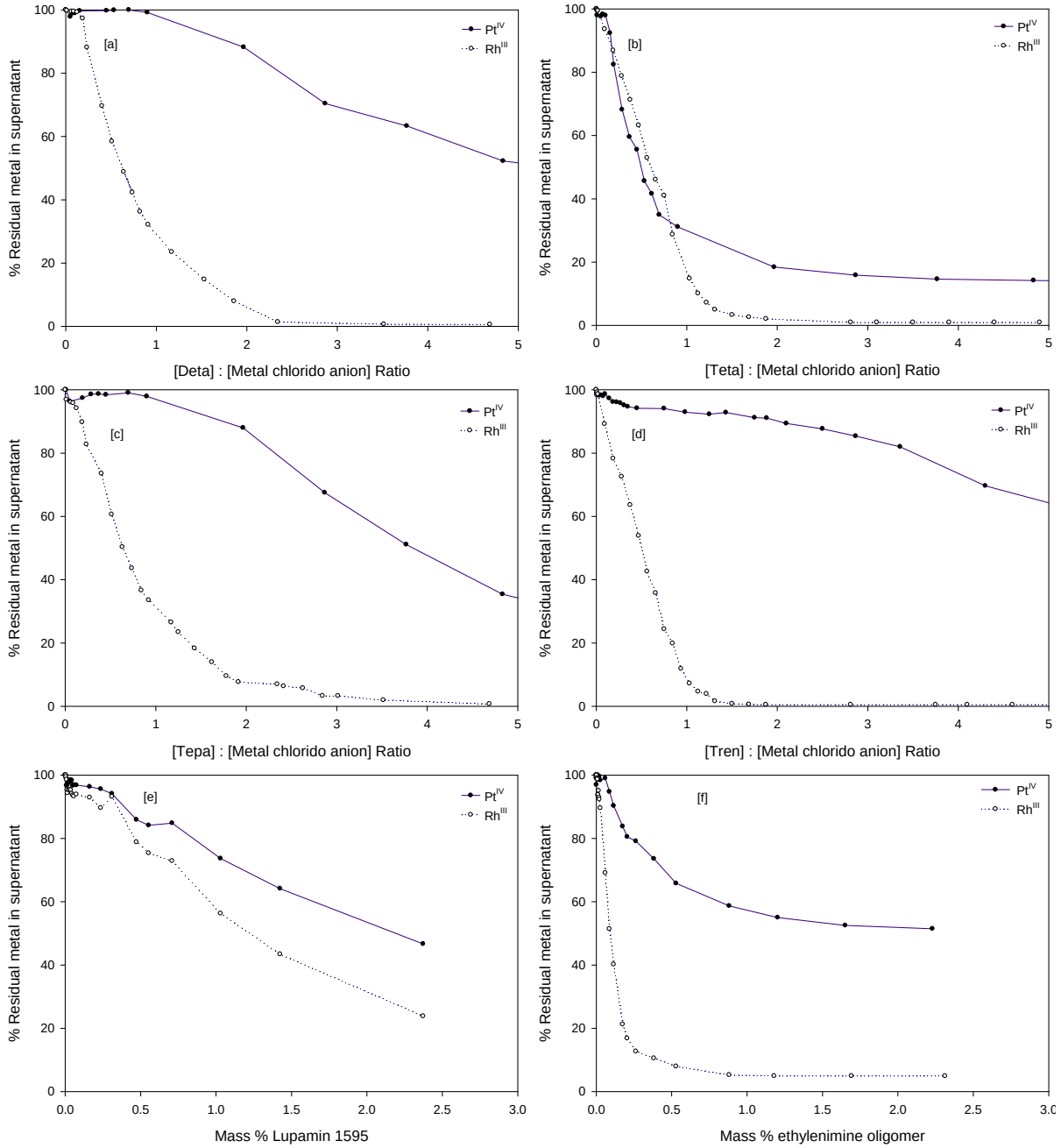

Figure 3.3: Comparison between the Pt – and Rh –precipitant titrations conducted for all the (poly)amines screened. [Pt] = 7.011 mM; [Rh] = 7.134 mM; [HCl] = 6.0 M.

3.3.3 Crystal structure of tetraethylenepentammonium diaqua hexachlororhodate(III) dichloride, (**Tepa**H_5)[$RhCl_6$]Cl_2·2H_2O

Structural data for $[RhCl_6]^{3-}$ complexes involving quintuply charged organic cations are unknown, even though these compounds are interesting from the perspective of obtaining information regarding the stoichiometric types and structures of the complex forms of Rh^{III} compounds, especially in acidic, halide-rich matrices. Furthermore, preparation of crystals

involving the $[RhCl_6]^{3-}$ complex anion is extremely difficult due to its thermodynamic and kinetic instability, especially toward aquation reactions. The aim of the present work is to describe the structure of the synthesized (**Tepa**H_5)$[RhCl_6]Cl_2 \cdot 2H_2O$ crystal; where **Tepa** is the quintuply charged protonated tetraethylenepentamine, $[H_3N((CH_2)_2NH_2)_3(CH2)NH_3]^{5+}$.

The structure of (**Tepa**H_5)$[RhCl_6]Cl_2 \cdot 2H_2O$ is of an "island type", consisting of $[$**Tepa**$H_5]^{5+}$ cations, discrete $[RhCl_6]^{3-}$ complex anions, uncoordinated Cl^- anions and a water of crystallization. Figure 3.4 illustrates the asymmetric structural unit cell with an atomic numbering scheme. The Rh atom in the complex anion resides in an octahedral environment consisting of six chlorine atoms. The average Rh-Cl bond length was established as 2.3503 (± 0.0075) Å. This bond length is consistent with that documented by Frank *et al* [25], who reported an average Rh-Cl bond length of 2.3497 (± 0.0071) Å in the diethylenetriammonium hexachlororhodate(III), (**Deta**H_3)$[RhCl_6]$, crystal structure. The maximal deviation of the bond angles from 90° is 1.63° in the *cis* position and 1.59° in the *trans* position, implying that the Rh atom resides in an octahedral environment. The intermolecular contacts between the $[RhCl_6]^{3-}$ complex anions was found to be 6.260 Å.

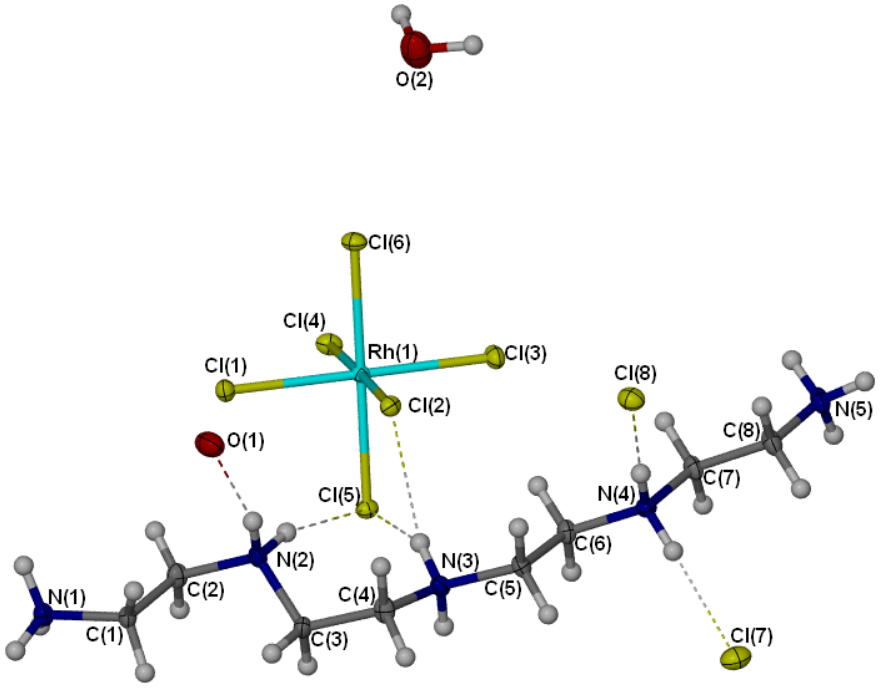

Figure 3.4: Asymmetric unit cell of (**Tepa**H_5)$[RhCl_6]Cl_2 \cdot 2H_2O$ with atomic numbering scheme

In the $[$**Tepa**$H_5]^{5+}$ cation, the average values of the N - C and C - C distances were established to be 1.490 Å and 1.517 Å, respectively; while the N - C - C bond angles were

found to vary from 107.41° to 114.38°, Table 3.7. These values were found to be consistent with that documented in literature for diethylenetriammonium hexachlororhodate(III), (**Deta**H_3)[$RhCl_6$], [24] and diethylenetriammonium hexachloroplatinate(IV) chloride, (**Deta**H_3)[$PtCl_6$]Cl, [25]. The packing arrangement of ions along the *c*-axis is illustrated in Figure 3.5.

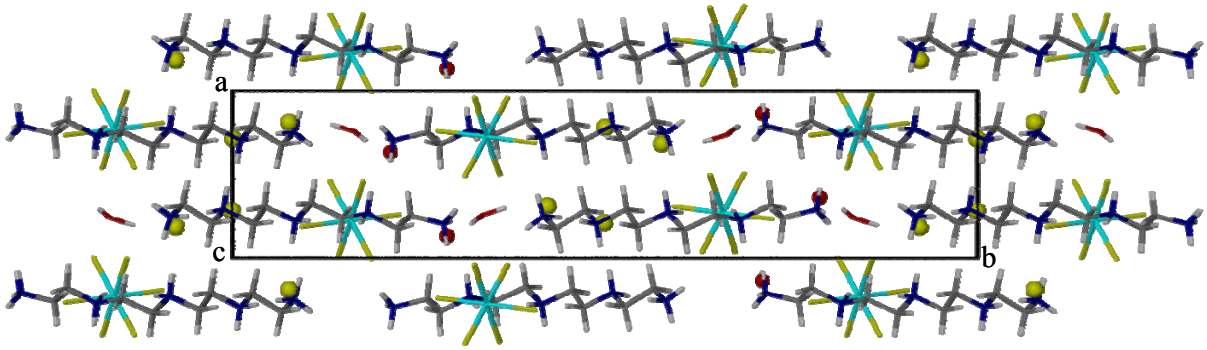

Figure 3.5: Extended crystal packing of ions viewed along the direction of the c-axis, from which it is evident that water molecules are entrained within the crystal packing arrangement

Table 3.6: Atomic coordinates and equivalent isotropic displacement parameters, U_{eq} (Å^2), of all the non-hydrogen atoms for (**Tepa**H_5)[$RhCl_6$]Cl_2·$2H_2O$

Atom	*x*	*y*	*z*	U_{eq}
Rh(1)	0.22835(12)	0.15849(13)	0.59312(11)	0.0106(13)
Cl(1)	0.4596(2)	0.13076(7)	0.73958(13)	0.0133(9)
Cl(2)	0.19041(2)	0.09376(15)	0.48522(1)	0.017(7)
Cl(3)	-0.00624(4)	0.18688(12)	0.45078(8)	0.0166(9)
Cl(4)	0.26223(6)	0.22422(3)	0.69944(4)	0.0145(5)
Cl(5)	0.00213(15)	0.14133(11)	0.75518(15)	0.0137(12)
Cl(6)	0.46161(9)	0.17517(10)	0.43933(17)	0.0159(10)
Cl(7)	0.81394(8)	0.07668(4)	0.04317(13)	0.0234(12)
Cl(8)	0.71505(13)	0.0006(14)	0.72752(12)	0.0193(12)
O(1)	0.13442(17)	0.28844(18)	0.46693(18)	0.0269(17)
O(2)	0.76(14)	0.16354(1)	0.16812(10)	0.0386(10)
N(1)	0.20755(13)	0.28384(10)	1.18763(12)	0.0146(14)
N(2)	0.26768(12)	0.18123(13)	1.00724(12)	0.0144(12)
N(3)	0.22539(12)	0.08457(10)	0.96508(11)	0.0134(12)
N(4)	0.29264(13)	-0.01067(12)	0.75151(14)	0.0137(13)
N(5)	0.24745(16)	-0.08182(11)	0.44975(11)	0.0186(11)
C(1)	0.25547(5)	0.23888(4)	1.17632(8)	0.0147(6)
C(2)	0.18029(2)	0.22237(4)	1.04275(13)	0.016(10)
C(3)	0.24177(6)	0.14791(4)	1.11291(8)	0.0163(8)
C(4)	0.32718(8)	0.10632(5)	1.07853(7)	0.0168(4)
C(5)	0.30799(5)	0.04363(3)	0.92642(6)	0.0139(7)
C(6)	0.20698(6)	0.02897(5)	0.79753(7)	0.015(4)
C(7)	0.21257(2)	-0.02629(3)	0.62116(7)	0.0161(8)
C(8)	0.31969(1)	-0.06569(5)	0.58185(8)	0.0184(9)

Table 3.7: Selected interatomic distances, *d* (Å), and angles, *ω* (deg), for tetraethylenepentammonium aqua hexachlororhodate(III) dichloride, (**Tepa**H_5)[$RhCl_6$]$Cl_2 \cdot H_2O$

Bond	*d* / Å	Angle	*ω* / deg	Angle	*ω* / deg
Rh(1) - Cl(1)	2.3512(4)	Cl(1) - Rh(1) - Cl(3)	178.73(1)	N(2) - C(2) - C(1)	111.51(4)
Rh(1) - Cl(2)	2.3398(5)	Cl(1) - Rh(1) - Cl(2)	91.23(3)	N(1) - C(7) - C(2)	108.98(3)
Rh(1) - Cl(3)	2.3518(8)	Cl(1) - Rh(1) - Cl(2)	89.62(3)	N(2) - C(3) - C(4)	114.38(3)
Rh(1) - Cl(4)	2.3582(6)	Cl(6) - Rh(1) - Cl(1)	88.95(2)	N(3) - C(5) - C(6)	107.41(1)
Rh(1) - Cl(5)	2.362(2)	Cl(5) - Rh(1) - Cl(6)	177.72(5)	N(4) - C(6) - C(5)	108.99(4)
Rh(1) - Cl(6)	2.3391(3)	Cl(5) - Rh(1) - Cl(4)	88.37(3)	N(3) - C(4) - C(3)	112.63(3)
N(1) - C(1)	1.4815(1)	Cl(5) - Rh(1) - Cl(1)	88.86(1)	N(4) - C(7) - C(8)	108.02(3)
N(2) - C(2)	1.5688(3)	Cl(5) - Rh(1) - Cl(3)	90.17(3)	N(5) - C(8) - C(7)	109.91(1)
N(2) - C(3)	1.5043(4)	Cl(5) - Rh(1) - Cl(2)	91.59(4)		
N(3) -C(4)	1.496(4)	Cl(6) - Rh(1) – Cl(4)	90.98(3)		
N(3) - C(5)	1.4882(8)	Cl(4) - Rh(1) – Cl(2)	89.79(2)		
N(4) - C(7)	1.4853(4)	Cl(6) - Rh(1) – Cl(3)	91.01(4)		
N(4) - C(6)	1.4821(4)	Cl(6) - Rh(1) - Cl(2)	89.11(3)		
N(5) - C(8)	1.4861(7)	Cl(4) - Rh(1) - Cl(3)	89.36(3)		
C(1) - C(2)	1.517(5)	Cl(4) - Rh(1) - Cl(2)	178.98(2)		
C(3) - C(4)	1.5041(3)	C(2) - N(2) - C(3)	113.63(2)		
C(5) - C(6)	1.5255(7)	C(6) - N(4) - C(7)	113.41(1)		
C(7) -C(8)	1.52796(2)	C(5) – N(3) - C(4)	114.19(4)		

3.3.4 Precipitation of Pt^{IV}, Rh^{III} chlorido-complexes from synthetic solutions containing both metals: Is selectivity possible?

Figure 3.6 illustrates the results obtained for the precipitation titrations of Pt^{IV}, present in a solution containing equimolar amounts of Pt^{IV} and Rh^{III}, as a function of increasing (poly)amine concentration. It is evident that **Teta**, **Tepa** and **Tren** is effective toward the precipitation of Pt^{IV} from aqueous solution, with 90 – 97% of Pt removed at [precipitant]:[metal chloride anion] ratios > 15. However, quantitative precipitation (> 98% removal) of Pt is only attained when using **Teta** as precipitant.

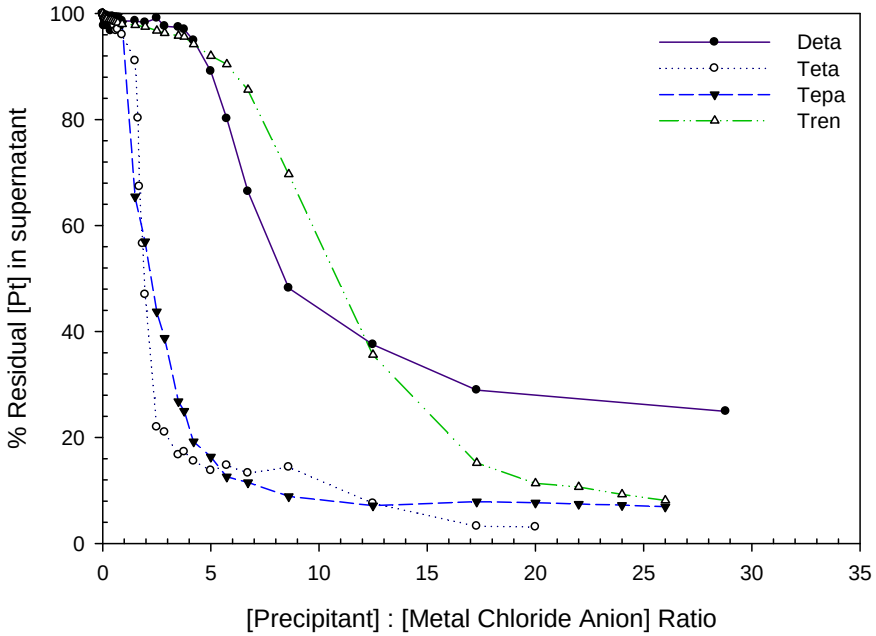

Figure 3.6: Residual [Pt] in the supernatant as a function of increasing [Precipitant]:[Metal chloride anion] ratio. [Pt] = 7.813 mM; [HCl] = 6.0 M. The precipitants used are denoted in the legend. Typical RSD values was below 7%.

The trend observed for the precipitation of Rh from a solution containing equimolar amounts of Pt^{IV} and Rh^{III} is illustrated in Figure 3.7. It is evident from Figure 3.7 that all the (poly)amines used in this study are highly efficient toward the precipitation of Rh^{III}, with 80% of the total Rh removed at a [precipitant]:[metal chloride anion ratio] of 1. Quantitative precipitation (> 98%) of Rh can be achieved at a [precipitant]:[metal chloride anion] ratio of 2.

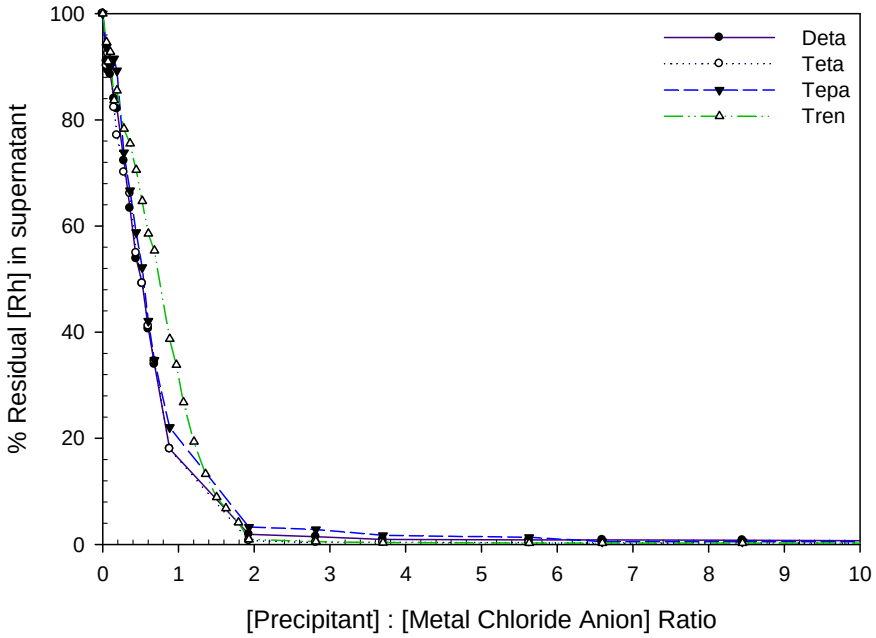

Figure 3.7: Residual [Rh] in the supernatant as a function of increasing [Precipitant]:[Metal chloride anion] ratio. [Rh] = 7.956 mM; [HCl] = 6.0 M. The precipitants used are denoted in the legend. Typical RSD values was below 7%.

Figure 3.8[a] - [f] compares the results obtained for the precipitation of Pt^{IV} and Rh^{III} from a solution containing both these metals in equimolar concentrations. The results of Lupamin® 1595 and the ethylenimine oligomer mixture are included for comparison, although the results cannot be accurately reproduced due to the formation of a colloidal suspension. Regarding the selectivity of the amines utilised during this study, only **Deta** and **Tren** can be considered as being selective toward the preferential precipitation of Rh^{III} above Pt^{IV}, Figure 3.8[a] and [d]. In the case of **Teta** and **Tepa**, Pt^{IV} is precipitated to a significant extent at a [precipitant]:[metal chloride anion] ratio of 2, with almost 50% of $[PtCl_6]^{2-}$ precipitated in both instances. However, when utilising **Deta** or **Tren** as the precipitating agent, less than 3% of the total Pt is precipitated at a [precipitant]:[metal chloride anion] ratio of 2. Furthermore, **Tren** allows for the addition of greater amounts of the precipitant, since Pt is not precipitated to any significant extent up to a [precipitant]:[metal chloride anion] ratio of 7, at which point Rh is quantitatively removed (> 98%), Figure 3.8[d].

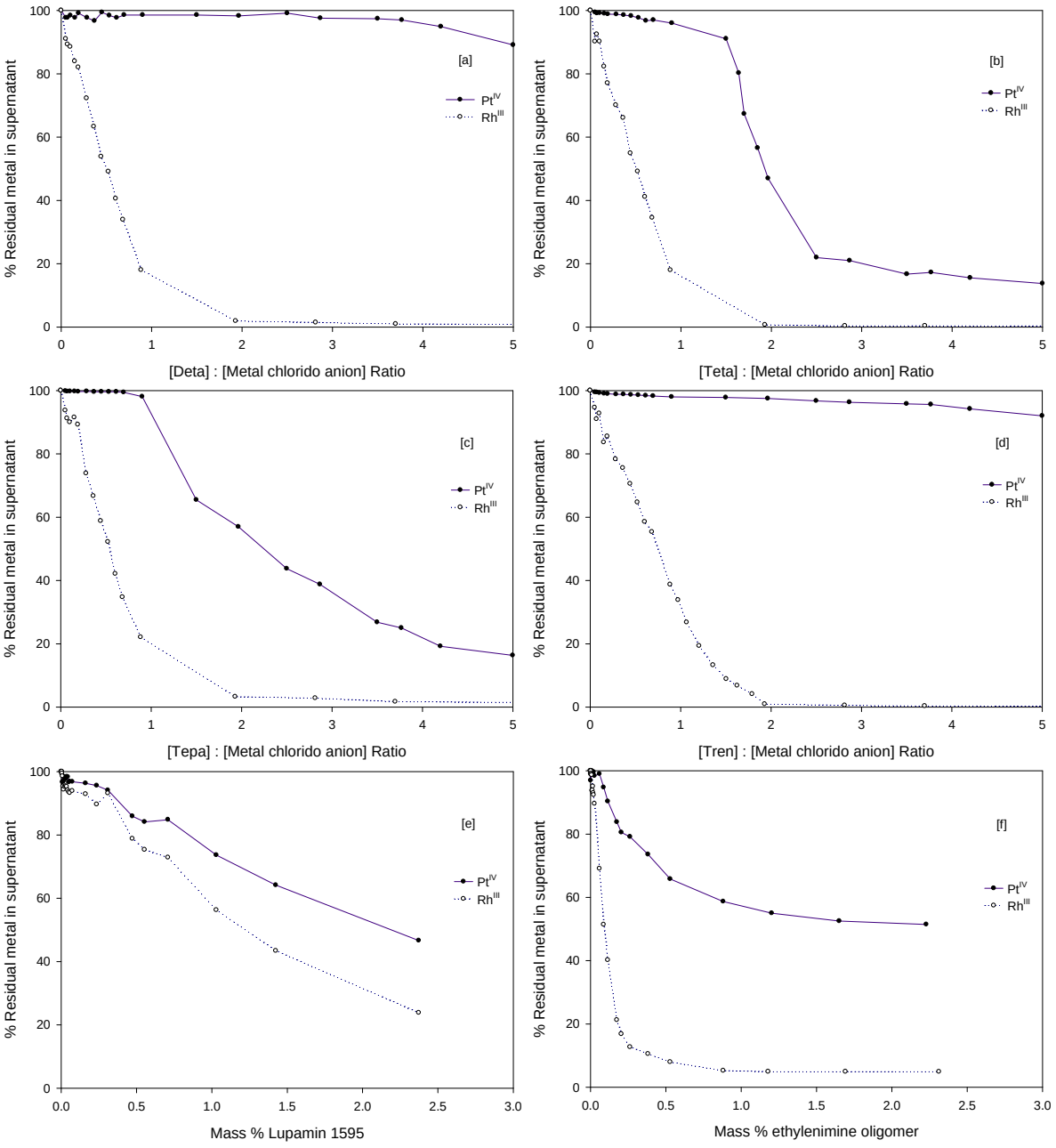

Figure 3.8: Comparison between the Pt – and Rh –precipitant titrations conducted for all the (poly)amines screened. [Pt] = 7.813 mM; [Rh] = 7.956 mM; [HCl] = 6.0 M

The selectivity factors of the (poly)amines **Deta**, **Teta**, **Tepa** and **Tren** toward the precipitation of Rh^{III} and Pt^{IV} were determined as a function of increasing (poly)amine concentration. During these precipitation investigations, the $[Pt^{IV}] / [Rh^{III}]$ ratio was varied while the total metal (Pt + Rh) concentration was kept constant. This enables us to ascertain which of the precipitants investigated is more selective toward the preferential precipitation of Rh^{III} in solutions containing a mixture of Pt^{IV} and Rh^{III}. The selectivity factor, β, is given

by $\beta = [Pt^{IV}] / [Rh^{III}]$. **Tren** exhibits the greatest selectivity for the preferential extraction of Rh^{III}, while **Tepa** is considered the least selective precipitant, Figure 3.9.

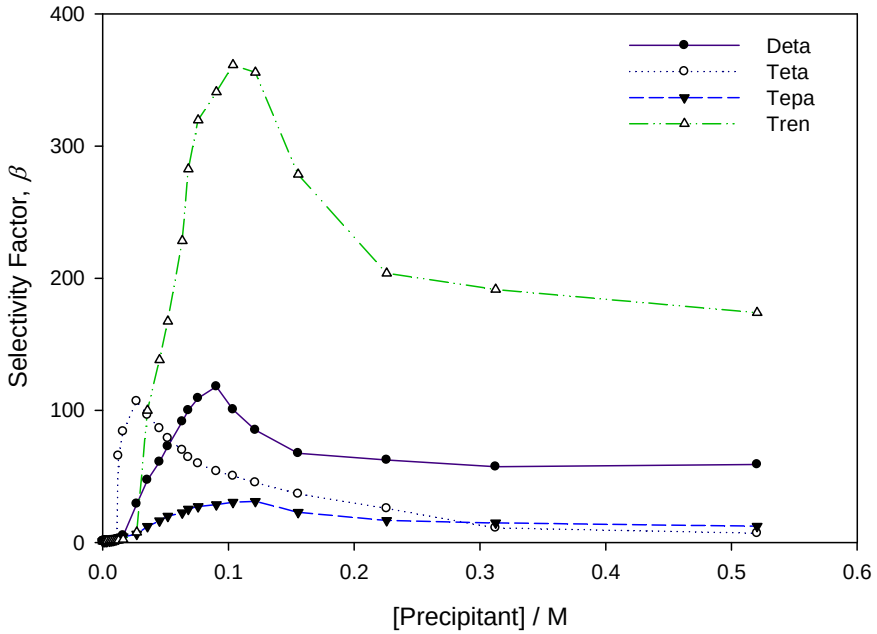

Figure 3.9: Selectivity factor, β, as a function of increasing precipitant concentration. Typical RSD values was below 7%

3.3.5 Precipitation of Pt and Rh from an authentic Heraeus industrial feed solution

The precipitation results presented so far demonstrate that quantitative and selective precipitation of Rh^{III} and Pt^{IV} is possible with the organic precipitants **Deta**, **Teta**, **Tepa** and **Tren**. However, this was only the case when applied to well-defined solutions, *i.e.* the respective Rh^{III} and Pt^{IV} chlorido-complexes are known. In this section, precipitation studies involving the use of authentic industrial process solutions containing PGMs as well as an array of associated transition metals (Table 3.2) will be examined. In this regard, only the relative amounts of each element in the industrial process solution is known, with no additional information relating to the chemical speciation of these elements. In spite of the lack of speciation information, precipitation studies were performed using an "unaltered" (*i.e.* no additional processing of this solution was performed) PGM-containing industrial feed solution

It is well established that the chemical speciation of PGM chlorido-complexes is of critical importance for the efficient separation and refining of PGMs [26-29]. In the case of Pt, the efficiency of the industrial separation schemes are strictly dependent on the knowledge and control of the species distribution of Pt^{IV} anionic chlorido-complexes in solution since, depending on the conditions, aquated $[PtCl_n(H_2O)_{6-n}]^{4-n}$ (n=0-6) complexes or even their hydrolysis products, $[PtCl_{6-n}(OH)_n]^{2-}$ (n=0-6) might be present. In this context, ^{195}Pt NMR spectroscopy was used to evaluate the speciation of Pt^{IV} chlorido-complexes present in a Heraeus industrial PGM containing feed solution in 4.008 M chloride matrix.

The ^{195}Pt NMR spectrum of the industrial feed solution is shown in Figure 3.10. Although various spectral windows were scanned, only one resonance signal was obtained at 25.5 ppm relative to a standard external Pt reference. The assignment of the signal is based on the detailed analysis of the $^{35}Cl/^{37}Cl$ isotope effects observed in 128.8 MHz ^{195}Pt NMR, which shows that the “fine-structure” of this resonance signal can be understood in terms of the unique isotopologue distribution of $[PtCl_6]^{2-}$ [26]; a topic that will be discussed in Chapter 5.

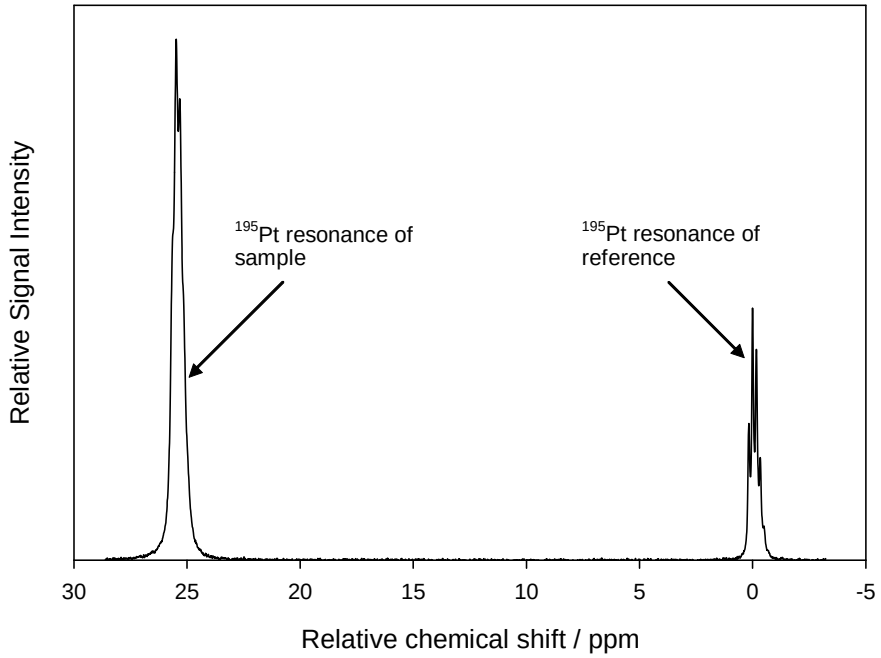

Figure 3.10: ^{195}Pt NMR spectrum of an authentic industrial feed solution

Through high-resolution ^{195}Pt NMR studies, it was shown that the Pt present in the feed solution exists only as the $[PtCl_6]^{2-}$ complex anion, and it is thus expected that the precipitation of Pt from the feed solution should provide similar trends to that observed for the laboratory prepared Pt containing solutions. Figure 3.11 illustrates the results obtained for the precipitation of Pt using the denoted organic precipitants. These trends are similar to that observed for the precipitation of Pt from a laboratory prepared mixed metal solution, Section 3.3.3. Quantitative precipitation of Pt (> 98%) is only achieved with **Teta** and **Tren**, at a [precipitant]:[metal chloride anion] ratio > 8. Furthermore, the titration curve obtained for Pt – **Teta** illustrates two end-points, which is consistent with the observations made in Section 3.3.1. Although vast excess of precipitant was used (in some instances up to 50 times excess) quantitative Pt removal could not be attained when using **Deta** and **Tepa** as precipitants, with only 85% of Pt removed when using **Deta** and 78% when using **Tepa**.

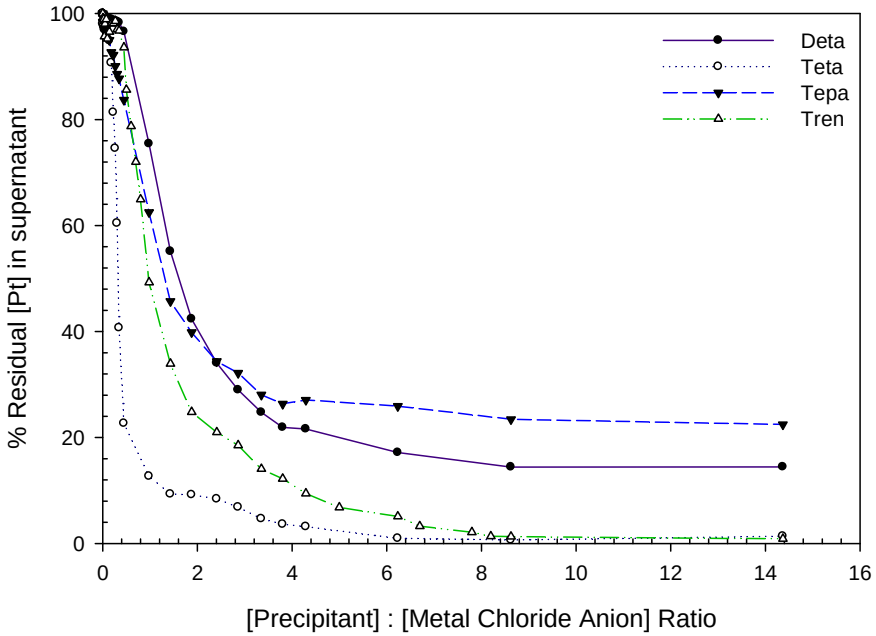

Figure 3.11: Residual [Pt^{IV}] in the supernatant as a function of increasing [Precipitant]:[Metal chloride anion] ratio. [Pt] = 18.68 mM; [Cl^-] = 4.008 M. Typical RSD values was below 7%

Figure 3.12 illustrates the results obtained for the precipitation of Rh^{III} using the denoted organic precipitants. The difference between the titration curves obtained for the industrial solutions and that of the laboratory prepared solutions is blatantly visible - quantitative precipitation of Rh from the industrial feed solution *could not* be achieved, irrespective of the type of precipitant or the amount thereof used. In all the cases, only 75.4% of the total Rh initially present was removed, Figure 3.12. This implies that 8.011 mM (824.4 $mg.L^{-1}$) of the total Rh (33.38 mM, 3435 $mg.L^{-1}$) initially present remains in the supernatant. This is in stark contrast to the results presented in Sections 3.3.1 and 3.3.3. These titrations were repeated using an industrial feed solution that was heated at 333.1 K for three days, in order to facilitate chloride anation of aquated Rh^{III} species, $[RhCl_n(H_2O)_{6-n}]^{3-n}$ (n=0-4). However, heat treatment did not provide an improvement in Rh precipitation, with only 78.6% of the total Rh initially present being removed, Figure 3.13.

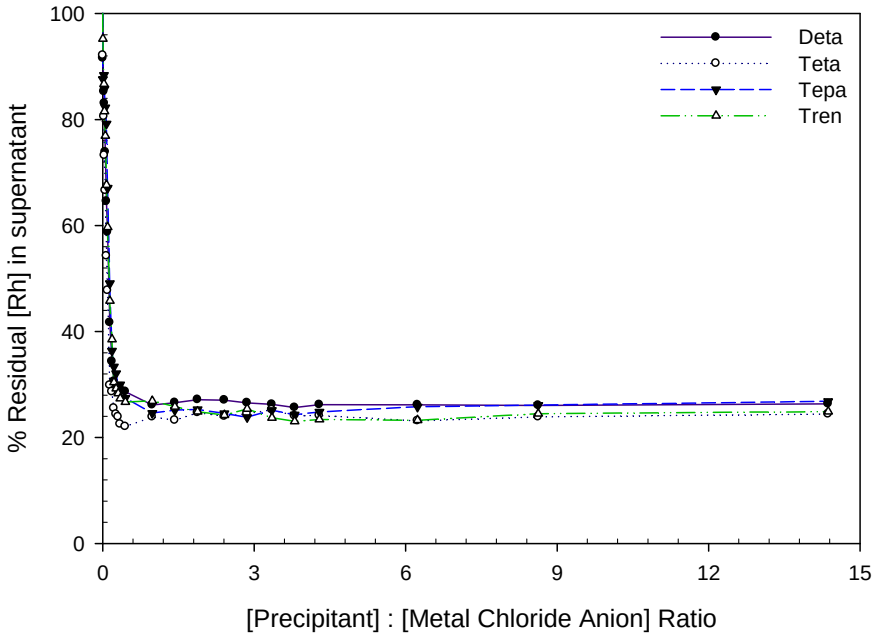

Figure 3.12: Residual [Rh^{III}] in the supernatant as a function of increasing [Precipitant]:[Metal chloride anion] ratio. [Rh] = 3.871 mM, [Cl^-] = 4.008 M. Typical RSD values was below 7%

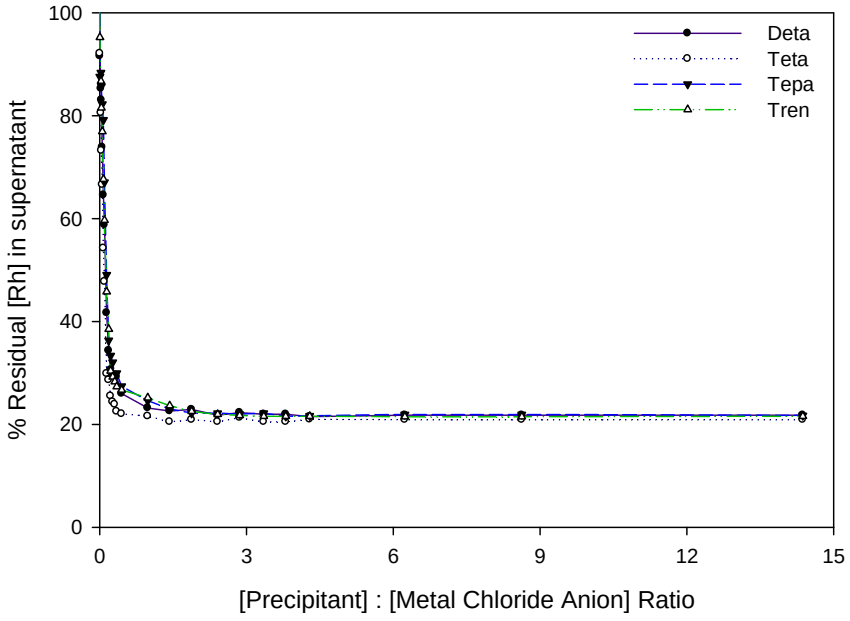

Figure 3.13: Residual [Rh^{III}] in the supernatant as a function of increasing [Precipitant]:[Metal chloride anion] ratio. Precipitation was repeated after the industrial feed solution was heated for 3 days at 333.1 K. [Rh] = 3.871 mM, [Cl^-] = 4.008 M. Typical RSD values was below 7%

This raises the question: What gives rise to the trends observed in Figure 3.12 and 3.13? Several explanations for these trends could be hypothesized, including:

(*i*) *Matrix interferences encountered during the quantification of Rh that may cause enhancement of the analyte signal.*

This possibility was easily eliminated by means of standard addition methods, where the industrial feed stock solution was "spiked" with known quantities of a standard Rh elemental reference. In this method, one portion of the industrial feed solution was measured as usual by ICP-OES. To the second portion of the feed solution, a known amount of the Rh elemental reference standard was added. The difference between the measured concentrations of the first and second portions constantly yielded the amount of Rh reference added to the solution. Furthermore, portions of the industrial feed solution were submitted for ICP-MS analysis (Central Analytical Facility – Stellenbosch University), the results of which was found to be consistent to that reported in this study.

(*ii*) *Rh^{III} aqua chlorido-species distribution*

A parameter that is very difficult to ascertain due to the complicated nature of the industrial feed solution, combined with the limited number of analytical techniques available to conduct comprehensive chemical speciation investigations. Although the total chloride concentration of the industrial feed solution was determined at 4.008 M, the free (unbound) chloride concentration is presumed to be significantly lower than this value; a conclusion validated by the indifference in the precipitation results after heat treatment (used to facilitate chloride anation) of the industrial feed solution. This lower free chloride concentration would result in the formation of higher aquated Rh^{III} chlorido-complexes, $[RhCl_n(H_2O)_{6-n}]^{3-n}$ (n=0-4), which are not precipitated. The low free chloride concentration is attributed to the presence of various transition metals Table 3.2, which would exist as their chlorido-complexes. In this regard, these metals would effectively act as "chloride binders", thereby decreasing the effective "free" (unbound) chloride concentration.

3.4 Concluding remarks

In summary, a recovery method for Rh and Pt, based on precipitation is proposed using various commercially available organic precipitants including **Deta**, **Teta**, **Tepa**, **Tren**, Lupamin® 1595, Lupamin® 9030 and polyethylenimine. Lupamin® 1595, Lupamin® 9030 and polyethylenimine produce a colloidal suspension upon addition to PGM containing solutions, resulting in poor reproducibility due to inconsistent separation of the aqueous/solid phases. The organic precipitants illustrating the greatest selectivity for Rh recovery included **Deta** and **Tren**, while **Teta** illustrated greater selectivity toward the precipitation of Pt. Moreover, it was found that both Rh and Pt could be recovered quantitatively from laboratory prepared Rh^{III} and Pt^{IV} containing solutions.

The first $[RhCl_6]^{3-}$ crystal structure involving the quintuply charged tetraethylenepentammonium cation, $[\mathbf{Tepa}H_5]^{5+}$, has been reported. The tetraethylene-pentammonium diaqua hexachlororhodate(III) dichloride complex, $(\mathbf{Tepa}H_5)[RhCl_6]Cl_2{\cdot}2H_2O$, illustrates a monoclinic crystal system with a $P21/n$ space group. Crystal data for the $C_8H_{31}Cl_8N_5O_2Rh$ complex was found to be $a = 7.1601(4)$ Å, $b = 31.9491(17)$ Å, $c = 9.8711(5)$ Å, $\beta = 91.057(1)°$, $\rho_{calc} = 1.812$ g.cm-3, $V = 2257.7(2)$ Å^3.

Precipitation of Pt from an unaltered industrial feed solution using the organic precipitants **Deta**, **Teta**, **Tepa** and **Tren** yielded similar results to that of the laboratory prepared Pt-containing solutions. This is attributed to the fact that the Pt present in the feed solution exists solely as the $[PtCl_6]^{2-}$ complex anion, which was confirmed by means of high-resolution ^{195}Pt NMR spectroscopy. Assignment of the ^{195}Pt resonance was based on the detailed analysis of the ^{35}Cl/^{37}Cl isotope effects observed in the 128.8 MHz ^{195}Pt NMR resonance of the $[Pt^{35}Cl_n{}^{37}Cl_{6-n}]^{2-}$ complex anion. The presence of resonances associated with aquated $[PtCl_n(H_2O)_{6-n}]^{4-n}$ (n=4-6) species were not observed in the ^{195}Pt NMR spectrum that was recorded.

Quantitative precipitation of Rh from an industrial feed solution using the aforementioned organic precipitants was not attained. The maximum Rh content recovered from the feed solution was 78.6% for all the precipitants investigated. This is in stark contrast to the results obtained when laboratory prepared Rh-containing solutions were used. Matrix

interference as a possible source of inaccurate Rh analysis, and consequently poor recovery from the industrial feed solution, was eliminated by the use of spike recovery. The current hypothesis for the large discrepancy seen in recovery is attributed to the presence of higher aquated Rh species, $[RhCl_n(H_2O)_{6-n}]^{3-n}$ (n=0-4), in the feed solution due to low free chloride concentration. Although the total chloride concentration in the feed solution is 4.008 M, the free chloride concentration is significantly lowered due to the presence of various metal ions, presumably present as their respective chlorido-complexes. Unfortunately, traditional analytical techniques (including polarography, UV-vis and hyphenated HPLC techniques) have limited capabilities, especially pertaining to the chemical speciation of metal ion complexes in complicated, acidic chloride-rich matrices. Transition metal (^{103}Rh) NMR spectroscopy has emerged as a powerful analytical tool for the *direct* detection, unambiguous characterisation and chemical speciation of transition metal complexes, without altering the chemical composition of a solution.

3.5 References

[1] H. Narita, K. Morisaku, M. Tanaka, *Chem. Commun.* (2008) 5921

[2] A. A. Mhaske, P. M. Dhadke, *Hydrometallurgy* **61** (2001) 143

[3] A. A. Mhaske, P. M. Dhadke, *Hydrometallurgy* **63** (2002) 143

[4] G. Levitin, G. Schmuckler, *React. & Funct. Polym.* **54** (2003) 149

[5] S. N. Ashrafizadeh, G. P. Demopoulos, *J. Chem. Tech. Biotechnol*. **67** (1996) 367

[6] N. G. Afzaletdinova, Yu. I. Murinov, Sh. Yu. Khazhiev, S. O. Bondareva, R. R. Muslukhov, *Zhurnal Neorganicheskoi Khimii*, **55** (2008) 481

[7] R. J. Warr, A. N. Westra, K. J. Bell, J. Chartres, R. Ellis, C. Tong, T. G. Simmance, A. Gadzhieva, A. J. Blake, P. A. Tasker, and M. Schröder, *Chem. Eur. J.*, **15** (2009) 4836

[8] J. G. H. Du Preez and U. Naidoo*, Solvent Extraction and Ion Exchange*, **23** (2005) 439

[9] L.G. Floyd, in: *2nd International Conference on New Process for Ruthenium, Rhodium and Iridium*, Int. Precious Metals Institute Inc., New York (1978)

[10] R.M. Izatt, J.S. Bradshaw, R.L. Bruening, N.E. Izatt, K.E. Krakowiak, in: K.C. Liddell, D.J. Chaiko (Eds.), *Metal Separation Technologies beyond 2000: Integrating Novel Chemistry with Processing*, Symposium Proceeding, Hawaii, June 13–18, TMS (1999) 357

[11] W. D. Crozier, R. A. Grant, Johnson Matthey PLC. *UK Patent 2 247 888A* (1992)

[12] Alessandro De Robertis, Claudia Foti, Ottavia Giuffre` , and Silvio Sammartano; *J. Chem. Eng. Data* **46** (2001) 1425

[13] Concetta De Stefano, Ottavia Giuffrè and Silvio Sammartano; *J. Chem. Eng. Data* **50** (2005) 1917

[14] *S.* A. Johnson and F. Basolo, *Inorg. Chem.*, I, (1962) 925

[15] *S.* Zipp, A. P. Zipp and S.K. Madan. *Coord. Chem. Rev*., **14** (1974) 29.

[16] S. G. Zipp and S. K. Madan, *Inorg. Nucl. Chem.* (1974) 221

[17] S. Ci. Zipp and S. K. Madan; *Inorg. Chim. Acta,* **14** (1975) 83-86

[18] Lupamin® 1595 & Lupamin® 9030, Technical data sheet, BASF corporation (2010)

[19] R. H. Blessing, *Acta Crystallogr.* **A51** (1995) 33-38

[20] G. M. Sheldrick, *SHELXS-97 & SHELXL-97*, University of Göttingen, Germany

[21] L. J. Barbour, *J. Supramol. Chem.* **1** (2001) 189

[22] J. L. Atwood, L. J. Barbour, *Cryst. Growth Des.* **3** (2003) 3

[23] S. M. Cohen, T. H. Brown, *J. Chem. Phys.* **61** (1974) 2985

[24] W. Frank and G. Reiβ, *Z. anorg. Allg. Chem.*, **622** (1996) 729

[25] E. V. Makotchenko, I. A. Baidina, and S. A. Gromilov, *Zhurnal Strukturnoi Khimii*, **48** (2007) 1222

[26] W. J. Gerber, P. Murray and K. R. Koch, *Dalton Trans.* (2008) 4113

[27] G. Schmuckler, *US patent 4 885 143*, United States of America (1989)

[28] G. Schmuckler, B. Limoni-Relis, *Sep. Sci. Technol*, **30** (1995) 337

[29] F. L. Bernardis, R. A. Grant and D. C. Sherrington, *React. Funct. Polym.*, **65** (2005) 205

Chapter 4

$^{35}Cl/^{37}Cl$ isotope effects in ^{103}Rh NMR of $[RhCl_n(H_2O)_{6-n}]^{3-n}$ complexes in hydrochloric acid solution as a unique 'NMR finger-print' for unambiguous characterization†

4.1 Introduction

South Africa is the world's leading primary producer of the platinum group metals (PGMs, Pt, Pd, Rh, Ru, Ir and Os), contributing more than three quarters of the world's supply of rhodium (>86%) and platinum (>76%), in addition to a significant proportion of the associated metals in 2009 [1]. The strong commercial demand for Rh, used almost exclusively in catalytic applications for automobile exhaust emission control systems as well as in the chemical industry, has resulted in this metal being one of the most expensive, with average prices per troy ounce of Rh ranging between 1592 and 6564 US$ in the years 2006–2009 [1].

In the context of the PGM refining industry, we have been applying methods for chemical speciation [2] to study PGM complexes in aqueous hydrochloric acid solutions as relevant to the separation and recovery of these metals as complex anions, *inter alia* by means of high-resolution ^{195}Pt nuclear magnetic resonance (NMR) spectroscopy [3]. Nuclear magnetic resonance spectroscopy is a powerful tool for direct speciation of the kinetically inert $[PtX_n(H_2O)_{6-n}]^{4-n}$ [4], as well as the corresponding hydroxido $[PtX_n(OH)_{6-n}]^{2-}$ ($X = Cl^-$ and Br^-) complex anions [5]. Recently, a novel ^{195}Pt NMR method was developed for the unambiguous speciation of $[PtCl_n(H_2O)_{6-n}]^{4-n}$ (n = 4–6) by exploiting the unique $^{35}Cl/^{37}Cl$ isotope effects visible in the ^{195}Pt NMR resonances obtained at high magnetic fields (14.08 T) in acidic solutions [6]. At high magnetic fields and controlled solution temperature, the ^{195}Pt NMR resonances of $[PtCl_n(H_2O)_{6-n}]^{4-n}$ (n = 4–5) show well resolved 'fine-structure' due the

† This chapter is based on the publication: T. E. Geswindt, W. J. Gerber, D. J. Brand, K. R. Koch, *Analytica Chimica Acta*, **730** (2012) 93-98

various possible isotopologues and isotopomers as a result of the natural $^{35}Cl/^{37}Cl$ isotopic distribution unique to each individual Pt^{IV} complex in solution, resulting in an unambiguous ^{195}Pt NMR 'finger-print' for each complex [6].

The nucleus of rhodium naturally occurs only as a single NMR active isotope ^{103}Rh ($I = (^1/_2)$), which has unfortunately a small negative gyromagnetic ratio (γ), and consequently a low resonance frequency Ξ = 3.16 MHz (requiring a special low-frequency NMR probe) relative to ^1H at 100.00 MHz. Moreover the relatively low overall ^{103}Rh NMR receptivity[4] of 0.186, makes routine ^{103}Rh NMR difficult and it is thus not widely practiced. With the more general availability of high magnetic field (>9.04 T) NMR spectrometers with higher sensitivity, ^{103}Rh NMR becomes potentially an attractive tool for speciation of complexes in process and effluent solutions relevant to the PGM refining industry, in which relatively high Rh concentrations may be found, particularly with the aim of developing novel and better separation and recovery methods given the high commercial value of rhodium. A survey of the literature shows only few NMR studies by directly detected ^{103}Rh NMR, particularly in aqueous solutions. On the other hand, if the Rh atom in a given molecule is bound to a nucleus with a high NMR receptivity, *e.g.* ^1H or ^{31}P, then modern indirectly detected NMR methods make the observation of ^{103}Rh spectroscopy more practically useful. The applications of ^{103}Rh NMR in rhodium chemistry have recently been reviewed [7].

Early work involving directly detected ^{103}Rh NMR is limited to the characterization of all ten $[RhCl_{6-x}Br_x]^{3-}$ (x = 0–6) anions [8], as well as some of the possible aquated species $[RhCl_n(H_2O)_{6-n}]^{3-n}$ (n = 0–6) by Mann and Spencer [9], as later confirmed by Sandström *et al.* [10]; nevertheless these studies demonstrate that ^{103}Rh NMR may be a viable tool for examining solutions of relevance to the refining industry, with potentially useful chemical data being obtainable by this means, exemplified by Glaser and Sandström who used ^{103}Rh NMR to examine the deceptively simple Rh^{III} chemistry in aqueous solutions rich in bromide ions [11]. These authors also examined some octahedral Rh^{III} complexes with sulfur-donor ligands, as well as complexes such as $[Rh(CN)_6]^{3-}$ and $[Rh(SCN)_6]^{3-}$ by ^{103}Rh NMR [12]. The latter study is interesting in that Glaser and Sandström postulate a direct correlation between the $\delta(^{103}Rh)$ chemical shift and the relevant thermodynamic formation constants ($\log \beta_6$) of such complexes. This suggests ^{103}Rh NMR to be a method for the estimation of

[4] Receptivity of ^{13}C at natural abundance is 1, and ^1H at 5870

the formation constants from δ(^{103}Rh) NMR, a conclusion which in our view, must be treated with some caution at this time. While these studies indicate that ^{103}Rh NMR spectroscopy can be used to identify various complex species such as $[RhCl_n(H_2O)_{6-n}]^{3-n}$ and $[RhBr_n(H_2O)_{6-n}]^{3-n}$ in aqueous solutions by their δ(^{103}Rh) chemical shift, the relatively high temperature, concentration and matrix dependence of δ(^{103}Rh) chemical shifts observed in these studies [9–12], makes the unambiguous identification (speciation) of rhodium complexes in such solutions under differing conditions uncertain, and rapid accurate assignments tedious.

In this study it is shown that at high magnetic fields with carefully controlled solution temperatures, the 19.11 MHz ^{103}Rh NMR signals of the series of $[RhCl_n(H_2O)_{6-n}]^{3-n}$ (n = 3-6) complexes in equilibrated hydrochloric acid solutions, are well resolved into a distinctive 'fine-structure' due to ^{35}Cl/^{37}Cl isotopologue and isotopomer effects, resulting in a unique NMR 'finger-print', with which it is possible to uniquely identify all chlorido containing Rh^{III} complexes. By this method the identity of the Rh^{III} complex can readily be obtained from the fine-structure of the ^{103}Rh peaks, without reference to accurate ^{103}Rh NMR chemical shifts. This is potentially a considerable advantage, given the absence of a convenient and universal reference compound for ^{103}Rh NMR [7]. Considerable experimental error is encountered when attempting to measure δ(^{103}Rh) chemical shifts, which can vary by as much as ± 129 ppm for even the 'simple' $[RhCl_6]^{3-}$ species [10]. Moreover, the relatively small δ(^{103}Rh) difference of 66 ppm between two Rh^{III} complex isomers such the *trans*-$[RhCl_2(H_2O)_4]^+$ and *cis*-$[RhCl_2(H_2O)_4]^+$ cations, makes it virtually impossible to reliably distinguish between this and other isomers in solution, on the basis of δ(^{103}Rh) chemical shifts alone. This emphasizes a need for a rapid additional means of unambiguously characterizing $[RhCl_n(H_2O)_{6-n}]^{3-n}$ (n=0-6) complexes, including possible *cis/trans* and *fac/mer* isomers, by means of ^{103}Rh NMR in solution.

4.2 Experimental

4.2.1 Preparation of Rh^{III} complex solutions

Two solutions of 0.86 M $[RhCl_n(H_2O)_{6-n}]^{3-n}$ (n = 3–6) were prepared by dissolving *ca* 0.9 g of commercially available $RhCl_3 \cdot nH_2O$ (Johnson Matthey) in 3.5 mL 29% ($^{v}/_{v}$) $^{2}H_2O/^{1}H_2O$ containing the appropriate quantity of concentrated (32% $^{v}/_{v}$) HCl: (*solution 1* = 6.02 M HCl, 0.868 M Rh; *solution 2* = 1.03 M HCl, 0.867 M Rh). These solutions were kept covered at 333 K for a week and thereafter allowed to equilibrate at 292 K for a further 5 days. The total rhodium and chloride concentration of these solutions was determined by means of ICP-OES (SPECTRO Arcos instrument); equipped with a Schott spray chamber and cross-flow nebulizer. The general ICP-OES conditions were: ICP RF power = 1400 W, coolant gas flow = 13.00 L min^{-1}, auxiliary gas flow = 1.00 L min^{-1}, nebulizer gas flow = 0.80 L min^{-1}. The most sensitive rhodium (343.489 nm) and chloride (134.742 nm) wavelengths were used for these determinations. An ULTRASPEC single element rhodium standard (De Bruyn Spectroscopic Solutions; 99.998% purity, 10% $^{v}/_{v}$ HCl) was used for rhodium standardisation, while dried sodium chloride (Sigma–Aldrich; 99.95% purity) was used for the chloride standardisation.

4.2.2 ^{103}Rh NMR Spectroscopy

^{103}Rh NMR spectra at 19.11 MHz were recorded at constant temperature (292.1 K ± 0.1 K) using a three channel Varian INOVA spectrometer (14.1 T magnet corresponding to 600 MHz ^{1}H resonance frequency) with a 10 mm HX Nalorac Z-spec ^{15}N-^{103}Rh (18–61 MHz) broad-band probe. It is important to allow sufficient time for the sample to achieve temperature equilibrium, following which optimal shimming is required. All NMR samples contained *ca* 30% ($^{v}/_{v}$) D_2O for locking purposes. Since the probe is not equipped for modern gradient shimming, together with the low receptivity of the ^{103}Rh nucleus, optimal shimming was carried out on FID of the D_2O while acquiring a D_2O spectrum in the conventional pulsed mode; with the X channel pre-tuned to ^{103}Rh. Once the best possible shim setting was obtained, the lock channel was used in the conventional mode, and final shimming adjusted for each ^{103}Rh NMR sample. In the absence of a suitable reference compound, chemical shifts (ppm) are reported to $\Xi(^{103}Rh)$ = 3.16 MHz on the TMS scale at 100.000 MHz, as proposed by Goodfellow [13]; the high-frequency positive-shift convention was used [7]. ^{103}Rh spectra were recorded with a spectral width of 19.11 kHz, using a 15.4 µs

excitation pulse at maximum practical power in an attempt to ensure approximately homogeneous RF excitation over the entire spectral width, with an acquisition time of 0.5 s and a 1.0 s pulse delay to ensure sufficient relaxation, under conditions of optimal resolution. A detailed search of the literature yielded no reliable measured estimates of ^{103}Rh T_1 relaxation times, particularly for octahedral Rh^{III} complexes as involved in this work. If the reasonable 'rule of thumb' by Sanders and Hunter [19] is used which allows for a rough estimate of the rotational correlation time τ_c, (τ_c / ps $\approx M_r$ where M_r is the relative molar mass of the molecule in question), then for $[RhCl_6]^{3-}$ we estimate a $\tau_c \approx 316$ ps. This means that at the ^{103}Rh resonance frequency of 19.11 MHz at our magnetic field, the condition $\omega_o\tau_c \approx 0.0190$ or $\omega_o\tau_c << 1$ is met, suggesting that the extreme narrowing condition for NMR is pertinent. In this region $T_2^* \leq T_2 \leq T_1$, so we can estimate the T_1 for the best resolved peaks of the $[RhCl_6]^{3-}$ species (Figure 4a) which has a line width of ~2.6 Hz, from which T_2, and thus T_1 of ≈ 0.12 s results. Thus, a pulse repetition rate of 5 × 0.12 s ≈ 0.612 s is adequate to ensure essentially complete relaxation for these Rh complexes. The very good agreement between the experimental and simulated peaks of the isotopologues shown in Figure 4, attest to this. Typically, due to the low receptivity of the ^{103}Rh nucleus, NMR spectra normally required *ca* 40,000 transients to achieve satisfactory signal/noise (S/N) ratios resulting in total experimental times ≥ 12 h. In the absence of artificial line-broadening (apodization) of the accumulated FIDs, the typical ^{103}Rh resonance line-widths ($\nu_{½}$ at half peak-height varied from 2.3 to 3.1 Hz at optimal resolution under careful temperature (292.1 ± 0.1 K) control.

SigmaPlot Version 11 (Systat Software Inc.) was used to perform the nonlinear least-squares fits on the ^{103}Rh experimental data. The SigmaPlot curve fitter uses the Marquardt–Levenberg algorithm to find the coefficients (parameters) of the independent variable(s) that give the best fit between the sum of several Lorentzian functions and the experimental data.

4.3 Results and discussion

At high magnetic fields (14.1 T) and carefully controlled conditions, the high-resolution ^{195}Pt NMR resonance signals of the series of complex anions $[PtCl_n(H_2O)_{6-n}]^{4-n}$ (n = 4–6) are resolved into a secondary structure, due to small chemical-shift differences as a result of both isotopologues and, the possible isotopomers[5] within each set of

[5] Isotopomer(s) with respect to whether a ^{35}Cl or ^{37}Cl is trans to a coordinated water molecule in the $[M^{IV/III}Cl_n(H_2O)_{6-n}]^{4/3-n}$ complex

$[Pt^{35}Cl/^{37}Cl_n(H_2O)_{6-n}]^{4-n}$ isotopologues [6], arising from the natural $^{35}Cl/^{37}Cl$ isotope distribution of the chlorido ligand(s) coordinated to Pt^{IV}. The resulting unique line shapes of the ^{195}Pt NMR resonances for this series of complexes, essentially constitutes an unequivocal $^{35}Cl/^{37}Cl$ isotope resolved 'fingerprint' for the identification of all species in this series, including stereoisomers such as *cis*- and *trans*-$[PtCl_4(H_2O)_2]$, provided at least one chlorido ligand remains bound to the Pt^{IV} complex and exchanges slowly on the NMR time scale.

Rhodium is separated and recovered on a commercial scale in the form of its chlorido $[RhCl_n(H_2O)_{6-n}]^{3-n}$ complex anions in hydrochloric acid, the available species distribution diagram in the literature however suggesting the presence of several species in solution depending on the hydrochloric acid concentration [15,16]. Provided at least one chlorido ligand is bound to Rh^{III}, these complexes can in principle exist as a set of four $^{35}Cl/^{37}Cl$ isotopologues and isotopomers[6] within each set of isotopologues illustrated for *fac*-$[Rh^{35}Cl_2{}^{37}Cl(H_2O)_3]$ and *mer*-$[Rh^{35}Cl_2{}^{37}Cl(H_2O)_3]$ by way of example, in Figure 4.1.

In the case of the *fac*-$[Rh^{35}Cl_2{}^{37}Cl(H_2O)_3]$ isotopologue, although *trans* $^{35}Cl/^{37}Cl$-Rh-(OH_2) configurations are possible in a statistical 2:1 ratio, these isotopomers are magnetically equivalent and result in the same chemical shift $\delta(^{103}Rh)$. By contrast for the *mer*-$[Rh^{35}Cl_2{}^{37}Cl(H_2O)_3]$ isotopologue, the isotopomer with a *trans* ^{37}Cl–Rh–(OH_2) configuration is *not* magnetically equivalent to the one with *trans* ^{35}Cl–Rh–(OH_2), which is twice as abundant than the former, resulting in a small chemical shift difference as manifested in the different 'fine-structures' of their respective ^{103}Rh NMR resonances. Similar considerations apply to the corresponding $[RhCl_5(H_2O)]^{2-}$, *cis*-$[RhCl_4(H_2O)_2]^-$ and *trans*-$[RhCl_4(H_2O)_2]^-$ species. Hence ^{103}Rh NMR spectroscopy at high magnetic fields ($\geq$14.1 T) is expected to be useful for the investigation of the species distribution of the $[RhCl_n(H_2O)_{6-n}]^{3-n}$ complex anions in hydrochloric acid, and in particular is likely also to show $^{35}Cl/^{37}Cl$ isotope resolved ^{103}Rh resonances, analogous to the Pt^{IV} complexes [6], referred to above.

[6] There is a misunderstanding regarding the usage of the terms *isotopologue* and *isotopomer* in the NMR literature. Generally, the term isotopomer has been used when in fact isotopologues were inferred. In this study, the term *isotopologue* is used to refer to a chemical species that differ only in isotopic composition of its constituent molecules or ions. *Isotopomers* are isomers having the same number of each isotopic atom, differing only in their relative positions in the molecule or ion.

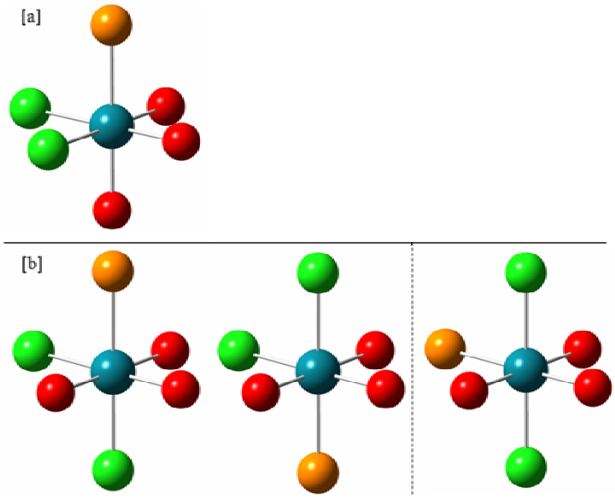

Figure 4.1: [a] The isotopologue of the *fac*-$[Rh^{35}Cl_2{}^{37}Cl(H_2O)_3]$ species; [b] Possible isotopomers associated with the isotopologue of the *mer*-$[Rh^{35}Cl_2{}^{37}Cl(H_2O)_3]$ species where the $^{35}Cl/^{37}Cl$ is coordinated *trans* with respect to water in a 2:1 ratio. ● = ^{35}Cl; ● = ^{37}Cl; ● = H_2O

As shown in Figure 4.2, these expectations are satisfactorily confirmed by the detailed 19.11 MHz ^{103}Rh NMR spectra of several $[RhCl_n(H_2O)_{6-n}]^{3-n}$ (n = 3–6) complexes at thermodynamic equilibrium at a fixed total Rh^{III} concentration of *ca* 0.87 M, obtained in solutions with 6.0 M and 1.0 M hydrochloric acid concentrations respectively. Figure 2[a]–[f] shows the well resolved fine-structure profile for each of the individual ^{103}Rh NMR resonances, recorded at a temperature of 292.1 ± 0.1 K, of the species $[RhCl_6]^{3-}$, $[RhCl_5(H_2O)]^{2-}$ in 6.0 M HCl and *cis*-$[RhCl_4(H_2O)_2]^-$, *trans*-$[RhCl_4(H_2O)_2]^-$, *fac*-$[RhCl_3(H_2O)_3]$ and *mer*-$[RhCl_3(H_2O)_3]$ present in solutions in 1.0 M hydrochloric acid. The well-resolved fine-structure profile of the ^{103}Rh NMR resonance for each species is due to $^{35}Cl/^{37}Cl$ isotope effects. Significantly, the ^{103}Rh resonance of the $[RhCl_6]^{3-}$ anion (Figure 2a) is resolved only into five of the seven expected $[Rh(^{35/37}Cl)_6]^{3-}$ isotopologues, very similar to what may be observed in the corresponding ^{195}Pt NMR spectrum of the $[Pt(^{35/37}Cl)_6]^{2-}$ complex [3].

In view of the relatively poor receptivity[#] of ^{103}Rh NMR, only five of the seven peaks due to the isotopologues $[Rh(^{35}Cl)_n(^{37}Cl)_r]^{3-}$ (n = 6–2, r = 2–6, $n + r = 6$), may be experimentally observed within a reasonable ^{103}Rh NMR acquisition time, since the statistically calculated abundance of $[Rh(^{35}Cl)(^{37}Cl)_5]^{3-}$ and $[Rh(^{37}Cl)_6]^{3-}$ isotopologues is very low (abundances of 0.38 and 0.02% respectively), Table 4.1. The relative statistical probability, P(n), for each possible isotopologue in the series of $[Rh^{35/37}Cl_n(H_2O)_{6-n}]^{3-n}$ (n = 3–6) complexes may be calculated as the fractional natural abundance (α) of ^{35}Cl (0.7553)

and ^{37}Cl (0.2447) using the binominal probability distribution function[7] for n ^{35}Cl and r ^{37}Cl chlorido ligands (n + r = 6). From a visual inspection of Figure 4.2[c]–[f], it can be seen however that the fine-structure of some of the ^{103}Rh resonances, particularly due to the stereoisomer pairs *cis*-$[RhCl_4(H_2O)_2]^-$, *trans*-$[RhCl_4(H_2O)_2]^-$, *fac*-$[RhCl_3(H_2O)_3]$ and *mer*-$[RhCl_3(H_2O)_3]$, respectively, differ significantly from a model which takes into account only the ^{35}Cl/^{37}Cl isotopologue distributions. The experimental ^{103}Rh NMR peak shapes and peak intensity ratios observed, suggest additional isotopomer induced fine-structure. The resolved fine-structure of the ^{103}Rh NMR resonances (Figure 4.2[b]–[f]) can only be accounted for by considering the possible isotopomers[2], within each possible set of isotopologues for the series of 'aquated' complexes $[RhCl_5(H_2O)]^{2-}$, *cis*-$[RhCl_4(H_2O)_2]^-$, *trans*-$[RhCl_4(H_2O)_2]^-$, *fac*-$[RhCl_3(H_2O)_3]$ and *mer*-$[RhCl_3(H_2O)_3]$. The relative statistical probability for each possible isotopomer, $S(n)$, in the series of $[Rh^{35/37}Cl_n(H_2O)_{6-n}]^{3-n}$ (n = 1–5) complexes was deduced as illustrated schematically in Figure 4.1. For the *fac*-$[RhCl_3(H_2O)_3]$ species the *trans* $^{35/37}$Cl–Rh–(OH_2) isotopomers are magnetically equivalent, while for the *mer*-$[RhCl_3(H_2O)_3]$ species two sets of magnetically inequivalent isotopomers are possible in a 2:1 statistical ratio (reasonably neglecting any possible ^{17}O/^{18}O isotope effects due to the very low natural abundances of these isotopes of oxygen of the coordinated water molecules).

Figure 4.2 shows the 'simulated' overall ^{103}Rh NMR line-shape obtained from the sum of several Lorentzian peaks of equal half-height peak width (2.64 Hz)[8] and fixed isotope chemical shift spacing per $^{35/37}$Cl isotope. This corresponds to all the possible isotopologues with probability $P(n)$, and the statistically likely but magnetically non-equivalent isotopomers[3] with probability $S(n)$ for each of the complexes listed. An excellent non-linear least-squares fit between the experimental and simulated ^{103}Rh NMR spectra using a 5.33 Hz (~0.279 ppm) shielding ('up-field' isotope shift) per $^{37}Cl^-$ coordinated to the Rh^{III} ion is observed. The essentially quantitative agreement of the experimental line-shape, within

---

[7] $P(n)= \sum_{n=0}^{n=\frac{(n+r)!}{(n!r!)}} (\alpha^{n}_{^{35}Cl}\alpha^{r}_{^{37}Cl})$

[8] In the likely event that ^{35}Cl/^{37}Cl quadrupolar relaxation is a dominant contribution to the overall ^{103}Rh relaxation, and thus the line-width, it might be expected that differing line-widths may pertain to differing $[RhCl_n(H_2O)_{6-n}]^{3-n}$ species and their isotopologues. However, for the well-resolved isotopologue peaks for the $[RhCl_6]^{3-}$ complex, a constant line-width leads to the best fit between the experimental and simulated peaks. For the other species where the ^{103}Rh isotopologue/isotopomer peaks are less-clearly resolved, differing line-widths lead to good fits shown in Figure 4.2.

experimental error, with the expected statistical isotopologue and isotopomer distributions are shown in Table 4.1 for all the $[Rh^{35/37}Cl_n(H_2O)_{6-n}]^{3-n}$ (n = 3–6) considered in this study.

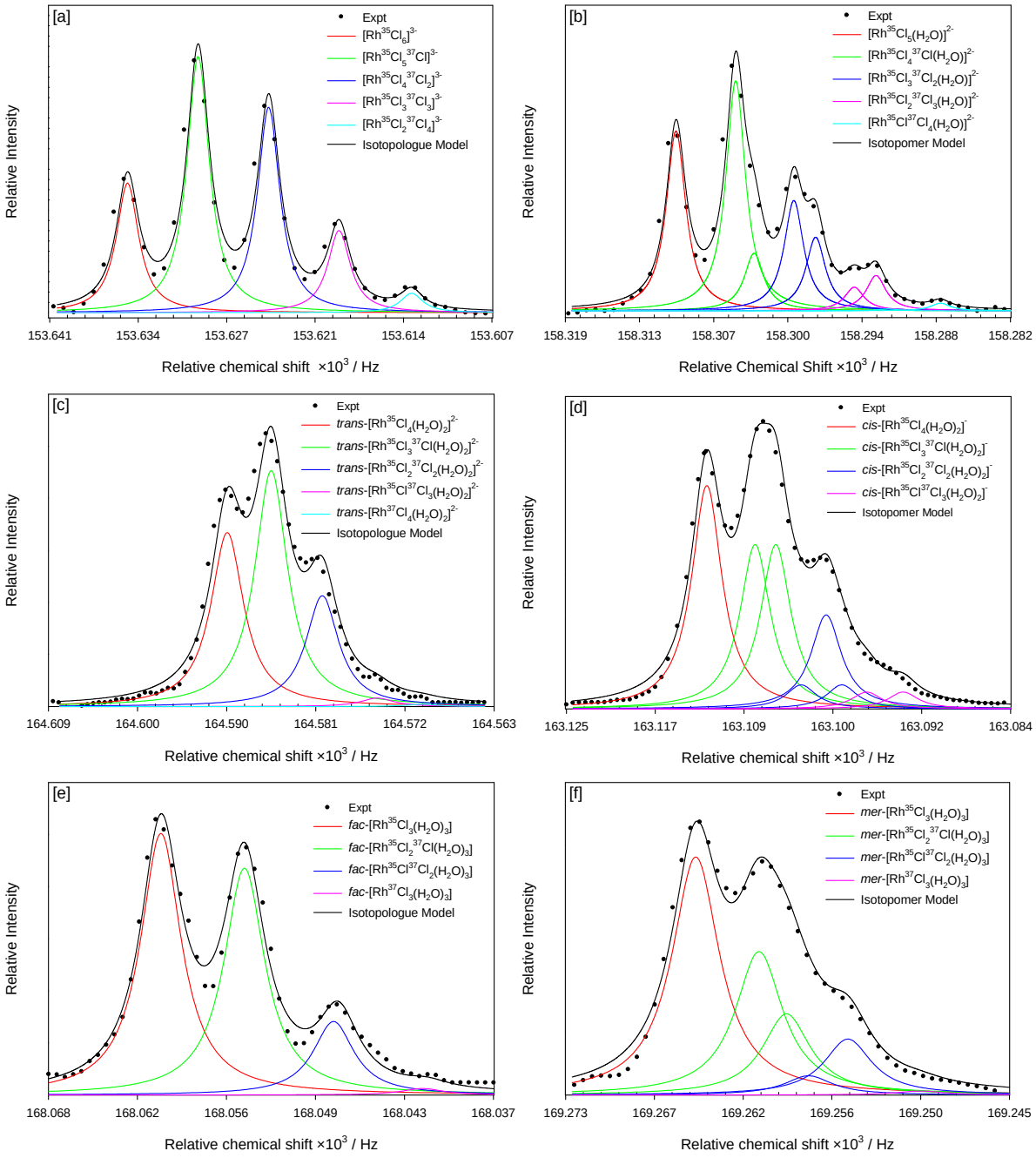

Figure 4.2: Experimental ^{103}Rh spectra of $[RhCl_n(H_2O)_{6-n}]^{3-n}$ (n = 3–6) species recorded at 292.1 K (symbols). The least-squares fits (solid lines) between experimental spectra of $[RhCl_6]^{3-}$ [a], *trans*-$[RhCl_4(H_2O)_2]^-$ [c] and *fac*-$[RhCl_3(H_2O)_3]$ [e] and the isotopologue model; the least-squares fits between the experimental spectra and the isotopologue model that includes isotopomers for the $[RhCl_5(H_2O)]^{2-}$, *cis*-$[RhCl_4(H_2O)_2]^-$ and *mer*-$[RhCl_3(H_2O)_3]$ species are denoted by [b], [d] and [f], respectively

Interestingly, in this context Sadler *et al.* reported similar resolved $^{35}Cl/^{37}Cl$ isotope effects in the ^{195}Pt NMR spectrum of $[PtCl_6]^{2-}$ complex more than 3 decades ago, at the then highest magnetic field spectrometer generally available [14], although these were erroneously ascribed to $^{35}Cl/^{37}Cl$ 'isotopomers'. As is now clear from this study as well as our recent work on the analogous Pt^{IV} complexes, in general for $[MCl_6]^{2/3-}$ ($M = Pt^{IV}$ or Rh^{III}) species, the resolved fine-structure in the ^{103}Rh (and ^{195}Pt) NMR resonances are only due to the various isotopologues in these complex anions, and no isotopomer effects are resolved for these particular species. To our knowledge no such isotopologues effects have been previously reported for the $[RhCl_6]^{3-}$ complex anion to date.

The isotopomer-induced $^{35}Cl/^{37}Cl$ 'fine-structure' effects visible in the ^{103}Rh NMR resonance of the isotopologues $[Rh^{35}Cl_4{}^{37}Cl(H_2O)]^{2-}$ and $[Rh^{35}Cl_3{}^{37}Cl_2(H_2O)]^{2-}$ *etc.*, are due to the possibility of trans ^{37}Cl-^{103}Rh-OH_2 and ^{35}Cl-^{103}Rh-OH_2 configurations within these isotopologues. Evidently, the additional fine-structure observed in the ^{103}Rh resonances of these complexes arises from small differences in ^{103}Rh shielding of these isotopomer configurations within a given complex. From the least-squares fitting of the experimental line-shapes, an effective $\Delta(\delta(^{103}Rh))$ of *ca* 0.141 ppm (2.7 Hz) between the *trans*- and *cis*-$[Rh^{35}Cl_4{}^{37}Cl(H_2O)]^{2-}$ isotopomers can be calculated, depending on whether a ^{37}Cl atom is respectively *trans* or *cis* to the coordinated water molecule. This finding emphasizes the remarkable sensitivity of $\delta(^{103}Rh)$ to very subtle effects on the ^{103}Rh shielding within these complexes, and the necessity of careful temperature control to achieve optimal NMR resolution. While a detailed explanation of the origin of the $^{35}Cl/^{37}Cl$ isotope effects must await a full computational (theoretical) investigation, these effects are likely to result from small differences in the vibrational stretching frequencies between the ^{37}Cl-^{103}Rh and ^{35}Cl-^{103}Rh bonds *trans* to the relatively weakly bound coordinated water molecules in these (as well as the corresponding Pt^{IV} [6]) complexes. This is a nice example of the elegant theoretical work by Jameson and Jameson on the 'rovibrational' averaging of nuclear shielding in MX^{6-} type molecules more than two decades ago [17]. In this context we have recently found in a density functional theory (DFT) study that, for the series of $[PtX_6]^{2-}$ ($X = F^-$, Cl^-, Br^-, I^-) complexes, the calculated ^{195}Pt NMR shielding of these complexes are extraordinarily sensitive to average Pt-halide bond distances Δ(Pt-Cl); for example the $d(\delta 195Pt)/d\Delta(Pt–Cl)$ for the Pt–Cl case is *ca* 183 ppm/picometer [18].

Table 4.1: Comparison of the experimental (simulated from Figures 2 [a]–[f]) and statistically expected isotopologue and isotopomer distributions for the $[Rh^{35/37}Cl_n(H_2O)_{6-n}]^{3-n}$ (n = 3–6) series.

$^{35/37}$Cl trans to H_2O	Rh^{III} isotopologue	Percent isotopomers		Sum percent of isotopomers to yield isotopologue amount	
		Experimental[a]	Statistical	Experimental[a]	Statistical
	$[Rh^{35}Cl_6]^{3-}$	-	-	18.69 ± 0.3	18.92
	$[Rh^{35}Cl_5{}^{37}Cl]^{3-}$	-	-	36.96 ± 0.2	36.31
	$[Rh^{35}Cl_4{}^{37}Cl_2]^{3-}$	-	-	29.67 ± 0.2	29.03
	$[Rh^{35}Cl_3{}^{37}Cl_3]^{3-}$	-	-	11.86 ± 0.2	12.38
	$[Rh^{35}Cl_2{}^{37}Cl_4]^{3-}$	-	-	2.81 ± 0.2	2.97
	$[Rh^{35}Cl^{37}Cl_5]^{3-}$	-	-	*Not reliably quantifiable*	0.38
	$[Rh^{37}Cl_6]^{3-}$	-	-	*Not reliably quantifiable*	0.02
^{35}Cl	$[Rh^{35}Cl_5(H_2O)]^{2-}$	24.99 ± 0.2	24.97	24.99 ± 0.2	24.97
^{35}Cl ^{37}Cl	$[Rh^{35}Cl_4{}^{37}Cl(H_2O)]^{2-}$	31.96 ± 0.2 8.00 ± 0.3	31.94 7.99	39.96 ± 0.6	39.93
^{35}Cl ^{37}Cl	$[Rh^{35}Cl_3{}^{37}Cl_2(H_2O)]^{2-}$	15.33 ± 0.2 10.23 ± 0.2	15.32 10.22	25.56 ± 0.5	25.54
^{35}Cl ^{37}Cl	$[Rh^{35}Cl_2{}^{37}Cl_3(H_2O)]^{2-}$	3.27 ± 0.1 4.90 ± 0.2	3.27 4.9	8.17 ± 0.4	8.17
^{35}Cl ^{37}Cl	$[Rh^{35}Cl^{37}Cl_4(H_2O)]^{2-}$	0.26 ± 0.2 1.05 ± 0.1	0.26 1.05	1.31 ± 0.4	1.31
^{37}Cl	$[Rh^{37}Cl_5(H_2O)]^{2-}$	*Not reliably quantifiable*	0.08	*Not reliably quantifiable*	0.08
^{35}Cl, ^{35}Cl	*cis*-$[Rh^{35}Cl_4(H_2O)_2]^{-}$	30.68 ± 0.3	32.96	30.68 ± 0.3	32.96
^{35}Cl, ^{35}Cl ^{35}Cl, ^{37}Cl	*cis*-$[Rh^{35}Cl_3{}^{37}Cl(H_2O)_2]^{-}$	22.56 ± 0.2 22.59 ± 0.2	21.08 21.08	45.15 ± 0.5	42.16
^{35}Cl, ^{35}Cl ^{35}Cl, ^{37}Cl ^{37}Cl, ^{37}Cl	*cis*-$[Rh^{35}Cl_2{}^{37}Cl_2(H_2O)_2]^{-}$	3.30 ± 0.2 12.91 ± 0.3 3.30 ± 0.2	3.37 13.48 3.37	19.15 ± 0.5	20.22
^{35}Cl, ^{37}Cl ^{37}Cl, ^{37}Cl	*cis*-$[Rh^{35}Cl^{37}Cl_3(H_2O)_2]^{-}$	2.31 ± 0.4 2.31 ± 0.4	2.16 2.16	4.62 ± 1.0	4.32
^{37}Cl, ^{37}Cl	*cis*-$[Rh^{37}Cl_4(H_2O)_2]^{-}$	*Not reliably quantifiable*	0.34	*Not reliably quantifiable*	0.34
	trans-$[Rh^{35}Cl_4(H_2O)_2]^{-}$	-	-	32.73 ± 0.5	32.96
	trans-$[Rh^{35}Cl_3{}^{37}Cl(H_2O)_2]^{-}$	-	-	42.40 ± 0.4	42.16
	trans-$[Rh^{35}Cl_2{}^{37}Cl_2(H_2O)_2]^{-}$	-	-	20.85 ± 0.9	20.22
	trans-$[Rh^{35}Cl^{37}Cl_3(H_2O)_2]^{-}$	-	-	3.60 ± 1.0	4.31
	trans-$[Rh^{37}Cl_4(H_2O)_2]^{-}$	-	-	0.42 ± 0.3	0.34
^{35}Cl	*mer*-$[Rh^{35}Cl_3(H_2O)_3]$	43.96 ± 0.9	43.50	43.96 ± 0.9	43.50
^{35}Cl ^{37}Cl	*mer*-$[Rh^{35}Cl_2{}^{37}Cl(H_2O)_3]$	26.48 ± 1.3 14.97 ± 1.0	27.82 13.91	41.45 ± 2.9	41.73
^{35}Cl ^{37}Cl	*mer*-$[Rh^{35}Cl^{37}Cl_2(H_2O)_3]$	3.55 ± 0.8 10.31 ± 1.0	4.45 8.90	13.86 ± 2.2	13.35
^{37}Cl	*mer*-$[Rh^{37}Cl_3(H_2O)_3]$	0.72 ± 0.5	1.40	0.72 ± 0.5	1.40
^{35}Cl, ^{35}Cl, ^{35}Cl	*fac*-$[Rh^{35}Cl_3(H_2O)_3]$	-	-	46.02 ± 1.3	43.50
^{35}Cl, ^{35}Cl, ^{37}Cl	*fac*-$[Rh^{35}Cl_2{}^{37}Cl(H_2O)_3]$	-	-	39.91 ± 2.5	41.73
^{35}Cl, ^{37}Cl, ^{37}Cl	*fac*-$[Rh^{35}Cl^{37}Cl_2(H_2O)_3]$	-	-	12.93 ± 1.3	13.35
^{37}Cl, ^{37}Cl, ^{37}Cl	*fac*-$[Rh^{37}Cl_3(H_2O)_3]$	-	-	1.13 ± 0.5	1.42

[a] The isotopologue/isotopomer model was fitted by non-linear least-square analysis to the experimental data from which the 95% confidence interval was estimated. ^{103}Rh NMR spectra of each solution were acquired three separate times, not in succession. For peaks of lower intensity the relative percentage deviation between experimental and fitted resonance intensities naturally is much larger compared to the intense ^{103}Rh peaks. Better agreement can only be obtained at the

On a more practical level, the $^{35}Cl/^{37}Cl$ isotope effects will assist in the establishment of a direct and definitive chemical speciation-distribution diagram for the full series of $[RhCl_n(H_2O)_{6-n}]^{3-n}$ in halide-rich aqueous solutions of interest to the Rh recovery and refining industry, using ^{103}Rh NMR spectroscopy.

Furthermore no observable secondary isotope effects, due to $^{1/2}H$ isotopes associated with the coordinated water molecules, were found upon increasing the $^2H_2O:H_2O$ ratio from 10 to 30%($^v/_v$) for the $[Rh^{35/37}Cl_n(^{1/2}H_2O)_{6-n}]^{3-n}$ (n = 3–5) complexes. Presumably, the $^1H/^2H$ exchange of water is rapid in solution, resulting in the averaging of any potential (small) isotope effects from this source. Moreover, application of ^1H-decoupling during acquisition of ^{103}Rh NMR spectra in this study resulted in significant loss of isotopologue/isotopomer resolution in the recorded ^{103}Rh resonances, in all probability due to significant RF absorption of the high ionic-strength aqueous solutions causing inevitable temperature fluctuations and/or convection currents within the 10 mm sample tube. Considering the significant temperature dependence of the ^{103}Rh NMR chemical shifts, reported to be in the range (0.5–3.0 ppm K^{-1})[9] [7–10] compared to those observed for this series of complex anions (e.g. *ca* 2.0 ppm.K^{-1} for $[RhCl_6]^{3-}$), the importance of careful temperature control to at least ± 0.1 K when acquiring high-resolution NMR spectra is highlighted. Moreover, in order to ensure complete thermal equilibrium of the sample in the 10 mm NMR tube, a waiting period of at least 35 min is recommended to achieve satisfactory thermal equilibrium within the sample. A significant deterioration in resolution of the ^{103}Rh NMR resonance signal for $[RhCl_n(H_2O)_{6-n}]^{3-n}$ (n = 3–6) complexes is observed upon exceeding a temperature of 300.0 K, very similar to that observed previously in the $[PtCl_n(H_2O)_{6-n}]^{4-n}$ (n = 4–6) complexes [6]. The possible reasons for this immense temperature dependence await a more detailed ^{103}Rh NMR spectroscopic study of the Rh complexes described here. Intra- and inter-molecular ligand exchange ($^{35/37}Cl^-$ or H_2O) is likely to be too slow at temperatures <300 K [15–18], to account for the loss of the isotopologue and isotopomer resolution in the ^{103}Rh NMR resonance structure. Moreover, such $^{35}Cl/^{37}Cl$ isotope effects reported here for the generally kinetically inert Rh^{III} complexes (and elsewhere for the Pt^{IV} complexes) would not be visible under conditions of fast chemical exchange on the NMR time scale such as may be expected at higher temperatures (>350 K), as can be confirmed by the preliminary

[9] Higher temperatures usually result in "down-field" shifts (higher δ) or lower shielding (σ), so that dσ/dT is usually reported as a negative value.

temperature dependence NMR experiments. The possibility of variable quadrupolar $^{35}Cl/^{37}Cl$ relaxation effects for ^{103}Rh in different species because of the temperature dependence of this relaxation mechanism is also likely to affect the observed line-widths of the ^{103}Rh resonance at differing temperatures, a topic in need of a more detailed study.

4.4 Concluding remarks

The remarkable isotopologue, and for some complexes isotopomer induced fine-structure of the ^{103}Rh NMR resonances (at high magnetic fields) of the series of aquated $[Rh^{35/37}Cl_n(H_2O)_{6-n}]^{3-n}$ (n = 3–6) complex anions in hydrochloric acid solutions constitutes a novel method of direct spectroscopic speciation of $[RhCl_n(H_2O)_{6-n}]^{3-n}$ (n = 3–6) complexes. This is possible without the need for accurate chemical shifts of these species, or the need for the comparison of authentic synthetic complexes many of which are not readily available or even separately synthesizable. Given the large chemical shift range of *ca* 12,000 ppm observed for diverse rhodium complexes to date [7], together with the extreme sensitivity of ^{103}Rh nuclear shielding to numerous effects such solvent, concentration, temperature, pressure and other effects [3], this makes the comparison of chemical shifts subject to considerable uncertainty. The use of $^{35}Cl/^{37}Cl$ isotope-resolved ^{103}Rh NMR resonance thus constitutes a significant advance as a convenient and reliable method for the identification of halide containing complexes, provided these are kinetically inert to ligand exchange on the NMR time scale. Particularly noteworthy is the possibility of the unambiguous assignment of stereoisomers such as the *trans*- or *cis*-$[RhCl_4(H_2O)_2]^-$ which differ in chemical shift by only *ca* 76 ± 3 ppm, or the uncharged *fac*-$[RhCl_3(H_2O)_3]$ and *mer*-$[RhCl_3(H_2O)_3]$ isomers differing only by *ca* 63 ± 3 ppm. These can now readily be identified based on their $^{35}Cl/^{37}Cl$ isotope induced 'NMR fingerprint', without reference to their accurate ^{103}Rh NMR chemical shifts or the need for a suitable reference compound.

4.5 References:

[1] D. Jollie, *Platinum 2010*, Johnson Matthey PLC, Royston, UK, 2010, 44 and 58.

[2] D.M. Templeton, F. Ariese, R. Cornelis, L.G. Danielsson, H. Muntau, H.P. van Leeuwen, R. Loinski, *Pure Appl. Chem*. **72** (2000) 1453

[3] K.R. Koch, M.R. Burger, J. Kramer, A.N. Westra, *Dalton Trans*. (2006) 3277

[4] J. Kramer, K.R. Koch, *Inorg. Chem*. **45** (2006) 7843

[5] J. Kramer, K.R. Koch, *Inorg. Chem*. **46** (2007) 7466

[6] W.J. Gerber, P. Murray, K.R. Koch, *Dalton Trans*. **31** (2008) 4113

[7] J.M. Ernsting, S. Gaemers, C.J. Elsevier, *Magn. Res. Chem*. **42** (2004) 721

[8] B.E. Mann, C.M. Spencer, *Inorg. Chim. Acta*, **76** (1983) L65

[9] B.E. Mann, C.M. Spencer, *Inorg. Chim. Acta*, **65** (1982) L57

[10] C. Carr, J. Glaser, M. Sandström, *Inorg. Chim. Acta*, **131** (1987) L53

[11] M.C. Read, J. Glaser, M. Sandström, *J. Chem. Soc., Dalton Trans*. (1992) 233

[12] M.C. Read, J. Glaser, I. Persson, M. Sandström, *J. Chem. Soc., Dalton Trans*. (1994) 3243

[13] R.J. Goodfellow, in: R.K. Harris, B.E. Mann (Eds.), *NMR and the Periodic Table*, Academic Press, London, 1978,

[14] I.M. Ismail, S.J.S. Kerrison, P.J. Sadler, *J. Chem. Soc., Chem. Commun*. (1980) 1175

[15] E. Benguerel, G.P. Demopoulos, G.B. Harris, *Hydrometallurgy*, **40** (1996) 135

[16] W.J. Gerber, K.R. Koch, H.E. Rohwer, E.C. Hosten, T.E. Geswindt, *Talanta*, **82** (2010) 348

[17] C.J. Jameson, A.K. Jameson, J. *Chem. Phys*. **85** (1986) 5484

[18] M.R. Burger, J. Kramer, H. Chermette, K.R. Koch, *Magn. Res. Chem*. **48** (2010) 38

[19] J.K.M. Sanders and B.K. Hunter, in *Modern NMR Spectroscopy*, 2nd Edition, Oxford University Press, (1993)

Chapter 5

High-resolution ^{103}Rh NMR spectroscopy as a tool for the *direct* speciation of Rh^{III} aqua chlorido-complexes: A comparative study[†]

5.1 Introduction

Cozzi and Pantani [1], who based their diagram on the stability constants obtained from polarographic data - Figure 5.1 [a], reported the earliest postulated speciation diagram for Rh^{III} aqua-chlorido complexes. Robb *et al* [2,3] subsequently conducted UV-vis kinetic experiments for the aquation reactions of $[RhCl_n(H_2O)_{6-n}]^{3-n}$ (n = 4-6) complexes, from which they calculated "kinetic-based" stability constants. In 1996, Benguerel *et al* [4] used the stability constants determined by Robb *et al* [2,3] in order to construct the speciation diagram depicted by Figure 5.1 [b]. In their argument, Benguerel *et al* [4] noted that Robb *et al* [2,3] did not account for the activity of water, which is known to be considerably lower than 1 in concentrated HCl solutions. As a result, they constructed a revised speciation diagram, based on the data obtained by Robb *et al* [2.3], in which the activity of water was accounted for [4], Figure 5.1 [c]. Both the polarographic method documented by Cozzi and Pantani [1] as well as the kinetic studies reported by Benguerel *et al* [4] suffer from the disadvantage that no distinction could be made between any of the stereoisomers. Recently a speciation diagram for the $[RhCl_n(H_2O)_{6-n}]^{3-n}$ (n=0-6) complexes, obtained by means of a hyphenated ion-pair HPLC-ICP-MS method was proposed [5], Figure 5.1 [d]. It is evident from Figures 5.1 [a]-[d] that there are large discrepancies between the literature reported speciation diagrams; most notably the composition of species present at 1.0 M and 6.0 M chloride concentration, and the chloride concentration at which a 1:1 ratio of $[RhCl_6]^{3-}$ and $[RhCl_5(H_2O)]^{2-}$ exists, as denoted in Figure 5.1. This prompted the re-evaluation of the Rh^{III} aqua-chlorido species distribution in an HCl matrix by means of a *direct* method, *i.e.* high-resolution ^{103}Rh NMR spectroscopy.

[†] This Chapter is partially based on the publication: T.E. Geswindt, W.J. Gerber and K.R. Koch, High-resolution ^{103}Rh NMR spectroscopy as an analytical tool for the *direct* chemical speciation of $[RhCl_n(H_2O)_{6-n}]^{3-n}$ (n=3-6) complexes, *Manuscript prepared for publication (2013)*

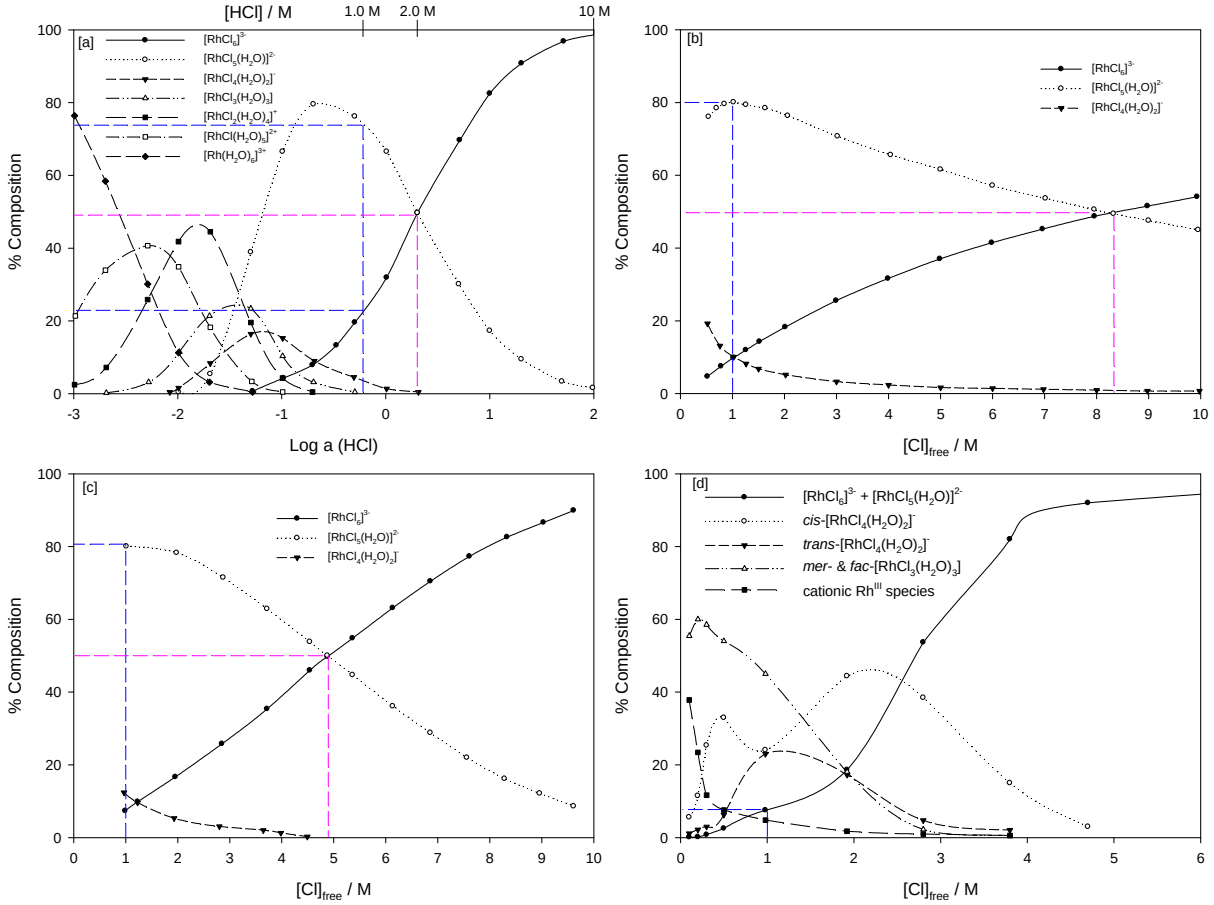

Figure 5.1: Literature documented Rh^{III} species distribution diagrams illustrating the large discrepancies existing between proposed diagrams. The dashed blue lines indicate the Rh^{III} species distribution at 1.0 M free chloride concentration, while the dashed pink lines indicate the free chloride concentration at which a 1:1 ratio of $[RhCl_6]^{3-}$ and $[RhCl_5(H_2O)]^{2-}$ exists

5.2 Experimental

5.2.1 Reagents and preparation of solutions containing Rh^{III} aqua-chlorido species used for ^{103}Rh NMR spectroscopic studies

A series of 12 Rh^{III} solutions was prepared by dissolving the appropriate amount of commercially available $RhCl_3{\cdot}nH_2O$ (Heraeus Chemicals GmbH) in 3.5 mL 29% ($^{v}/_{v}$) $^{2}H_2O/^{1}H_2O$ (Sigma Aldrich) containing the appropriate quantity of concentrated (32% $^{v}/_{v}$) HCl (Merck Chemicals). Each of these solutions contained a different amount of HCl such that the ***free*** Cl^- concentration of the 12 solutions varied between 0.721 and 5.694 M. These solutions were sealed and stored at a temperature of 333.1 K for two weeks and thereafter the solutions were allowed to equilibrate at 292.1 K for a further two weeks. The ionic strength

of these solutions was not kept constant in order to simulate authentic mining feed solution conditions. The total rhodium and chloride concentrations were determined by means of ICP-OES (SPECTRO Arcos). A rhodium elemental standard (De Bruyn Spectroscopy - 1000 ± 3ppm, 99.99% purity) was used for rhodium determination while dried NaCl (Sigma Aldrich; 99.5% UltraPure) was used for total chloride determination. Although unconventional, ICP-OES was used for quantification of the total chloride concentration. To date, there have been few reports in literature documenting the use of ICP-OES in the quantification of halogens [1,2]. This is probably due to the relatively low emissivity of the halogen atoms. In addition, the halogen atoms/ions emit well below 160 nm, while most modern ICP-OES spectrometers are unable to detect in these low ultraviolet ranges. Nonetheless, it has been shown that (Cl), (Br) and (I) can satisfactorily be quantified in waste oils [6,7], and more recently in acidic halide-rich aqueous solutions containing PGMs [8]. The optimal ICP-OES spectrometer settings used were: RF power = 1400 W, Argon coolant flow = 13.0 $L.min^{-1}$, auxiliary flow = 1.0 $L.min^{-1}$, nebulizer flow = 0.80 $L.min^{-1}$.

5.2.2 ^{103}Rh NMR spectroscopy

^{103}Rh NMR spectra at 19.11 MHz were recorded at constant temperature (292.1 K ± 0.1K) using a three channel Varian INOVA spectrometer (14.1 Tesla magnet corresponding to 600 MHz ^{1}H resonance frequency) with a 10mm HX Nalorac Z-spec ^{15}N-^{103}Rh (18 – 61 MHz) broad-band probe. It is important to allow sufficient time for the sample to achieve temperature equilibrium, where after optimal shimming is required. All NMR samples contained *ca* 30% (*v/v*) D_2O for locking purposes. Since the probe is not equipped for modern gradient shimming, together with the low receptivity of the ^{103}Rh nucleus, optimal shimming was carried out on FID of the D_2O while acquiring a D_2O spectrum in the conventional pulsed mode; with the X channel pre-tuned to ^{103}Rh. Once the best possible shim setting was obtained, the lock channel was used in the conventional mode, and final shimming adjusted for each ^{103}Rh NMR sample. Recently, we developed a ^{103}Rh NMR method for the unambiguous speciation and characterization of $[RhCl_n(H_2O)_{6-n}]^{3-n}$ (n=3-6) complex anions by exploiting the unique ^{35}Cl/^{37}Cl isotope effects visible in the ^{103}Rh NMR resonances obtained at high magnetic fields (14.08 Tesla) in acidic chloride solutions [9]. Although this method does not require the use of conventional referencing methods, the chemical shifts (ppm) are reported Ξ (^{103}Rh) = 3.16 MHz on the TMS scale at 100.000 MHz, as proposed by

Goodfellow [10]; the high-frequency positive-shift convention was used [11]. ^{103}Rh spectra were recorded with a spectral width of 19.11 KHz (1000 ppm), using a 8.0 µs excitation pulse at maximum practical power in an attempt to ensure approximately homogeneous RF excitation over the entire spectral width, with an acquisition time of 0.5 s and a 2 s pulse delay to ensure relaxation, under conditions of optimal resolution. Typically, due to the low receptivity of the ^{103}Rh nucleus, NMR spectra normally required *ca* 50 000 transients to achieve satisfactory S/N ratios resulting in total experimental times ≥ 12 h. In the absence of artificial line-broadening (apodization) of the accumulated FIDs, the typical ^{103}Rh resonance line-width at half peak-height ($\nu_{½}$) varied from 2.3 - 3.1 Hz at optimal resolution under careful temperature control (292.1 K ± 0.1K). ^{103}Rh NMR measurements were repeated a year after the solutions were prepared in order to verify that no significant changes in the original ^{103}Rh NMR spectra were observed. The MestReNova V6.02 software package (Mestrelab Research S. L.) was used for the processing of ^{103}Rh NMR spectra and integration of the relative peak areas of each resonance peak.

5.2.3 Reversed-phase high-performance liquid chromatography separation of $[RhCl_n(H_2O)_{6-n}]^{3-n}$ (n=5,6) complexes

5.2.3.1 Reagents utilised

HPLC grade methanol was obtained from Merck chemicals. All aqueous solutions were prepared using ultrapure Milli-Q water. Analytical grade tetrabutylammonium chloride (TBA^+Cl^-), sodium acetate and glacial acetic acid were obtained from Sigma–Aldrich. The chromatographic mobile phase was prepared by the addition of methanol to stock solutions of 0.05 M tetrabutylammonium chloride and 0.1 M acetate buffer (pH = 4.6) to yield a 30% ($^v/_v$) MeOH:H_2O solution. This mobile phase was filtered through 0.45 µm HV filters (Millipore Corporation, HVLP04700) under vacuum and degassed for 15 – 20 min in an ultrasonic bath before use. The preparation of solutions containing mixed aqua chlorido-species of Rh^{III} was previously described in Section 5.2.1.

5.2.3.2 High-performance liquid chromatography coupled to ICP-OES for detection

Chromatographic separations were performed with a Varian Prostar liquid chromatograph equipped with a binary 210 delivery module, a 410 auto-sampler operating at an optimized mobile phase flow-rate of 0.8 $mL.min^{-1}$. The column used throughout this study was a Gemini C18, 250 mm × 4.6 mm internal diameter, 5 µm particle size, with a mirror-finish interior wall. The efficiency of the column was examined by the injection of a solution comprising of acetophenone, phenol, aniline, caffeine, uracil, pyridine, benzene and 30% ($^{v}/_{v}$) acetonitrile. Column conditioning comprised of the passage of mobile phase through the column for 1 hour prior to analysis, followed by a 45 min post-analysis rinse with pure methanol.

It is well known that the most important factors in IP-RP-HPLC that influence the retention time of anionic analytes are the concentration of the ion-pairing agent ($TBA^{+}Cl^{-}$) in the mobile phase, as well as the eluent composition of the MeOH:H_2O ($^{v}/_{v}$) ratio. For a constant eluent composition (MeOH:H_2O $^{v}/_{v}$ ratio), increasing the $TBA^{+}Cl^{-}$ concentration would result in an increased amount of ion-pairing agent partitioned in the stationary phase, resulting in an increase in the retention factor (k) of the analyte [12]. Methanol was used as an organic modifier since acetonitrile is known to form, presumably, coordination compounds of Rh^{III} [13-15]. Increasing the percentage volume of methanol in the mobile phase, at a constant $TBA^{+}Cl^{-}$ concentration, results in a decrease in the retention factor (k) of the analyte, as a result of an increased quantity of the analyte partitioned in the mobile phase as opposed to the stationary phase. Thus, to retain a balance between resolution and analysis time, it was found that a mobile phase composition consisting of 9.0 mM $TBA^{+}Cl^{-}$ and 30% ($^{v}/_{v}$) MeOH:H_2O with a 0.01 M sodium acetate buffer (pH = 4.6) was optimal.

Several Rh^{III} solutions, prepared as outlined in section 5.2.1, were diluted such that the final Rh concentration was 0.200 mM while the final HCl concentration varied between 0.401 – 3.451 mM. These samples were prepared in a matrix consisting of 9.0mM $TBA^{+}Cl^{-}$, 30% ($^{v}/_{v}$) MeOH:H_2O and 0.01 M sodium acetate buffer, *i.e.* the composition of the mobile phase. The diluted samples were thoroughly mixed for ± 45 s, after which a 20.0 µL aliquot of the diluted sample was injected onto the C_{18} column. The average time elapsed from stock sample dilution until injection never exceeded 90 s.

Detection of Rh emission at 343.489 nm was performed using a SPECTRO Arcos ICP-OES, equipped with a Burgener T2002 nebulizer and a cyclonic spray chamber for homogenous sample delivery. The sample was transferred directly from the HPLC column to the nebulizer by PEEK tubing with an internal diameter equal to 0.12 mm. The optimal ICP-OES operating conditions were: RF power = 1600 W, coolant gas flow = 16.00 $L.min^{-1}$, auxiliary gas flow = 2.00 $L.min^{-1}$, nebulizer gas flow = 0.60 $L.min^{-1}$.

5.2.4 Precipitation of $[RhCl_n(H_2O)_{6-n}]^{3-n}$ (n=5,6) complex anions using organic (poly)amines

A 0.103 M Rh^{III} stock solution was prepared by dissolving the appropriate amount of $RhCl_3 \cdot nH_2O$ (Heraeus Chemicals GmBH) in 25 mL MilliQ water. The vessel was sealed and the solution was aged at 333.1 K for a week.

Diethylenetriamine (**Deta** - Riedel-de Haën), triethylenetetramine (**Teta** - Fluka), tetraethylenepentamine (**Tepa** – Sigma-Aldrich) and tris(2-aminoethyl)amine (**Tren** - Fluka) were utilized as the organic precipitants and used without further purification. A stock 0.100 M solution of each organic precipitant was prepared using MilliQ water as a diluent.

The Rh^{III} stock solution was used to prepare several solutions, each containing 5.0 mM rhodium. The HCl concentration of each solution was adjusted by the addition of the desired amount of 32% HCl (Merck Chemicals). The HCl concentration of these solutions ranged from 0 to 4.986 M. These solutions were made up to a pre-determined volume using MilliQ water, the vessels sealed and the solutions allowed to age at elevated temperature (333.1 K) for a week, and then at 298.1 K for another week. This was done in order to ensure "complete" equilibrium of the $[RhCl_n(H_2O)_{6-n}]^{3-n}$ (n=3-6) complex anions.
Once equilibrium had been reached, a specific volume of the stock organic precipitant was added to each of the Rh^{III} solutions such that the final precipitant concentration was 25.0 mM (5× excess over the rhodium concentration). The added HCl would act as an appropriate "*in situ*" protonating agent. Precipitation was allowed to proceed for three days, after which the solutions were centrifuged at 6500 rpm, the supernatant decanted and its Rh content analysed by means of ICP-OES.

This experiment was repeated using $HClO_4$ (70% $^{v}/_{v}$ - Fluka) as a protonating agent for the precipitants, in the event that the H^+ concentration was insufficient to fully protonate

the precipitants, particularly at lower HCl concentrations. In this instance, 0.100 M stock solutions of the organic precipitants were prepared in 3.0 M $HClO_4$. The precipitation reactions were then conducted in a similar manner as previously described.

5.2.5 Rh^{III} precipitation from a chloride *"adjusted"* industrial feed solution using organic (poly)amines

The precipitation of Rh^{III} from an industrial feed solution (Heraeus chemicals GmbH) was reinvestigated using the organic precipitants diethylenetriamine (**Deta** – Riedel de Haën), triethylenetetramine (**Teta** - Fluka), tetraethylenepentamine (**Tepa** – Sigma-Aldrich) and tris(2-aminoethyl)amine (**Tren** - Fluka), in the presence of an appropriate protonating agent, *viz.* hydrochloric acid. The composition of the industrial solution is shown in Table 3.1. Prior to precipitation, the total chloride concentration of the industrial feed solution was adjusted to 8.01 M by the addition of the appropriate volume of 32% ($^{v}/_{v}$) HCl (reagent grade - Merck chemicals). Following the addition of HCl, the "adjusted" feed solution was equilibrated at elevated temperature (333.1 ± 0.5 K) for five days; thereafter allowing it to equilibrate for a further five days at 298.1 K prior to its use. The total chloride concentration was confirmed by ICP-OES analysis, as outlined in Chapter 3.

The organic precipitants were prepared in 6.0 M HCl, as described in Chapter 3.2.

Table 3.1: Elemental composition and concentration of the industrial feed solution used throughout this study.

Element	mg/L	M
Au	1	5×10^{-6}
Ag	95	8.8×10^{-4}
Pt	30646	1.5712×10^{-1}
Pd	12827	1.2054×10^{-1}
Ir	997	5.18×10^{-3}
Rh	3435	3.338×10^{-2}
Ru	273	2.70×10^{-3}
Re	< 1	-
Al	164	6.08×10^{-3}
As	7	9×10^{-5}
Co	203	3.44×10^{-3}
Cr	24	4.6×10^{-4}
Cu	2051	3.228×10^{-2}
Fe	21271	3.8091×10^{-1}
Ni	3514	5.987×10^{-2}
Pb	4235	2.044×10^{-2}
Se	< 1	-
Si	318	1.13×10^{-2}
Te	1468	1.150×10^{-2}
Zn	8	1×10^{-4}

The precipitation titration consisted of a series of 25-30 samples in which the same volume of the adjusted feed solution was used, while the organic precipitant concentration was gradually increased along the series. The precipitation reaction was allowed to proceed for three days at 298.1 K, after which the samples were centrifuged at 6500 rpm and the supernatant decanted. The metal content of the supernatant was analysed by means of ICP-OES, and that of the precipitate inferred by mass balance of the metal content in the aqueous phase before and after the precipitation reaction.

5.3 Results and discussion

5.3.1 ^{103}Rh NMR spectroscopy – A revised Rh^{III} aqua chlorido speciation diagram

In order to determine the concentration of any particular Rh^{III} species when several $[RhCl_n(H_2O)_{6-n}]^{3-n}$ (n=3-6) aqua-chlorido complexes are simultaneously present, with the proposed high-resolution ^{103}Rh NMR spectroscopic speciation technique, it first necessitates the characterization of each of the Rh^{III} species present at any given HCl concentration. Recently, it was demonstrated that at high magnetic fields (14.1 Tesla) and carefully controlled experimental conditions, the high-resolution ^{103}Rh NMR resonance signals of the series of complex anions $[RhCl_n(H_2O)_{6-n}]^{3-n}$ (n=3-6) are resolved into a secondary structure due to small chemical shift differences as a result of both isotopologues and the possible isotopomers within each set of $[Rh^{35/37}Cl_n(H_2O)_{6-n}]^{3-n}$ isotopologues [9]. This arises from the natural $^{35/37}$Cl isotope distribution of the chlorido ligand(s) coordinated to Rh^{III}. The resulting line-shapes of the ^{103}Rh NMR resonances for this series of complexes essentially constitute an explicit $^{35/37}$Cl isotope-resolved "fingerprint" for the characterization of all the species in this series including stereoisomers, for instance *cis*- or *trans*-$[RhCl_4(H_2O)_2]^-$, provided that at least one chloride ligand remains bound to the Rh^{III} metal-centre and exchanges slowly on an NMR time-scale. Therefore, the $^{35/37}$Cl isotope resolved ^{103}Rh NMR resonances are effortlessly assigned without the need for accurate $\delta(^{103}Rh)$ chemical shifts. The major intricacy arising when relying on accurate $\delta(^{103}Rh)$ chemical shifts for species identification is that chemical shifts, especially of heavy nuclei, is extremely sensitive toward a variety of secondary effects such as concentration, type of solvent, composition of matrix and

temperature. These effects essentially render accurate $\delta(^{103}Rh)$ chemical shifts relatively tentative in solutions that are of relevance to the PGM refining industry.

Nuclear magnetic resonance, by definition, is a quantitative spectroscopic tool because the area of a resonance peak is directly proportional to the number of resonant nuclei contributing to the peak. In this regard the longitudinal (spin-lattice) relaxation time (T_1) measurements play an integral role in establishing whether or not quantitative conditions in NMR spectroscopy have been met. However, due to the low receptivity of the ^{103}Rh nucleus, it would be unrealistic to conduct elaborate experiments to determine the T_1 relaxation time of each $[RhCl_n(H_2O)_{6-n}]^{3-n}$ (n=3-6) species since the time required to obtain a ^{103}Rh NMR spectrum with an acceptable S/N ratio is in the order of ≥ 12 hours, depending on the Rh concentration of the sample. Moreover, a detailed search of the literature yielded no reliable measured estimates of ^{103}Rh T_1 relaxation times, particularly for the octahedral Rh^{III} complexes involved in this study. In order to crudely ascertain if quantitative conditions of the proposed ^{103}Rh NMR speciation method have been met, several ^{103}Rh NMR spectra of a single sample were acquired. For each repeat, the relaxation delay between pulses was varied from 2 to 13 s, while keeping all other spectrometer parameters constant. It stands to reason that if the T_1 relaxation time is long, then the area of the resonance peaks for each spectrum acquired as a function of increasing relaxation delay would differ substantially. However, it was found that the resulting spectra were identical in all regards, and yielded the same integrated peak areas (within experimental error) for the $[RhCl_n(H_2O)_{6-n}]^{3-n}$ (n = 5,6) species investigated. This is clearly reflected when the ratio of the integrated peak area, $A([RhCl_6]^{3-})/A([RhCl_5(H_2O)]^{2-})$, is plotted as a function of the relaxation delay time applied, Figure 1. This figure illustrates a relaxation delay ≥ 2 s would suffice in order to achieve quantitative NMR conditions. Furthermore, the rotational correlation time, τ_c, normally determined through relaxation time measurements, was roughly estimated using the guideline described by Sanders and Hunter [16]. The rotational correlation time for "small" molecules in aqueous phase at room temperature can be given by τ_c / ps ≈ M_r, where M_r is the relative molecular mass. Thus, for $[RhCl_6]^{3-}$, the correlation time would be ≈ 315.62 ps, implying fast molecular motion. In the event of fast molecular motion, it is often assumed that $T_1 \approx T_2$. The effective transverse relaxation time, T_2^*, can be obtained by the following equation:

$$T_2^* = \frac{1}{\pi \, \Delta\upsilon_{1/2}} \qquad (5.1)$$

where $\Delta\nu_{1/2}$ is the peak width at half peak height

For $[RhCl_6]^{3-}$, the average $\Delta\nu_{½}$ = 35 Hz and when substituting this value into equation (5.1), T_2^* = 0.01 s. Therefore, T_1 for $[RhCl_6]^{3-}$ can be estimated to be 0.01 s which implies that quantitative conditions have been met since a total recycle time of 2.5 seconds, which is greater than five times T_1, was used throughout this study.

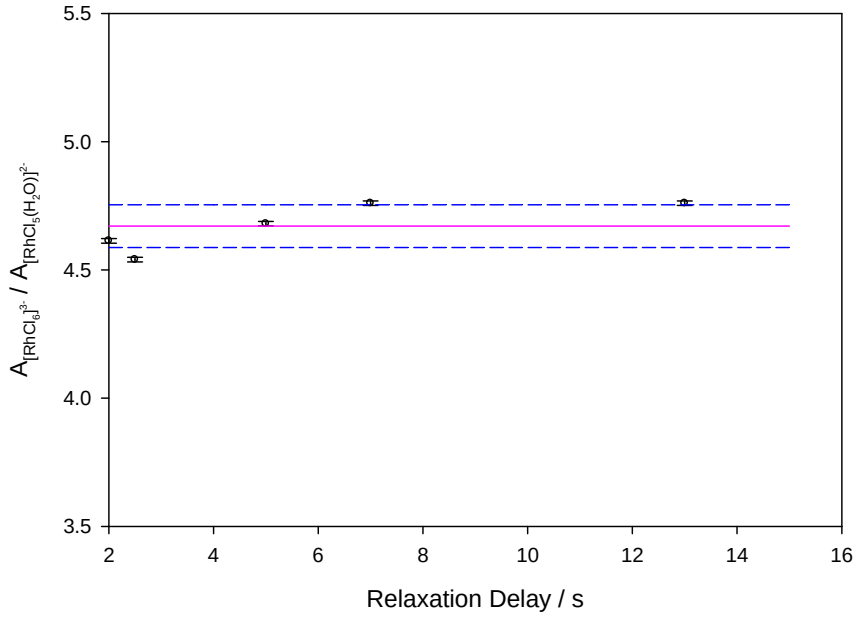

Figure 5.2: The ratio of the integrated peak area A($[RhCl_6]^{3-}$)/A($[RhCl_5(H_2O)]^{2-}$) as a function of the relaxation time applied. The horizontal lines shows the 95% confidence interval (blue dashed lines) of the average peak area ratio (solid pink line)

The ^{103}Rh NMR spectra recorded for several solutions that contain varying HCl concentrations illustrate that an increase in the free chloride concentration leads to an increase in chloride anation, as the aqua ligands are successively substituted with chlorido ligands, Figure 5.2[10] and equation 5.2.

$$[RhCl_{6-n}(H_2O)_n]^{3-n}(aq) + nCl^-(aq) \rightleftharpoons_{\beta_n} [RhCl_6]^{3-}(aq) + n\,H_2O\,(l) \quad (n=1\text{-}6) \quad (5.2)$$

$$\text{where: } \beta_n = \frac{[RhCl_6^{3-}]}{[RhCl_{6-n}(H_2O)_n^{3-n}][Cl^-]^n} \quad (5.3)$$

[10] A nominal peak area of 1.00 was allocated to the $[RhCl_5(H_2O)]^{2-}$ species and the peak area of all other species were scaled relative to that of the $[RhCl_5(H_2O)]^{2-}$ species' peak area, since this species was observed at all the HCl concentrations investigated.

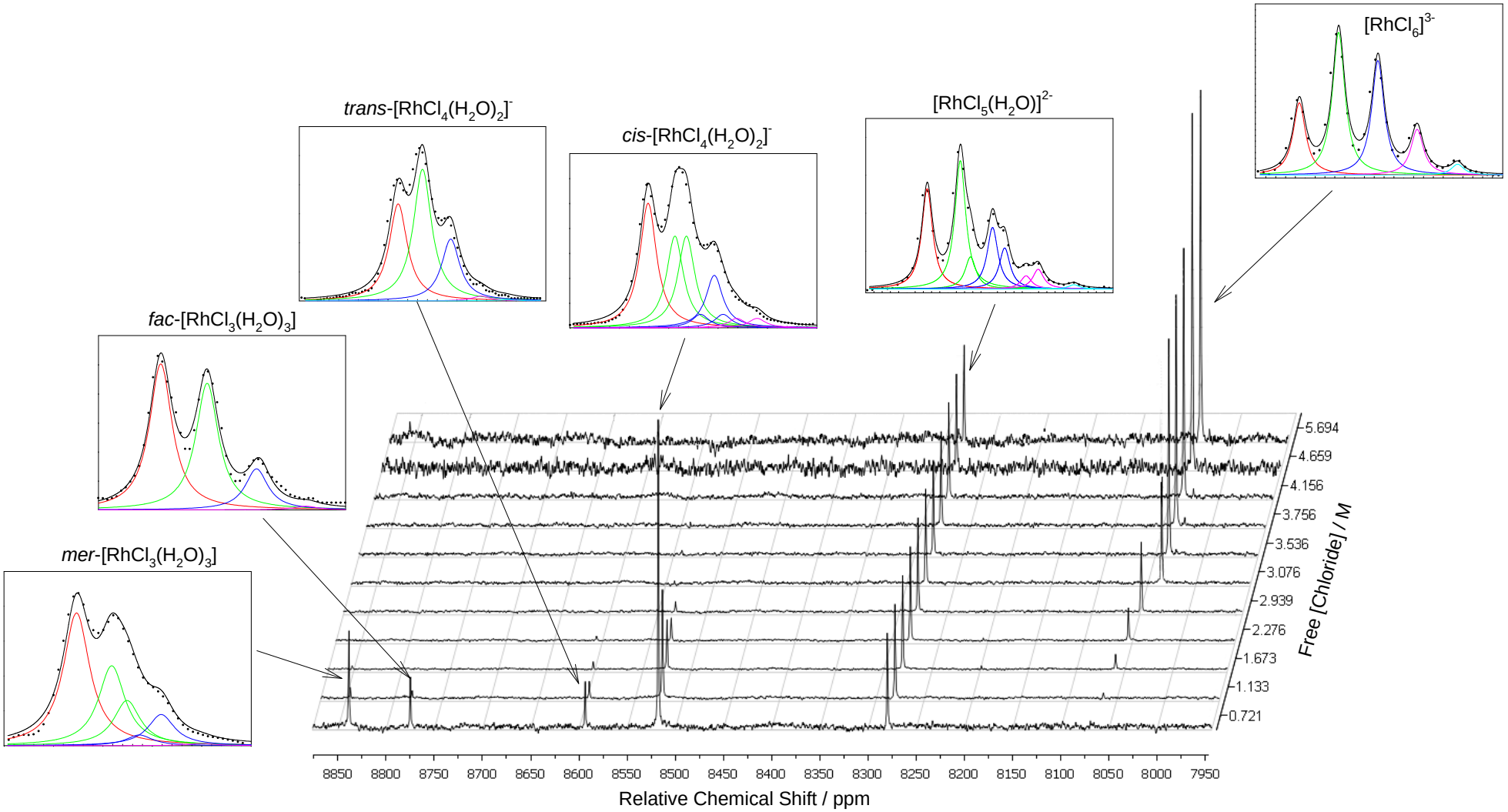

Figure 5.3: Change in the ^{103}Rh NMR resonances of the $[RhCl_n(H_2O)_{6-n}]^{3-n}$ (n=3-6) complexes as a function of free chloride concentration. The assignment of the resonances is based on the $^{35}Cl/^{37}Cl$ isotope effects, as exhibited by the insert figures.

Quantification of the respective Rh^{III} species was performed by integrating each individual ^{103}Rh NMR resonance peak. Division of the individual peak area by the total sum of all the Rh^{III} species' peak areas yields the mole fraction of each individual Rh^{III} species. Multiplication of the mole fraction of the Rh^{III} species by the known total rhodium concentration yields the individual concentration of each Rh^{III} aqua-chlorido species. The free chloride concentration was quantified by multiplying the concentration of the individual Rh^{III} species with the number of chloride ligands coordinated to the metal centre and then subtracting the sum value of the coordinated chloride ligands from the known total chloride concentration.

A partial Rh^{III} speciation diagram was constructed as a function of free chloride concentration, Figure 5.4. Comparing the postulated species distribution with that documented in literature at selected chloride concentrations, Table 5.1, highlights several interesting facts. (*i*) The documented HCl concentrations at which a 1:1 ratio of $[RhCl_6]^{3-}$ and $[RhCl_5(H_2O)]^{2-}$ species exists varies between 0.04 to 8.3 M [4]. As may be seen from Figure 5.4, the HCl concentration at which a 1:1 ratio of these species exists is 3.08 M. (*ii*) The higher aquated Rh^{III} species, $[RhCl_n(H_2O)_{6-n}]^{3-n}$ (n=3-4), persists in appreciable concentrations up to approximately 3.0 M HCl [4,5]. However, the most important difference, from a solvent- or solid phase extraction perspective, occurs at 1.0 M HCl. At this HCl concentration it was found that, based on the postulated species distribution diagram (Figure 5.4), the $[RhCl_5(H_2O)]^{2-}$ species is in 34% abundance. This is in stark contrast to the data published by Cozzi and Pantani [1] and Benguerel *et al* [4] claiming 70 and 80% abundances, respectively. It is also in contrast to the recent studies reported by Gerber *et al* [5], that claim a $[RhCl_5(H_2O)]^{2-}$ species abundance of 8-10% at an HCl concentration of 1.0 M. Furthermore, the equilibrium constant for the reaction illustrated by equation (5.2), for n = 1, calculated in this study was found to vary between 0.67 – 0.82 $L.mol^{-1}$, which is inconsistent with the value of 0.10-0.12 $L.mol^{-1}$ documented in literature [2-5]. This high equilibrium constant can be attributed to the high ionic strength at which the experiments were conducted. An increase in the ionic strength implies a decrease in the activity of water (as highlighted in Chapter 2), which suppresses the aquation of the $[RhCl_6]^{3-}$ complex anion thereby leading to an inherently larger calculated equilibrium constant. It should also be noted that the speciation diagram proposed in this study was conducted as a function of HCl concentration and no attempt was made to keep the ionic strength of the examined solutions constant, as reported in literature [4], so as to better reflect authentic industrial process

solution conditions. The Rh^{III} samples prepared in this study thus reflect what can be expected in the mining industry for a Rh feed solution, since "all" base and associated PGMs are removed prior to rhodium recovery. The validity of the ^{103}Rh NMR spectroscopic method was tested by periodically repeating measurements over a period of one year in order to ensure (*i*) that chemical equilibrium has been attained, and (*ii*) the reproducibility of the method under identical experimental conditions, Figure 5.4. It is evident that even after one year the measurements were reproducible, which also indicates that chemical equilibrium was achieved, Figure 5.4.

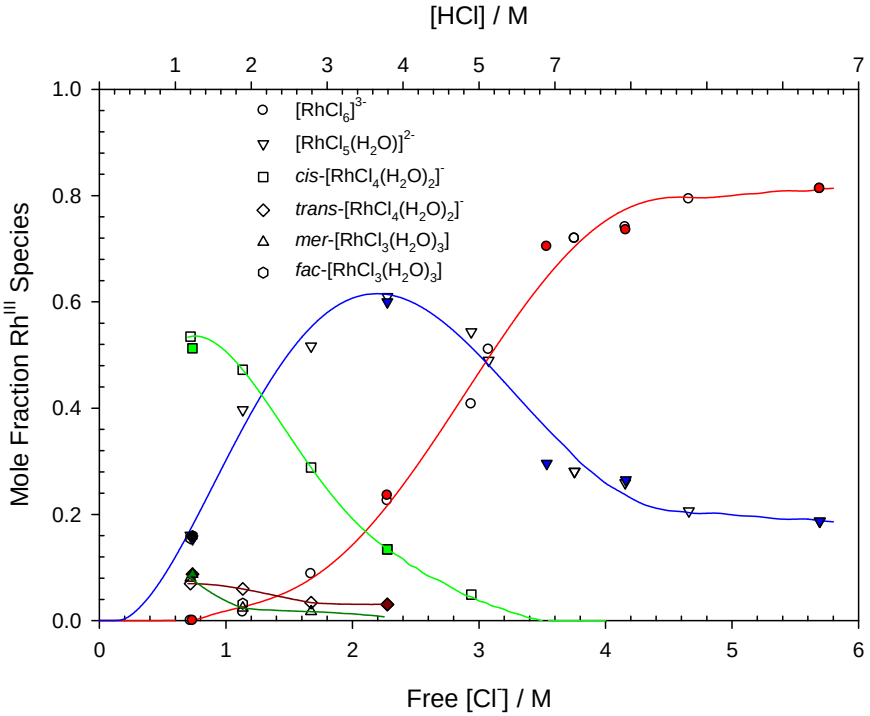

Figure 5.4: Partial species distribution diagram as a function of HCl concentration for all $[RhCl_n(H_2O)_{6-n}]^{3-n}$ (n=3-6) species, including stereoisomers. The open symbols represent data obtained directly after sample preparation; the closed (coloured) symbols represent data obtained after the samples have equilibrated at 298.1 K for a year.

Further validation for the proposed Rh^{III} speciation diagram, Figure 5.3, is based on the aquation kinetics of the $[RhCl_n(H_2O)_{6-n}]^{3-n}$ (n=5,6) complex anions, Figure 5.4. It is evident from Figure 5.4 that at an ionic strength of 3.012 M HCl, minimal aquation of the $[RhCl_5(H_2O)]^{2-}$ complex anion takes place, which is indicated by the absence of the second set of isosbestic points commonly associated with the aquation of the $[RhCl_5(H_2O)]^{2-}$ complex anion. At a free chloride concentration of 3.076 M, the species distribution was calculated at 51.2% $[RhCl_6]^{2-}$ and 48.8% $[RhCl_5(H_2O)]^{2-}$, with no formation of the *cis*-

$[RhCl_4(H_2O)_2]^-$ species, Figure 5.4, which is corroborated with the kinetic observations made in Figure 5.5.

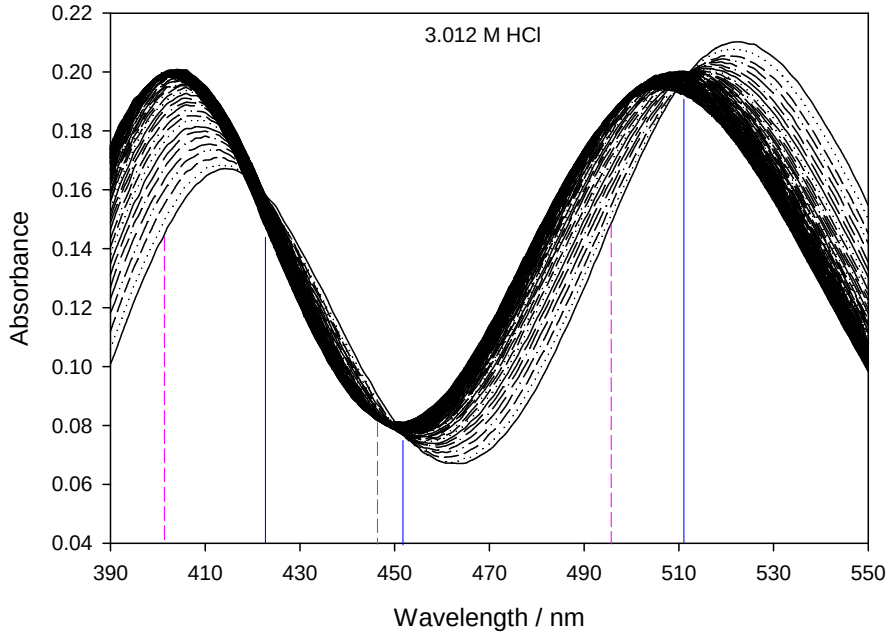

Figure 5.5: The change in the UV-vis spectrum as a function of time (90 minutes) upon dilution of a 0.1038 M Rh^{III} stock solution equilibrated in 10.18 M HCl to a 3.012 M HCl matrix (292.1 K)

Table 5.2: Comparison of the mole fraction $[RhCl_n(H_2O)_{6-n}]^{3-n}$ (n=3-6) species at various $[Cl^-]_{free}$ between this study and that reported in literature. The $[Cl^-]$ of the $[RhCl_n(H_2O)_{6-n}]^{3-n}$ (n=5,6) species' cross-over points are also included for comparison

REF	[HCl] / M	Mole Fraction Rh^{III} species						$[Cl^-]_{free}$ of $[RhCl_n(H_2O)_{6-n}]^{3-n}$ (n=5,6) cross–over point / M
		$[RhCl_6]^{3-}$	$[RhCl_5(H_2O)]^{2-}$	$[RhCl_4(H_2O)_2]^-$		$[RhCl_3(H_2O)_3]$		
				cis-$[RhCl_4(H_2O)_2]^-$	*trans*-$[RhCl_4(H_2O)_2]^-$	*fac*-$[RhCl_3(H_2O)_3]$	*mer*-$[RhCl_3(H_2O)_3]$	
[7]	1	0.32	0.66	0.02[a]		-		2.01
	3	0.70	0.30	-		-		
	5	0.89	0.11	-		-		
[8,9]	1	0.10	0.80	0.10[a]		-		8.33
	3	0.26	0.71	0.03[a]		-		
	5	0.36	0.62	0.02[a]		-		
[10]	1	0.13	0.80	0.07[a]		-		4.92
	3	0.27	0.70	0.03[a]		-		
	5	0.51	0.49	-		-		
[11]	1		0.08[b]	0.24	0.23	0.05	0.45	-
	3		0.54[b]	0.38	0.04	-	0.02	
	5		0.92[b]	0.03	-	-	-	
This Study	1	0.02	0.31	0.50	0.07	0.03	0.06	3.05
	3	0.46	0.51	0.04	-	-	-	
	5	0.80	0.20	-	-	-	-	

[a] The polarographic and UV-vis methods documented by references [7] and [8,9], respectively, cannot discern between stereoisomers. The mole fraction of the $[RhCl_4(H_2O)_2]^-$ species is thus given as a sum mole fraction of the *cis/trans* stereoisomers

[b] The hyphenated ion-pair HPLC-ICP-MS method developed by Gerber *et al* [11] did not allow for the separation of the $[RhCl_n(H_2O)_{6-n}]^{3-n}$ (n=5,6) species, since these species eluted as a single band. The sum of the mole fraction of these two species is presented.

5.3.2 Hyphenated reversed-phase ion-pair HPLC-ICP-OES separation and chemical speciation of $RhCl_n(H_2O)_{6-n}]^{3-n}$ (n=3-6) complex anions – correlation to ^{103}Rh NMR derived speciation diagram

Gerber *et al* [5] recently reported a reversed-phase ion-pair HPLC-ICP-MS method for the separation and quantification of $[RhCl_n(H_2O)_{6-n}]^{3-n}$ (n=0-6) aqua-chlorido complexes. Based on these studies, a revised $[RhCl_n(H_2O)_{6-n}]^{3-n}$ speciation diagram, differing extensively from that previously reported in literature [2-5], is proposed. Despite the comprehensive investigation pursued by Gerber *et al* [5], a detailed species distribution of $[RhCl_n(H_2O)_{6-n}]^{3-n}$ (n=5,6) complex anions *via* this method is still lacking, since the authors could not successfully separate these two species from each other. This is attributed to the relatively fast aquation of the $[RhCl_6]^{3-}$ species combined with the fact that a 50 µm spherical ODS (octadecyl silane) silica gel was used as the HPLC column stationary phase [5]. It was therefore of interest to explore the developed chromatographic method in order to establish whether an effective separation of these two complex anions could be achieved using modified chromatographic conditions. Furthermore, the results obtained could be used for further validation of the speciation diagram determined by the ^{103}Rh NMR method (*vide infra*).

A critical requirement for the separation of $[RhCl_n(H_2O)_{6-n}]^{3-n}$ (n=3-6) complexes would be that the Rh^{III} aqua-chlorido complexes do not undergo extensive aquation/anation, *i.e.* the species distribution should not change. This is particularly problematic since the aquation of $[RhCl_6]^{3-}$ is known to occur rapidly; with a documented $t_{1/2}$ = 1.3 min at an ionic strength of 0.1 mol.kg^{-1} HCl at 298.1 K (Chapter 2). Thus, to minimize aquation of the $[RhCl_6]^{3-}$ complex anion during a chromatographic run, the chromatographic separation should be rapidly completed. It was found that a mobile phase constituency of 9.0 mM tetrabutylamonium chloride (TBA^+Cl^-), 1.0 mM acetate buffer and 30% ($^v/_v$) methanol and water gave the best results in terms of a 'relatively' rapid ion-pair separation; with methanol acting as a column modifier leading to decreased retention times of the Rh^{III} complexes. The possibility of the formation of Rh^{III} methanolic and/or acetato species, in the given time-frame during which a chromatographic run was conducted, is negated based on the UV-vis spectra recorded as a function of time, Figure 5.6. These figures illustrate (*i*) that no change in the characteristic UV-vis spectra of both $[RhCl_6]^{3-}$ and $[RhCl_5(H_2O)]^{2-}$ was observed, and

(*ii*) the rate of aquation of $[RhCl_6]^{3-}$ is slower than that observed in the absence of added methanol, acetate buffer and TBA^+Cl^-.

The slower Rh^{III} aquation kinetics (when diluting a 0.1038 M Rh^{III} stock solution, initially equilibrated in 10.181 M HCl, in a matrix consisting of 9.0 mM TBA^+Cl^-, 1.0 mM acetate buffer and 30% $^v/_v$ methanol) is attributed to the decreased water activity compared to a Rh solution prepared in the absence of these reagents, Figure 5.5. The aquation model denoted by equations (2.1) and (2.2) was used to simulate the experimental kinetic data. Due to the low chloride concentration, the chloride anation reactions are considered to occur to a negligible extent.

$$[RhCl_6]^{3-} + H_2O \underset{k_{56}}{\overset{k_{65}}{\rightleftharpoons}} [RhCl_5(H_2O)]^{2-} + Cl^- \qquad (2.1)$$

$$[RhCl_5(H_2O)]^{2-} + H_2O \underset{k_{45}}{\overset{k_{54}}{\rightleftharpoons}} \textit{cis}\text{-}[RhCl_4(H_2O)_2]^- + Cl^- \qquad (2.2)$$

The simulated pseudo first-order aquation model resulted in exceptional fits to the experimental data, Figure 5.5 [c], thus validating the proposed aquation model. Moreover, the calculated rate constants, k_{65} and k_{54}, are shown in Table 5.3, and demonstrates that the rate of aquation of both the $[RhCl_6]^{3-}$ and $[RhCl_5(H_2O)]^{2-}$ complex anions is significantly slower when the Rh^{III} stock solution is diluted in a matrix consisting of TBA^+Cl^-, acetate buffer and methanol when compared to a solution prepared in the absence of these reagents.

Diluting the Rh^{III} samples used for ^{103}Rh NMR spectroscopic studies to a 10 mM HCl matrix (in the presence of TBA^+Cl^-, sodium acetate buffer and MeOH – *i.e.* constitution of the chromatographic mobile phase), followed by rapid injection of the diluted sample onto the column yields the chromatographic traces depicted in Figure 5.7. From Figure 5.7, it is evident that the peak eluting at 418 s demonstrates pronounced tailing which is indicative of species interconversion / aquation occurring during the chromatographic run. More importantly, the chromatograms in Figure 5.7 illustrate that an increase in the chloride concentration leads to an increase in the intensity of the peak eluting at 1220 s; with a corresponding decrease in the peaks eluting at 418, 247 and 208 s, respectively. The peak at eluting at 1220 s could be due to either the $[RhCl_6]^{3-}$ or $[RhCl_5(H_2O)]^{2-}$ complex anions, based on the presumption that high chloride concentration would lead to an increase in chloride anation. Conversely, the decreasing intensity of the peaks eluting at 418, 247 and 208 s with increasing chloride concentration leads to the assumption that these peaks are attributed to the higher aquated species, *i.e.* $[RhCl_n(H_2O)_{6-n}]^{3-n}$ (n=3,4); however, definitive assignments can only be made upon quantification of each of the eluted Rh^{III} aqua-chlorido complexes.

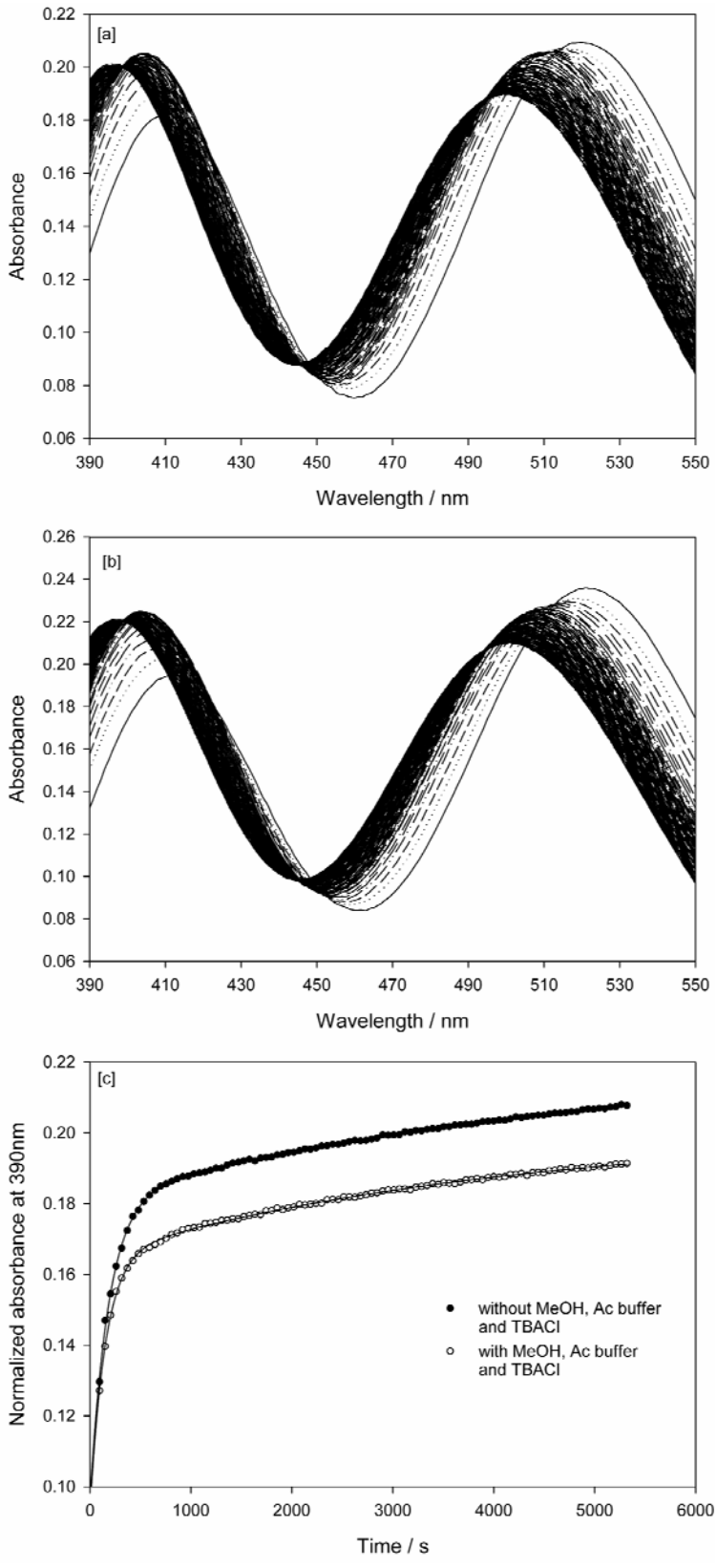

Figure 5.6: Change in Rh^{III} UV-vis spectrum as a function of time (90 minutes) upon dilution of a 0.1038 M Rh^{III} stock solution equilibrated in 10.181 M HCl to a 0.1018 HCl matrix. [a] Rh solution prepared in the absence of MeOH, sodium acetate buffer and $TBA^{+}Cl^{-}$; [b] Rh solution prepared in the presence of MeOH, Ac buffer and $TBA^{+}Cl^{-}$. [c] Kinetic traces illustrating the change in absorbance at 390 nm; symbols = Expt data, Lines = Simulated kinetic fits of the aquation model

Table 5.3: Aquation rate constants of $[RhCl_n(H_2O)_{6-n}]^{3-n}$ (n=5,6) complex anions in (1) the absence of MeOH, Acetate buffer (Ac buffer) and tetrabutylammonium chloride (TBA^+Cl^-), and (2) the presence of MeOH, Ac buffer and TBA^+Cl^-

Sample	Aquation rate constants	
	k_{65} / $\times 10^{-3}$ s^{-1}	k_{54} / $\times 10^{-4}$ s^{-1}
(1) Rh^{III} solution prepared *without* MeOH, Ac buffer and TBA^+Cl^-	8.75	2.39
(2) Rh^{III} solution prepared *with* MeOH, Ac buffer and TBA^+Cl^-	5.19	1.78

Quantification of the Rh^{III} species was done by integrating the entire transient signal as well as the individual peaks. Division of the individual peak area by the total transient signal area yields the mole fraction of the particular species. Multiplication of the mole fraction of the species with the total known rhodium concentration yields the individual Rh^{III} species concentration.

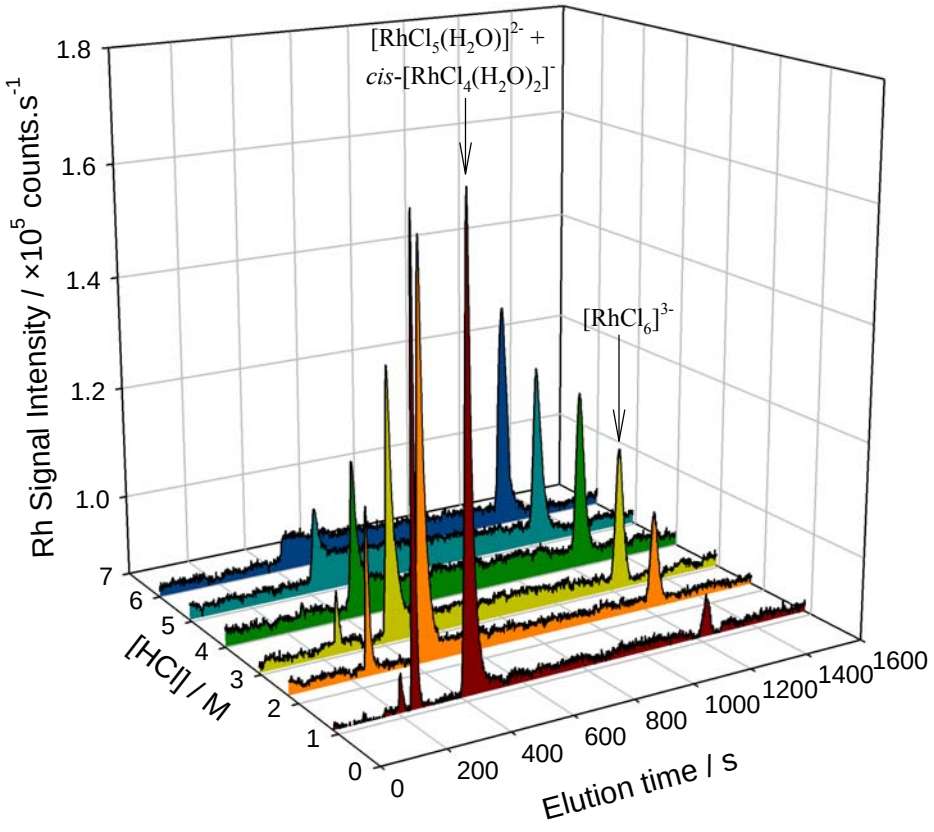

Figure 5.7: Chromatographic traces obtained when injecting Rh^{III} stock samples, initially equilibrated in varying HCl (0.714 – 5.998 M) concentrations, immediately after the appropriate dilution to a 10 mM HCl matrix. Temp = 298.1 K. Several chromatograms were excluded for clarity.

Figure 5.8 shows the partial $[RhCl_n(H_2O)_{6-n}]^{3-n}$ species distribution diagram for the Rh^{III} complexes eluting at 1220 and 418 s, respectively. At first glance, it seems that the species distribution diagram depicted by Figure 5.8 does not correlate well when compared to that depicted in Figure 5.4, with the mole fraction of the Rh^{III} species eluting at 418 s being substantially greater than expected.

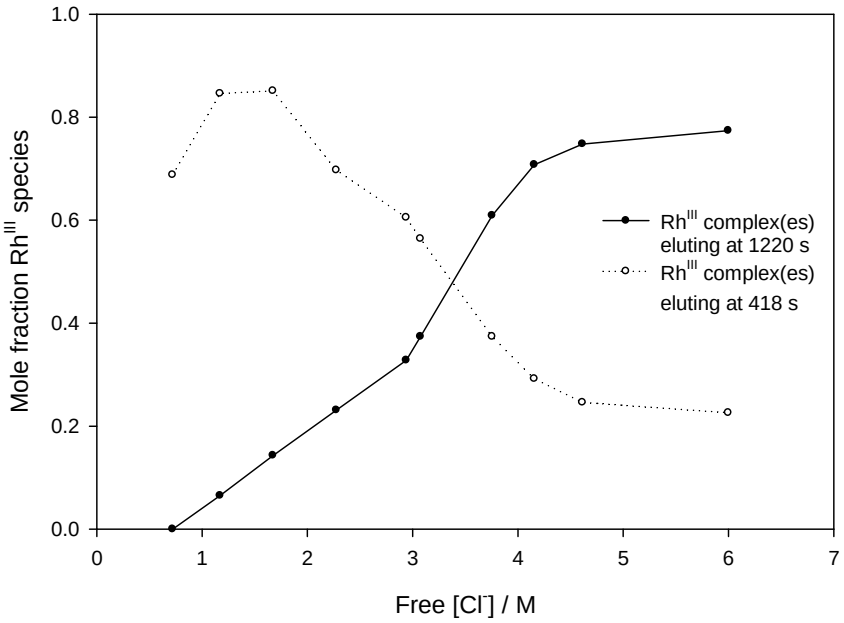

Figure 5.8: Partial $[RhCl_n(H_2O)_{6-n}]^{3-n}$ species distribution diagram as a function of HCl concentration, derived from a modified RP-IP-HPLC-ICP-OES method. The total Rh^{III} concentration of each sample injected was 0.200 mM and the typical RSD for the mole fraction was below 5.5%

Assignment of the Rh^{III} species eluting at 1220 and 418 s, Figure 5.7, was done by comparison of the species distribution of the Rh^{III} aqua-chlorido complexes obtained by the hyphenated RP-IP-HPLC-ICP-OES method to that obtained by means of ^{103}Rh NMR spectroscopic studies, Figure 5.9. Careful inspection of Figure 5.9 reveals that the Rh^{III} species eluting at 1220 s can be ascribed to the $[RhCl_6]^{3-}$ complex anion, as seen from the good correlation between the $[RhCl_6]^{3-}$ distribution determined from the ^{103}Rh NMR spectroscopic study and that of the hyphenated HPLC-ICP-OES method. The distribution of the Rh^{III} species eluting at 418 s can be rationalized by considering that more than one Rh^{III} species elute simultaneously, leading to the unexpected high mole fraction calculated for this "species". In this case, the most likely species to elute as a single band would be the $[RhCl_5(H_2O)]^{2-}$ and *cis*-$[RhCl_4(H_2O)_2]^-$ complex anions. This was confirmed by taking the sum of the mole fraction of these two species, obtained from the ^{103}Rh NMR study, and comparing it with the species distribution of the Rh^{III} species eluting at 418 s, which shows an excellent correlation, Figure 5.9. Therefore, the Rh^{III} species eluting at 1220 s can be

attributed to the $[RhCl_6]^{3-}$ complex anion, while that eluting at 418 s is attributed to both the $[RhCl_5(H_2O)]^{2-}$ and *cis*-$[RhCl_4(H_2O)_2]^{-}$ complex anions. Furthermore, it should be highlighted that this is the first time that the $[RhCl_6]^{3-}$ complex anion was successfully separated from the $[RhCl_5(H_2O)]^{2-}$ complex anion.

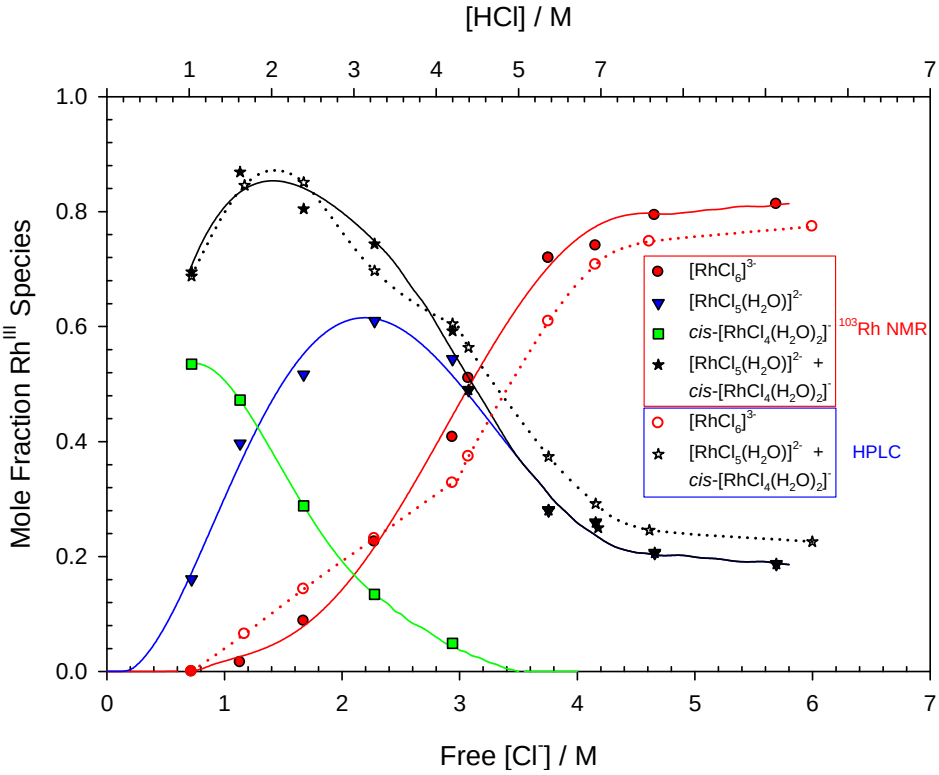

Figure 5.9: Partial $[RhCl_n(H_2O)_{6-n}]^{3-n}$ (n=4-6) species distribution diagram as a function of HCl concentration comparing the data obtained from HPLC-ICP-OES separations (dashed lines & open symbols) to that of the ^{103}Rh NMR spectroscopic data (solid lines & coloured symbols)

5.3.3 Ion-pair (poly)amine precipitation of $[RhCl_n(H_2O)_{6-n}]^{3-n}$ (n=5,6) species as a function of HCl concentration – The effect of Rh^{III} speciation

It is well known that PGMs can be separated by solvent extraction as well as "selective" precipitation [17]. The "selective" precipitation of Rh^{III} aqua-chlorido species from complex PGM-rich media have been highlighted by Crozier and Grant [17]. In this regard, it was reported [17] that various (poly)amine compounds, such as diethylenetriamine, have been used for the precipitation of Rh^{III} aqua-chlorido complexes. To this extent, the HCl concentration at which precipitation should be conducted becomes important for two reasons. (*i*) The H^+ concentration should be sufficient in order to ensure complete protonation of the (poly)amine in question. (*ii*) The Cl^- concentration should be adequate for the formation of predominantly the $[RhCl_6]^{3-}$ complex anion, in view of the fact that only this species is presumably precipitated from solution.

In this study the focal point was to use diethylenetriamine, triethylenetetramine, tetraethylenepentamine and tris(2-aminoethyl)amine for the precipitation of the Rh^{III} aqua chlorido-species to establish the effect of Cl^- concentration on not only the precipitation of these species from solution, but also to probe the extent of correlation between this study and the speciation results obtained from the ^{103}Rh NMR spectroscopic study.

Figure 5.10[a] visually illustrates the effect of the HCl concentration on the speciation of Rh^{III} aqua chlorido-complexes. Addition of unprotonated (poly)amine to each of the Rh^{III} containing solutions leads to the following observations (with the (poly)amine : Rh^{III} mole ratio precipitation titration curves illustrated in Figures 5.11[a] & [b]):
(*i*) Addition of unprotonated (poly)amine to Rh^{III} solutions containing less than 0.10 M HCl results in the formation of a yellow precipitate, Figure 5.10[b] (*solutions 1 and 2*) and Figure 5.11[a]. This is presumably due to hydrolyzed Rh^{III} species, $[RhCl_n(OH)_{6-n}]^{3-}$ (n=0-6), which is known to be sparingly soluble in aqueous media.
This was confirmed when repeating the experiments by preparing the (poly)amine stock solutions in a 3.0 M $HClO_4$ matrix in order to facilitate complete protonation of the (poly)amines. Addition of this stock solution, under identical experimental conditions, is associated with the complete absence of (yellow) precipitate formation up to [HCl] > 0.68 M, Figure 5.11[b]. It is, however, important to note that the repeated results cannot be directly correlated to that observed when the (poly)amines were prepared in the absence of $HClO_4$,

since the presence of ClO_4^- anions would affect the solubility-product constant (K_{sp}) of formation of the Rh^{III} - (poly)ammonium precipitate.

(*ii*) At HCl concentrations ranging from 0.10 to 0.6 M (a factor of 20 - 120 times excess HCl over the Rh concentration) no precipitate formation is observed, Figure 5.10[b] (*solutions 3 - 6*) and Figure 5.11[a]. Similar observations were made when the (poly)amine stock solutions, prepared in a 3.0 M $HClO_4$ matrix, were added to the Rh^{III} containing solutions; thus negating the possibility that these trends are due to insufficient / incomplete protonation of the (poly)amines, Figure 5.11[b].

(*iii*) At [HCl] > 0.60 M the formation of a deep rose-red coloured precipitate is formed (Figure 5.10[a] *solutions 7 – 10*), which is characteristic of the Rh^{III}-(poly)ammonium ion-pair. Thus, at [HCl] > 0.60 M, the typical (poly)ammonium : Rh^{III} mole ratio precipitation titration curves are exhibited, Figure 5.11.

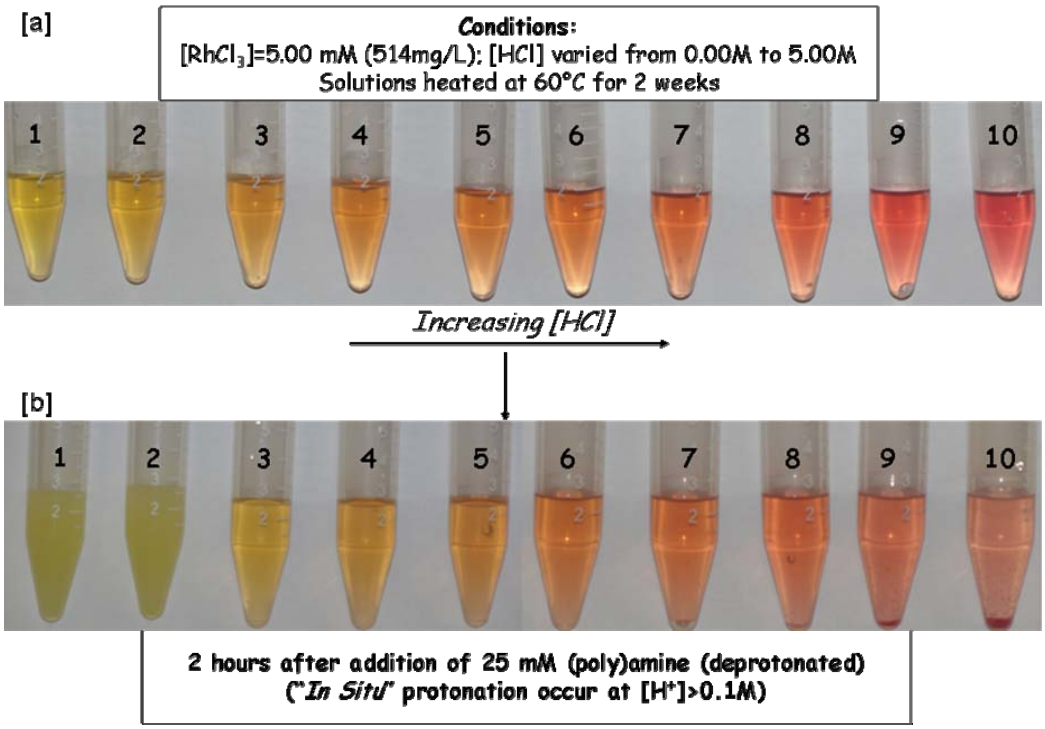

Figure 5.10: Visual illustration of 5.00 mM Rh^{III} solutions equilibrated at various HCl concentrations (0.00 – 5.00 M). [a] before addition of (poly)amines, [b] 2 hours after addition of the (poly)amines. The (poly)amine concentration added to each solution was always 5 times excess over the Rh concentration, which is sufficient to achieve quantitative precipitation of Rh.

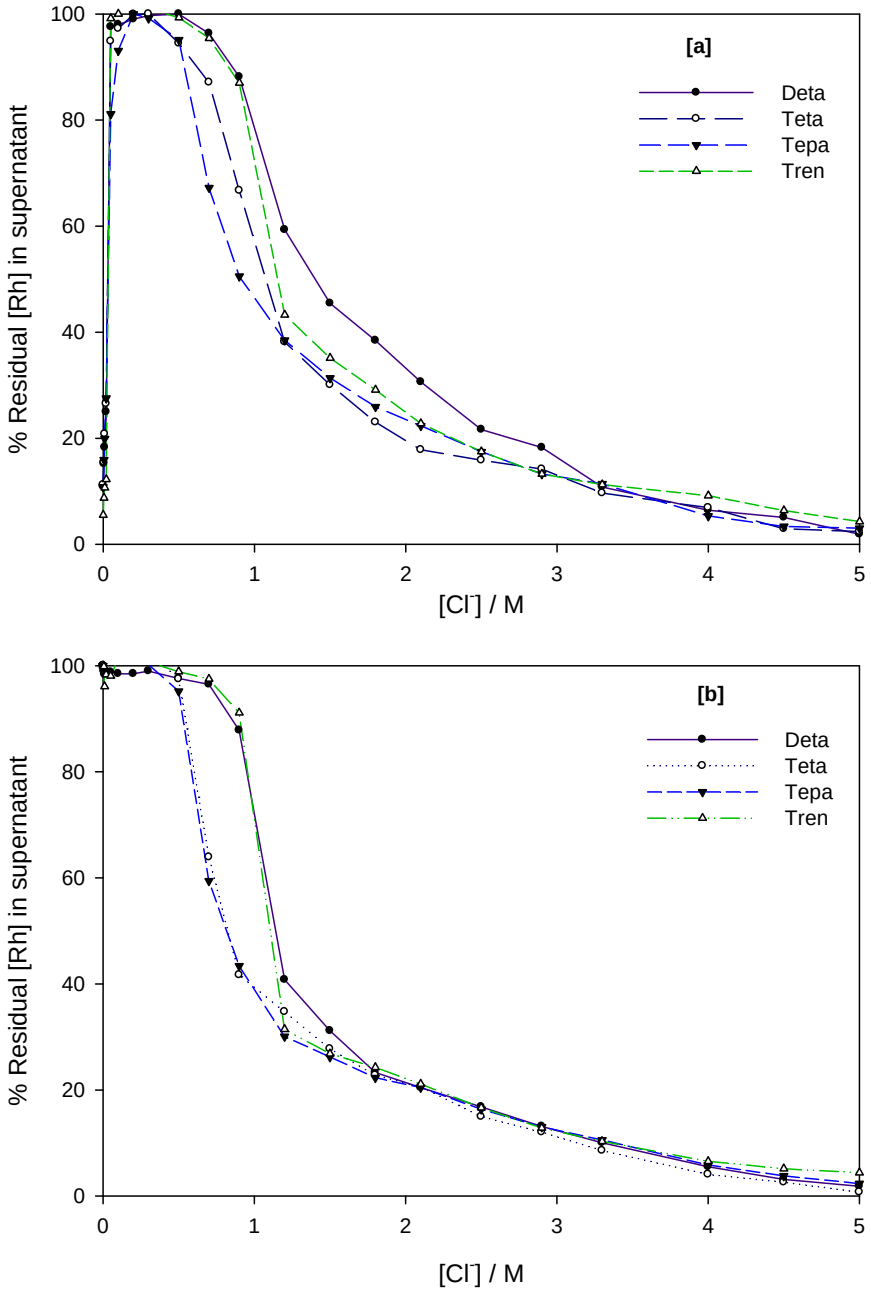

Figure 5.11: Rh^{III} precipitation conducted as a function of chloride concentration. The organic (poly)amines used are denoted in the legend. [a] Precipitation studies conducted by "*in situ*" protonation of the (poly)amines, which typically occur at [HCl] > 0.100 M; [b] Precipitation studies conducted by protonating the (poly)amine, using a 3.0 M $HClO_4$ matrix, prior to addition of the (poly)amine stock solutions to the Rh^{III} containing solutions. [Rh] = 5.00 mM, [Amine] = 25.00 mM. All precipitation studies were conducted at 298.1 K and repeated in triplicate. Typical RSD values for the [Rh] were below 5%.

From Figure 5.11 it becomes evident that the chloride concentration, and hence the $[RhCl_n(H_2O)]_{6-n}]^{3-}$ (n=0-6) species distribution, plays an important role in the quantitative recovery of Rh from aqueous chloride solutions. In each of these series of precipitation titrations, the quantitative precipitation (> 98%) of Rh^{III} is observed at HCl concentrations greater than 4.497 M, Figure 5.11. Since the total Rh^{III} concentration can be accurately determined, the total mole fraction of the Rh^{III} aqua-chlorido complex anions can be determined as a function of the total HCl concentration, equation (5.4).

$$\text{Mole Fraction } Rh^{III} = 1 - \left(\frac{[Rh]_{Precipitated}}{[Rh]_{Total}} \right) \qquad (5.4)$$

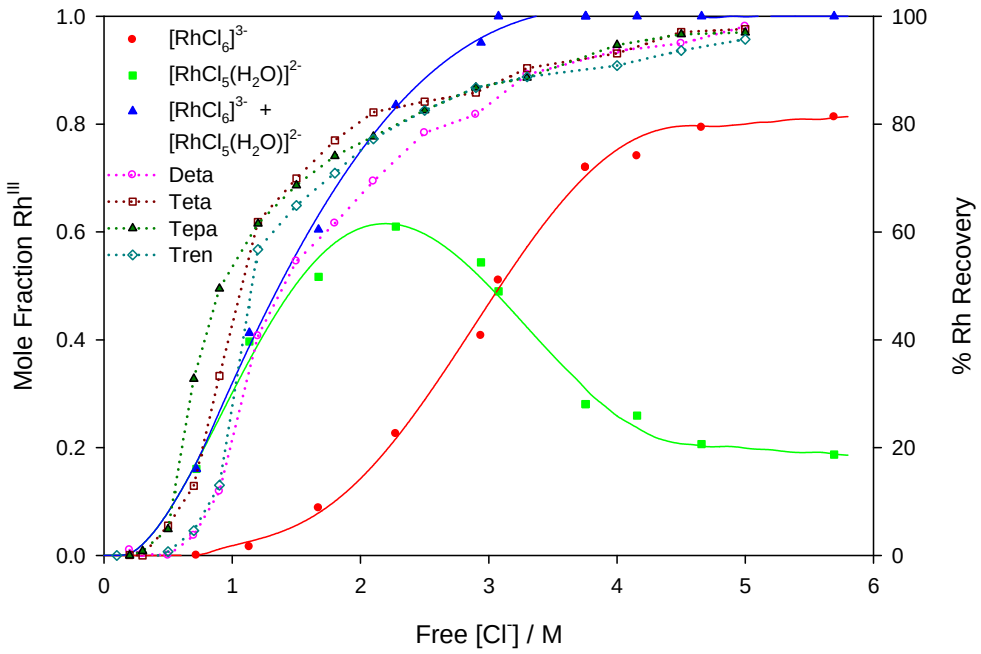

Figure 5.12: Partial $[RhCl_n(H_2O)_{6-n}]^{3-n}$ (n=5,6) species distribution diagram as a function of HCl concentration comparing the data obtained from precipitation titrations (dashed lines & open symbols) to that of the ^{103}Rh NMR experiments (solid lines and closed symbols)

The species distribution calculated from the precipitation studies however does not correlate with that of the $[RhCl_6]^{3-}$ or $[RhCl_5(H_2O)]^{2-}$ species distributions determined from the ^{103}Rh NMR measurements. Thus, the possibility that both the $[RhCl_6]^{3-}$ and $[RhCl_5(H_2O)]^{2-}$ species can be precipitated [20,21] should be taken into account when corroborating the precipitation data with that of the ^{103}Rh NMR experiments. By taking the sum of the mole fraction of the $[RhCl_n(H_2O)_{6-n}]^{3-n}$ (n=5,6) anions obtained from the ^{103}Rh NMR spectroscopic experiments excellent correlation to the precipitation data is observed,

Figure 5.12, substantiating the notion that both the $[RhCl_n(H_2O)_{6-n}]^{3-n}$ (n=5,6) anions can be precipitated from solution. Regarding the latter rationale, the structure of both $K_3[RhCl_6]$ as well as $K_2[RhCl_5(H_2O)]$ have recently been elucidated through X-ray crystallographic studies [18]. Moreover, the crystal structure of several (poly)ammonium-Rh^{III} compounds have been reported, including diethylenetriammonium hexachlororhodate(III) [19], $(H_3N(CH_2)_2NH_2(CH_2)_2NH_3)[RhCl_6]$, triammonium hexachlororhodate(III) [20], $(NH_4)_3[RhCl_6]$ and the diammonium aquapentachlororhodate(III) [21], $(NH_4)_2[RhCl_5(H_2O)]$, complexes. From these studies it is thus evident that both the $[RhCl_n(H_2O)_{6-n}]^{3-n}$ (n=5,6) aqua-chlorido species could be precipitated from a chloride-rich matrix. Furthermore, there is an unmistakable change in the colour of the precipitate, from dark purple to light pink, as the HCl concentration of the solutions were increased. In addition, by decreasing the HCl concentration there is a substantial decrease in the amount of Rh^{III} precipitated, Figures 5.11 and 5.12, which is attributed to the formation of the higher aquated species, $[RhCl_n(H_2O)_{6-n}]^{3-n}$ (n=0-4), at lower chloride concentrations. These findings highlight the profound effect of Rh^{III} species distribution in the determination of appropriate conditions for Rh recovery. Furthermore, it aids in the understanding of anomalies observed in documented literature [22-25], which would provide insight for the possible enhancement of Rh^{III} separation and refining on an industrial scale.

5.3.4 Transition metal (^{195}Pt and ^{103}Rh) NMR spectroscopic studies of authentic industrial feed solutions

Up to this point, the speciation of Rh^{III} aqua chlorido-species has been thoroughly described and the use of ^{103}Rh NMR spectroscopy as an analytical tool for the unambiguous characterisation and speciation has been highlighted. However, these studies were only conducted on laboratory prepared Rh^{III} solutions. In this part of the discussion, the practical relevance of transition metal (more specifically ^{195}Pt and ^{103}Rh) NMR spectroscopy will be extended to authentic industrial feed solutions, as pertinent to the PGM industry.

5.3.4.1 ^{195}Pt NMR spectroscopic study of an authentic Heraeus industrial feed solution

It is well established that the chemical speciation of PGM chlorido-complexes is of critical importance for the efficient separation and refining of PGMs [26-29]. In the case of Pt, the efficiency of the industrial separation schemes are strictly dependent on the knowledge and control of the species distribution of Pt^{IV} anionic chlorido-complexes in solution since, depending on the conditions, aquated $[PtCl_n(H_2O)_{6-n}]^{4-n}$ (n=0-6) complexes or even their hydrolysis products, $[PtCl_{6-n}(OH)_n]^{2-}$ (n=0-6) might be present. In this context, ^{195}Pt NMR spectroscopy was used to evaluate the speciation of Pt^{IV} chlorido-complexes present in a Heraeus PGM containing industrial feed solution in 4.008 M chloride matrix.

The ^{195}Pt NMR spectrum of the industrial feed solution is shown in Figure 5.13. Although various spectral windows were scanned, only one resonance signal was obtained at 25.5 ppm relative to a standard external Pt reference. The assignment of the signal is based on the **deta**iled analysis of the ^{35}Cl/^{37}Cl isotope effects observed in 128.8 MHz ^{195}Pt NMR, which shows that the "fine-structure" of this resonance signal can be understood in terms of the unique isotopologue distribution of $[PtCl_6]^{2-}$ [26]. These ^{35}Cl/^{37}Cl isotope effects in the ^{195}Pt NMR resonance of the $[Pt^{35/37}Cl_6]^{2-}$ complex anion manifest only as a result of the statistically expected ^{35}Cl/^{37}Cl isotopologues. The ^{195}Pt NMR resonance structure thus serves as a unique "finger-print" that can be used for the unambiguous characterization of $[PtCl_n(H_2O)_{6-n}]^{4-n}$ (n=4-6) complexes [26].

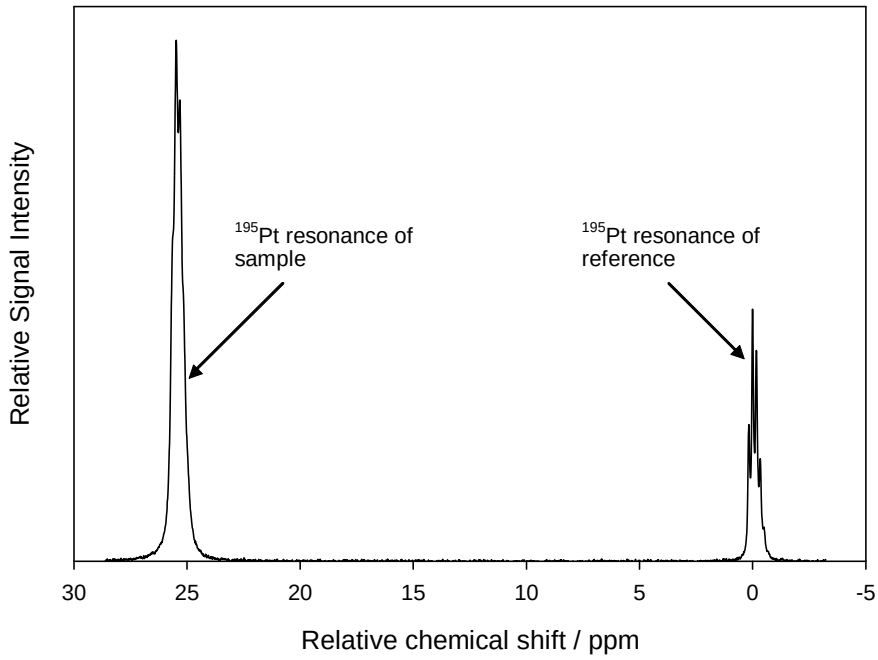

Figure 5.13: ^{195}Pt NMR spectrum of an authentic industrial feed solution

Figure 5.14 shows the well-resolved fine-structure profile for each individual ^{195}Pt NMR resonance, recorded at 292.1 ± 0.1 K, of the $[PtCl_6]^{2-}$ complex anion. This spectrum was obtained from the co-axial reference insert. The well-resolved fine-structure profile of the ^{195}Pt NMR resonance in $[PtCl_6]^{2-}$ is attributed to the ^{35}Cl/^{37}Cl isotope effects. Significantly, the $[PtCl_6]^{2-}$ complex anion is resolved only into six of the seven expected $[Pt^{35/37}Cl_6]^{2-}$ isotopologues, similar to that obtained by Koch *et al* [26]. Only six of the seven peaks attributed to the isotopologues $[Pt^{35}Cl_n{}^{37}Cl_{6-n}]^{2-}$ (n=1-6) were observed experimentally since the statistically calculated abundance of the $[Pt^{37}Cl_6]^{2-}$ isotopologue occur at a very low abundance of 0.02%.

SigmaPlot Version 11 (Systat Software Inc.) was used to perform the non-linear least-squares fits on the ^{195}Pt NMR experimental data. The SigmaPlot curve fitter uses the Marquardt-Levenberg algorithm to find the coefficients/parameters of the independent variable(s) that provide the best fit between the sum of several Lorentzian functions and the experimental data. The non-linear least-squares fit between the experimental and simulated ^{195}Pt spectrum of $[Pt^{35}Cl_n{}^{37}Cl_{6-n}]^{2-}$ (n=1-6) is excellent, which validates the proposed model, Figure 5.14. Furthermore, there is a 22.1 Hz (0.171 ppm) down-field shift upon exchange of a $^{35}Cl^-$ with $^{37}Cl^-$, which is consistent with that found by Koch *et al* [26].

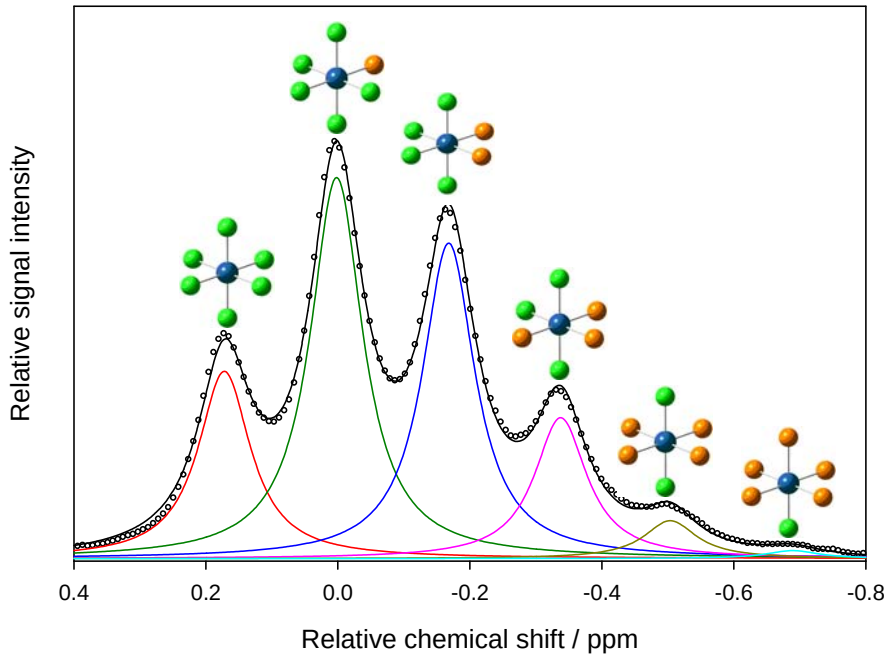

Figure 5.14: ^{195}Pt NMR spectrum (enlarged), recorded at 293.1 K, of the co-axial reference insert, containing pure $[PtCl_6]^{2-}$, illustrating the $^{35/37}$Cl isotopologue induced splitting of the ^{195}Pt resonance signal. The symbols illustrate the experimental data while the solid lines illustrate the isotopologue model fitted to the experimental data. ● = ^{35}Cl; ● = ^{37}Cl

In order to attain optimal correlation between the simulated and experimental data, it is important to equilibrate the solution in the spectrometer for at least 20-30 minutes at the desired temperature (292.1 ± 0.1 K) and conditions under which the magnetic field homogeneity has been optimized. Spectra were recorded at 292.1 K since the $[Pt^{35}Cl_n{}^{37}Cl_{6-n}]^{2-}$ (n=1-6) line-widths are extremely dependent on temperature, with significant loss of resolution (due to line-broadening) reported at temperatures below 283.0 K and higher than 293.0 K [26].

Figure 5.15 shows the ^{195}Pt NMR spectrum of the authentic industrial feed solution, recorded at 292.1 ± 0.1 K. The ^{195}Pt NMR spectrum was subsequently simulated in a similar manner to the reference insert. The non-linear least-squares fit between the experimental and simulated ^{195}Pt NMR spectrum of the $[Pt^{35}Cl_n{}^{37}Cl_{6-n}]^{2-}$ (n=1-6) isotopologue model is excellent, Figure 5.15, thus confirming the isotopologue model. Furthermore, the relative statistical probability, *P(n)*, for each possible isotopologue of the $[Pt^{35}Cl_n{}^{37}Cl_{6-n}]^{2-}$ (n=1-6) complex anion may be calculated at the fractional natural abundance of ^{35}Cl (0.7553) and ^{37}Cl (0.2447) using the binominal probability function, Equation 3.1, where *n* and *r* is the number of coordinated ^{35}Cl and ^{37}Cl, respectively; Table 5.4.

As may be seen from Table 5.4, the agreement between the experimentally calculated and statistically expected isotopologue distribution using the resonance areas is excellent.

$$P(n) = \sum_{n=0}^{n=\frac{(n+r)!}{n!r!}} \left(\alpha^{n}{}_{^{35}\mathrm{Cl}}\alpha^{r}{}_{^{37}\mathrm{Cl}}\right) \qquad (5.5)$$

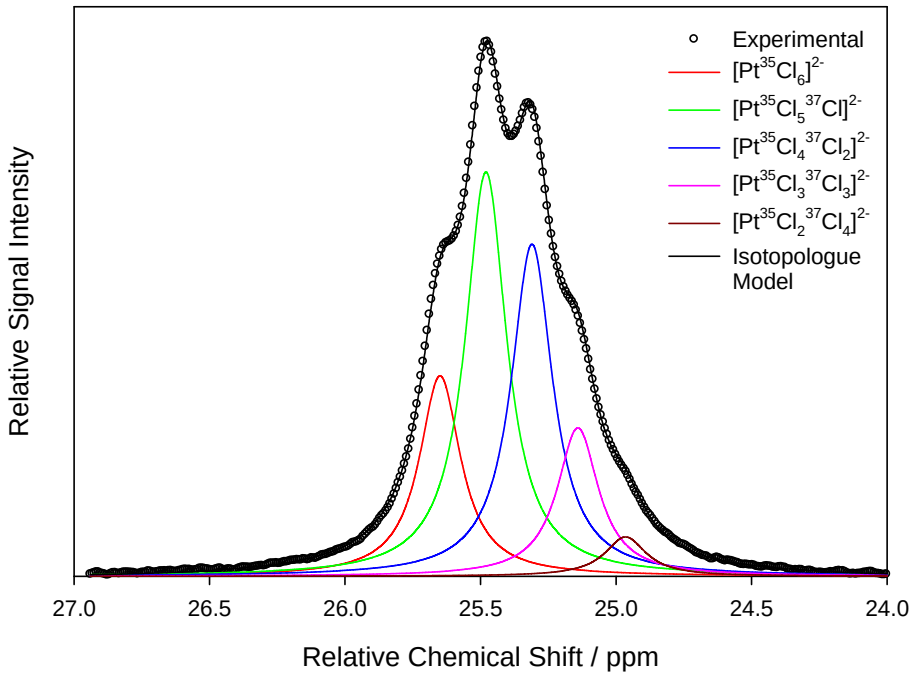

Figure 5.15: Experimental ^{195}Pt NMR spectrum (enlarged) of an authentic industrial feed solution illustrating the "fine-structure" of the ^{195}Pt resonance. The solid lines represent the non-linear least-squares fits of the isotopologue model to the experimental ^{195}Pt NMR spectroscopic data. The symbols represent the experimental data while the solid lines represent the isotopologue model fits.

Table 5.4: Comparison between the experimental and statistical isotopologue distributions for the $[Pt^{35/37}Cl_6]^{2-}$ complex anion

Isotopologue	Percentage $[PtCl_6]^{2-}$ Isotopologue distribution		
	Experimental[a]	Statistical	Literature [26]
$[Pt^{35}Cl_6]^{2-}$	17.82 ± 0.13	18.92	18.78
$[Pt^{35}Cl_5{}^{37}Cl]^{2-}$	35.95 ± 0.09	36.31	36.47
$[Pt^{35}Cl_4{}^{37}Cl_2]^{2-}$	29.53 ± 0.07	29.03	29.03
$[Pt^{35}Cl_3{}^{37}Cl_3]^{2-}$	13.20 ± 0.08	12.38	12.36
$[Pt^{35}Cl_2{}^{37}Cl_4]^{2-}$	3.24 ± 0.02	2.97	2.97
$[Pt^{35}Cl{}^{37}Cl_5]^{2-}$	0.34 ± 0.02	0.38	0.39
$[Pt^{37}Cl_6]^{2-}$	*N. A.*	0.02	*N. A.*

[a] The isotopologue model was fitted by non-linear least-squares analysis to the experimental data (^{195}Pt NMR spectrum of the industrial feed solution – Fig. 3.13[b]) from which the 95% confidence interval was estimated. ^{195}Pt NMR spectra were acquired three separate times, not in succession.

It is evident from Figure 5.15 that there is a significant loss in resolution observed in the ^{195}Pt NMR resonance for the industrial feed solution. This is not ascribed to temperature effects, since the ^{195}Pt resonance observed for the co-axial reference insert displayed well-resolved $[Pt^{35}Cl_n{}^{37}Cl_{6-n}]^{2-}$ (n=1-6) isotopologue resonances. The loss in resolution may be attributed to the presence of low levels of paramagnetic species, e.g. Ir^{IV}, present in the industrial feed solution. However, this is purely speculative as a variety of factors could lead to the loss in resolution. These factors include intra- and inter-molecular chloride exchange, solvent viscosity effects that may influence the processes dependent on molecular correlation times (τ_c) and spin-rotation relaxation mechanisms. Nevertheless, all the $[Pt^{35}Cl_n{}^{37}Cl_{6-n}]^{2-}$ (n=1-6) could be deconvoluted and each ^{195}Pt resonance was assigned, confirming that the Pt present in the feed solution exists exclusively as the $[PtCl_6]^{2-}$ complex anion. The fact that quantitative precipitation of Pt is observed for this industrial solution (Chapter 3) can therefore be attributed to the exclusive existence of the $[PtCl_6]^{2-}$ complex anion in this solution.

5.3.4.2 ^{103}Rh NMR spectroscopic study of an authentic Anglo Platinum industrial feed solution

In order to analyze the practical relevance of the developed ^{103}Rh NMR speciation method, the ^{103}Rh NMR spectrum of an authentic industrial Rh^{III} feed solution (Anglo Platinum PLC) in an HCl matrix was acquired, Figure 5.16. The sample was provided without any additional information from the supplier, except that it *only* contained Rh^{III}, since this was a feed solution prepared for final Rh purification (presumably by diethylenetriammonium precipitation). ICP-OES analysis of the Anglo Platinum Rh feed solution revealed that the total chloride concentration was 2.121 M, and the Rh concentration 0.2109 M[11]. The low Rh concentration results in a decrease in the S/N ratio, which is evident from Figure 5.16.

[11] It should be noted that the feed solution contained a significantly lower Rh concentration (0.2109 M) than was typically used. This is the reason attributed for the decreased S/N ratio, Figure 5.16. Higher resolution (at this Rh concentration) could not be obtained, since this would require unrealistically long acquisition times. For the spectrum depicted in Figure 5.16, 100.000 transients were acquired, corresponding to a total acquisition time of 70 hours.

Three ^{103}Rh NMR resonances were observed at $\delta(^{103}Rh)$ = -84.672 ppm, 159.288 ppm and 235.130 ppm, respectively. Assignment of the observed resonances was based on the $^{35}Cl/^{37}Cl$ isotope effects (as outlined in Chapter 4) revealing that the solution only contained $[RhCl_5(H_2O)]^{2-}$, *cis*-$[RhCl_4(H_2O)_2]^-$ and *trans*-$[RhCl_4(H_2O)_2]^-$ complex anions in appreciable concentrations. An excellent non-linear least-squares fit between the experimental and simulated $^{35}Cl/^{37}Cl$ isotopomer model was obtained for both the $[RhCl_5(H_2O)]^{2-}$ and *cis*-$[RhCl_4(H_2O)_2]^-$ complex anions, Figure 5.17, confirming the assignment of these species. Table 5.5 illustrates the quantitative agreement between the experimentally calculated and the statistically expected isotopomer distribution model for the $[RhCl_5(H_2O)]^{2-}$ and *cis*-$[RhCl_4(H_2O)_2]^-$ complex anions. Due to the low S/N ratio, the *trans*-$[RhCl_4(H_2O)_2]^-$ complex anion [$\delta(^{103}Rh)$ = 235.130 ppm] could not be reliably quantified by means of $^{35}Cl/^{37}Cl$ isotope effects; however, its assignment was confirmed using ^{103}Rh NMR chemical-shift trend analysis [29,30].

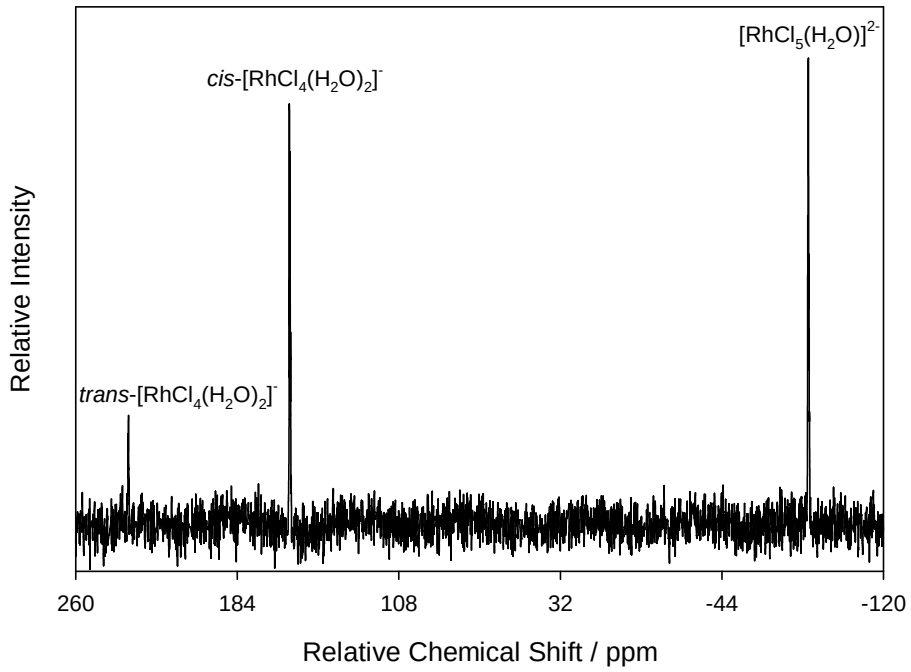

Figure 5.16: ^{103}Rh NMR spectrum of an authentic industrial rhodium feed solution recorded at 292.1 K. $[Rh]_{tot}$ = 0.2109 M; $[Cl^-]_{tot}$ = 2.121 M

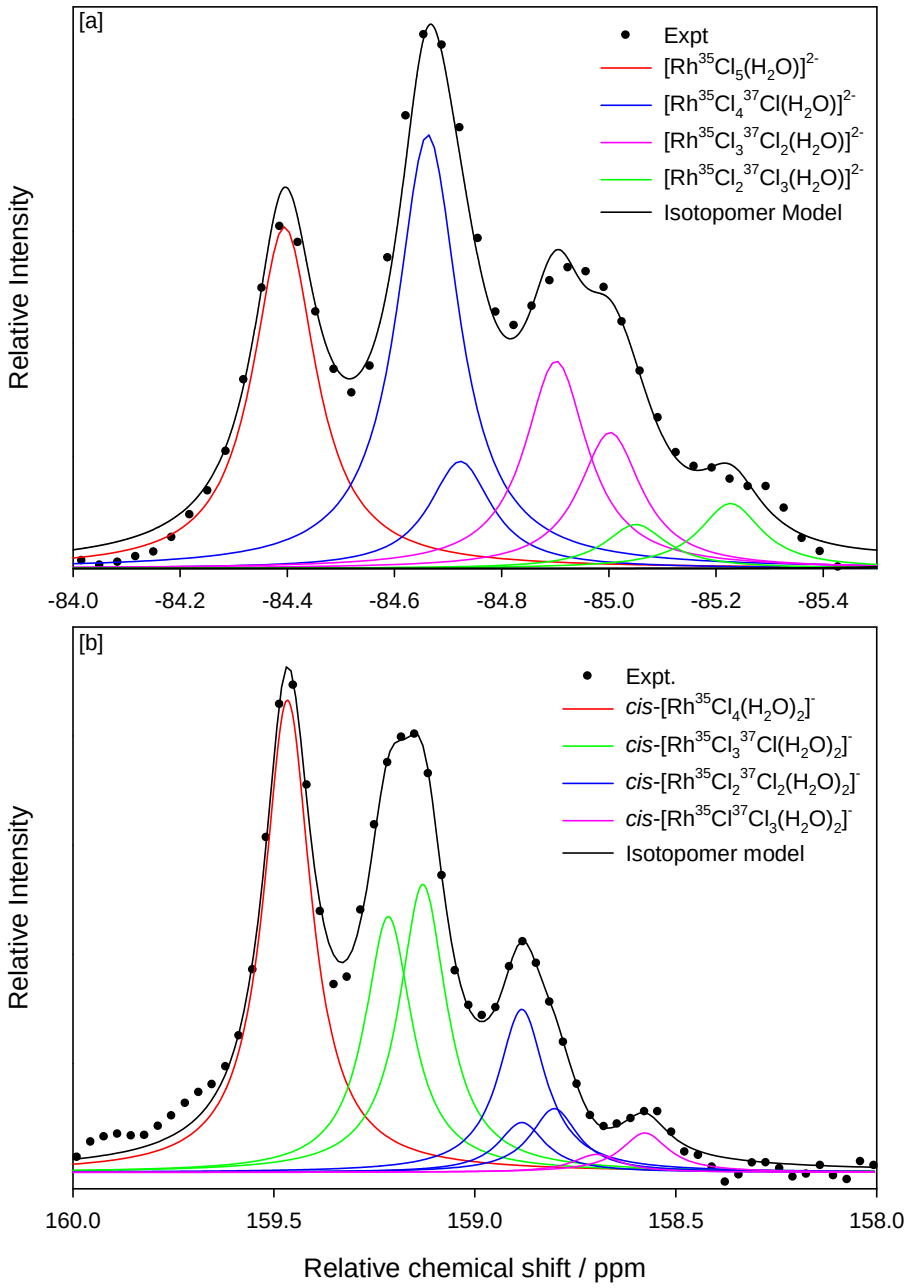

Figure 5.17: Experimental ^{103}Rh NMR spectra of the $[RhCl_n(H_2O)_{6-n}]^{3-n}$ (n=4,5) complex anions recorded at 292.1 K (symbols). [a] $[Rh^{35/37}Cl_5(H_2O)]^{2-}$ complex anion; [b] *cis*-$[Rh^{35/37}Cl_4(H_2O)_2]^-$ complex anion. The non-linear least-squares fits between the experimental spectra and the isotopologue model that includes isotopomers is denoted by the solid lines.

Table 5.5: Comparison of the experimental (simulated from Figure 5.17) and statistically expected isotopomer distributions for the $[Rh^{35/37}Cl_5(H_2O)]^{2-}$ and *cis*-$[Rh^{35/37}Cl_4(H_2O)_2]^-$ complex anions

$^{35/37}Cl$ *trans* to H_2O	Rh^{III} isotopologue	Percent isotopomers		Sum percent of isotopomers to yield isotopologue amount	
		Experimental	Statistical	Experimental	Statistical
^{35}Cl	$[Rh^{35}Cl_5(H_2O)]^{2-}$	25.26	24.97	25.26	24.97
^{35}Cl	$[Rh^{35}Cl_4{}^{37}Cl(H_2O)]^{2-}$	32.07	31.94	40.00	39.93
^{37}Cl		7.93	7.99		
^{35}Cl	$[Rh^{35}Cl_3{}^{37}Cl_2(H_2O)]^{2-}$	15.34	15.32	25.41	25.54
^{37}Cl		10.07	10.22		
^{35}Cl	$[Rh^{35}Cl_2{}^{37}Cl_3(H_2O)]^{2-}$	3.26	3.27	8.07	8.17
^{37}Cl		4.81	4.9		
^{35}Cl	$[Rh^{35}Cl^{37}Cl_4(H_2O)]^{2-}$	0.33	0.26	1.26	1.31
^{37}Cl		0.93	1.05		
^{37}Cl	$[Rh^{37}Cl_5(H_2O)]^{2-}$	*Not reliably quantifiable*	0.08	*Not reliably quantifiable*	0.08
^{35}Cl, ^{35}Cl	*cis*-$[Rh^{35}Cl_4(H_2O)_2]^-$	36.31	32.96	36.31	32.96
^{35}Cl,^{35}Cl	*cis*-$[Rh^{35}Cl_3{}^{37}Cl(H_2O)_2]^-$	19.66	21.08	41.80	42.16
^{35}Cl, ^{37}Cl		22.14	21.08		
^{35}Cl, ^{35}Cl	*cis*-$[Rh^{35}Cl_2{}^{37}Cl_2(H_2O)_2]^-$	2.80	3.37	18.12	20.22
^{35}Cl, ^{37}Cl		12.53	13.48		
^{37}Cl,^{37}Cl		2.79	3.37		
^{35}Cl, ^{37}Cl	*cis*-$[Rh^{35}Cl^{37}Cl_3(H_2O)_2]^-$	1.39	2.16	2.77	4.32
^{37}Cl, ^{37}Cl		1.38	2.16		
^{37}Cl, ^{37}Cl	*cis*-$[Rh^{37}Cl_4(H_2O)_2]^-$	*Not reliably quantifiable*	0.34	*Not reliably quantifiable*	0.34

Quantification of the respective Rh^{III} species present in the feed solution was performed by integrating each individual ^{103}Rh NMR resonance peak. Division of the individual peak area by the total sum of all the Rh^{III} species' peak areas yields the mole fraction of each individual Rh^{III} species. From the mole fraction of the RhIII species and the total Rh concentration, the individual concentration of each RhIII species can be calculated. The free chloride concentration was quantified by multiplying the concentration of each individual Rh^{III} species with the number of chloride ligands presumed to coordinate to the metal centre, followed by subtracting the sum concentration of the coordinated chloride ligands from the known total chloride concentration. The calculated free chloride concentration of the feed solution was 1.188 M. From the proposed species distribution diagram, Figure 5.4, the $[RhCl_n(H_2O)_{6-n}]^{3-n}$ (n=4,5) species distribution was predicted at a free chloride concentration of 1.188 M, and compared to that calculated from direct measurement of the ^{103}Rh NMR spectrum of the Rh feed solution, Table 5.6. The excellent correlation between the predicted and calculated $[RhCl_n(H_2O)_{6-n}]^{3-n}$ (n=4,5) species

distribution, Table 5.6, provides further evidence in support of the postulated species distribution diagram, Figure 5.4, proposed in this study. Unfortunately, the industrial PGM feed solution obtained from Heraeus chemicals could not be used for direct ^{103}Rh NMR spectroscopic studies, since the Rh concentration (33.4 mM) is too low and would thus lead to unrealistically long acquisition times.

Table 5.6: Comparison of the mole fraction $[RhCl_n(H_2O)_{6-n}]^{3-n}$ (n=4,5) species, at $[Cl^-]_{free}$ = 1.188 M, predicted by the proposed speciation diagram (Fig. 5.4) with that calculated from the ^{103}Rh NMR spectrum of an authentic Rh feed solution

Rh^{III} species	Mole fraction $[RhCl_n(H_2O)_{6-n}]^{3-n}$ (n=4,5) species	
	Predicted	Expt. obtained
$[RhCl_5(H_2O)]^{2-}$	0.39	0.42
cis-$[RhCl_4(H_2O)_2]^-$	0.45	0.47
trans-$[RhCl_4(H_2O)_2]^-$	0.070	0.10

5.3.5 Reinvestigation of Rh^{III} precipitation from an "adjusted" industrial feed solution – The importance of chemical speciation

It is evident, from the results discussed thus far, that the speciation of the $[RhCl_n(H_2O)_{6-n}]^{3-}$ (n=0-6) complexes in chloride solutions is the most likely cause for the poor recovery of Rh from a Heraeus PGM feed solution, Figure 3.16 (Chapter 3). However, this could not be established *directly* by means of high-resolution ^{103}Rh NMR, due to the low levels of Rh present in these PGM feed solutions, Table 3.1. In order to substantiate this hypothesis, the precipitation of Rh^{III} from these feed solutions was re-investigated, as a function of amine concentration, by "adjusting" the total chloride concentration of the feed stock solution to 8.01 M. Furthermore, this solution was heated at 354.1 K (65°C) for approximately two weeks in order to facilitate chloride anation of possible higher aquated Rh^{III} species, $[RhCl_n(H_2O)_{6-n}]^{3-n}$ (n=0-4).

Figure 5.18 illustrates the mole ratio precipitation curves of Rh^{III} as a function of increasing organic precipitant (**Deta**, **Teta**, **Tepa** and **Tren**) concentration, obtained from a chloride "adjusted" industrial feed solution. It is evident that adjusting the chloride concentration of the feed solution, followed by heat treatment to facilitate chloride anation, increased the amount of Rh precipitated by up to 98%, Figure 5.18.

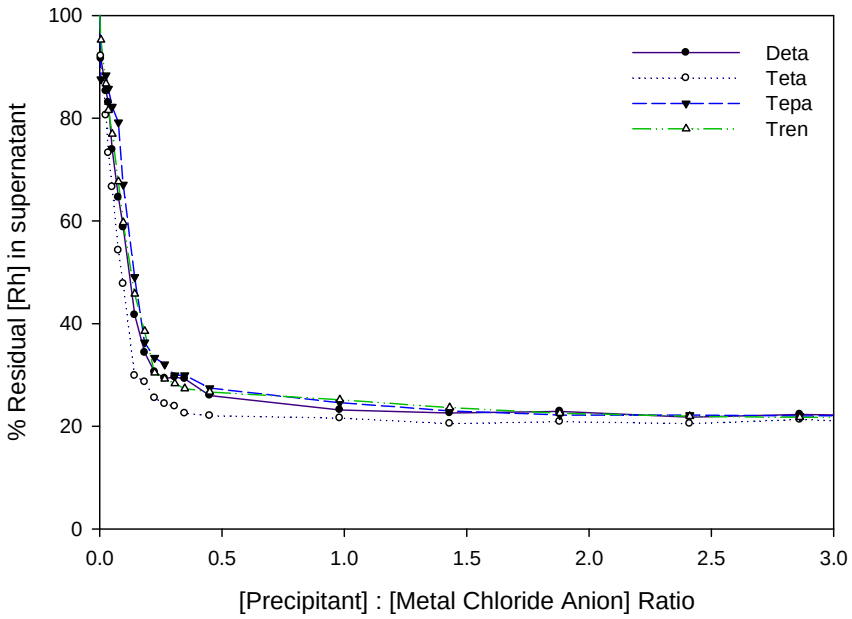

Figure 3.16: Residual [Rh] in the supernatant as a function of increasing [Precipitant]:[Metal chloride anion] ratio. [Rh] = 3.871 mM, [Cl^-] = 4.008 M

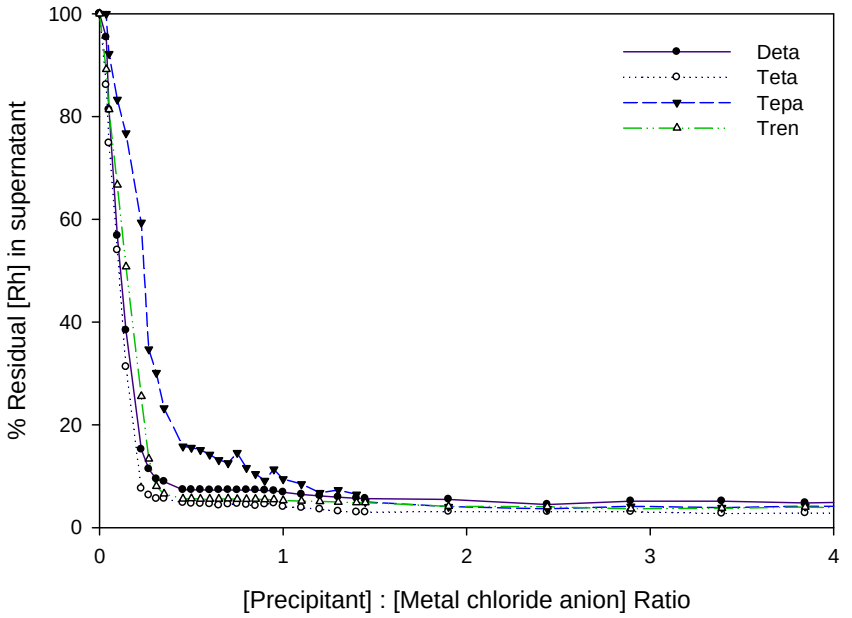

Figure 5.18: Residual [Rh] in the supernatant as a function of increasing [Precipitant]:[Metal chloride anion] ratio. The chloride concentration of the raw feed solution was adjusted to 8.01 M and the solution heated at 354.1 K for 2 weeks prior to performing precipitation titrations. [Rh] = 3.903 mM, [Cl^-] = 8.01 M, Precipitation titrations were conducted at 298.1 K.

The mole ratio precipitation curves illustrated in Figure 5.18 provides further support in favour of the hypothesis that $[RhCl_n(H_2O)_{6-n}]^{3-n}$ (n=0-6) speciation effects is responsible for the poor recovery of Rh from an "unaltered" industrial feed solution. Although the total chloride concentration of the "unaltered" industrial feed solution was in significant excess compared to the Rh concentration ($[Cl^-]$ = 4.008 M; [Rh] = 33.38 mM), the effect of other transition metals present in this solution should also be taken into account. By way of example: from ^{195}Pt NMR spectroscopic studies, it is known that Pt exists only as the $[PtCl_6]^{2-}$ complex anion in the "unaltered" industrial feed solution. The concentration of Pt in this solution is 0.1511 M (Table 5.1), implying that the concentration of chloride ligands coordinated to the Pt metal centre is 0.9426 M (6 × 0.1511 M). Therefore, the presence of Pt lowers the total chloride concentration by 0.9426 M. This rationale can be extended for all the metals present in solution, if the speciation of all the metal chlorido-complexes is accurately known. The presence of other metals would therefore significantly lower the total chloride concentration, and thus the free chloride concentration. The lowered free chloride concentration, in turn, would enhance the extent at which aquation of the $[RhCl_n(H_2O)_{6-n}]^{3-n}$ (n=5,6) species occur, thus leading to the poor Rh recovery as the higher aquated, $[RhCl_n(H_2O)_{6-n}]^{3-n}$ (n=0-4) species is more prevalent. Furthermore, chloride anation reactions would be negligible due to the low chloride concentration. However, upon increasing the chloride concentration, coupled with thermal treatment of the solution to enhance chloride concentration of the higher aquated Rh^{III} species, $[RhCl_n(H_2O)_{6-n}]^{3-n}$ (n=0-4), the recovery of Rh by organic precipitation of Rh is significantly enhance, Figure 5.18. Moreover, at a [precipitant]:[metal chloride anion] ratio of 1, quantitative precipitation (> 95%) of Rh is achieved for all the organic precipitants investigated.

Figure 5.19 shows the [precipitant]:[metal chloride anion] mole ratio precipitation titration curves of Pt, obtained from a chloride adjusted feed solution, using the denoted organic precipitants. It is evident that quantitative precipitation (> 98%) is achieved for triethylenetetramine (**Teta**) and tris(2-aminoethyl)amine (**Tren**) at [precipitant]:[metal chloride anion] ratios greater than 3 and 4, respectively. Furthermore, 95% of Pt was recovered using diethylenetriamine and tetraethylenepentamine, which is an improvement when compared to the results obtained from an "unaltered" industrial feed solution (Chapter 3, Figure 3.14). This is attributed to the increased chloride concentration used to maintain charge balance in the crystal lattice.

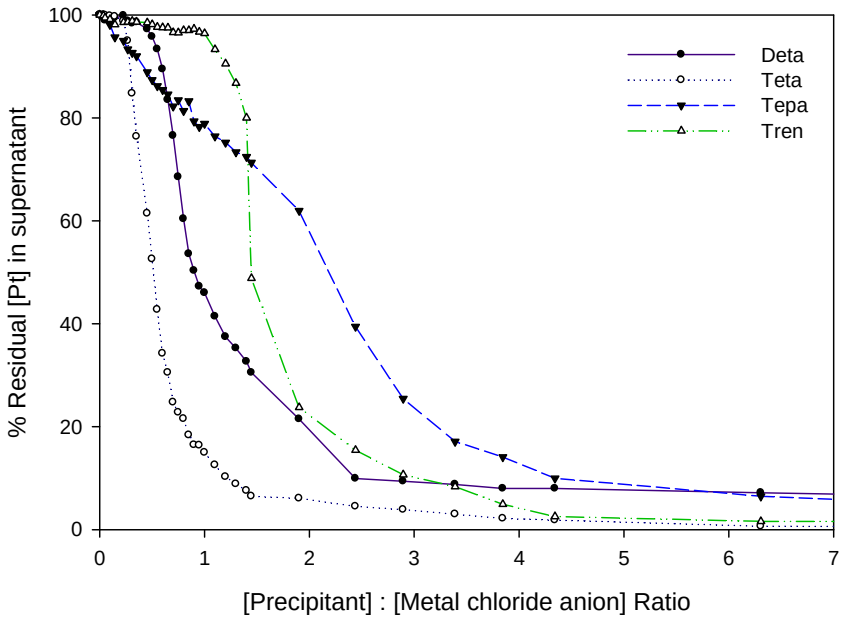

Figure 5.19: Residual [Pt] in the supernatant as a function of increasing [Precipitant]:[Metal chloride anion] ratio. [Rh] = 3.903 mM, [Cl^-] = 8.01 M, Precipitation titrations were conducted at 298.1 K.

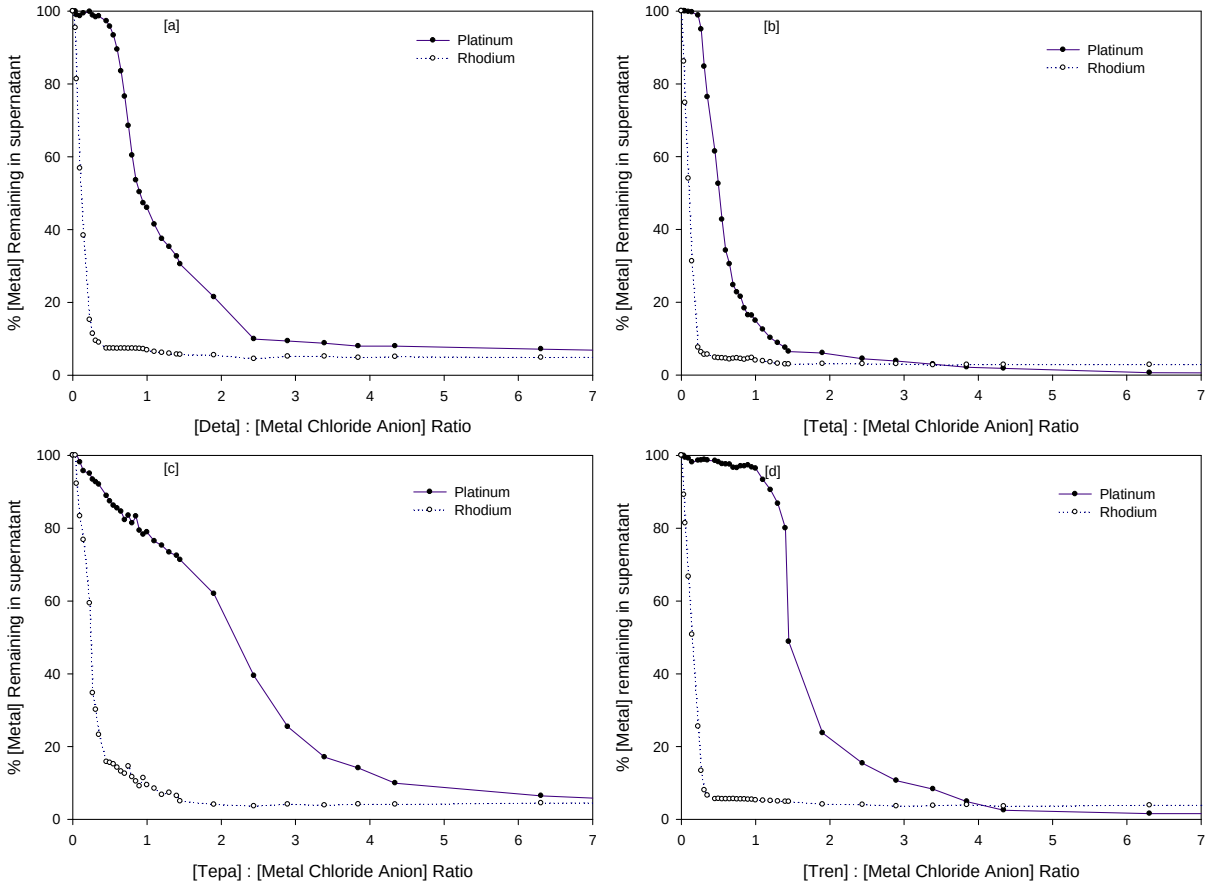

Figure 5.20: Comparison between the Pt- and Rh-precipitant titration curves for the organic precipitants used throughout this study. [Pt] = 18.79 mM; [Rh] = 3.903 mM, [Cl^-] = 8.01 M

Consider the following two equations (5.6) and (5.7):

$$[PtCl_6]^{2-}\ (aq) + [\mathbf{Deta}H_3]^{3+}\ (aq) + Cl^-\ (aq) \rightarrow (\mathbf{Deta}H_3)[PtCl_6]Cl\ (s) \qquad (5.6)$$

$$[PtCl_6]^{2-}\ (aq) + [\mathbf{Tepa}H_5]^{5+}\ (aq) + 3Cl^-\ (aq) \rightarrow (\mathbf{Tepa}H_5)[PtCl_6]Cl_3\ (s) \qquad (5.7)$$

In order to precipitate Pt using the organic precipitants denoted in equations (5.6) and (5.7), chloride anions is required to maintain charge balance. However, in the "unaltered" industrial feed solution, the free chloride concentration is too low and thus no chloride anions is incorporated into the crystal lattice, leading to a decrease in Pt recovery for these precipitates. In contrast, triethylenetetrammonium is highly efficient for the precipitation of Pt, mainly due to its +4 charge. In this instance, two $[PtCl_6]^{2-}$ anions can form an ion-pair with a single triethylenetetrammonium cation, thereby conserving charge balance.

Figure 5.20[a]-[d] compares the [precipitant]:[metal chloride anion] mole ratio precipitation titration curves of Rh and Pt obtained from an industrial feed solution. Comparing the various organic precipitants used, at a [precipitant]:[metal chloride anion] ratio of 1, it is evident that tris(2-aminoethyl)amine (**Tren**) shows the greatest selectivity toward the precipitation of Rh^{III} above $[PtCl_6]^{2-}$, Figure 5.20[d]; while triethylenetetramine is considered to be the least selective, Figure 5.20[b]. At a [precipitant]:[metal chloride anion] ratio of 1, for the tris(2-aminoethyl)amine precipitation curve, 95% Rh is precipitated as opposed to 4.7% for Pt, illustrating that tris(2-aminoethyl)amine could, under carefully controlled conditions, be used as a highly selective organic precipitant for the "upfront" recovery of Rh, *i.e.* before the recovery of Pt, and possibly other associated PGMs – Pd, Ir and Ru.

5.4 Concluding remarks

A ^{103}Rh NMR spectroscopic technique was developed for the unambiguous speciation of the Rh^{III} aqua chlorido-complexes, $[RhCl_n(H_2O)_{6-n}]^{3-n}$ (n=3-6), present in acidic, chloride-rich media. Under optimal NMR conditions, it was possible to unambiguously characterize and quantify all six $[RhCl_n(H_2O)_{6-n}]^{3-n}$ (n=3-6) species, including the *mer*- & *fac*-$[RhCl_3(H_2O)_3]$ as well as the *cis*- & *trans*-$[RhCl_4(H_2O)_2]^-$ species, present in a 0.721 M chloride matrix. An advantage of the developed technique, compared to previously reported speciation studies [1-5], is that it was possible to identify and quantify the $[RhCl_n(H_2O)_{6-n}]^{3-n}$ (n=3,4) stereoisomers. Moreover, cationic $[RhCl_n(H_2O)_{6-n}]^{3-n}$ (n=0-4) species was not observed, presumably due to the slow aquation of the *mer*-$[RhCl_3(H_2O)_3]$, *trans*-$[RhCl_2(H_2O)_4]^+$ and $[RhCl(H_2O)_5]^{2+}$ species; with negligibly small aquation rate constants documented for these cations [31].

Rh^{III} containing solutions, equilibrated in differing HCl concentrations for a year at 298 K, was analyzed by means of ^{103}Rh NMR spectroscopy. The analysis provided a partial $[RhCl_n(H_2O)_{6-n}]^{3-n}$ (n=3-6) species distribution diagram as a function of free chloride concentration. It was found that highly aquated $[RhCl_n(H_2O)_{6-n}]^{3-n}$ (n=3,4) species may persist up to free chloride concentrations of 3.0 M. Furthermore, at a free chloride concentration of 1.0 M, the abundance of $[RhCl_6]^{3-}$ and $[RhCl_5(H_2O)]^{2-}$ was found to be 2% and 31%, respectively; which is in stark contrast to that previously documented in literature [1-5]. In addition, the $[RhCl_6]^{3-}$ complex anion only becomes abundant (> 80%) at free chloride concentrations > 5.0 M.

The reversed-phase (C_{18}) ion-pair (TBA^+Cl^-) HPLC-ICP-OES method developed by Gerber *et al* [5] was adapted and used to separate and quantify the Rh^{III} aqua chlorido-complexes present in an acidic, chloride-rich matrix (*i.e.* the solutions prepared for ^{103}Rh NMR studies). Under optimal chromatographic conditions it was possible to separate and quantify the $[RhCl_6]^{3-}$, $[RhCl_5(H_2O)]^{2-}$ and the *cis*-$[RhCl_4(H_2O)2]^-$ complex anions, with the latter species eluting as a single band. Although further studies on this subject is required to separate all the Rh^{III} aqua chlorido complexes, it is noteworthy to mention that, for the first time, the $[RhCl_6]^{3-}$ complex anion has been successfully separated from the $[RhCl_5(H_2O)]^{2-}$ complex anion. Assignment of the eluted species was based on the correlation of the species distribution of the Rh^{III} aqua chlorido-complexes obtained through HPLC investigations to

that proposed by ^{103}Rh NMR studies. Excellent correlation between the two studies was obtained.

The precipitation of Rh^{III} aqua chlorido-complexes (by the organic precipitants diethylenetriamine, triethylenetetramine, tetraethylenepentamine and tris(2-aminoehtyl)amine) was performed as a function of HCl concentration. It was observed that the percentage Rh recovered from these solutions increased upon increasing HCl concentration. From the precipitation studies, the mole fraction Rh^{III} aqua chlorido-complexes precipitate was determined as a function of increasing HCl concentration. It was established that the speciation trends calculated from the precipitation studies could only be understood by considering that both the $[RhCl_6]^{3-}$ and $[RhCl_5(H_2O)]^{2-}$ species are precipitated from solution. An excellent correlation between the species distribution of the Rh^{III} aqua chlorido-complexes calculated from the precipitation studies was obtained when compared to the sum of the mole fractions of the $[RhCl_6]^{3-}$ and $[RhCl_5(H_2O)]^{2-}$ complex anions determined by means of high-resolution ^{103}Rh NMR spectroscopy, Figure 5.12.

High-resolution ^{195}Pt and ^{103}Rh NMR spectroscopic studies were performed on authentic industrial feed solutions. Assignment of the ^{195}Pt and ^{103}Rh resonances was based on the ^{35}Cl/^{37}Cl isotope effects, which manifest only as a result of the statistically expected ^{35}Cl/^{37}Cl isotopologues and, in some cases, isotopomers within each class of isotopologues – as highlighted in Chapter 4. These studies revealed that in a Heraeus PGM feed solution, Pt exists exclusively as the $[PtCl_6]^{2-}$ complex anion, exemplified by the excellent comparison between the experimental and statistical isotopologue distributions calculated for the $[Pt^{35/37}Cl_6]^{2-}$ complex anion, Table 5.4. Unfortunately, the industrial PGM feed solution obtained from Heraeus chemicals could not be used for direct ^{103}Rh NMR studies, since the Rh concentration was found to be too low.

In order to validate the practical relevance of the developed speciation method derived by means of high-resolution ^{103}Rh NMR spectroscopy, the ^{103}Rh NMR spectrum of an authentic industrial Rh^{III} feed solution, supplied by Anglo Platinum PLC, was recorded. Three ^{103}Rh resonances were observed at $\delta(^{103}Rh) = -84.6$, 159 and 235 ppm, which was assigned to the $[RhCl_5(H_2O)]^{2-}$, *cis*-$[RhCl_4(H_2O)_2]^-$ and *trans*-$[RhCl_4(H_2O)_2]^-$ species, respectively; Figure 5.17 and Table 5.5. Furthermore, the concentration of free chloride and all the Rh^{III} aqua chlorido-complexes were quantified, from which it was determined that the

abundance of the Rh^{III} species were 39.3% for the $[RhCl_5(H_2O)]^{2-}$ species, 45.4% for the *cis*-$[RhCl_4(H_2O)_2]^-$ and 6.9% for the *trans*-$[RhCl_4(H_2O)_2]^-$ species; all of which were accurately predicted by the Rh^{III} species distribution diagram developed by means of ^{103}Rh NMR spectroscopy, Table 5.6.

From the results discussed throughout this study, it becomes more evident that the speciation of Rh^{III} aqua chlorido-complexes is the most likely cause for the poor recovery of Rh from a Heraeus PGM feed solution - as highlighted in Chapter 3. The low concentration of Rh in this feed solution renders high-resolution ^{103}Rh NMR spectroscopy unfeasible in this instance. In order to validate the hypothesis that speciation of Rh^{III} aqua chlorido-complexes is responsible for the poor Rh recovery from a Heraeus PGM feed solution, the precipitation of Rh, by several organic precipitants, was re-evaluated. The chloride concentration of the PGM feed solution was increased and the solution was treated thermally for several days in order to increase the rate of chloride anation of Rh^{III} aquated species. Under the revised precipitation conditions, the percentage Rh recovered from the PGM feed solution increased from 78% (from an unaltered feed solution) to > 95%, validating the hypothesis that speciation effects were responsible for the poor Rh recovery, Figure 5.18. Moreover, tris(2-aminoethyl)amine (**Tren**) was highlighted as the most selective organic precipitant for the recovery of Rh, removing 95% of the Rh initially present, compared to 4.7% Pt at a [precipitant]:[metal chloride anion] ratio of 1. It is therefore evident that, under carefully optimized conditions, tris(2-aminoethyl)amine, **Tren**, could be used as a highly selective organic precipitant for the upfront recovery of Rh.

5.5 References

1. D. Cozzi, F. Pantani, *J. Inorg. Nucl. Chem*. **8** (1958) 385
2. W. Robb, G.M. Harris, *J. Am. Chem. Soc*. **87** (1965) 4472
3. W. Robb, M.M. de V. Steyn, *Inorg. Chem*. **6** (1967) 616
4. E. Benguerel, G.P. Demopoulos, G.B. Harris, *Hydrometallurgy* **40** (1996) 135
5. W. J. Gerber, K. R. Koch, H. E. Rohwer, E. C. Hosten, T. E. Geswindt, *Talanta*, **82** (2010) 348
6. K. Krengel-Rothensee, U. Richter and P. Heitland, *J. Anal. At. Spectrom.*, **14** (1999) 699
7. J. Naozuka, M. A. Mesquita Silva da Veiga, P. V. Oliveira and E. de Oliveira, *J. Anal. At. Spectrom.*, **18** (2003) 917
8. P-H. van Wyk, W. J. Gerber and K. R. Koch, *J. Anal. At. Spectrom.*, **27** (2012) 577
9. Theodor E. Geswindt, Wilhelmus J. Gerber and Klaus R. Koch, *Analytica Chimica Acta*, **730** (2012) 93
10. R.J. Goodfellow, in: R.K. Harris, B.E. Mann (Eds.), *NMR and the Periodic Table*, Academic Press, London, 1978, 244
11. I.M. Ismail, S.J.S. Kerrison, P.J. Sadler, *J. Chem. Soc., Chem. Commun*. (1980) 1175
12. R. Vlasankova, L. Sommer, *Chromatographia* **52** (2000) 692
13. B. D. Catsikis, M. L. Good. *Inorg. Chem*. **8** (5) (1969) 1095
14. M. Pillinger, C. D. Nunes, P. D. Vaz, A. A. Valente, I. S. Gonçalves, P. J. A. Ribeiro-Claro, J. Rocha and F. E. Kühn, *Phys. Chem. Chem. Phys*. **4** (2002) 3098
15. K. R. Dunbar, *J. Am. Chem. Soc*. **110** (1988) 8247
16. J.K.M. Sanders and B.K. Hunter, in *Modern NMR Spectroscopy*, 2nd Edition, Oxford University Press, (1993)
17. W. D. Crozier, R. A. Grant, Johnson Matthey PLC. *UK Patent 2 247 888A*, 1992
18. G. Bugli, *J. Appl. Cryst*. **14** (1981) 143
19. W. Frank and G. J. Reiss, *Z. Anorg. Allg. Chem*. **622** (1996) 729
20. S. S. Tavale, V. G. Puranik, P. Umapathy, C. S. Dorai, *Journal of Crystallographic and Spectroscopic Research*, **23** (1) (1993)
21. V. G. Puranik, S. S. Tavale, P. Umapathy, C. S. Dorai, *Journal of Crystallographic and Spectroscopic Research*, **23** (4) (1993)
22. G. Schmukler, B. Limoni-Relis, *Sep. Sci. Technol*. **30** (3) (1995) 337
23. H. Narita, K. Morisaku, M. Tanaka, *Chem. Commun.* (2008) 5921
24. A. A. Mhaske, P. M. Dhadke, *Hydrometallurgy* **61** (2001) 143

25. A. A. Mhaske, P. M. Dhadke, *Hydrometallurgy* **63** (2002).143

26. W. J. Gerber, P. Murray, K. R. Koch, *Dalton transactions* **31** (2008) 4113

27. G. Schmuckler, *US patent 4 885 143*, United States of America (1989)

28. F. L. Bernardis, R. A. Grant and D. C. Sherrington, *React. Funct. Polym.* **65** (2005) 205

29. J. Kramer, K.R. Koch, *Inorg. Chem*. **45** (2006) 7843

30. J. Kramer, K.R. Koch, *Inorg. Chem*. **46** (2007) 7466

31. D.A. Palmer, G.M. Harris, *Inorg. Chem*. **14** (1975) 1316

Chapter 6

Conclusions

In this thesis, high-resolution ^{103}Rh NMR spectroscopy was used as an analytical tool for the detection, unambiguous characterisation and *direct* chemical speciation of $[RhCl_n(H_2O)_{6-n}]^{3-n}$ (n=3-6) complexes, without the necessity to alter the chemical composition of the aqueous, chloride-rich Rh-containing solutions. The associated results obtained throughout this study was necessitated to substantiate arguments in favour of the revised $[RhCl_n(H_2O)_{6-n}]^{3-n}$ (n=3-6) species distribution diagram, obtained by direct ^{103}Rh NMR spectroscopic measurements. Furthermore, these studies were required for the correct interpretation of phenomena typically encountered in the industrial separation and recovery of Rh.

6.1 Rh^{III} ligand exchange kinetics

The aquation kinetics of $[RhCl_6]^{3-}$ and $[RhCl_5(H_2O)]^{2-}$ were investigated as a function of ionic strength and temperature. Under the experimental conditions defined in this study, the aquation (and chloride anation) reactions of the $[RhCl_6]^{3-}$ and $[RhCl_5(H_2O)]^{2-}$ complex anions follow pseudo first-order kinetics. Furthermore, the aquation rate constants for the $[RhCl_6]^{3-}$ and $[RhCl_5(H_2O)]^{2-}$ species were determined as a function of ionic strength and temperature. The aquation rate constants determined at an ionic strength of 4.0 M $HClO_4$ and 298.1 K were consistent with those reported in literature. Moreover, it was found that a change in the ionic strength influenced the observed pseudo first-order aquation rate constants more than was reported in literature. This is presumably due to the changes in the activity coefficients of the reagents, *i.e.* H_2O, Cl^- and Rh^{III}. An increase in the charge density of the respective Rh^{III} species would lead to an increase in the extent to which ionic strength influences the rate of ligand exchange. This implies a decrease in the rate of aquation for the $[RhCl_n(H_2O)_{6-n}]^{3-n}$ (n=4-6) complex anions upon increasing ionic strength.

Temperature has a profound effect on the rate of ligand substitution, with an increase in temperature leading to an increase in the rate of aquation of the $[RhCl_n(H_2O)_{6-n}]^{3-n}$ (n=5,6) complex anions. Furthermore, the transition state activation energies (E_a) for the aquation of the $[RhCl_6]^{3-}$ and $[RhCl_5(H_2O)]^{2-}$ species were calculated, from which it was found that these

activation energies are independent of the ionic strength. Ionic strength and temperature thus have profound effects on the species distribution of $[RhCl_n(H_2O)_{6-n}]^{3-n}$ (n=0-6) complexes which would have to be accurately accounted for prior to reporting a "kinetic based" Rh^{III} speciation diagram. Errors in the reported Rh^{III} speciation diagrams would have a profound (negative) effect on Rh^{III} recovery studies such as liquid-liquid extraction, solid-phase extraction or organic precipitation studies, since most of these studies optimize experimental conditions according to the data reported in proposed speciation diagrams.

6.2 Recovery of Rh and Pt by means of organic precipitation

Several commercially available *N*-containing organic compounds were used as organic precipitants for the "selective" recovery of Rh from aqueous, chloride-rich media. These compounds included **Deta**, **Teta**, **Tepa**, **Tren**, polyethylenimine, Lupamin® 1595 and Lupamin® 9030, of which only **Deta**, **Teta**, **Tepa** and **Tren** were subsequently used for further study. Applied to laboratory prepared PGM (Pt and Rh) containing solutions, in which the species distribution of the respective metal-chlorido complexes are accurately known, all of the precipitants illustrated quantitative recovery of Rh. Furthermore, preferential recovery of Rh, rather than Pt, was attained when using **Deta** and **Tren**, with **Tren** exhibiting the greatest selectivity toward the recovery of Rh. Regarding the selectivity of the organic precipitants toward the preferential recovery of Rh, no trend was observed upon increasing the chain-length (and thus the formal charge from +3 to +5) of the organic precipitants. Moreover, no recovery trends could be observed when using organic precipitants having a linear motif as opposed to those having a branched motif.

Quantitative recovery of Rh from an authentic Heraeus industrial feed solution was not obtained with any of the precipitants used, while Pt was recovered quantitatively using **Teta** and **Tren**. The fact that Pt could be recovered quantitatively from this feed solution was attributed to the Pt present in the industrial feed solution existing solely as the $[PtCl_6]^{2-}$ complex anion, which was confirmed by means of high-resolution ^{195}Pt NMR spectroscopy. The poor recovery of Rh from an Heraeus industrial feed solution was hypothesized to be due to $[RhCl_n(H_2O)_{6-n}]^{3-n}$ (n=0-6) species distribution, with the decrease in recovery attributed to the dominance of higher aquated Rh^{III} species, $[RhCl_n(H_2O)_{6-n}]^{3-n}$ (n=0-4).

Traditional analytical techniques (polarography, UV-vis spectrophotometry and hyphenated HPLC techniques) have limited capabilities when investigating the chemical speciation of metal-chloride complexes in complicated, acidic chloride-rich media. In this regard, ^{103}Rh NMR spectroscopy was used as an analytical tool for the detection, unambiguous characterisation and chemical speciation of $[RhCl_n(H_2O)_{6-n}]^{3-n}$ (n=3-6) complexes.

6.3 Characterisation of ^{103}Rh resonances observed in high-resolution ^{103}Rh NMR spectra

The application of ^{103}Rh NMR spectroscopy as an analytical tool for the direct speciation of $[RhCl_n(H_2O)_{6-n}]^{3-n}$ (n=3-6) first necessitated the characterization of each of the ^{103}Rh resonances. A detailed analysis of the ^{35}Cl/^{37}Cl isotope effects observed in the 19.11 MHz ^{103}Rh NMR resonances of $[RhCl_n(H_2O)_{6-n}]^{3-n}$ complexes (n = 3–6) in acidic solution at 292.1 K, showed that the 'fine structure' of each ^{103}Rh resonance can be understood in terms of the unique *isotopologue* and, in certain instances, the *isotopomer* distribution in each of these complexes. These ^{35}Cl/^{37}Cl isotope effects in the ^{103}Rh NMR resonance of the $[Rh^{35/37}Cl_6]^{3-}$ species manifest only as a result of the statistically expected ^{35}Cl/^{37}Cl isotopologues, whereas for the aquated species such as the $[Rh^{35/37}Cl_5(H_2O)]^{2-}$, *cis*-$[Rh^{35/37}Cl_4(H_2O)_2]^-$ as well as the *mer*-$[Rh^{35/37}Cl_3(H_2O)_3]$ complexes, additional fine-structure due to the various possible isotopomers within each class of isotopologues, is visible. Of particular interest was the direct identification of stereoisomers *cis*-$[RhCl_4(H_2O)_2]^-$, *trans*-$[RhCl_4(H_2O)_2]^-$, *fac*-$[RhCl_3(H_2O)_3]$ and *mer*-$[RhCl_3(H_2O)_3]$, based on the ^{103}Rh NMR line shape, rather than on the basis of their very similar $\delta(^{103}Rh)$ chemical shift, which differ by only *ca* 76 ± 3 ppm for the anionic *trans*- and *cis*-$[RhCl_4(H_2O)_2]^-$ isomers and by *ca* 63 ± 3 ppm for the uncharged *fac*-$[RhCl_3(H_2O)_3]$ and *mer*-$[RhCl_3(H_2O)_3]$ isomers. The use of ^{35}Cl/^{37}Cl isotope-resolved ^{103}Rh NMR resonance thus constitutes a significant advance as a convenient and reliable method for the identification of halide containing complexes, provided these complexes are kinetically inert to ligand exchange on the NMR time scale. These complexes are therefore readily identified based on their ^{35}Cl/^{37}Cl isotope induced 'NMR fingerprint', without reference to their accurate ^{103}Rh NMR chemical shifts or the need for a suitable reference compound.

6.4 Direct speciation of $[RhCl_n(H_2O)_{6-n}]^{3-n}$ complexes by means of high-resolution ^{103}Rh NMR spectroscopy

A ^{103}Rh NMR spectroscopic technique was developed for the direct speciation of Rh^{III} aqua chlorido-complexes, $[RhCl_n(H_2O)_{6-n}]^{3-n}$ (n=3-6), present in acidic, chloride-rich media. In order to ascertain if quantitative NMR conditions have been met, the rotational correlation time, τ_c, normally obtained through relaxation time measurements, was estimated using the guideline outlined by Sanders and Hunter (in "Modern NMR Spectroscopy", 2nd Ed., Oxford University Press, 1993). This guideline allows for the estimation of the longitudinal relaxation time, T_1, from which it was ascertained that a total recycle time of 2.5 s was sufficient to obtain quantitative NMR conditions.

The ^{103}Rh NMR spectroscopic measurements conducted on concentrated Rh^{III} solutions allowed for the construction of a partial $[RhCl_n(H_2O)_{6-n}]^{3-n}$ species distribution diagram, as a function of the "free" (unbound) chloride concentration. This speciation diagram is considered to be the most accurate currently available, mainly because published species distribution diagrams for Rh^{III} aqua chlorido-complexes have been generally constructed using data from *indirect* (kinetic and spectrophotometric) measurements in dilute Rh^{III} solutions, at nominally higher HCl concentrations, for which the Rh^{III}:Cl^- mole ratio is far greater than that expected in authentic process solutions. Furthermore, in order to analyze the practical relevance of the developed ^{103}Rh NMR spectroscopic technique, the ^{103}Rh NMR spectrum of an authentic industrial Rh feed solution (Anglo Platinum PLC) was recorded. Detailed analysis of this spectrum revealed that the solution contained only the $[RhCl_5(H_2O)]^{2-}$ and *cis*-$[RhCl_4(H_2O)_2]^-$ complex anions in appreciable concentrations (*i.e.* 39.3% and 45.4%, respectively), while the *trans*-$[RhCl_4(H_2O)_2]^-$ complex anion was present at considerably lower abundance, 6.9%. The proposed Rh^{III} species distribution diagram accurately predicted these abundances, at a "free" chloride concentration of 1.188 M.

The reason for the poor Rh recovery from an authentic Heraeus industrial feed solution can therefore be attributed to Rh^{III} speciation effects, with the presence of other metals (often present in higher concentrations than Rh) decreasing the "free" (unbound) chloride concentration, by acting as chloride "binders". The decrease in the "free" chloride concentration would consequently lead to an increase in the extent to which aquation of Rh^{III}

occurs. This implies that the higher aquated Rh^{III} chlorido-complexes, $[RhCl_n(H_2O)_{6-n}]^{3-n}$ (n=0-4), would be the dominant Rh^{III} species present in these process solutions. Subsequently, the organic precipitation conditions were optimized by adjusting the total chloride concentration of the industrial feed solution to 8.01 M, followed by thermal treatment to enhance chloride anation of the higher aquated Rh^{III} complexes. Under these conditions, the recovery of Rh improved dramatically, with up to 95.8% of the Rh initially present recovered. Furthermore, it was concluded that tris(2-aminoethyl)amine (**Tren**), under very carefully controlled conditions, was a more "selective" precipitant toward the preferential recovery of Rh, when compared to the recovery of Pt.

In summary, it is evident that ^{103}Rh NMR spectroscopy is a powerful spectroscopic technique for investigating the chemistry of Rh^{III} aqua chlorido-complexes in solutions which are pertinent to the refining industry. The understanding of the speciation of metal-chloride complexes as a function of the chloride ion concentration can potentially result in the optimization of Rh recovery by careful speciation control, as exemplified in this study. However, ^{103}Rh NMR spectroscopy does have limitations, which include primarily the high cost associated with high-field NMR spectrometers combined with the fact that these instruments are not readily available within the industrial setting. Furthermore, due to its low receptivity, the relative sensitivity of ^{103}Rh NMR spectroscopy is low, which implies that lower levels of detection of species concentrations are limited to the (milli)molar concentration levels. Therefore, comparably higher Rh concentrations (> 0.2 M) combined with extended acquisition times (> 12 hours) are required to attain optimal S/N ratios.

Addendum A

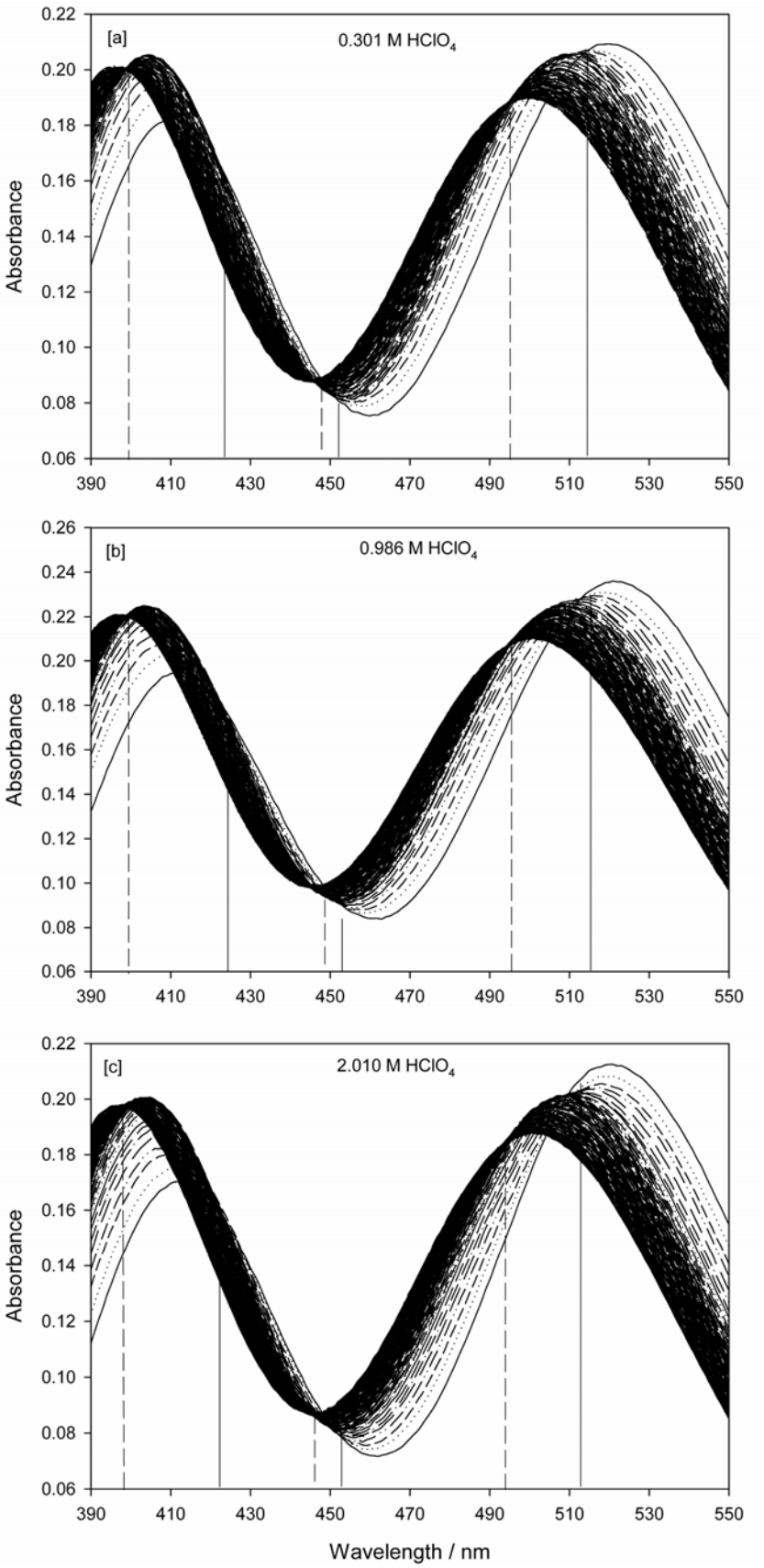

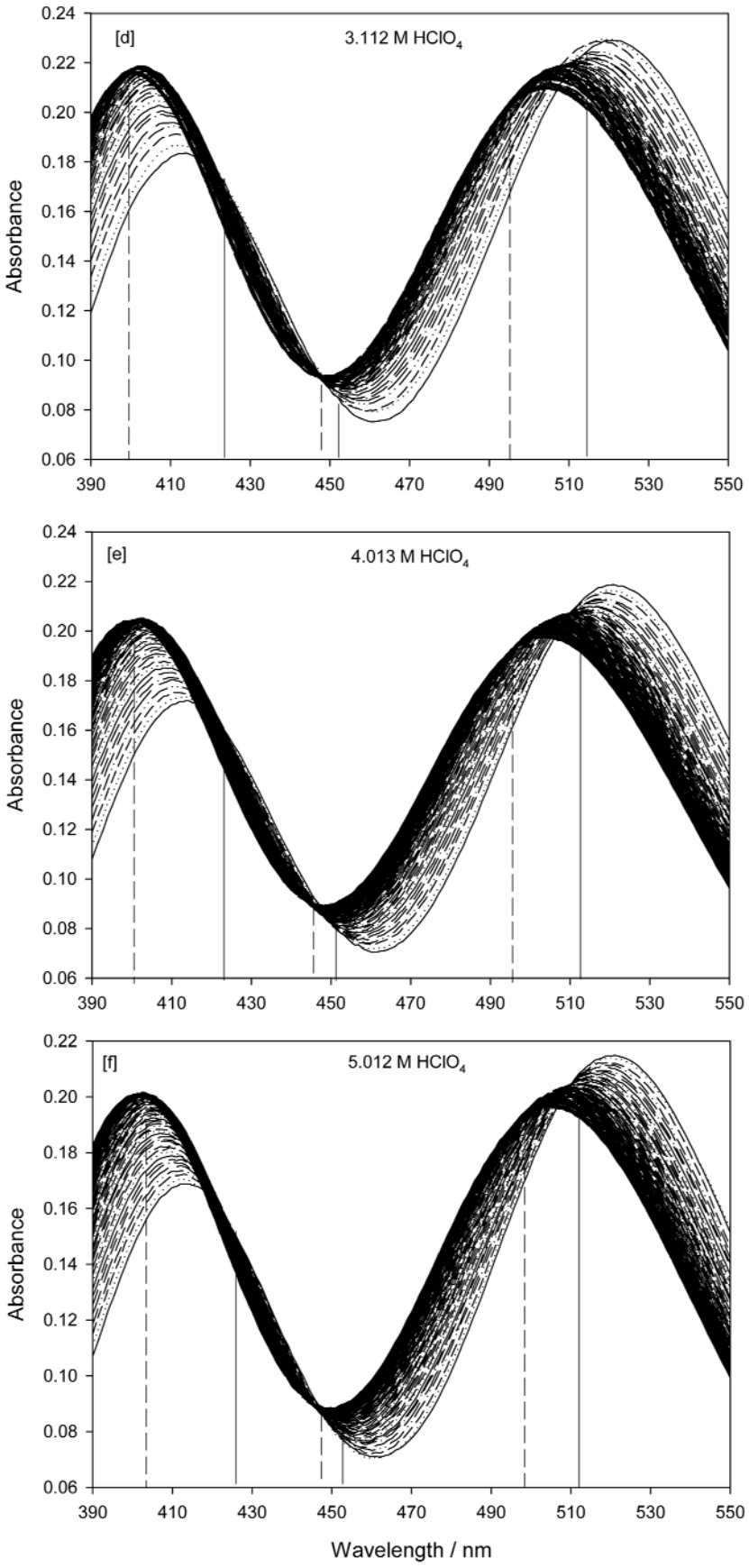

Figure A6.1: Change in UV-vis spectra as a function of time upon diluting a 0.1021 M Rh^{III} solution initially equilibrated in 10.181 M HCl to a final HCl concentration of 0.1018 M. The ionic strength was varied from 0.301 M to 5.012 M, as denoted in the respective figures [a] – [f]. Spectra were recorded at 298 K

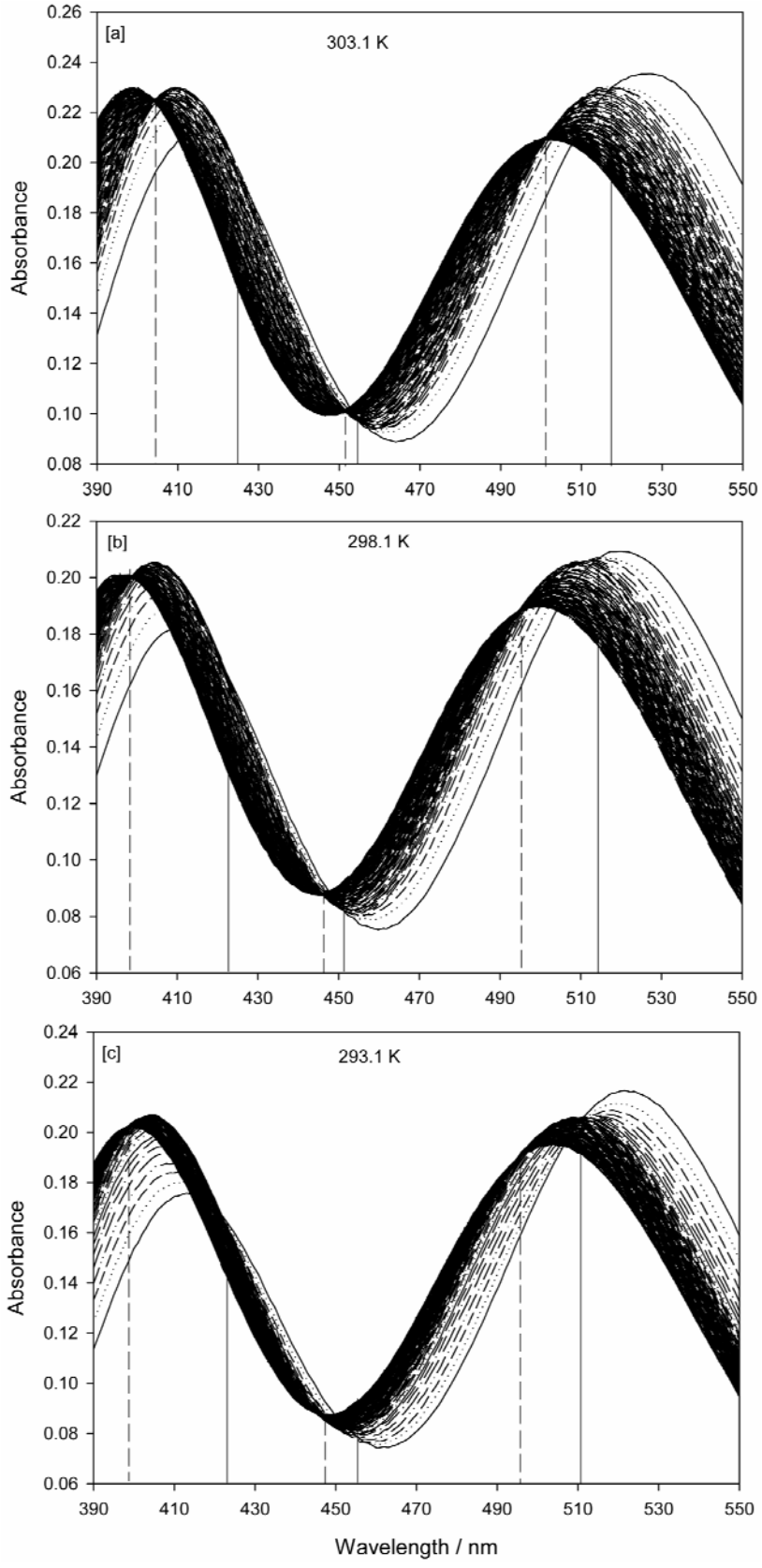

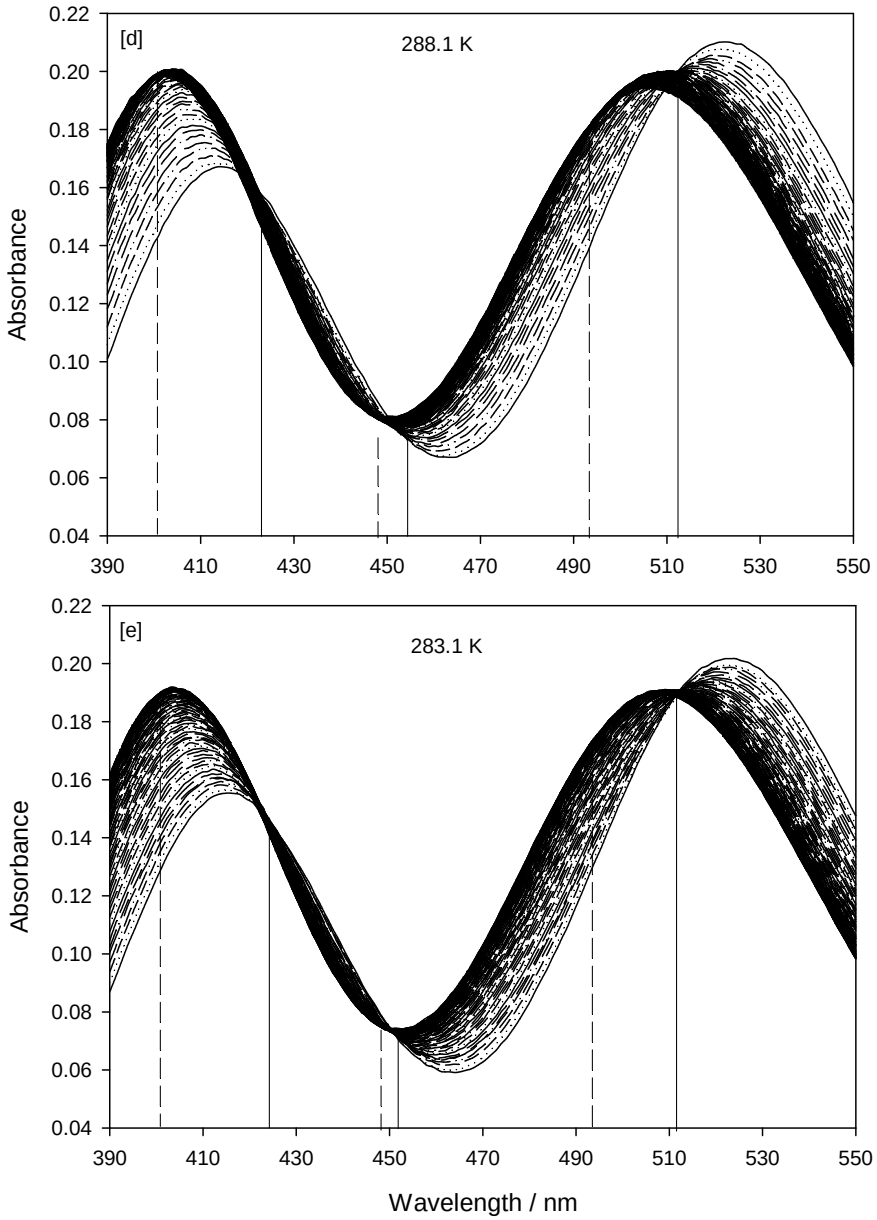

Figure A2.2: Change in UV-vis spectra as a function of time upon diluting a 0.1021 M Rh^{III} solution initially equilibrated in 10.181 M HCl to a final HCl concentration of 0.1018 M. The temperature was varied from 303.1 K – 283.1 K, as denoted in the respective figures [a] – [e]. The denoted spectra were recorded at a constant ionic strength of 0.301 M $HClO_4$

Addendum B

List of publications by T. E. Geswindt

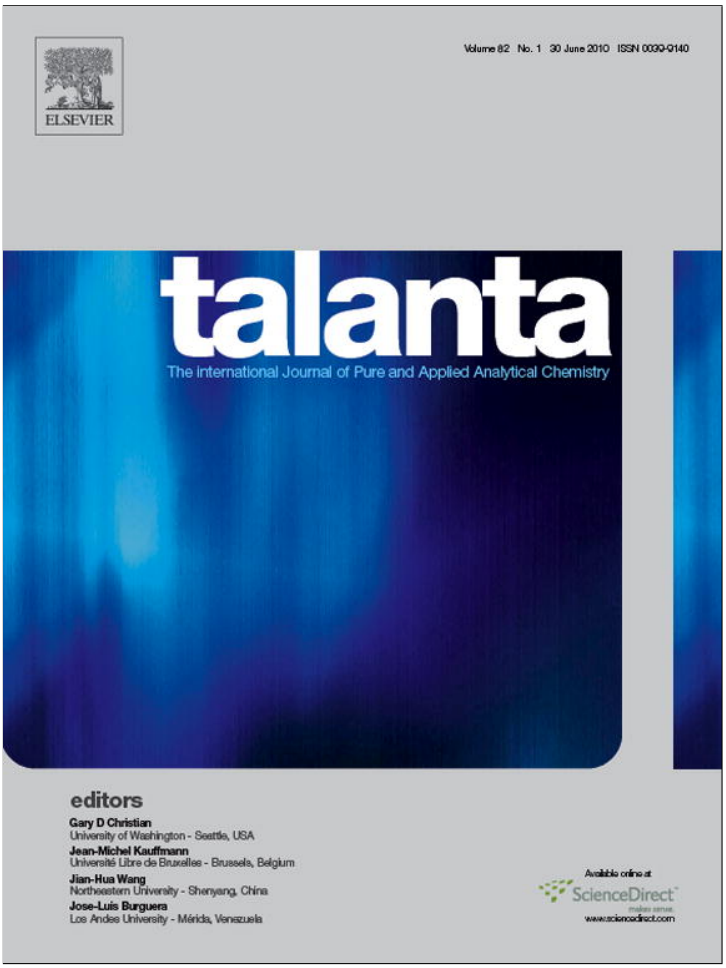

Talanta 82 (2010) 348–358

Contents lists available at ScienceDirect

Talanta

journal homepage: www.elsevier.com/locate/talanta

Separation and quantification of $[RhCl_n(H_2O)_{6-n}]^{3-n}$ (n = 0–6) complexes, including stereoisomers, by means of ion-pair HPLC–ICP-MS

Wilhelmus J. Gerber[a,*], Klaus R. Koch[a], Hans E. Rohwer[b], Eric C. Hosten[b], Theodor E. Geswindt[a]

[a] Research Group of PGM Chemistry, Department of Chemistry and Polymer Science, Stellenbosch University, Private Bag XI, Stellenbosch 7602, Western Cape, South Africa
[b] Department of Chemistry, Nelson Mandela Metropolitan University, PO Box 77000, Port Elizabeth 6031, South Africa

ARTICLE INFO

Article history:
Received 6 January 2010
Received in revised form 22 April 2010
Accepted 23 April 2010
Available online 15 May 2010

Keywords:
Rh(III) aqua chlorido-complexes
Speciation
Ion-pair chromatography
Kinetics
HPLC
ICP-MS

ABSTRACT

A hyphenated ion-pair (tetrabutylammonium chloride—TBACl) reversed phase (C_{18}) HPLC–ICP-MS method (High Performance Liquid Chromatography Inductively Coupled Plasma Mass Spectroscopy) for anionic Rh(III) aqua chlorido-complexes present in an HCl matrix has been developed. Under optimum chromatographic conditions it was possible to separate and quantify cationic Rh(III) complexes (eluted as a single band), $[RhCl_3(H_2O)_3]$, *cis*-$[RhCl_4(H_2O)_2]^-$, *trans*-$[RhCl_4(H_2O)_2]^-$ and $[RhCl_n(H_2O)_{6-n}]^{3-n}$ (n = 5, 6) species. The $[RhCl_n(H_2O)_{6-n}]^{3-n}$ (n = 5, 6) complex anions eluted as a single band due to the relatively fast aquation of $[RhCl_6]^{3-}$ in a 0.1 mol L^{-1} TBACl ionic strength mobile phase matrix. Moreover, the calculated $t_{1/2}$ of 1.3 min for $[RhCl_6]^{3-}$ aquation at 0.1 mol kg^{-1} HCl ionic strength is significantly lower than the reported $t_{1/2}$ of 6.3 min at 4.0 mol kg^{-1} $HClO_4$ ionic strength. Ionic strength or the activity of water in this context is a key parameter that determines whether $[RhCl_n(H_2O)_{6-n}]^{3-n}$ (n = 5, 6) species can be chromatographically separated. In addition, aquation/anation rate constants were determined for $[RhCl_n(H_2O)_{6-n}]^{3-n}$ (n = 3–6) complexes at low ionic strength (0.1 mol kg^{-1} HCl) by means of spectrophotometry and independently with the developed ion-pair HPLC–ICP-MS technique for species assignment validation. The Rh(III) samples that was equilibrated in differing HCl concentrations for 2.8 years at 298 K was analyzed with the ion-pair HPLC method. This analysis yielded a partial Rh(III) aqua chlorido-complex species distribution diagram as a function of HCl concentration. For the first time the distribution of the *cis*- and *trans*-$[RhCl_4(H_2O)_2]^-$ stereoisomers have been obtained. Furthermore, it was found that relatively large amounts of 'highly' aquated $[RhCl_n(H_2O)_{6-n}]^{3-n}$ (n = 0–4) species persist in up to 2.8 mol L^{-1} HCl and in 1.0 mol L^{-1} HCl the abundance of the $[RhCl_5(H_2O)]^{2-}$ species is only 8–10% of the total, far from the 70–80% as previously proposed. A 95% abundance of the $[RhCl_6]^{3-}$ complex anion occurs only when the HCl concentration is above 6 mol L^{-1}. The detection limit for a Rh(III) species eluted from the column is below 0.147 mg L^{-1}.

1. Introduction

Separation and refining of platinum group metals (PGM) is based predominantly on the subtle difference between their anionic chlorido-complexes such as $[PtCl_6]^{2-}$, $[PdCl_4]^{2-}$, $[RhCl_6]^{3-}$ and $[IrCl_6]^{2/3-}$, while Ru and Os are generally separated by means of oxidative distillation [1,2]. Currently, rhodium is recovered last from PGM mining feed streams in South Africa using either solvent-extraction or ion-exchange followed by precipitation [2]. A possible reason for the 'late' recovery of Rh(III) is presumably due to the presence of aquated species, $[RhCl_n(H_2O)_{6-n}]^{3-n}$ (n = 3–5), even in strong chloride media [2,3]. To design more efficient refining methods, chemical speciation and the quantification of Rh(III) aqua chlorido-complexes in process solutions is of critical importance. The need for a detailed investigation of the species distribution of Rh(III) aqua chlorido-complexes in an HCl matrix is clearly reflected by the large differences between proposed species distribution diagrams, e.g. the reported HCl concentrations where a 1:1 ratio of $[RhCl_6]^{3-}$ and $[RhCl_5(H_2O)]^{2-}$ species exist varies from 0.04 to 8.3 mol L^{-1} HCl [3]. These large differences between proposed species distribution diagrams are indicative of the difficulty involved to develop an analytical technique for the separation and quantification of Rh(III) aqua chlorido-complexes present in an HCl matrix.

Sandström and co-workers [4,5] was able to characterize all $[RhX_n(H_2O)_{6-n}]^{3-n}$ (X = Cl^-, Br^- and n = 0–6) complexes, while Mann and Spencer [6] characterized the series of $[RhCl_nBr_{6-n}]^{3-n}$ (n = 0–6) complex anions by means of ^{103}Rh NMR. Unfortunately the relatively low magnetogyric ratio of the ^{103}Rh nucleus precludes ^{103}Rh NMR for relatively rapid speciation and quantification, particularly in dilute solutions [4–7]. Recent capillary electrophoresis (CE) speciation studies of Rh(III) present in several acidic

* Corresponding author. Tel.: +27 021 808 2699; fax: +27 021 808 3342.
E-mail address: wgerber@sun.ac.za (W.J. Gerber).

0039-9140/$ – see front matter © 2010 Elsevier B.V. All rights reserved.
doi:10.1016/j.talanta.2010.04.049

matrices (HCl, HNO_3, H_2SO_4) illustrated that several Rh(III) species could be separated with some peaks tentatively assigned to particular species [8–11]. However, separation and unambiguous assignment of in particular $[RhCl_n(H_2O)_{6-n}]^{3-n}$ (n = 2–4) stereoisomers has not yet been reported using any chromatographic technique. UV–VIS spectroscopy is of 'limited' use for speciation of Rh(III) aqua chlorido-complexes when more than two species are simultaneously present, due to the relatively small difference in molar extinction coefficient spectra of $[RhCl_n(H_2O)_{6-n}]^{3-n}$ (n = 0–6) species coupled with discrepancies between reported molar extinction coefficient spectra [12,13]. Matrix-assisted laser desorption ionization time-of-flight mass spectrometry (MALDI-TOF) does not reflect the species distribution in solution and cannot differentiate between stereoisomers, e.g. *cis*- or *trans*-$[RhCl_4(H_2O)_2]^-$ [11].

As part of our interest in developing speciation techniques for PGM [14–16] complexes present in HCl solutions similar to mining feed and effluent streams, we aimed to develop an ion-pair reversed phase (C_{18}) chromatographic speciation method for $[RhCl_n(H_2O)_{6-n}]^{3-n}$ (n = 0–6) species including stereoisomers, followed by detection by means of inductively coupled plasma mass spectrometry (ICP-MS). Despite the relatively 'uncomplicated' sample matrix (water and hydrochloric acid) the chromatographic separation and identification of these complexes is challenging due to the difference in the net charge, the kinetic lability of Rh(III) complexes and presence of stereoisomers which might be expected to exhibit only subtle retention differences in a chromatographic separation. Moreover, the mobile phase composition for a reversed phase ion-pair chromatographic separation is inevitably different from the HCl sample matrix which may lead to the interconversion of kinetically labile Rh(III) aqua chlorido-complexes [17–23] during a chromatographic run. This matter is exemplified by Salvadó and co-workers [11] who argued that the relatively rapid aquation of $[RhCl_6]^{3-}$ made it impossible to observe a peak for $[RhCl_6]^{3-}$ using CE, whereas Aleksenko et al. [10] claims the contrary. In this regard, we re-investigated the anation/aquation kinetics of Rh(III) aqua chlorido-complexes to evaluate the extent of species interconversion that might be expected during a chromatographic run. In particular, the rate of aquation at low ionic strength (0.1 mol L^{-1} HCl) conditions was studied since previous investigations [17–23] were conducted at relatively high ionic strengths (≥2.0 mol L^{-1} HCl or $HClO_4$); such conditions are not compatible with the intended reversed phase ion-pair chromatographic separation. The assignment of eluted Rh(III) aqua chlorido-complexes by this means entailed a detailed kinetic study utilizing the developed reversed phase chromatographic speciation method and when possible results were compared for validation with an independent UV–VIS study conducted in parallel. This paper describes the development of an ion-pair HPLC–ICP-MS method for the separation and the quantification of $[RhCl_n(H_2O)_{6-n}]^{3-n}$ (n = 0–6) complexes present in an HCl matrix without the need for chelation of the metal cation [24] by ligands such as dithiocarbamates and 8-hydroxyquinoline prior to separation.

2. Experimental

2.1. Apparatus

The HPLC instrumentation used comprises of a Shimadzu LC-9A pump coupled to a Perkin-Elmer Sciex Elan 6100 ICP quadrupole MS detector (for breakthrough curve determination a Shimadzu CDD-6A conductivity detector was used) and steel tubing with inner diameter of 0.20 mm. The injection valve used was a Rheodyne (model number 7125) mounted with a 20 μL sample loop. The flow rate (u) of the mobile phase was 1.0 mL min^{-1}. The cylindrical steel columns had lengths (L) varying between 5 and 25 cm and an inner diameter (D_C) of 0.5 cm with mirror-finish interior walls. The room temperature was regulated at 25 ± 1 °C. The general ICP-MS operating conditions used were; nebulizer argon gas flow 0.97 L min^{-1}, ICP RF-Power 1100 W, isotope used: m/z 103, nebulizer type: cross flow. UV–VIS spectra were recorded with a Perkin-Elmer Lambda 12 double-beam UV–VIS spectrometer. Quartz cuvettes were used and the slit width was set at 1 nm. The room temperature was regulated at 25 ± 1 °C. A Grant KD100 circulating thermostatic controller, mounted on a Grant W6 tank with cooling coil, was used to regulate the temperature when the sample is prepared and within the sample chamber of the spectrometer at 25.0 ± 0.1 °C. pH measurements were performed using a Metrohm 691 pH-meter and a Metrohm 6.0232.100 combined glass pH electrode. Potentiometric standardization titrations were recorded and performed using a Metrohm 716 DMS Titrino with Metrohm 728 stirrer. A Metrohm 6.0404.100 combined massive silver electrode was used for argentiometric determination of chloride and bromide anions.

2.2. Reagents

0.1 mol L^{-1} stock solutions of tetrabutylammonium chloride (TBACl), tetrabutylammonium bromide (TBABr), potassium bromide (KBr) and tetrabutylphosphonium bromide (TBPBr) (Fluka) were prepared and used for subsequent dilutions. All solution preparations used Milli-Q water with resistivity levels of 18.1 MΩ cm. The stationary phase was Silica gel 100 C_{18} (Fluka 60757, CAS 112926-00-8). The C_{18} surface coverage is 17–18% or 4.0 μmol m^{-2} and the remaining surface hydroxyl groups are end-capped with methyl. The silica column material has an average diameter of 50 μm and the pore diameter is approximately 100 Å. Ethanol absolute, CH_3CH_2OH (Saarchem), was used as discussed in the column preparation section. Several stock Rh(III) solutions of approximately 1 mmol L^{-1} and 0.1 mol L^{-1} were prepared by dissolving $[RhCl_3]\cdot x(H_2O)$ (Alfa Aesar) in water at the desired HCl concentration. Total Rh concentration was determined using the ICP-MS and calibration was done with a certified multi-element PGM standard (Spectrascan 8313).

2.3. C_{18} column packing and conditioning

The "tap-fill" dry-pack method [25] was used for column packing. Evidence that the columns were properly packed was inferred from the 'perfect' Gaussian peak shape of eluted analytes, Fig. 1a, which implies no column voids and upon opening the columns no bed compression was found after weeks of use.

The reversed phase column was initially conditioned by passage of an ethanol/water (80:20, v/v) mixture through the column for at least 40 min, after which elution of the EtOH was affected by passage of a mobile phase that contained ion-pair reagent dissolved in water at the desired concentration for approximately 3 h [26]. After these conditioning steps the columns were ready for use. When a column was not used for an extended time period it was stored in 100% EtOH.

2.4. Chromatographic injection procedure for all Rh(III) samples

As an example, 1.0 mL of a ~1.0×10^{-3} mol L^{-1} Rh(III) stock sample was first diluted, 100-fold, to a total volume of 100.00 mL, such that the matrix of the diluted sample was 0.1 mol L^{-1} HCl at 298 K. The diluted sample was thoroughly mixed by means of a magnetic follower for ±45 s, after which a 20 μL aliquot of the diluted sample was injected onto the C_{18} column. The time taken from stock sample dilution until injection was, on average, approximately 114 s.

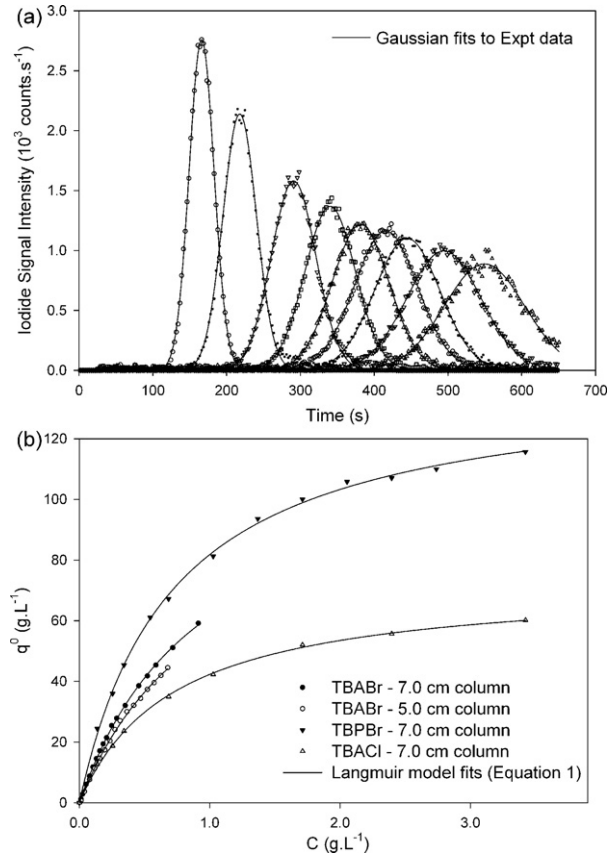

Fig. 1. (a) Typical iodide test sample Gaussian chromatographic traces as a function of mobile phase TBACl concentration. Column length = 5.0 cm, mobile phase = distilled water + (0.01, 0.015, 0.02, . . ., 0.05 M) TBACl + 0.01 mol L^{-1} HCl. (b) Ion-pair adsorption isotherms obtained by means of frontal analysis and the corresponding Langmuir model fits. The composition of the mobile phases consisted of the relevant ion-pair reagent dissolved in water.

2.5. Adsorption isotherm measurements by means of frontal analysis

One pump of the HPLC instrument was used to deliver a mobile phase that consists of water. A second pump delivered a mobile phase that consisted of ion-pair reagent (either TBABr or TBPBr or TBACl) dissolved in water. The break through curves shown in the supplemental information, Fig. S1a, were recorded successively at a flow rate of 1.0 mL min^{-1}, with an adequate delay between each break through curve to establish the re-equilibration of the column with the mobile phase that consists only of water. Using a set of KBr solutions of known concentration, the conductivity signal response was shown to be proportional to the injected KBr concentration. KBr is not retained at all in the column and effectively takes the column hold-up volume into account, Fig. S1b.

3. Computational details

3.1. The Langmuir isotherm

The Langmuir model [27] relates the amount of ion-pair reagent adsorbed, q^o, to the mobile phase concentration of ion-pair reagent, C, Eq. (1); where q_s is the monolayer saturation capacity and K_{ad} is the adsorption equilibrium constant:

$$q^o = q_s \left(\frac{K_{ad} C}{1 + K_{ad} C} \right) \quad (1)$$

The amount of ion-pair reagent adsorbed is given by Eq. (2), where V_{eq}, V_a and C are the elution volume, volume of the stationary phase and ion-pair mobile phase concentration, respectively:

$$q^o = \frac{C V_{eq}}{V_a} \quad (2)$$

3.2. Kinetic data analysis

The program Kinetic$_5$Ver [28] (Visual Basic 6) was written for the least-squares fitting of rate law(s), derived from reaction models, to experimental data (spectrophotometric and chromatographic). The program has two main components that work in tandem; a routine to numerically integrate the differential equations using a Runge–Kutta algorithm [29] and a routine to execute the least-squares fitting using the Simplex algorithm [30]. Validation of program, Kinetic$_5$Ver, was performed by generating artificial data via analytical integration of several rate models in varying complexity with chosen rate constants and molar extinction coefficients. The artificial data sets were then manipulated with the aid of a random number generator such that each data point had an absolute error varying from 0 to 3%. These augmented data sets were then analyzed with program Kinetic$_5$Ver and in all cases the calculated parameters with Kinetic$_5$Ver agreed within 2% with the chosen parameters used in the analytical integration.

3.3. Mauser plots

The theory of Mauser space diagrams has been extensively discussed by Polster and co-worker [31,32]. In particular, we were interested in the absorbance triangle plot for a linear reaction system (e.g. relation (3)) with two consecutive reactions in order to calculate the molar extinction coefficients from UV–VIS spectra for several Rh(III) species:

$$A \rightarrow B \rightarrow C \quad (3)$$

To obtain all the molar extinction coefficients in the wavelength region (390–550 nm) would require literally, 25,600 absorbance (λ_y) versus absorbance (λ_x) plots. This large amount of graphs results from plotting all wavelengths against each other. To achieve this task, a program called Mauser$_1$Ver was written in VB.Net [33].

4. Results and discussion

4.1. Ion-pair C_{18} HPLC column capacity and column overload

The extent of separation or resolution between Rh(III) aqua chlorido-complexes can be controlled by varying the surface concentration of ion-pair reagent, column length and competing ion-pair reactions. The surface concentration of ion-pair reagent (TBACl, TBABr, TBPBr) at a specific mobile phase ion-pair reagent concentration and the column monolayer saturation capacity, q_s, were determined by means of frontal analysis. The adsorption isotherms obtained and the least-squares fits with the Langmuir model, Eq. (1), are shown in Fig. 1b. The good least-squares fits, Fig. 1b, combined with the agreement in the calculated column monolayer saturation capacity, Table 1, using different ion-pair reagents and column lengths validate the Langmuir model. The calculated adsorption constants, K_{ad}, are listed in Table 1.

Relatively rapid interconversion of Rh(III) aqua chlorido-complexes (due to aquation or anation) during a chromatographic run as well as column overload [34], will result in non-Gaussian peak shapes. To estimate at what ion-pair reagent concentration column overload occurred in this ion-pair HPLC system, sodium iodide test samples were injected as a function of mobile phase ion-pair concentration, Fig. 1a. The sample matrix of the iodide test

Table 1
From the Langmuir model fits the C_{18} monolayer saturation capacity, q_s, and ion-pair reagent adsorption constants, K_{ad}, at 298 K were calculated. The internal diameter of these columns was 0.2 cm. L = column length.

Ion-pair reagent	K_{ad} (L g^{-1})	q_s (g L^{-1})	L (cm)
TBABr	1.03 (±0.04)	120 (±5)	7.0
TBABr	0.99 (±0.06)	132 (±4)	5.0
TBPBr	1.43 (±0.04)	137 (±8)	7.0
TBACl	0.78 (±0.05)	128 (±8)	7.0

samples were the same as for the injected Rh(III) samples and the highest concentration of iodide was 20 times that of the total Rh(III) concentration injected in this study. As 'perfect' iodide Gaussian peaks (Fig. 1a) were obtained, column overload can be ruled out as a possible cause for non-Gaussian peak shapes obtained in this study (*vide infra*). Moreover, to monitor column degradation and to measure the efficiency of newly packed columns, daily injection of the iodide test samples were carried out.

4.2. Kinetic based speciation of $[RhCl_n(H_2O)_{6-n}]^{3-n}$ (n = 3–6) at low HCl ionic strength

The difficulty of assigning Rh(III) aqua chlorido-complexes that elute during a chromatographic separation is due, in part, that several Rh(III) species are simultaneously present even at relatively high HCl concentrations [2]. This problem was addressed by exploiting the well documented *trans* effect [17–23,35] when Rh(III) aqua chlorido-complexes undergo ligand exchange reactions. Of particular interest in this study was the possible stereo-specific substitution of successive aquation of the $[RhCl_6]^{3-}$ complex anion based on the *trans* effect, i.e. $[RhCl_6]^{3-} \rightarrow [RhCl_5(H_2O)]^{2-} \rightarrow$ *cis*-$[RhCl_4(H_2O)_2]^{-} \rightarrow$ *fac*-$[RhCl_3(H_2O)_3]$ [12]. This reaction sequence was exploited for Rh(III) species assignment since it is relatively easy to carry out practically, by diluting a Rh(III) sample equilibrated in concentrated HCl (>9.0 mol L^{-1}) to a 0.1 mol L^{-1} HCl matrix and following this process by UV–VIS spectroscopy. Harris and co-workers [12,17–19] conducted extensive kinetic studies concerning the ligand exchange rates of Rh(III) aqua chlorido-complexes. However, the ionic strength at which these investigations were conducted varied from approximately 2 mol kg^{-1} (HCl or $HClO_4$) upwards and are not suitable (*vide infra*) for an ion-pair reversed phase chromatographic separation. As the ionic strength can significantly alter the rate of ligand exchange, we re-investigated the aquation rates of $[RhCl_n(H_2O)_{6-n}]^{3-n}$ (n = 4–6) species in a relatively low ionic strength environment of 0.1 mol kg^{-1} HCl. A 0.1 mol L^{-1} ionic strength was chosen since it closely resembles the mobile phase composition used in this study and the kinetic study is likely to establish the extent by which Rh(III) species interconversion might occur during a chromatographic run. In addition, comparison of the kinetic data (*vide infra*) obtained with the UV–VIS study and independently with the developed ion-pair HPLC–ICP-MS study, enable the correct assignment of the Rh(III) aqua chlorido-complexes separated chromatographically.

Available species distribution diagrams suggest that in a 9.5 mol L^{-1} HCl matrix only $[RhCl_6]^{3-}$ and $[RhCl_5(H_2O)]^{2-}$ species are present in significant quantities [3]. Dilution of a stock Rh(III) sample equilibrated in 9.464 mol L^{-1} HCl to a 0.101 mol L^{-1} HCl matrix results in relatively rapid successive aquation reactions of the Rh(III) species. The ensuing UV–VIS spectral change was monitored as a function of time at 298.1 K, Fig. 2a. The first set of isosbestic points formed within 6 min, indicated by the solid vertical lines in Fig. 2a, after which a second set of isosbestic points was observed as indicated by the vertical dashed lines. The two sets of isosbestic points confirm that only two Rh(III) species are predominant at a time during the sequential aquation reactions (4) and (5),

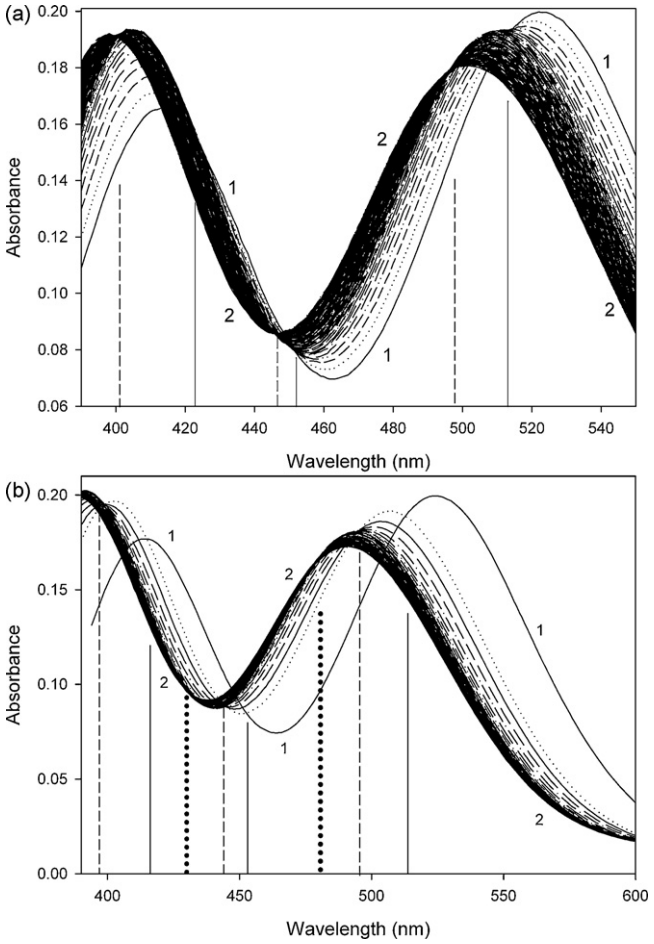

Fig. 2. The UV–VIS spectral change as a function of time when diluting a 0.1963 mol L^{-1} Rh(III) sample equilibrated in 9.464 mol L^{-1} HCl, 100-fold, to a 0.101 mol L^{-1} HCl matrix, (a) represents the first 90 min and (b) 3 days of recording after dilution. Solid, dashed and dotted vertical lines indicate the three sets of isosbestic points observed and are associated with the successive aquation reactions $[RhCl_6]^{3-} \rightarrow [RhCl_5(H_2O)]^{2-} \rightarrow$ *cis*-$[RhCl_4(H_2O)_2]^{-} \rightarrow$ *fac*-$[RhCl_3(H_2O)_3]$, respectively.

respectively. Moreover, the second set of isosbestic points corroborate that aquation of $[RhCl_5(H_2O)]^{2-}$ is most likely to yield only the *cis*-$[RhCl_4(H_2O)_2]^{-}$ stereoisomer, as a result of the higher *trans* effect of the coordinated chloride ion compared to water [17].

From Fig. 2a it is observed that 90 min after dilution the rate by which the UV–VIS spectrum change decrease considerably. This is associated with the relatively slower rate of aquation of the *cis*-$[RhCl_4(H_2O)_2]^{-}$ complex and it was therefore necessary to record the UV–VIS spectrum of the diluted sample over a period of at least 4 days to observe the formation of the third set of isosbestic points at 431 and 478 nm, Fig. 2b. The third set of isosbestic points confirm the stereo-specific substitution route of successive aquation reactions, leading to the conclusion that aquation of *cis*-$[RhCl_4(H_2O)_2]^{-}$ yields the *fac*-$[RhCl_3(H_2O)_3]$ stereoisomer, relation (6):

$$[RhCl_6]^{3-} + H_2O \underset{k_{56}}{\rightleftharpoons} [RhCl_5(H_2O)]^{2-} + Cl^{-} \quad (4)$$

$$[RhCl_5(H_2O)]^{2-} + H_2O \underset{k_{45}}{\overset{k_{54}}{\rightleftharpoons}} cis\text{-}[RhCl_4(H_2O)_2]^{-} + Cl^{-} \quad (5)$$

$$cis\text{-}[RhCl_4(H_2O)_2]^{-}_{(aq)} + H_2O \underset{k_{34}}{\overset{k_{43}}{\rightleftharpoons}} fac\text{-}[RhCl_3(H_2O)_3] + Cl^{-} \quad (6)$$

For the calculation of the relevant aquation/anation rate constants from the data, of which Fig. 2a is a typical example, the same rate laws, Eqs. (7)–(9), proposed by Harris and co-workers

Table 2
Comparison of the calculated Rh(III) aqua chlorido-complexes pseudo-first-order aquation and anation rate constants by means of UV–VIS spectroscopy and independently with the ion-pair HPLC method at 298.1 K and 0.101 mol kg^{-1} HCl ionic strength.

Aquation/anation rate constants	Experimental technique		
	UV–VIS	Ion-pair HPLC–ICP-MS	Literature[a]
k_{65} (min^{-1})	5.52 (±0.23) × 10^{-1}	–	1.1 × 10^{-1}[b]
k_{54} (min^{-1})	1.51 (±0.07) × 10^{-2}	1.48 (±0.06) × 10^{-2}[c]	2.32 × 10^{-3}[b]
cis–fac k_{43} (min^{-1})	1.24 (±0.04) × 10^{-4}	1.31 (±0.05) × 10^{-4}[d] 1.28 (±0.06) × 10^{-4}[e] 1.26 (±0.07) × 10^{-4}[f]	–
fac–cis k_{34} (M^{-1} min^{-1})	3.46 (±0.11) × 10^{-4}	3.52 (±0.14) × 10^{-4}[d] 3.49 (±0.17) × 10^{-4}[f]	–
trans–mer k_{43} (min^{-1})	–	4.28 (±0.21) × 10^{-4}[e] 4.32 (±0.23) × 10^{-4}[f]	–
mer–trans k_{34} (M^{-1} min^{-1})	–	1.42 (±0.03) × 10^{-4}[f]	–

The corresponding pseudo-first-order anation rate constants calculated were negligibly small at 0.1 mol kg^{-1} HCl ionic strength experimental conditions.
[a] Refs. [3,17].
[b] Aquation rate constants determined at 4.0 mol kg^{-1} ionic strength.
[c] Fig. 4c.
[d] Fig. 5c.
[e] Fig. 8c.
[f] Fig. 8d.

[12,17] three decades ago were used. Due to the significant lower rate of aquation of *cis*-$[RhCl_4(H_2O)_2]^-$ compared to $[RhCl_5(H_2O)]^{2-}$, the aquation of *cis*-$[RhCl_4(H_2O)_2]^-$ was not included in the reaction model fitted. Using the program Kinetic$_5$Ver the rate laws, Eqs. (7)–(9), were simulated and non-linear least-squares regression fits at several wavelengths were carried out. The agreement between the experimental and simulated data is excellent and the fit at 550 nm is shown in Fig. 3a. The good least-squares fits validate the rate laws and the calculated rate constants listed in Table 2 are the average of at least four separate experiments:

$$\frac{d(A)}{dt} = -k_{65}(A) + k_{56}(B)(Cl^-) \quad (7)$$

$$\frac{d(B)}{dt} = k_{65}(A) - k_{56}(B)(Cl^-) - k_{54}(B) + k_{45}(E)(Cl^-) \quad (8)$$

$$\frac{d(E)}{dt} = k_{54}(B) - k_{45}(E)(Cl^-) \quad (9)$$

$A = [RhCl_6]^{3-}$, $B = [RhCl_5(H_2O)]^{2-}$ and E = *cis*-$[RhCl_4(H_2O)_2]^-$.

We find that the pseudo-first-order aquation rate constants, k_{65} and k_{54}, are much larger compared with those reported in literature [3,17], Table 2. As ionic strength is the only difference between our experiments and that reported in the literature [17], the effect of ionic strength on the rate of aquation was investigated at a fixed chloride concentration of 0.1 mol L^{-1}. This was done by diluting a Rh(III) sample equilibrated in 9.464 mol L^{-1} HCl such that the matrix of the diluted sample contained 0.101 mol L^{-1} HCl and the desired concentration of $HClO_4$, which was varied from 0.1 to 5.6 mol L^{-1}. From Fig. 3a it is observed that as the ionic strength increase, the rate of aquation associated with reactions (4) and (5) decreases substantially. The least-squares fits obtained using program Kinetic$_5$Ver are shown in Fig. 3a and the computed rate constants are listed in Table 3. The calculated aquation rate constants, k_{65} and k_{54}, Table 3 at an ionic strength of 4.0 mol kg^{-1} $HClO_4$ agree satisfactorily with those reported by Harris and co-worker [17] (Table 2) and validates our kinetic analyses. The relatively large decrease of the aquation rates with an increase in ionic strength can be attributed to a decrease of the activity of water and the Rh(III) aqua chlorido-complexes.

In order to calculate the relevant aquation/anation rate constants for reaction (6) from the data, of which Fig. 2b is a typical example, the rate laws, Eqs. (7), (8) and (10), were used. Similar as before, using the program Kinetic$_5$Ver Eqs. (7), (8) and (10) were

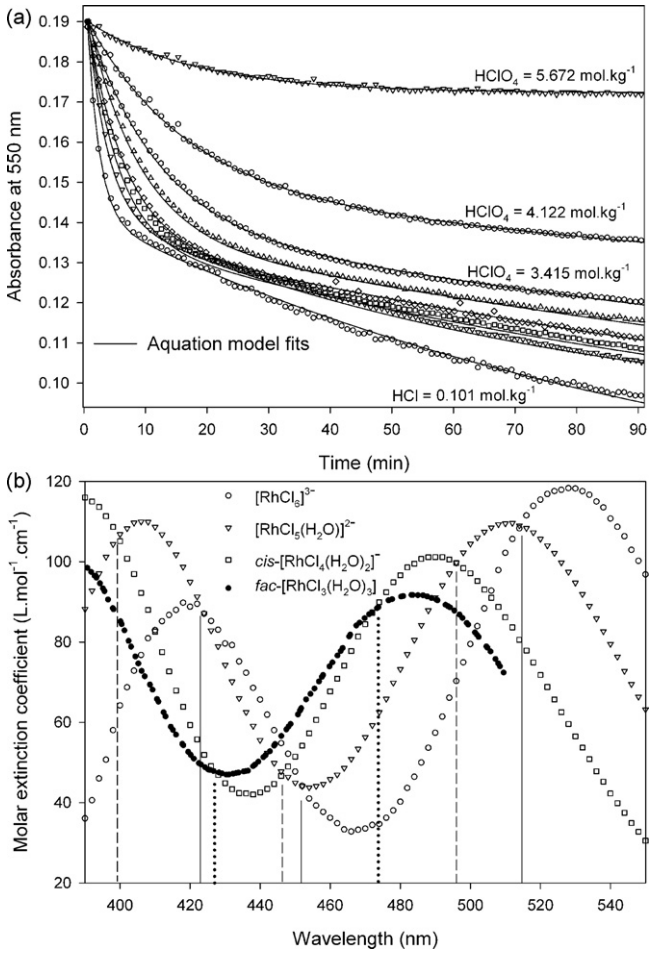

Fig. 3. (a) The symbols represent the absorbance change as a function of time when diluting 0.1963 mol L^{-1} Rh(III) samples equilibrated in 9.464 mol L^{-1} HCl, 100-fold, to a 0.101 mol L^{-1} HCl and specified concentration of $HClO_4$. The aquation model least-squares fits (solid lines) are excellent and the concentrations of $HClO_4$ used in each case are listed in Table 3. (b) Calculated molar extinction coefficients for $[RhCl_n(H_2O)_{6-n}]^{3-n}$ (n = 3–5) complexes using the program Mauser$_1$Ver.

Table 3
Calculated pseudo-first-order aquation rate constants for the $[RhCl_n(H_2O)_{6-n}]^{3-n}$ ($n = 5, 6$) complex anions as a function of ionic strength (perchloric acid) at 298.1 K.

Ionic strength	Aquation rate constants	
$HClO_4$ (mol kg^{-1})	k_{65} (min^{-1})	k_{54} (min^{-1})
0.109	$5.42\ (\pm0.21) \times 10^{-1}$	$1.53\ (\pm0.05) \times 10^{-2}$
0.912	$3.15\ (\pm0.17) \times 10^{-1}$	$1.26\ (\pm0.04) \times 10^{-2}$
1.84	$2.03\ (\pm0.13) \times 10^{-1}$	$6.77\ (\pm0.33) \times 10^{-3}$
2.34	$1.62\ (\pm0.08) \times 10^{-1}$	$4.94\ (\pm0.19) \times 10^{-3}$
2.66	$1.21\ (\pm0.08) \times 10^{-1}$	$4.01\ (\pm0.16) \times 10^{-3}$
3.41	$8.78\ (\pm0.29) \times 10^{-2}$	$2.40\ (\pm0.07) \times 10^{-3}$
4.12	$6.19\ (\pm0.31) \times 10^{-2}$	$1.64\ (\pm0.05) \times 10^{-3}$
5.66	$4.66\ (\pm0.23) \times 10^{-2}$	–

simulated and non-linear least-squares regression fits at several wavelengths resulted in excellent agreement between the experimental and simulated data illustrated for 490 and 520 nm in the supplementary information, Fig. S2. The calculated aquation and anation rate constants, k_{43} and k_{34}, are listed in Table 2:

$$\frac{d(E)}{dt} = k_{54}(B) - k_{43}(E) + k_{34}(G)(Cl^-) - k_{45}(E)(Cl^-) \quad (10)$$

$B = [RhCl_5(H_2O)]^{2-}$, $E = cis\text{-}[RhCl_4(H_2O)_2]^-$ and $G = fac\text{-}[RhCl_3(H_2O)_3]$.

The least-squares fits to the kinetic data discussed above not only yield the relevant aquation/anation rate constants but also the molar extinction coefficients of the Rh(III) aqua chlorido-complexes at several wavelengths. To further validate the kinetic analyses, the molar extinction coefficients of $[RhCl_5(H_2O)]^{2-}$, $cis\text{-}[RhCl_4(H_2O)_2]^-$ and $fac\text{-}[RhCl_3(H_2O)_3]$, were independently re-calculated using Mauser diagrams, Fig. 3b. A typical Mauser diagram obtained with program Mauser$_1$Ver is shown in the supplementary data, Fig. S3. The agreement between the molar extinction coefficients calculated for the Rh(III) complexes with the two differing computational methods is excellent and confirm the results from the kinetic analyses performed. The molar extinction coefficient spectrum for $[RhCl_6]^{3-}$ could not be calculated from the Mauser plots and it was assumed as in the literature [12,13], that in concentrated (>9 mol L^{-1}) HCl essentially only the $[RhCl_6]^{3-}$ species is present. The calculated molar extinction coefficient spectra for the $[RhCl_n(H_2O)_{6-n}]^{3-n}$ ($n = 3$–5) species intersect at all the experimentally found isosbestic points and indicates that the aquation/anation model used is internally consistent, Fig. 3b. Interestingly, the UV–VIS molar extinction coefficients for the $[RhCl_n(H_2O)_{6-n}]^{3-n}$ ($n = 3$–6) species reported by Kleinberg and co-workers [13] and Harris and co-worker [12] differ substantially from one another, but our calculated ε data agree well with those reported by Harris and co-worker [12].

4.3. Chromatographic separation and the assignment of $[RhCl_6]^{3-}$, $[RhCl_5(H_2O)]^{2-}$, $cis\text{-}[RhCl_4(H_2O)_2]^-$ and $fac\text{-}[RhCl_3(H_2O)_3]$ complexes

The need for a speciation analysis of Rh(III) aqua chlorido-complexes in an HCl matrix is clearly reflected by the large differences between proposed species distribution diagrams [3]. In order to measure the concentration of a Rh(III) species when several $[RhCl_n(H_2O)_{6-n}]^{3-n}$ ($n = 0$–6) aqua chlorido-complexes are simultaneously present with the proposed ion-pair HPLC–ICP-MS speciation method, it is first necessary to assign the separated Rh(III) species. Utilizing the kinetic results obtained from the UV–VIS study above, which confirmed a stereo-specific substitution course of successive aquation of the $[RhCl_6]^{3-}$ complex anion, assignment of several of the Rh(III) aqua chlorido-complexes of interest separated with the ion-pair HPLC method (*vide infra*) becomes possible. A crucial component of the separation 'step' is that the Rh(III) aqua chlorido-complexes speciation must not change. This is potentially problematic for the separation of $[RhCl_5(H_2O)]^{2-}$ and $[RhCl_6]^{3-}$ species since the $t_{1/2}$ for aquation of the $[RhCl_6]^{3-}$ species was found to be 1.3 min at 0.1 mol kg^{-1} HCl ionic strength and 298 K in contrast to 4.5 min [17] at 4.0 mol kg^{-1} HCl ionic strength. Hence to minimize aquation of the $[RhCl_6]^{3-}$ complex anion during a chromatographic run, the intended separation should be completed as rapidly as possible and at 'high' ionic strength. It was found that a 5.0 cm column and a mobile phase of 0.1 mol L^{-1} TBACl, 0.01 mol L^{-1} HCl and water gave the best results in terms of a relatively rapid ion-pair HPLC separation. Diluting a Rh(III) sample equilibrated in 9.464 mol L^{-1} HCl to a 0.101 mol L^{-1} HCl matrix, followed by injection of the diluted sample as a function of time yields the chromatographic traces shown in Fig. 4a and b. From the UV–VIS data it can be confidently inferred that 10 min after dilution the sample only contains the $[RhCl_5(H_2O)]^{2-}$ and $cis\text{-}[RhCl_4(H_2O)_2]^-$ complex anions to any significant extent. It is thus reasonable that the Rh(III) species which elutes at 90 s (Fig. 4b), 10 min after dilution can be assigned to the $[RhCl_5(H_2O)]^{2-}$ species. Quantification of the Rh(III) species was done by integrating the entire transient signal and individual peaks. Division of individual peak area by the total transient signal area yields the mole fraction of a Rh(III) species. Multiplication of the mole fraction of a species with the known total Rh concentration yields the individual Rh(III) species concentration. A plot of $\ln([RhCl_5(H_2O)]^{2-})$ versus time, Eq. (11), yields a linear trend (Fig. 4c) confirming a pseudo-first-order aquation reaction. The aquation rate constant, k_{54}, obtained from the slope of the linear regression fit in Fig. 4c agree quantitatively with the k_{54} calculated for the $[RhCl_5(H_2O)]^{2-}$ species from the UV–VIS data (Table 2) confirming the assignment here. Moreover, when the diluted sample was injected 5.4 h after preparation, which is sufficient time for all the $[RhCl_5(H_2O)]^{2-}$ species to undergo aquation to form the $cis\text{-}[RhCl_4(H_2O)_2]^-$ species, no Rh(III) eluted at 90 s and proves that $[RhCl_n(H_2O)_{6-n}]^{3-n}$ ($n = 0$–4) species do not elute at 90 s. It is now apparent that the relatively broad peak in Fig. 4a at 90 s is due to a combination of $[RhCl_5(H_2O)]^{2-}$ and $[RhCl_6]^{3-}$ species. The relatively fast aquation of $[RhCl_6]^{3-}$ and the fact that a dilution step before injection is necessary makes it difficult or nearly impossible to choose chromatographic conditions with this system such that peaks for both $[RhCl_6]^{3-}$ and $[RhCl_5(H_2O)]^{2-}$ species can be observed in agreement with the CE study done by Salvadó and co-workers [11]:

$$\ln([B]_o) = -k_{54}t + \ln([B]_i) \quad (11)$$

The chromatographic conditions used to separate $cis\text{-}[RhCl_4(H_2O)_2]^-$ and $[RhCl_5(H_2O)]^{2-}$, Fig. 4b, is clearly not appropriate for the separation of $[RhCl_n(H_2O)_{6-n}]^{3-n}$ ($n = 3, 4$) complexes including stereoisomers. The optimum chromatographic parameters found for such a separation of $[RhCl_n(H_2O)_{6-n}]^{3-n}$ ($n = 3$, 4) complexes was determined to be a column of length 25.0 cm and the mobile phase consisted of water, 0.05 mol L^{-1} TBACl and 0.01 mol L^{-1} HCl. Diluting a stock Rh(III) sample equilibrated in 9.464 mol L^{-1} HCl to a 0.101 mol L^{-1} HCl matrix, followed by injection of the diluted sample as a function of time yielded the chromatographic traces shown in Fig. 5a and b. The pronounced tailing observed beyond 600 s in Fig. 5a for the sample injected 2.5 min after dilution suggests that only $[RhCl_5(H_2O)]^{2-}$ and $[RhCl_6]^{3-}$ complex anions are present shortly after dilution and considerable aquation of these species occurs during the chromatographic run. The second injection of the diluted Rh(III) sample (Fig. 5a) was 61 min after dilution and exhibit much less tailing compared to the first injection. The decrease in tailing is expected since 61 min after sample dilution all of the $[RhCl_6]^{3-}$ and approximately 66% of the $[RhCl_5(H_2O)]^{2-}$ species had undergone aquation to yield the $cis\text{-}[RhCl_4(H_2O)_2]^-$ species and therefore contains much less $[RhCl_5(H_2O)]^{2-}$ species that can

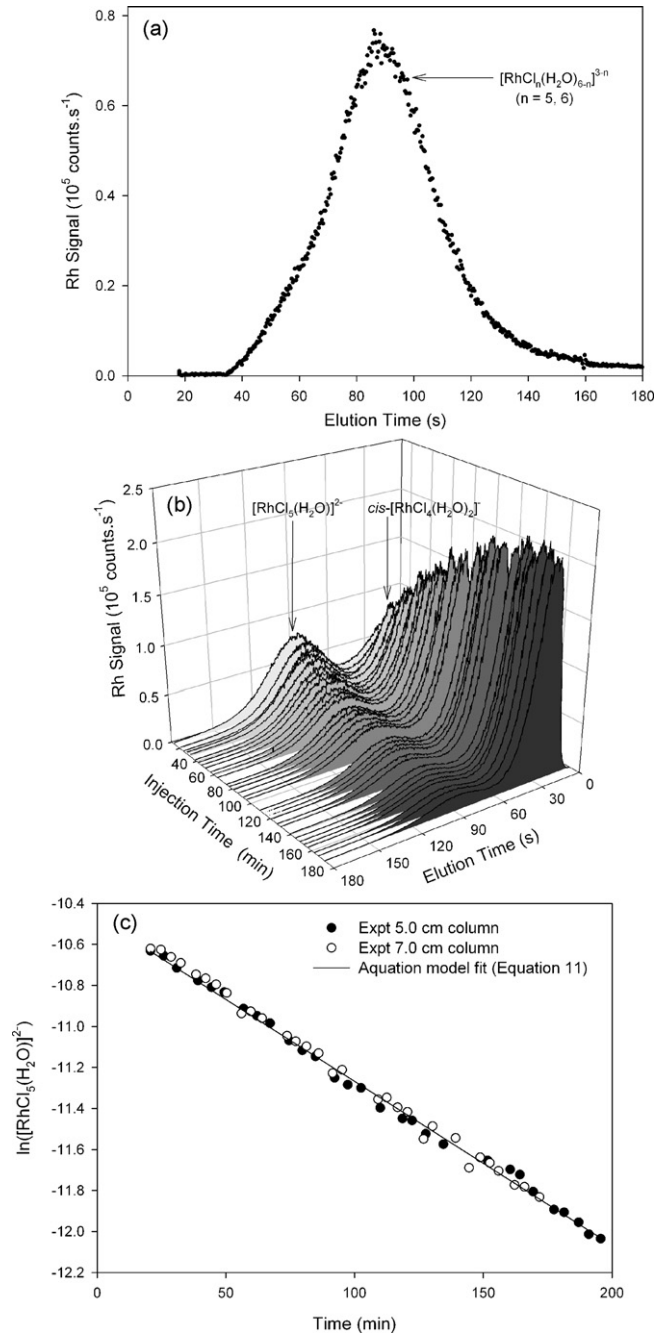

Fig. 4. Chromatographic traces obtained when diluting a 2.983 mmol L^{-1} Rh(III) sample equilibrated in 9.464 mol L^{-1} HCl, 100-fold, to a 0.101 mol L^{-1} HCl matrix and (a) injecting the sample immediately after dilution (114 s) and (b) as a function of time. (c) A plot of ln($[RhCl_5(H_2O)]^{2-}$) versus time yielded a linear trend confirming pseudo-first-order aquation kinetics. Mobile phase = water + 0.1 mol L^{-1} TBACl + 0.01 mol L^{-1} HCl, column length = 5.0 cm. The RSD (relative standard deviation) for peak area determination was below 5%.

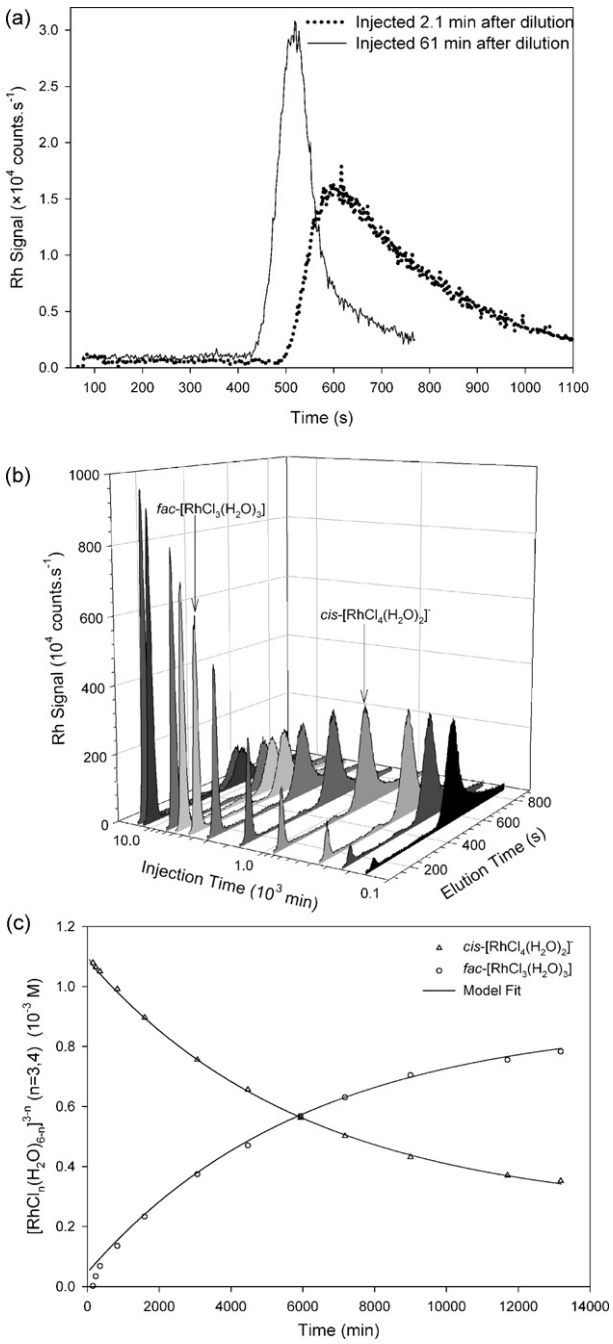

Fig. 5. Chromatographic traces (a) and (b) obtained when diluting a 0.1123 mol L^{-1} Rh(III) sample equilibrated in 9.464 mol L^{-1} HCl, 100-fold, to a 0.101 mol L^{-1} HCl matrix after which the diluted sample was injected as a function of time; (c) excellent aquation/anation model fit. Column length = 25.0 cm, mobile phase = water + 0.05 mol L^{-1} TBACl + 0.01 mol L^{-1} HCl.

aquate during the chromatographic run. In Fig. 5b the peak at 550 s initially intensify due to further aquation of $[RhCl_5(H_2O)]^{2-}$ and subsequently decreased in intensity with time. At the same time a peak at 180 s appears and only intensifies with time. These trends are consistent with the stereo-specific substitution course of successive aquation of the $[RhCl_6]^{3-}$ complex anion and it is thus reasonable to conclude that the peaks at 180 and 550 s are due to the *fac*-$[RhCl_3(H_2O)_3]$ and *cis*-$[RhCl_4(H_2O)_2]^-$ species, respectively. Simulation of the rate laws Eqs. (7), (8) and (10) using program Kinetic$_5$Ver resulted in an excellent least-squares fit to the data in Fig. 5b shown in Fig. 5c. The quantitative agreement between the calculated k_{43} and k_{34} rate constants, relation (6), determined chromatographically and independently with UV–VIS (Section 4.2 and Table 2) confirms the peak assignments.

In summary, the stereo-specific substitution course of successive aquation of the $[RhCl_6]^{3-}$ complex anion relations (4)–(6), were monitored using UV–VIS spectroscopy and independently with the ion-pair HPLC–ICP-MS method. The agreement between the UV–VIS and ion-pair HPLC data is excellent, Fig. 6, and the rate of each successive aquation reaction decreases by approximately an order of magnitude.

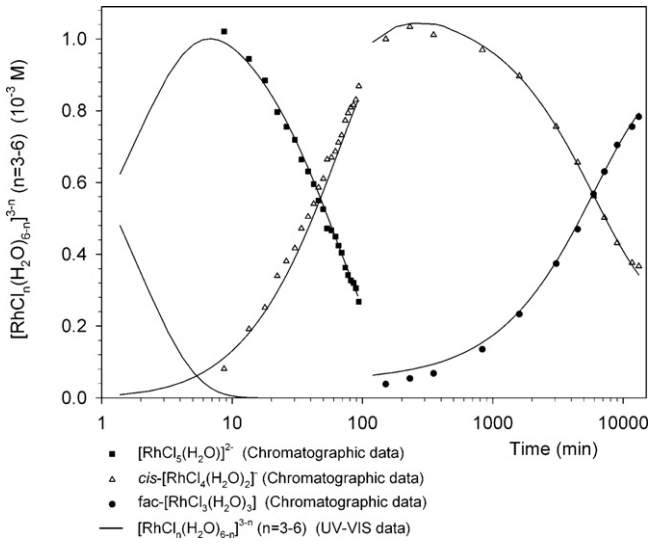

Fig. 6. Diluting a Rh(III) sample equilibrated in 9.462 mol L^{-1} HCl to a 0.101 mol L^{-1} HCl matrix results in successive aquation reactions. The calculated species concentration profiles from the UV–VIS data agree quantitatively with that determined 'directly' with the developed ion-pair HPLC speciation method and illustrate the internal consistency of the chromatographic peak assignments made.

4.4. 'Equilibrium' species distribution of $[RhCl_n(H_2O)_{6-n}]^{3-n}$ (n = 0–6) complexes as a function of HCl concentration

For the reaction conditions chosen in Sections 4.2 and 4.3, several of the Rh(III) aqua chlorido-complexes (cationic, *mer*-$[RhCl_3(H_2O)_3]$ and *trans*-$[RhCl_4(H_2O)_2]^-$) are not present in these solutions due to the stereo-specific substitution course of successive ligand exchange and the relatively slow aquation of the *cis*-$[RhCl_4(H_2O)_2]^-$ and *fac*-$[RhCl_3(H_2O)_3]$ species. Hence several stock Rh(III) samples were prepared with differing HCl concentration matrices (0.1–9.5 mol L^{-1} HCl) and allowed to equilibrate for ±2.8 years at 298 K. Injection of these Rh(III) stock samples resulted in the chromatographic traces shown in Fig. 7a and b. Before injection of a Rh(III) stock sample it is necessary to rapidly dilute it to a 0.1 mol L^{-1} HCl matrix, the time taken from dilution to injection was approximately 114 s for each sample.

For increasing HCl concentration in the stock samples, the area of the peak at 90 s (Fig. 7a) associated with the $[RhCl_n(H_2O)_{6-n}]^{3-n}$ (n = 5, 6) complex anions is seen to increase and for the stock sample with a 9.5 mol L^{-1} HCl matrix no peak is observed at 30 s. Despite the difficulty to obtain a clean baseline chromatographic separation of the $[RhCl_6]^{3-}$ and $[RhCl_5(H_2O)]^{2-}$ species, the chromatographic traces illustrated in Figs. 4a and 7a however represents an accurate technique to quantify the combined concentration of these complex anions present in a sample. During the dilution step and chromatographic run only approximately 5% of the $[RhCl_5(H_2O)]^{2-}$ species undergo aquation which slightly changes the species abundance relative to the undiluted sample, based on the rate of aquation data in Table 2.

The chromatographic traces shown in Fig. 7b exhibit several interesting features: (i) an un-retained peak at 120 s which decreases relatively fast in intensity as the chloride concentration in the Rh(III) stock solutions increase and above 4.0 mol L^{-1} chloride it was no longer observed. Although the manufacturer states that "all" residual surface silanol groups are endcapped with methyl, a relatively small percentage remain which can potentially act as cation-exchange sites. To obtain confirmation that cationic species is not retained several chloride salts Li^+, Na^+, Cs^+ and Ba^{2+} were injected separately under the same chromatographic conditions and concentration as done for the Rh(III) samples. All of the

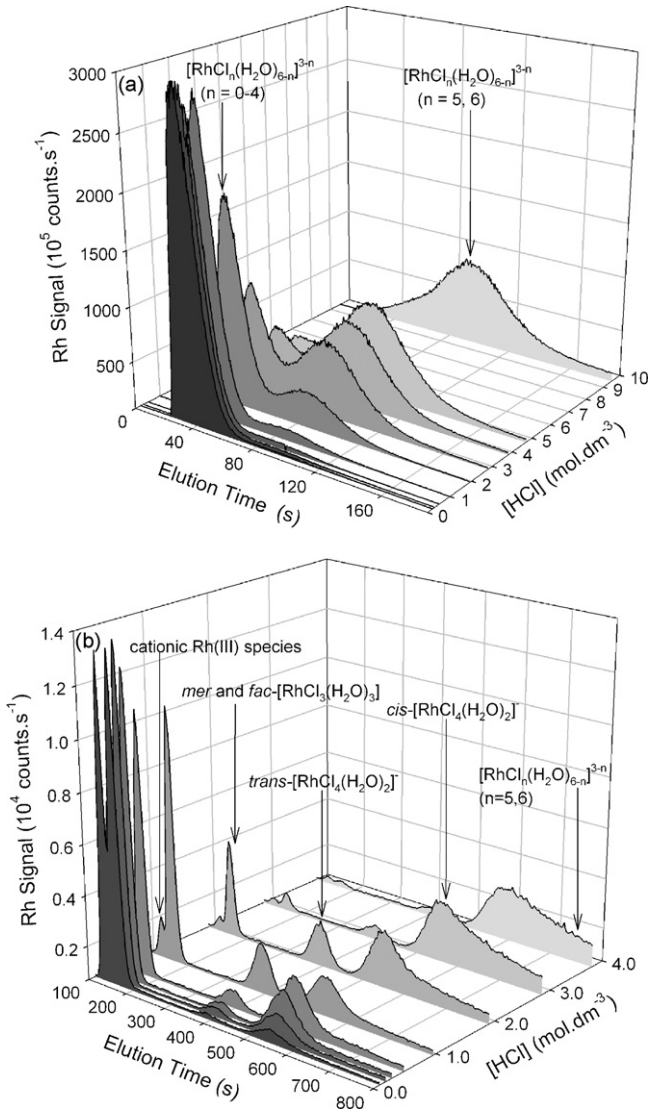

Fig. 7. Chromatographic traces (a) and (b) obtained when injecting the Rh(III) stock samples that were equilibrated in differing HCl matrices immediately (114 s) after dilution to a 0.101 mol L^{-1} HCl matrix. Total Rh(III) concentration for each sample was 1.283 mmol L^{-1}. Chromatographic conditions for (a) column length = 5.0 cm, mobile phase = water + 0.1 mol L^{-1} TBACl + 0.01 mol L^{-1} HCl and (b) column length = 25.0 cm, mobile phase = water + 0.05 mol L^{-1} TBACl + 0.01 mol L^{-1} HCl. The RSD for peak area determination in (a) and (b) was below 5 and 4%, respectively.

cationic metal ions eluted as Gaussian profiles at 120 s. Moreover, the TBA^+ concentration in the mobile phase is in 5000 times excess compared to the total Rh(III) concentration or the group 1 and 2 cationic metal ions injected and will strongly compete for the possible cation-exchange sites. As cationic species are not retained under the above-mentioned chromatographic conditions the peak at 120 s is assigned to cationic Rh(III) aqua chlorido-complexes. (ii) It was established that the Rh(III) species eluting at 180 s is due to the *fac*-$[RhCl_3(H_2O)_3]$ complex, Fig. 5b. During the 2.8 years that the Rh(III) stock solutions were aged it is accepted that the *mer*-$[RhCl_3(H_2O)_3]$ species will be present in addition to *fac*-$[RhCl_3(H_2O)_3]$. These Rh(III) complexes are not charged and it is possible that they are retained due to adsorption on the neutral C_{18} stationary phase. Another possible retention mechanism could be ascribed to partial hydrolysis of these species at the mobile phase pH of 2 to form $[RhCl_3(H_2O)_2(OH)]^-$ complex anions that can "ion-pair" with TBA^+. However, the reported pK_a values by

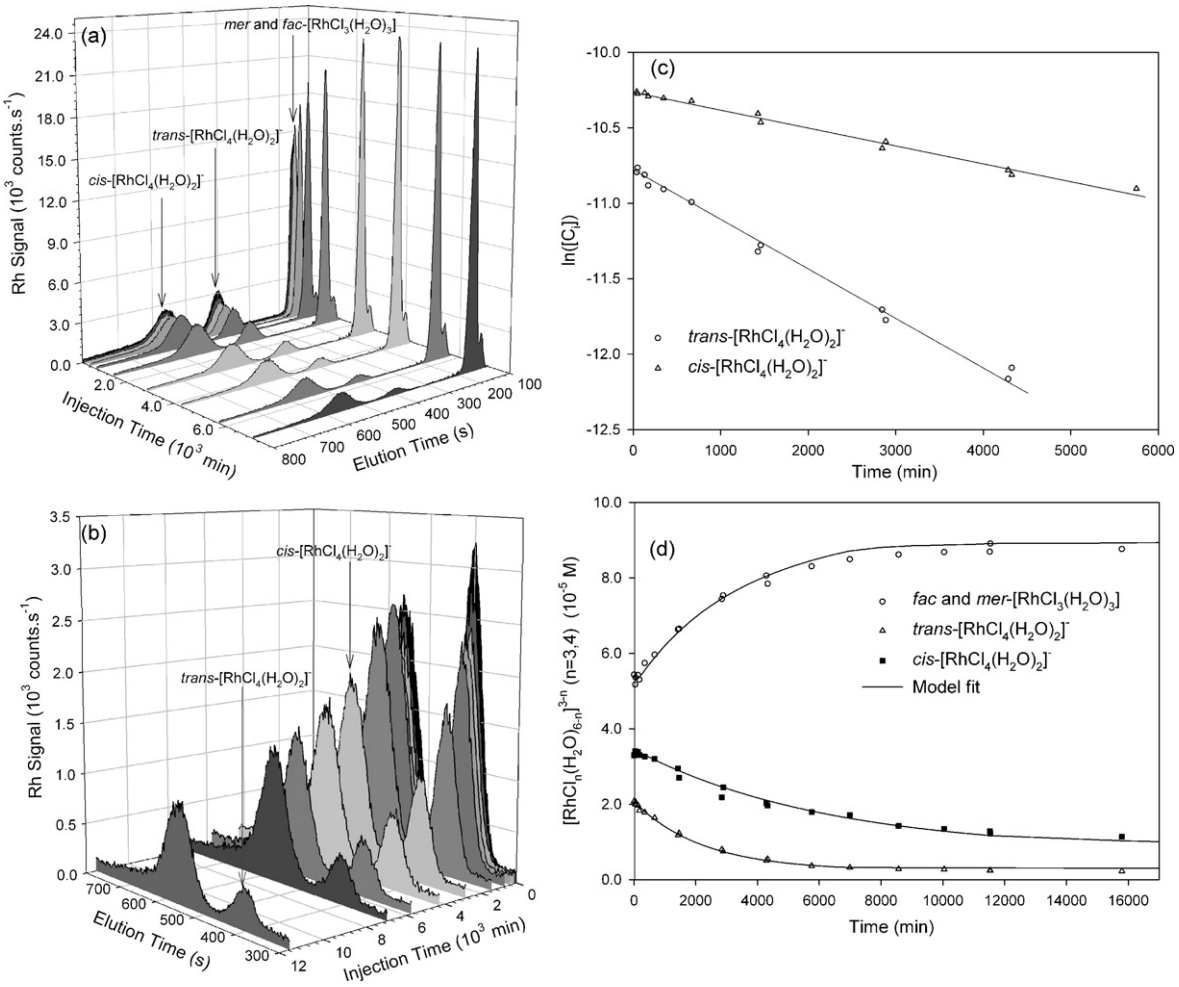

Fig. 8. Chromatographic traces obtained (a) when diluting a Rh(III) sample equilibrated in 9.464 mol L^{-1} HCl to a 0.998 mol L^{-1} HCl matrix and injecting the diluted sample as a function of time, (b) is an enlargement of the *cis*- and *trans*-$[RhCl_4(H_2O)_2]^-$ species elution profiles, (c) pseudo-first-order aquation model fits and (d) model fits that take into account anation in addition to aquation for the relevant species. Column length = 25.0 cm, mobile phase = distilled water + 0.05 mol L^{-1} TBACl + 0.01 mol L^{-1} HCl. The RSD for peak area determination is below 4%.

Harris and co-worker [12] of 7.31 and 6.96 for the *fac* and *mer* species respectively suggest that only a negligibly small fraction of these species are hydrolyzed at a pH of 2. Moreover, increasing the pH of the mobile phase to 7 (by replacing the added 0.01 mol L^{-1} HCl with 0.01 mol L^{-1} NaCl in the mobile phase) did not influence the retention times of eluting species. The intensity of the peak at 180 s decreases slower as the chloride concentration in the Rh(III) stock solutions increase compared to the peak at 120 s. This can be rationalized when considering that the *fac*- and *mer*-$[RhCl_3(H_2O)_3]$ species will increase relative to cationic Rh(III) species at higher chloride concentrations. For now, we tentatively assign the peak at 180 s to be a combination of *fac*- and *mer*-$[RhCl_3(H_2O)_3]$ and confirm this assumption below. (iii) It was conclusively shown that the *cis*-$[RhCl_4(H_2O)_2]^-$ species elutes at 550 s, Fig. 5b. To assign the peak at 400 s, Fig. 7b, the following should be noted; it is unlikely that the *mer*-$[RhCl_3(H_2O)_3]$ complex would exhibit such a large difference in retention behavior compared to the *fac*-$[RhCl_3(H_2O)_3]$ species, $[RhCl_n(H_2O)_{6-n}]^{3-n}$ ($n = 5$, 6) species undergo aquation during the chromatographic run which is the cause of the tailing beyond 600 s, the pK_a of *cis*-$[RhCl_4(H_2O)_2]^-$ species is larger than 7 ensuring negligible hydrolysis at a pH of 2 and the concentration of Rh(III) in the stock samples (~1.0 mmol L^{-1}) is to low for dimerization to occur. The only plausible species that remains is the *trans*-$[RhCl_4(H_2O)_2]^-$ complex anion and the peak at 400 s, Fig. 7b, is assigned as such. The *trans*-$[RhCl_4(H_2O)_2]^-$ species is present at highest concentration in a 1.0 mol L^{-1} HCl matrix taking several months to form when Rh(III) equilibrated in a 9.464 mol L^{-1} HCl is diluted to a 1.0 mol L^{-1} HCl matrix at 298 K. The relatively long time required for the formation of the *trans*-$[RhCl_4(H_2O)_2]^-$ species can be explained by the stereo-specific course of ligand substitution due to the *trans* effect, as proposed by Harris and co-worker [12], i.e. $[RhCl_6]^{3-} \rightarrow [RhCl_5(H_2O)]^{2-} \rightarrow$ *cis*-$[RhCl_4(H_2O)_2]^- \rightarrow$ *fac*-$[RhCl_3(H_2O)_3] \rightarrow$ *cis*-$[RhCl_2(H_2O)_4]^+ \rightarrow$ *mer*-$[RhCl_3(H_2O)_3] \rightarrow$ *trans*-$[RhCl_4(H_2O)_2]^-$.

According to the study by Harris and co-worker [12] the *trans*-$[RhCl_4(H_2O)_2]^-$ species undergoes aquation more rapidly than the *cis*-$[RhCl_4(H_2O)_2]^-$. In order to confirm the *mer*-$[RhCl_3(H_2O)_3]$ and *trans*-$[RhCl_4(H_2O)_2]^-$ peak assignments we measured the rate of aquation of the *cis*- and *trans*-$[RhCl_4(H_2O)_2]^-$ species. For these kinetic experiments, the Rh(III) stock solution equilibrated in a 0.995 mol L^{-1} HCl matrix for 2.8 years was diluted to a 0.101 mol L^{-1} HCl matrix, followed by injection of the diluted sample as a function of time. The results for one of these experiments are shown in Fig. 8a and b, from which it is observed that the peak at 550 s (*cis*-$[RhCl_4(H_2O)_2]^-$) initially increase due to the aquation of $[RhCl_5(H_2O)]^{2-}$ (first 150 min) after which the peaks at 400 and 550 s both decrease in intensity with time due to aquation of the *trans*- and *cis*-$[RhCl_4(H_2O)_2]^-$ species, respectively. The *cis*- and *trans*-$[RhCl_4(H_2O)_2]^-$ aquation products are the *fac*- and *mer*-$[RhCl_3(H_2O)_3]$ species respectively and it is observed (Fig. 8a) that only the peak at 180 s increase in intensity as a function of time, consistent with the assignment that the *fac*- and *mer*-

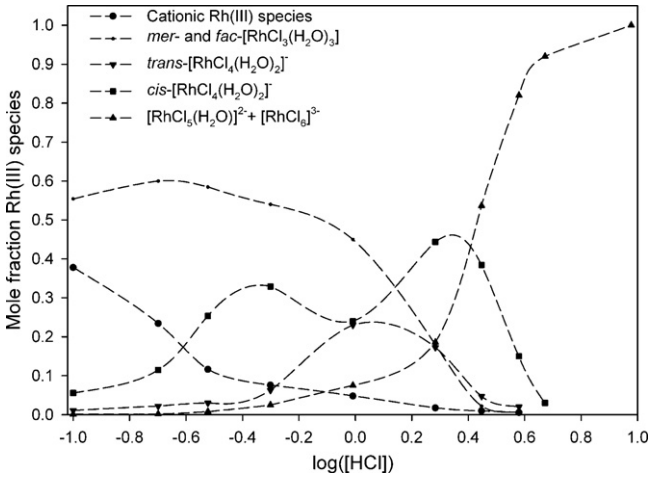

Fig. 9. $[RhCl_n(H_2O)_{6-n}]^{3-n}$ species distribution diagram as a function of HCl concentration. The total Rh(III) concentration for each sample was 1.283 mmol L^{-1}. The RSD for species abundance is below 5%.

$[RhCl_3(H_2O)_3]$ species elute as a single band at 180 s. Moreover, up to approximately 5000 min after dilution anation of *mer*- and *fac*-$[RhCl_3(H_2O)_3]$ is negligible and therefore plots of ln([*cis*- or *trans*-$[RhCl_4(H_2O)_2]^-$]) versus time, Eq. (11), were done and is illustrated in Fig. 8c. The good linear least-squares regression fits, Fig. 8c, confirmed pseudo-first-order aquation reactions and the calculated *cis* and *trans* k_{43} aquation rate constants are listed in Table 2. After 5450 min, anation of *mer*- and *fac*-$[RhCl_3(H_2O)_3]$ species must be taken into account and it was therefore necessary to do a non-linear least-squares fit with the rate model given by Eqs. (8), (10) and (12), as shown in Fig. 8d. The aquation rate constants calculated with the linear and non-linear least-squares fits, Table 2, agree quantitatively. Furthermore, the aquation rate constant for the *cis*-$[RhCl_4(H_2O)_2]^-$ complex agrees quantitatively with that determined previously using UV–VIS, Fig. S2, and chromatographically, Fig. 5, shown in Table 2. In addition, due to the *trans*-$[RhCl_4(H_2O)_2]^-$ species having two sites for chloride exchange compared to the one chloride site for the *cis*-$[RhCl_4(H_2O)_2]^-$ species, aquation of the *trans* stereoisomer is slightly faster than the *cis* stereoisomer.

$$\frac{d(F)}{dt} = -k_{43}(F) + k_{34}(H)(Cl^-) \quad (12)$$

F = *trans*-$[RhCl_4(H_2O)_2]^-$ and H = *mer*-$[RhCl_3(H_2O)_3]$.

A partial Rh(III) species distribution diagram as a function of HCl concentration, Fig. 9, was constructed by integrating the respective peaks in Fig. 7a and b. Due to the relatively fast aquation of $[RhCl_6]^{3-}$ only the combined amount of $[RhCl_n(H_2O)_{6-n}]^{3-n}$ (n = 5, 6) can be determined. Moreover, aquation of the $[RhCl_n(H_2O)_{6-n}]^{3-n}$ (n = 0–5) species is slow enough such that the speciation of the Rh(III) system do not change in the time taken to dilute and inject the stock samples. In addition, the chloride concentration in the diluted sample and in the mobile phase is always lower or equal to the Rh(III) stock samples and anation of Rh(III) species is therefore of no concern and will not change the species amounts during the dilution step or chromatographic run. Comparing our proposed speciation diagram with those shown in the review by Benguerel et al. [3] several differences are observed. Firstly, highly aquated $[RhCl_n(H_2O)_{6-n}]^{3-n}$ (n = 0–4) complexes persist in appreciable amounts up to 3.0 mol L^{-1} HCl. From a solvent- or solid phase extraction perspective [2,3] the most important difference occurs at 1.0 mol L^{-1} HCl where it was found that the $[RhCl_5(H_2O)]^{2-}$ species is only in 8–10% abundance which is in stark contrast to the data of Cozzi and Pantani [37] and Benguerel et al. [3] that claim 70 and 80% abundance, respectively. This large discrepancy was easily resolved with the following kinetic experiments. When Rh(III) equilibrated in 9.464 mol L^{-1} HCl was diluted to a 1.0 mol L^{-1} HCl matrix the UV–VIS spectral change as a function of time, Fig. S4a, clearly indicate that $[RhCl_5(H_2O)]^{2-}$ undergo significant aquation. From the kinetic model fit it is calculated, Fig. S4b, that only 44% of $[RhCl_5(H_2O)]^{2-}$ species remains after 90 min and it can be seen from Fig. S4b that significant aquation will continue to occur with time. Confirmation of these results were obtained by diluting Rh(III) equilibrated in 9.464 mol L^{-1} HCl to HCl matrices which varied from 0.1 to 6.5 mol L^{-1}, Fig. S5. The kinetic analyses performed on the data set shown in Fig. S5 clearly indicate that even in a 2.8 mol L^{-1} HCl matrix significant aquation of $[RhCl_5(H_2O)]^{2-}$ occurs. Interestingly only above a HCl concentration of 6 mol L^{-1}, no UV–VIS spectral change is observed as a function of time. This suggests that the $[RhCl_6]^{3-}$ species is in 95% or higher abundance when present in 6.0 mol L^{-1} HCl. These experiments confirm our chromatographic speciation data, Fig. 9, and also explains several anomalous Rh(III) extraction results found by Schmuckler and co-worker [1,36]. Moreover, the kinetic-based speciation diagram proposed by Benguerel et al. [3] only take into account $[RhCl_n(H_2O)_{6-n}]^{3-n}$ (n = 4–6) species thereby neglecting further aquation and stereoisomers. It should also be noted that our proposed species distribution diagram is as a function of HCl concentration and no attempt was made to keep ionic strength constant as done in literature [3,17,37], to better reflect actual industrial process solution conditions. Metal ions such as copper and strontium are not present in the samples prepared in this study and hence possible polyatomic interferences caused by $^{40}Ar^{63}Cu^+$ and $^{86}Sr^{16}OH^+$ are absent. The Rh(III) samples prepared in this study reflect what can be expected in the mining industry, since "all" base and platinum group metals are 'removed' prior to Rh recovery [2]. Moreover, the HPLC separation step can minimize polyatomic interference since each possible interfering species will presumably have a different retention time compared to the Rh(III) species and hence minimize possible peak overlap. In addition, metal ions present in group 1 and 2, such as ^{86}Sr in particular, will not form negatively charged chlorido complexes and will elute as an un-retained peak with no peak overlap with $[RhCl_n(H_2O)_{6-n}]^{3-n}$ (n = 3–6) species.

In addition to the Rh(III) species reported in several CE [9–11] studies, it was possible with the ion-pair HPLC technique to obtain a baseline separation of the $[RhCl_4(H_2O)_2]^-$ stereoisomers and assign them as well. In effect, more information regarding the speciation of Rh(III) aqua chlorido-complexes present in an HCl matrix, Fig. 9, was gained using the ion-pair HPLC technique compared to CE studies. Lastly, the ion-pair HPLC method has considerable scope for improvement by decreasing the column material particle size from 50 μm currently used to 5 μm or smaller and of course selecting different types of ion-pair reagents.

5. Conclusions

We developed an ion-pair (TBACl) reversed phase (C_{18}) HPLC–ICP-MS speciation method for Rh(III) aqua chlorido-complexes present in an HCl matrix. Under optimum chromatographic conditions it was possible, to separate and quantify cationic Rh(III) species (eluted as one band), $[RhCl_3(H_2O)_3]$, *cis*-$[RhCl_4(H_2O)_2]^-$, *trans*-$[RhCl_4(H_2O)_2]^-$ and $[RhCl_n(H_2O)_{6-n}]^{3-n}$ (n = 5, 6). The $[RhCl_n(H_2O)_{6-n}]^{3-n}$ (n = 5, 6) complex anions eluted as one band due to the relatively fast aquation of $[RhCl_6]^{3-}$ ($t_{1/2}$ = 1.3 min) in a low ionic strength (0.1 mol kg^{-1}) chloride matrix. It was found that the $t_{1/2}$ for $[RhCl_6]^{3-}$ aquation decreased significantly from 6.5 to 1.3 min when decreasing the ionic strength from 4.0 to 0.1 mol kg^{-1} $HClO_4$. In this context ionic strength or the activity of water is a key parameter that determines whether $[RhCl_n(H_2O)_{6-n}]^{3-n}$ (n = 5, 6) complex anions can be chromatographically separated. An advantage of the developed ion-pair HPLC

speciation method compared to previous CE speciation studies [9–11] is that it is possible to separate, quantify and identify the *cis*- and *trans*-$[RhCl_4(H_2O)_2]^-$ stereoisomers.

The Rh(III) samples that was equilibrated in differing HCl concentrations for 2.8 years at 298 K was analyzed with the ion-pair HPLC method. This analysis yielded a partial Rh(III) aqua chlorido-complex species distribution diagram as a function of HCl concentration. This diagram for the first time show the distribution of the *cis*- and *trans*-$[RhCl_4(H_2O)_2]^-$ stereoisomers. Furthermore, it was found that relatively large amounts of 'highly' aquated $[RhCl_n(H_2O)_{6-n}]^{3-n}$ (n = 0–4) species persist in up to 3.0 mol L^{-1} HCl and in 1.0 mol L^{-1} HCl the abundance of the $[RhCl_5(H_2O)]^{2-}$ species is only 8–10% far from the 70–80% proposed previously [3]. Interestingly a 95% abundance of the $[RhCl_6]^{3-}$ complex anion occurs only when the HCl concentration is above 6 mol L^{-1}. Work on extending the analysis of Rh(III) aqua halido-complexes speciation and to the other PGM are currently under way.

Acknowledgements

We gratefully acknowledge the financial support by Anglo-platinum Ltd., Nelson Mandela Metropolitan and Stellenbosch Universities.

Appendix A. Supplementary data

Supplementary data associated with this article can be found, in the online version, at doi:10.1016/j.talanta.2010.04.049.

References

[1] G. Schmukler, B. Limoni-Relis, Sep. Sci. Technol. 30 (3) (1995) 337.
[2] F.L. Bernardis, R.A. Grant, D.C. Sherrington, React. Funct. Polym. 65 (2005) 205.
[3] E. Benguerel, G.P. Demopoulos, G.B. Harris, Hydrometallurgy 40 (1996) 135.
[4] M.C. Read, J. Glaser, M. Sandström, J. Chem. Soc., Dalton Trans. 2 (1992) 233.
[5] C. Carr, J. Glaser, M. Sandström, Inorg. Chim. Acta 131 (1987) 153.
[6] B.E. Mann, C.M. Spencer, Inorg. Chim. Acta 76 (1983) L65.
[7] J.M. Ernsting, S. Gaemers, C.J. Elsevier, Magn. Reson. Chem. 42 (2004) 721.
[8] S.S. Aleksenko, A.P. Gumenyuk, S.P. Mushtakova, L.F. Kozhina, A.R. Timerbaev, Talanta 61 (2003) 195.
[9] S.S. Aleksenko, A.P. Gumenyuk, S.P. Mushtakova, J. Anal. Chem. 57 (2002) 215.
[10] S.S. Aleksenko, A.P. Gumenyuk, S.P. Mushtakova, A.R. Timerbaev, Fresenius J. Anal. Chem. 370 (2001) 865.
[11] J.M. Sánchez, M. Hidalgo, J. Havel, V. Salvadó, Talanta 56 (2002) 1061.
[12] D.A. Palmer, G.M. Harris, Inorg. Chem. 14 (1975) 1316.
[13] W.C. Wolsey, C.A. Reynolds, J. Kleinberg, Inorg. Chem. 2 (1963) 463.
[14] J. Kramer, K.R. Koch, Inorg. Chem. 45 (2006) 7843.
[15] J. Kramer, K.R. Koch, Inorg. Chem. 46 (2007) 7466.
[16] W.J. Gerber, P. Murray, K.R. Koch, Dalton Trans. 31 (2008) 4113.
[17] W. Robb, G.M. Harris, J. Am. Chem. Soc. 87 (1965) 4472.
[18] W. Robb, M.M. de V. Steyn, Inorg. Chem. 6 (1966 or 1967) 616.
[19] W. Robb, M.M. de, V. Steyn, H. Kruger, Inorg. Chim. Acta 3 (1969) 383.
[20] S.F. Chan, G.M. Harris, Inorg. Chem. 18 (1979) 717.
[21] R.J. Buchacek, G.M. Harris, Inorg. Chem. 15 (1976) 926.
[22] M.J. Pavelich, G.M. Harris, Inorg. Chem. 12 (1973) 423.
[23] K. Swaminathan, G.M. Harris, J. Am. Chem. Soc. 88 (1966) 4411.
[24] J.M. Sánchez, V. Salvadó, J. Havel, J. Chromatogr. A 834 (1999) 329.
[25] J.J. Kirkland, J.J. DeStefano, J. Chromatogr. A 1126 (2006) 50.
[26] R.K. Gilpin, M.E. Gangoda, A.E. Krishen, J. Chromatogr. Sci. 20 (1982) 345.
[27] R.J. Silby, R.A. Alberty, M.G. Bawendi, Physical Chemistry, 4th ed., John Wiley & Sons, Inc., New York, USA, 2005.
[28] W.J. Gerber, Ph.D. Dissertation, University of Port Elizabeth, South Africa, 2005.
[29] R.L. Burden, J.D. Faires, Numerical Analysis, 6th ed., Brooks/Cole Publishing Company, 1997.
[30] J.A. Nelder, R. Mead, Comput. J. 7 (1965) 308.
[31] J. Polster, H. Dithmar, Phys. Chem. Chem. Phys. 3 (2001) 993.
[32] J. Polster, Chem. Phys. 240 (1999) 331.
[33] T.E. Geswindt, M.Sc. Dissertation, Nelson Mandela Metropolitan University, South Africa, 2009.
[34] D.V. McCalley, Anal. Chem. 78 (2006) 2532.
[35] W. Preetz, G. Peters, D. Bublitz, Chem. Rev. 96 (1996) 977.
[36] G. Levitin, G. Schmuckler, React. Funct. Polym. 54 (2003) 149.
[37] D. Cozzi, F. Pantani, J. Inorg. Nucl. Chem. 8 (1958) 385.

Dalton Transactions

Cite this: *Dalton Trans.*, 2011, **40**, 8581

www.rsc.org/dalton

PAPER

A kinetic and thermodynamic study of the unexpected comproportionation reaction between *cis*-$[Os^{VIII}O_4(OH)_2]^{2-}$ and *trans*-$[Os^{VI}O_2(OH)_4]^{2-}$ to form a postulated $[Os^{VII}O_3(OH)_3]^{2-}$ complex anion†

Theodor E. Geswindt,[a] Wilhelmus J. Gerber,*[a] Hans E. Rohwer[b] and Klaus R. Koch[a]

Received 21st February 2011, Accepted 13th June 2011
DOI: 10.1039/c1dt10290g

A kinetic study of $[OsO_4]$ reduction by aliphatic alcohols (MeOH and EtOH) was performed in a 2.0 M NaOH matrix at 298.1 K. The rate model that best fitted the UV-VIS data supports a one-step, two electron reduction of Os^{VIII} (present as both the $[Os^{VIII}O_4(OH)]^-$ and *cis*-$[Os^{VIII}O_4(OH)_2]^{2-}$ species in a ratio of 0.34 : 0.66) to form the *trans*-$[Os^{VI}O_2(OH)_4]^{2-}$ species. The formed *trans*-$[Os^{VI}O_2(OH)_4]^{2-}$ species subsequently reacts relatively rapidly with the *cis*-$[Os^{VIII}O_4(OH)_2]^{2-}$ complex anion to form a postulated $[Os^{VII}O_3(OH)_3]^{2-}$ species according to: *cis*-$[Os^{VIII}O_4(OH)_2]^{2-}$ + *trans*-$[Os^{VI}O_2(OH)_4]^{2-}$ $\underset{k_{-2}}{\overset{k_{+2}}{\rightleftharpoons}}$ $2[Os^{VII}O_3(OH)_3]^{2-}$. The calculated forward, k_{+2}, and reverse, k_{-2}, reaction rate constants of this comproportionation reaction are 620.9 ± 14.6 M^{-1} s^{-1} and 65.7 ± 1.2 M^{-1} s^{-1} respectively. Interestingly, it was found that the postulated $[Os^{VII}O_3(OH)_3]^{2-}$ complex anion does not oxidize MeOH or EtOH. Furthermore, the reduction of Os^{VIII} with MeOH or EtOH is first order with respect to the aliphatic alcohol concentration. In order to corroborate the formation of the $[Os^{VII}O_3(OH)_3]^{2-}$ species predicted with the rate model simulations, several Os^{VIII}/Os^{VI} mole fraction and mole ratio titrations were conducted in a 2.0 M NaOH matrix at 298.1 K under equilibrium conditions. These titrations confirmed that the *cis*-$[Os^{VIII}O_4(OH)_2]^{2-}$ and *trans*-$[Os^{VI}O_2(OH)_4]^{2-}$ species react in a 1 : 1 ratio with a calculated equilibrium constant, K_{COM}, of 9.3 ± 0.4. The ratio of rate constants k_{+2} and k_{-2} agrees quantitatively with K_{COM}, satisfying the principle of detailed balance. In addition, for the first time, the molar extinction coefficient spectrum of the postulated $[Os^{VII}O_3(OH)_3]^{2-}$ complex anion is reported.

Introduction

There is extensive literature dealing with the use of $[OsO_4]$ as a homogenous catalyst for the oxidation of several organic compounds, of which the $[OsO_4]$ catalyzed Sharpless asymmetric dihydroxylation of alkenes to form vicinal diols is probably the best known example.[1,2] Remarkably, the oxidation of olefins is considerably accelerated by ligation of tertiary amines to the $[OsO_4]$ metal centre[3] to form $[OsO_4L_n]$ type complexes. Recently, Mayer *et al.*[4] demonstrated that the rate of $[OsO_4]$ reduction with molecular hydrogen significantly increases as a function of aqueous solution pH. This was attributed to co-ordination expansion of $[OsO_4]$ to form the $[Os^{VIII}O_4(OH)]^-$ and *cis*-$[Os^{VIII}O_4(OH)_2]^{2-}$ complex anions at relatively high hydroxide concentration. Moreover, experimental results[5a–e] as well as density functional theory calculations[2,4,5a,b,6] favour a concerted [3 + 2] addition of 'organic' substrate across two oxo groups of Os^{VIII}, Scheme 1, as an integral part of the mechanism of Os^{VIII} catalysis, in contrast to a [2 + 2] or an oxidative addition reaction.[2,5a,b,e7]

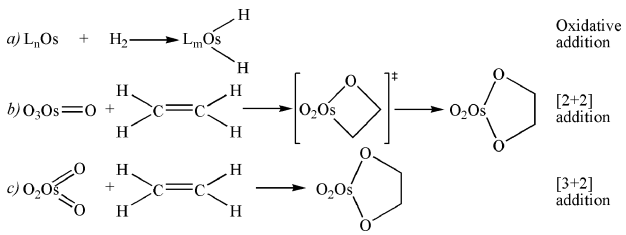

Scheme 1 Cartoon representation of possible substrate oxidation pathways.

The reduction of $[OsO_4]$ in aqueous basic media by the addition of ethanol is routinely performed in the mining industry after the separation of $[OsO_4]$ from solutions containing platinum group metals (PGMs) by means of oxidative distillation.[8–10] Reported kinetic investigations in the past four decades[4,11–21] pertaining to the reduction of $[OsO_4]$ with molecular hydrogen, alcohols, diols

[a]*Research Group of PGM Chemistry, Dept of Chemistry and Polymer Science, Stellenbosch University, Private Bag X1, Stellenbosch 7602, Western Cape, South Africa. E-mail: wgerber@sun.ac.za; Fax: +2721 808 3342; Tel: +2721 808 2699*
[b]*Dept of Chemistry, Nelson Mandela Metropolitan University, PO Box 77000, Port Elizabeth, 6031, South Africa*

† Electronic supplementary information (ESI) available: Supplementary UV-VIS spectra, kinetic traces and derivations. See DOI: 10.1039/c1dt10290g

and α-hydroxy acids in aqueous basic media are in agreement that Os^{VIII} is reduced to the *trans*-$[Os^{VI}O_2(OH)_4]^{2-}$ complex anion in a single, two-electron transfer step. Furthermore, the reduction of Os^{VIII} with the mentioned reducing agents is reported[4,11–21] to be first order with respect to the reducing agent and the total Os^{VIII} concentration in a relatively low hydroxide concentration matrix. However, EPR (electron paramagnetic resonance)[22,23] and polarographic[24] data obtained in the late 1960's, in a relatively high hydroxide concentration matrix, support the formation of an uncharacterized Os^{VII} species during the reduction of $[OsO_4]$ in basic media, which contradicts the observations reported by 4,11–21.

If an Os^{VII} species is present in appreciable amounts during the reduction of $[OsO_4]$ it might have possible ramifications for the PGM refining process and also for the mechanistic interpretation of Os^{VIII} catalytic reactions or alternatively "poisoning" of a catalytically 'active' Os^{VIII} species. As part of our interest in examining the chemistry of PGM in well defined industrial solutions,[25,26] we report here a detailed kinetic study concerning the reduction of Os^{VIII} by aliphatic alcohols in basic media.‡ The aim of this study is to establish whether Os^{VII} species exist in appreciable amounts in basic media and to measure the kinetic and thermodynamic parameters that define the formation of such a species. In this context we also present chemical equilibrium modelling of Os^{VIII}/Os^{VI} mole fraction and mole ratio titrations in order to support the results of our Os^{VIII} reduction kinetic investigation.

Experimental

Materials

Batches of high purity potassium osmate crystals, $K_2[Os^{VI}O_2(OH)_4]$, were obtained from Anglo Platinum Ltd (South Africa). Thiourea and sodium hydroxide salts (SMM Instruments) were of analytical grade. Analytical grade orthophosphoric acid (H_3PO_4), hydrogen peroxide (H_2O_2) and carbon tetrachloride (CCl_4) (Merck Chemicals) were used in the preparation of osmium tetroxide $[OsO_4]$ stock solutions. Spectroscopic grade methanol and ethanol (Merck Chemicals) were used in the kinetic investigations. Potassium hydrogen phthalate was used for the standardization of all NaOH stock solutions. All aqueous solutions were prepared and diluted to a desired concentration using MilliQ water with a resistivity of 18.2 MΩ cm.

Instrumentation

UV-VIS spectra were recorded with a Perkin-Elmer Lambda 12 double beam spectrophotometer using a slit width setting of 1 nm. Quartz cuvettes with a 1.0 cm path length were used. The room temperature was regulated at 298.0 ± 1.0 K. A Grant KD100 circulating thermostatic controller, mounted on a Grant W6 tank with cooling coil was used to regulate the temperature during sample preparation and within the sample chamber of the spectrophotometer at 298.1 ± 0.1 K. Mole ratio titrations were performed using a Metrohm 716 DMS titroprocessor, connected to a Metrohm 662 photometer. The photometer light path was 1.0 cm.

Preparation of Os^{VIII} and Os^{VI} stock solutions

$[OsO_4]$ solutions were prepared by oxidative distillation of the pure $K_2[Os^{VI}O_2(OH)_4]$ salt using 10% (v/v) H_2O_2 in an aqueous 45% (v/v) H_3PO_4 matrix. The evolved $[OsO_4]$ vapour was trapped in CCl_4. The UV-VIS spectrum of the $[OsO_4]$ in CCl_4 was identical to that reported in literature,[29a,b] supplementary information Figure S1,† and confirmed that only $[OsO_4]$ is present in the CCl_4. Aqueous $[OsO_4]$ solutions were prepared by extraction of $[OsO_4]$ from the CCl_4 stock solution into MilliQ water. Stock *trans*-$[Os^{VI}O_2(OH)_4]^{2-}$ solutions were prepared by dissolving the pure $K_2[Os^{VI}O_2(OH)_4]$ salt in a standardised 2.0 M NaOH matrix under inert Ar(g) conditions. In all cases the total Os concentration was determined by the thiourea colorimetric method.[30]

Os^{VIII} reduction kinetic experiments

The rate of Os^{VIII} reduction was investigated as a function of aliphatic alcohol (methanol, ethanol) concentration in a 2.0 M NaOH aqueous matrix. In these experiments the reactants were mixed thoroughly in a thermostatic reaction vessel maintained at 298.1 K under inert Ar(g) conditions and the final reaction mixture volume was 25.0 mL in a 2.0 M NaOH matrix. Prior to each kinetic reaction, a reaction "blank" was obtained, where the Os^{VIII} spectrum in a 2.0 M NaOH matrix was recorded in the absence of aliphatic alcohol. This was required in order to obtain the initial UV-VIS Os^{VIII} spectrum at time equals zero. No more than 30 s elapsed from initiating the reaction to the first spectral recording being made.

Os^{VIII}/Os^{VI} mole fraction and mole ratio titrations

Os^{VIII}/Os^{VI} mole fraction experiments were conducted by preparing a series of solutions in which the total Os concentration was kept constant, while the mole fraction $([Os^{VI}]/([Os^{VIII}]+[Os^{VI}]))$ was varied. Constant reaction volume, 25.0 mL, and hydroxide concentration, 2.0 M NaOH, were maintained for each solution in the series under inert Ar(g) conditions at 298.1 K. Each solution was allowed to equilibrate for approximately 60 s prior to recording UV-VIS spectra. The Os^{VIII}/Os^{VI} mole fraction experiment was done using several total Os concentrations up to 7.003×10^{-4} M.

The mole ratio titrations were performed by titrating an Os^{VIII} solution, prepared in a standardized 2.0 M NaOH matrix, against a *trans*-$[Os^{VI}O_2(OH)_4]^{2-}$ solution also prepared in 2.0 M NaOH. These titrations were performed under inert Ar(g) conditions at 298.1 K and were done using several total Os^{VI} and Os^{VIII} concentrations. The reaction solution was continuously agitated, but not vigorously, so as to prevent splashes and the formation of air bubbles in the light path of the photometer probe. Following each addition of potassium osmate dispensed from the titroprocessor, the reaction solution was allowed to equilibrate for 60 s, after which its absorbance at 400 nm was recorded.

‡ Note: Os^{VIII} in our study refers specifically to a combination of the $[Os^{VIII}O_4(OH)]^-$ and *cis*-$[Os^{VIII}O_4(OH)_2]^{2-}$ complex anions that are simultaneously present in a 2.0 M NaOH matrix.

Computational details

The program Mol$_1$Frak is a set of routines developed in-house using Matlab 7.0.1 in order to calculate equilibrium constants and species molar extinction coefficients. This was done by means of simulating a reaction model and performing non-linear least-squares fits to mole fraction and mole ratio UV-VIS spectroscopic data. The general workflow of program Mol$_1$Frak is similar to that described by Meloun *et al.*[31] The Newton–Raphson method for a non-linear system of equations[32] is used to calculate the free concentration of the relevant chemical species and for the minimization of the respective non-linear least-squares objective functions.

The program Kinetic$_5$Ver was developed in-house in the Visual Basic 6 environment in order to calculate reaction rate constants and species molar extinction coefficients. This was done by means of simulating reaction rate law(s) and performing non-linear least squares fits to UV-VIS spectroscopic data.[25] The Runga–Kutta algorithm was used to solve the set of differential equations while the Simplex algorithm[33] was used for the minimization of the respective non-linear least-squares objective functions.

Results and discussion

Several studies[4,34,35] have reported the relatively slow, spontaneous reduction of $[OsO_4]$ in an aqueous alkaline matrix to form the osmate, *trans*-$[Os^{VI}O_2(OH)_4]^{2-}$, complex anion. To obtain an indication of the actual time-frame of Os^{VIII} reduction in an aqueous alkaline matrix, $[OsO_4]$ was extracted from CCl_4 into water. After separation of the two phases, a NaOH solution was added to the aqueous $[OsO_4]$ aliquot such that the final NaOH concentration was 2.0 M. The UV-VIS spectrum of this aqueous solution was subsequently monitored over a period of six days at 298.1 K, Fig. 1.

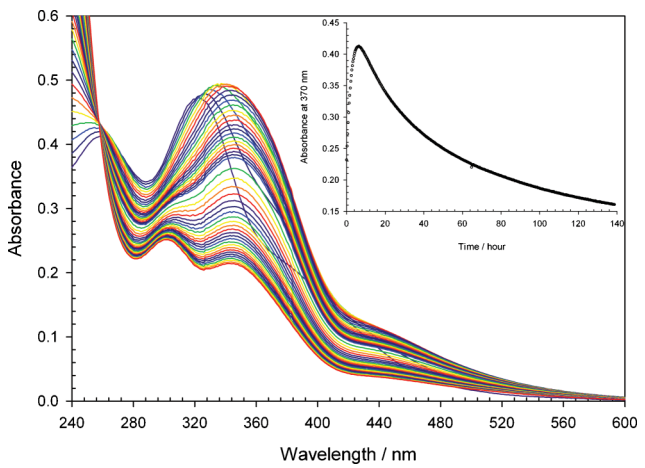

Fig. 1 Change in the Os^{VIII} UV-VIS spectrum as a function of time in a 2.0 M NaOH matrix. The insert figure illustrates the absorbance maximum at 370 nm after 6.39 h. $[Os]_T = 1.772 \times 10^{-4}$ M.

It is apparent from Fig. 1 that even after six days not all of the Os^{VIII} was reduced to the *trans*-$[Os^{VI}O_2(OH)_4]^{2-}$ species (*vide infra*). However, it is interesting to note that in the wavelength region of 305 to 480 nm, Fig. 1, the absorbance initially increases until a maximum is reached and subsequently decreases as a function of time. Considering that the 'osmium complexes' are the only species that absorb light in this wavelength region the observed absorbance maximum, Fig. 1, suggests two possible scenarios (i) relatively slow interconversion between $[Os^{VIII}O_4(OH)]^-$ and *cis*-$[Os^{VIII}O_4(OH)_2]^{2-}$ species during the reduction of Os^{VIII} to Os^{VI} or (ii) that at least one high oxidation state osmium species that has not been characterized before, is present during the reduction of Os^{VIII}.

In order to substantiate that a hitherto unknown Os complex is formed during the reduction of Os^{VIII} to Os^{VI}, it must first be established that the speciation of Os^{VIII} and Os^{VI} in a 2.0 M NaOH matrix is not responsible for the observed absorbance maximum, Fig. 1. Numerous studies[4,21] have shown that the reduction of Os^{VIII} results in the formation of only the *trans*-$[Os^{VI}O_2(OH)_4]^{2-}$ complex anion. Moreover, it is well documented[4,34] that $[OsO_4]$, in alkaline media, reacts with hydroxide to only form the $[Os^{VIII}O_4(OH)]^-$ and *cis*-$[Os^{VIII}O_4(OH)_2]^{2-}$ species, depicted by reactions 1 and 2. These reactions occur rapidly as is evident from the immediate solution colour change from colourless to bright yellow when hydroxide is added to $[OsO_4]$. Moreover, after the time, approximately 30 s, between adding hydroxide to $[OsO_4]$ and making the first UV-VIS spectral recording no change in absorbance occurs.

$$[Os^{VIII}O_4] + OH^- \underset{}{\overset{K_1}{\rightleftharpoons}} [Os^{VIII}O_4(OH)]^- \quad (1)$$

$$[Os^{VIII}O_4(OH)]^- + OH^- \overset{K_2}{\rightleftharpoons} cis\text{-}[Os^{VIII}O_4(OH)_2]^{2-} \quad (2)$$

As the Os^{VIII} speciation studies in alkaline media[4,34] are in good agreement over a relatively wide range of solution ionic strengths, we took the average of the reported stepwise equilibrium constants for reactions 1 and 2 ($K_1 = 135 \pm 11$, $K_2 = 0.93 \pm 0.07$) in order to calculate the Os^{VIII} species distribution diagram as a function of hydroxide concentration, Fig. 2. At a hydroxide concentration of 2.0 M the ratio of the $[Os^{VIII}O_4(OH)]^-$: *cis*-$[Os^{VIII}O_4(OH)_2]^{2-}$ species is approximately 0.34 : 0.66 and the amount of $[OsO_4]$ present is negligible. Furthermore, since reactions 1 and 2 are relatively rapid, especially when compared to the duration over which the data in Fig. 1 was recorded, and the hydroxide concentration is in large excess (2.0 M) compared to the total Os^{VIII}

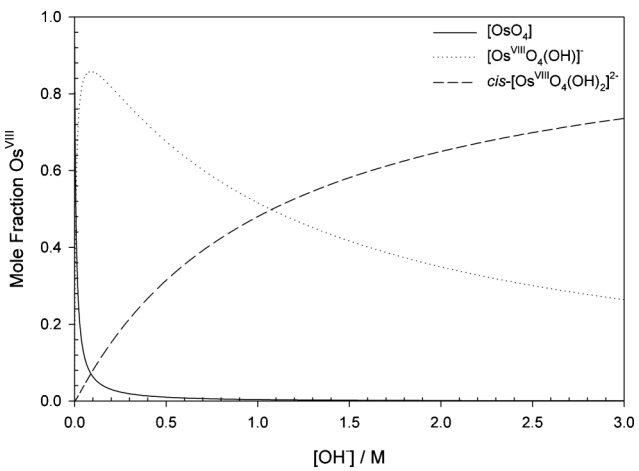

Fig. 2 Os^{VIII} species distribution diagram as a function of hydroxide concentration. Matlab 7.0.1 was used to calculate the species distribution.

concentration (1.772×10^{-4} M) used, it was assumed that during the reduction of Os^{VIII}, Fig. 1, the ratio of $[Os^{VIII}O_4(OH)]^-$ and *cis*-$[Os^{VIII}O_4(OH)_2]^{2-}$ species remains constant (*vide infra*). As the ratio of $[Os^{VIII}O_4(OH)]^-$ and *cis*-$[Os^{VIII}O_4(OH)_2]^{2-}$ species remains constant, combined with the fact that there is only one Os^{VI} species present in 2.0 M NaOH during the reduction of Os^{VIII}, Fig. 1, it was anticipated that the absorbance change at a wavelength would either only increase, decrease or remain constant as a function of time. It is therefore evident, if our assumption holds, that the speciation of Os^{VIII} and Os^{VI} in a 2.0 M NaOH matrix cannot account for the observed absorbance maximum, Fig. 1.

To investigate why an absorbance maximum occurs during the reduction of Os^{VIII} in a systematic manner, the rate of Os^{VIII} reduction was monitored as a function of organic substrate (MeOH or EtOH) concentration in a 2.0 M NaOH matrix at 298.1 K, Fig. 3a and 3b. When comparing Fig. 1 and 3 it is clear that the rate of Os^{VIII} reduction increases by orders of magnitude when MeOH or EtOH is added to the 2.0 M NaOH matrix. If the reduction of Os^{VIII} is allowed to proceed to completion, by addition of an excess amount of aliphatic alcohol, only the *trans*-$[Os^{VI}O_2(OH)_4]^{2-}$ species remains. This was confirmed by comparing the resultant UV-VIS spectrum obtained when

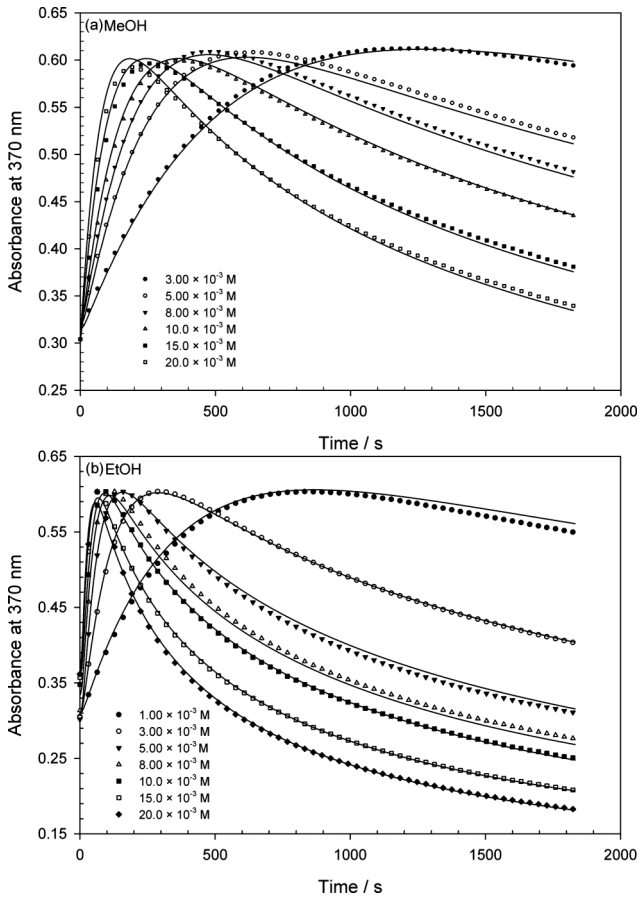

Fig. 3 Kinetic traces depicting the change in absorbance as a function of time for the reaction between Os^{VIII} and varying aliphatic alcohol concentrations at 298.1 K. (a) [Os] = 2.631×10^{-4} M; [OH^-] = 2.0 M; [MeOH] shown in the legend. (b) [Os] = 2.590×10^{-4} M; [OH^-] = 2.0 M; [EtOH] shown in the legend. Symbols = expt data; solid lines = model fits of eqn (9)–(11) using the parameters listed in Tables 1 and 2.

dissolving potassium osmate, $K_2[Os^{VI}O_2(OH)_4]$, crystals in 2.0 M NaOH and comparison with the spectra reported in literature.[4,21]

Several reaction models can be envisaged which could account for the observed kinetic traces illustrated in Fig. 3a and 3b. The first of several models considered was two consecutive one-electron reduction reactions according to; Os^{VIII} + $RCH_2OH \rightarrow Os^{VII}$ + $RCH_2OH \rightarrow Os^{VI}$. However, this model, as well as more elaborate variations failed to fit the experimental data. The simplest model that satisfactorily fitted all the data accumulated during this study is given by reactions 1–5.

$$[Os^{VIII}O_4(OH)]^- + RCH_2OH + OH^- \xrightarrow{k_x} trans\text{-}[Os^{VI}O_2(OH)_4]^{2-} + RCHO \quad (3)$$

$$cis\text{-}[Os^{VIII}O_4(OH)_2]^{2-} + RCH_2OH \xrightarrow{k_y} trans\text{-}[Os^{VI}O_2(OH)_4]^{2-} + RCHO \quad (4)$$

$$cis\text{-}[Os^{VIII}O_4(OH)_2]^{2-} + trans\text{-}[Os^{VI}O_2(OH)_4]^{2-} \underset{k_{-2}}{\overset{k_{+2}}{\rightleftharpoons}} 2\,[Os^{VII}O_3(OH)_3]^{2-} \quad (5)$$

The assumptions made in our proposed model are summarized below. As there is no evidence to the contrary, we assume that both the $[Os^{VIII}O_4(OH)]^-$ and *cis*-$[Os^{VIII}O_4(OH)_2]^{2-}$ complex anions oxidize aliphatic alcohols to produce the corresponding aldehyde and the *trans*-$[Os^{VI}O_2(OH)_4]^{2-}$ species, as depicted in reactions 3 and 4.[4,36] However, the formed aldehydes can also be further oxidized to their corresponding carboxylic acids.[11–18] We justify not taking this reaction into account two-fold; the alcohol concentration is always in relatively large excess compared to the corresponding aldehyde concentration during the kinetic run, and preliminary experimental results indicate that the observed rate for aldehyde oxidation is of the same order of magnitude as the oxidation of the corresponding alcohol.§ Furthermore, it is assumed here that only the *cis*-$[Os^{VIII}O_4(OH)_2]^{2-}$ and not the $[Os^{VIII}O_4(OH)]^-$ species reacts with the *trans*-$[Os^{VI}O_2(OH)_4]^{2-}$ complex anion, reaction 5. In support of this assumption the rate of Os^{VIII} reduction was measured as a function of hydroxide concentration (0.1–3.0 M NaOH) at 298.1 K and 1.0×10^{-2} M EtOH, Fig. 4. No attempt was made to keep the ionic strength constant for these explorative experiments. From Fig. 4 it is observed that the rate of Os^{VIII} reduction and the absorbance maximum value attained during the kinetic run increases considerably when the hydroxide concentration is varied from 0.1 to 3.0 M. If our assumption is valid that only the *cis*-$[Os^{VIII}O_4(OH)_2]^{2-}$ and not the $[Os^{VIII}O_4(OH)]^-$ species reacts with the *trans*-$[Os^{VI}O_2(OH)_4]^{2-}$ complex anion, it is expected that an increase in the hydroxide concentration would produce a corresponding increase in the amount of *cis*-$[Os^{VIII}O_4(OH)_2]^{2-}$ species, Fig. 2, which in turn leads to an increase in the extent of $[Os^{VII}O_3(OH)_3]^{2-}$ species formation, reaction 5, and consequently an increase in the absorbance maximum value. The significant increase of the absorbance maximum value correlates well with the large increase in the mole fraction of the *cis*-$[Os^{VIII}O_4(OH)_2]^{2-}$ species from 0.08 in 0.1 M NaOH to 0.73 in 3.0 M NaOH, Fig. 2, which suggests that the *cis*-$[Os^{VIII}O_4(OH)_2]^{2-}$ and not the

§ If necessary the oxidation of aldehydes can easily be incorporated in the rate model at a later stage for a better approximation

Table 1 The ratio of the absorbance maximum value at 370 nm (A_{max}) as a function of total osmium concentration

	$[Os^{VIII}]_{tot}$/M	A_{max} at 370 nm	A_{max} : $[Os^{VIII}]_{tot}$/M^{-1}
Fig. 1	1.772×10^{-4}	0.4118	2324
Fig. 3a[b]	2.631×10^{-4}	0.6118, 0.6088, 0.6088, 0.5999, 0.5964, 0.5927	2325, 2314, 2314, 2280, 2266, 2253
Fig. 3b[b]	2.590×10^{-4}	0.6007, 0.6014, 0.6014, 0.5992, 0.6001, 0.5956, 0.5889	2319, 2322, 2322, 2313, 2316, 2299, 2273
Fig. 5a [1][a]	3.485×10^{-4}	0.7814	2242
Fig. 5a[2][a]	7.003×10^{-4}	1.5957	2279

[a] Infer that the total osmium concentration was used. [b] The data is listed from the lowest to highest alcohol concentration

Table 2 Comparison of the calculated and experimental high oxidation state Os species'molar extinction coefficients at 370 nm

				Kinetic Data		
	Expt	Mole fraction	Mole ratio	MeOH	EtOH	Literature[4,21]
$\varepsilon_{trans\text{-}[Os^{VI}O_2(OH)_4]^{2-}}$/L mol^{-1} cm^{-1}	210.6 ± 6.4	203.4 ± 12.9	211.2 ± 9.4	188.4 ± 13.4	203.6 ± 16.5	231.2
$\varepsilon_{([Os^{VIII}O_4(OH)]^- + cis\text{-}([Os^{VIII}O_4(OH)^{2-}]}$/L mol^{-1} cm^{-1}	1159.7 ± 7.1	1201.3 ± 15.6	1213.7 ± 17.1	1217.8 ± 15.4	1266.1 ± 14.8	1165.6
$\varepsilon_{[Os^{VII}O_3(OH)_3]^{2-}}$ /L mol^{-1} cm^{-1}	—	5798.8 ± 56.3	5746.7 ± 61.5	5824.1 ± 57.6	5850.9 ± 49.6	—

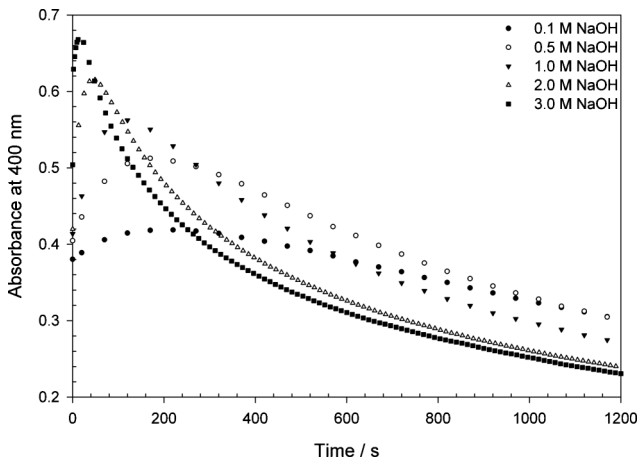

Fig. 4 Kinetic traces depicting the change in absorbance as a function of time and varying hydroxide concentration at 298.1 K. NaOH concentration is denoted in the legend. [Os] = 5.231×10^{-4} M and [EtOH] = 1.0×10^{-2} M.

$[Os^{VIII}O_4(OH)]^-$ species is involved in the comproportionation reaction.

In addition, the relatively slow reduction of Os^{VIII} in 2.0 M NaOH in the absence of aliphatic alcohol, Fig. 1, will have a negligible influence on the calculated results. Lastly, it is assumed that reactions 1 and 2 occur so rapidly compared to Os^{VIII} reduction that equilibrium is maintained at all times with respect to these two reactions. To support this assumption consider the following. If the ratio of $[Os^{VIII}O_4(OH)]^-$ and *cis*-$[Os^{VIII}O_4(OH)_2]^{2-}$ species changes during Os^{VIII} reduction to Os^{VI} then it stands to reason that when the rate of Os^{VIII} reduction to Os^{VI} increase the observed absorbance maximum value must decrease since the time that $[Os^{VIII}O_4(OH)]^-$ and *cis*-$[Os^{VIII}O_4(OH)_2]^{2-}$ species have to interconvert decreases. Now consider the data presented in Fig. 1, 3 and Table 1. The data in Fig. 1 was collected over six days whereas the data in Fig. 3 was collected in 30 min, a fraction of the time. In both cases the 'same' ratio of A_{max} : Total Os concentration, Table 1, is observed. The fact that essentially the same ratio of A_{max} : Total Os concentration is found, irrespective of the time available for $[Os^{VIII}O_4(OH)]^-$ and *cis*-$[Os^{VIII}O_4(OH)_2]^{2-}$ species interconversion, implies that the observed absorbance maximum value as a function of time is not due to slow $[Os^{VIII}O_4(OH)]^-$ and *cis*-$[Os^{VIII}O_4(OH)_2]^{2-}$ species interconversion. Moreover, it can be inferred that the ratio of $[Os^{VIII}O_4(OH)]^-$ and *cis*-$[Os^{VIII}O_4(OH)_2]^{2-}$ species remains, to a good approximation, constant during the reduction of Os^{VIII} to Os^{VI} or else the ratio of A_{max} : Total Os concentration would vary, Table 1.

The derivation of the rate model corresponding to reactions 1–5 in a 2.0 M NaOH matrix is given by eqn (6)–(11). The $[Os^{VIII}O_4(OH)]^-$ and *cis*-$[Os^{VIII}O_4(OH)_2]^{2-}$ concentrations are first expressed in terms of the total Os^{VIII} concentration in 2.0 M NaOH, eqn (6) and 7, respectively.

$$[E] = \frac{[A]}{K_2[OH^-] + 1} \quad (6)$$

$$[F] = \frac{K_2[OH^-][A]}{K_2[OH^-] + 1} \quad (7)$$

$$[A] = [Os^{VIII}]_T = [Os^{VIII}O_4(OH)^-] + [cis\text{-}Os^{VIII}O_4(OH)_2{}^{2-}] = [E] + [F]$$

$$[E] = [Os^{VIII}O_4(OH)^-]$$

$$[F] = [cis\text{-}Os^{VIII}O_4(OH)_2{}^{2-}]$$

Taking reactions 3–5 into account, the change in the total Os^{VIII} concentration as a function of time can be expressed as:

$$\frac{d[A]}{dt} = \frac{d[E]}{dt} + \frac{d[F]}{dt} = -k_x[OH^-][E][S] - k_y[F][S] - k_{+2}[F][B] + k_{-2}[C]^2 \quad (8)$$

$$[B] = [trans\text{-}Os^{VI}O_2(OH)_4{}^{2-}]$$

$$[S] = [MeOH] \text{ or } [EtOH]$$

$$[C] = [Os^{VII}O_3(OH)_3{}^{2-}]$$

Substituting eqn (6) and 7 into 8 and rearranging yields relationship 9:

$$\frac{d[A]}{dt} = -\left(\frac{k_x[OH^-] + k_y K_2[OH^-]}{K_2[OH^-]+1}\right)[A][S] - \left(\frac{k_{+2}K_2[OH^-]}{K_2[OH^-]+1}\right)[A][B] + k_{-2}[C]^2$$
$$= -k_{obs1}[A][S] - k_{obs2}[A][B] + k_{-2}[C]^2 \quad (9)$$

In a similar manner, eqn (10) and 11 can be derived.

$$\frac{d[B]}{dt} = \left(\frac{k_x[OH^-] + k_y K_2[OH^-]}{K_2[OH^-]+1}\right)[A][S] - \left(\frac{k_{+2}K_2[OH^-]}{K_2[OH^-]+1}\right)[A][B] + k_{-2}[C]^2$$
$$= k_{obs1}[A][S] - k_{obs2}[A][B] + k_{-2}[C]^2 \quad (10)$$

$$\frac{d[C]}{dt} = \left(\frac{k_{+2}K_2[OH^-]}{K_2[OH^-]+1}\right)[A][B] - k_{-2}[C]^2$$
$$= k_{obs2}[A][B] - k_{-2}[C]^2 \quad (11)$$

Using the program Kinetic$_5$Ver, the rate model eqn (9)–(11) were simulated and the non-linear least-squares fits obtained for the MeOH and EtOH data, Fig. 3a and 3b, are excellent.¶ The calculated Os species molar extinction coefficients and reaction rate constants are listed in Tables 1 and 2 respectively. The excellent non-linear least-squares fits, coupled with the quantitative agreement of the calculated comproportionation forward and reverse reaction rate constants, k_{+2} and k_{-2}, for both the MeOH and EtOH cases and the good agreement of calculated molar extinction coefficients with reported literature values validate the proposed kinetic model. The reduction rate of Os^{VIII} increases approximately five-fold with an increase in the alkyl chain length from methyl to ethyl. Moreover, the reduction of Os^{VIII} is first order with respect to aliphatic alcohol (MeOH or EtOH) concentration, Fig. S3.† The good fits and agreement between the calculated Os^{VII} species molar extinction coefficients for both the MeOH and EtOH cases coupled with the fact that an absorbance maximum occurs, Fig. 1, in the absence of aliphatic alcohols implies that an Os–alcohol adduct is not responsible for the observed absorbance maximum, Fig. 1 and 3, during the reduction of Os^{VIII}. Interestingly, from the simulations performed it can be deduced that the postulated $[Os^{VII}O_3(OH)_3]^{2-}$ complex anion does not react with MeOH or EtOH. Furthermore, the comproportionation reaction 5 severely impedes the rate of the overall conversion of $[Os^{VIII}O_4(OH)]^-$ and *cis*-$[Os^{VIII}O_4(OH)_2]^{2-}$ to *trans*-$[Os^{VI}O_2(OH)_4]^{2-}$ by lowering the Os^{VIII} concentration. In this context care should be taken when interpreting previous kinetic study results, in particular the free hydroxide concentration under which experiments were performed,[4,11–21] regarding Os^{VIII} reduction in basic media.

The analysis of Os^{VIII} reduction rates led to the inference that *cis*-$[Os^{VIII}O_4(OH)_2]^{2-}$ reacts with *trans*-$[Os^{VI}O_2(OH)_4]^{2-}$ to yield the $[Os^{VII}O_3(OH)_3]^{2-}$ complex anion, reaction 5. To corroborate that this comproportionation reaction occurs, Os^{VI}/Os^{VIII} mole fraction (Job's method of continuous variation) and mole ratio titrations, were performed, Fig. 5a and 5b, in a 2.0 M NaOH matrix at 298.1 K under equilibrium conditions. The relatively slow reduction of Os^{VIII} in a 2.0 M NaOH matrix made these experiments viable with freshly prepared osmium and NaOH solutions. The Job diagrams, Fig. 5a, are not simply an addition of the respective *trans*-$[Os^{VI}O_2(OH)_4]^{2-}$ and Os^{VIII} species' absorbance (Fig. S2†) and therefore imply that a reaction is occurring. The intersection of the least-square fits to the "linear" regions of the Job curves occur at mole fractions of 0.54 and 0.53, Fig. 5a. This is indicative of a 1 : 1 reaction between the *trans*-$[Os^{VI}O_2(OH)_4]^{2-}$ and *cis*-$[Os^{VIII}O_4(OH)_2]^{2-}$ species. The formation of a 2 : 2 complex was negated based on the fact that the "sides" of the Job plot would be concave.[37] Furthermore, the intersection of the least-square fits to the "linear" regions of the mole ratio titration curves is 1.05 (± 0.04), Fig. 5b, and corroborate the conclusions drawn from the Job diagrams.

In order to calculate the equilibrium constant for reaction 5 and Os species molar extinction coefficients, the program Mol$_1$Frak was used to simulate reactions 1, 2 and 5 and perform non-linear least-squares fits. The non-linear least squares fits obtained for both the Job plots and mole ratio titration curves, Fig. 5a and 5b, are excellent. The calculated Os^{VIII}, Os^{VII} and Os^{VI} molar extinction coefficients and the equilibrium constant, K_{COM}, are listed in Tables 1 and 2, respectively. The calculated osmium species distribution corresponding to the mole fraction data is shown in Fig. 5c. The osmium species' molar extinction coefficients, Table 2, calculated from the kinetic and equilibrium investigations together with the values reported in literature agree quantitatively. Moreover, it was possible to calculate, for the first time, the molar extinction coefficient spectrum of the postulated $[Os^{VII}O_3(OH)_3]^{2-}$ complex anion, Fig. 6. Note, the molar extinction coefficient spectrum of the $[Os^{VIII}O_4(OH)]^-$ and *cis*-$[Os^{VIII}O_4(OH)_2]^{2-}$ species is represented as a composite spectrum in Fig. 6; since, by maintaining the $[OH^-]$ at 2.0 M, the ratio of $[Os^{VIII}O_4(OH)]^-$ and *cis*-$[Os^{VIII}O_4(OH)_2]^{2-}$ species (0.34 : 0.66) remains constant.

The quantitative agreement of the calculated comproportionation reaction equilibrium constant, K_{COM}, listed in Table 3 and Os species molar extinction coefficients, Table 2, together with the excellent model fits of the mole fraction and mole ratio data, Fig. 5a and 5b, substantiate the proposed comproportionation reaction between the *trans*-$[Os^{VI}O_2(OH)_4]^{2-}$ and *cis*-$[Os^{VIII}O_4(OH)_2]^{2-}$ complex anions. From the mole fraction data (Fig. 5a), where kinetics are of no concern, we would like to emphasize the following point: Since the separate solutions of Os^{VI} and Os^{VIII} both have a 2.0 M NaOH matrix there is no thermodynamic reason that the ratio of $[Os^{VIII}O_4(OH)]^-$ and *cis*-$[Os^{VIII}O_4(OH)_2]^{2-}$ species will change when mixing the two solutions, hence the absorbance maximum observed at a mole fraction of 0.5, Table 1, is not due to a change in the $[Os^{VIII}O_4(OH)]^-$ and *cis*-$[Os^{VIII}O_4(OH)_2]^{2-}$ species ratio but rather due to a reaction between Os^{VIII} and Os^{VI} as the mole fraction and mole ratio data unmistakably illustrate. Furthermore, the A_{max} : Total Os concentration ratio, Table 1, is the same as that found for the data in Fig. 1 and 3 excluding the possibility for an Os–alcohol adduct. The ratio of the forward, k_{+2}, and reverse, k_{-2}, rate constants (reaction 5) obtained from the kinetic simulations agrees quantitatively with K_{COM}, Table 3, and satisfies the principle of detailed balance. The remarkable agreement between the diverse methods to calculate the comproportionation reaction equilibrium constant, K_{COM}, and molar extinction coefficients of the various

¶ Interestingly, when considering the possible permutations of the comproportionation reaction 5, all yield a mathematical equivalent rate law (compare equations 9, 10 and 11 with equations shown in the supplementary information†); apart from the fact that the composite rate constants (k_{obs}) would naturally differ.

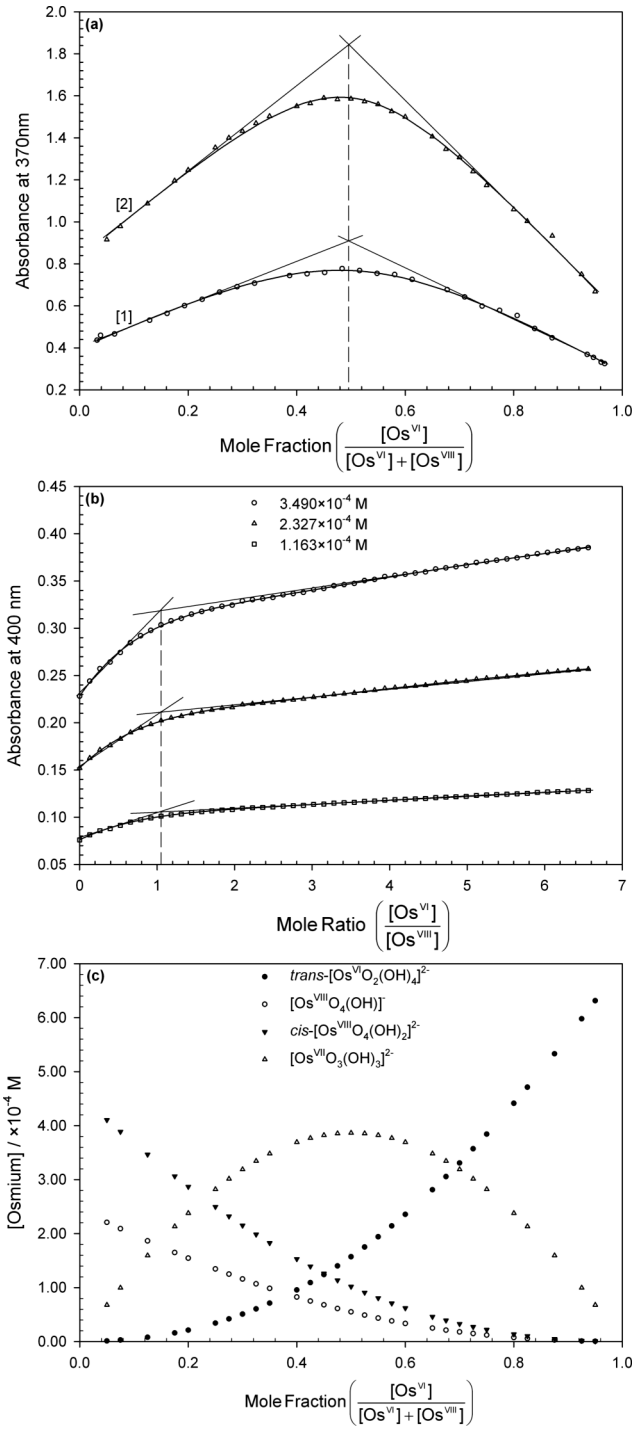

Fig. 5 (a) Job diagrams and (b) mole ratio titrations between Os^{VIII} and Os^{VI} in a 2.0 M NaOH at 298.1 K. (a):,1 $[Os^{VI}] + [Os^{VIII}] = 3.485 \times 10^{-4}$ M;,2 7.003×10^{-4} M; (b) The initial Os^{VIII} concentrations are denoted in the legend. Symbols = expt data, solid lines = model fit of reactions 1, 2 and 5. (c) Calculated Os species distribution for the mole fraction experiment at a total $[Os] = 7.003 \times 10^{-4}$ M.

Os species indicate that the proposed equilibrium and kinetic model are internally consistent. From Fig. 5c it is evident that the proposed $[Os^{VII}O_3(OH)_3]^{2-}$ species is present in relatively high concentration. However, it could not be determined whether the $[Os^{VII}O_3(OH)_3]^{2-}$ complex is the *fac* or *mer* stereoisomer or rule out

Table 3 Calculated rate and equilibrium constants for reactions 3–5

	Kinetic data			
	MeOH	EtOH	Mole ratio	Job's method
$k_{obs1}/M^{-1}\ s^{-1}$	0.29 ± 0.02	1.36 ± 0.09	—	—
$k_{+2}/M^{-1}\ s^{-1}$	621.2 ± 14.6	620.8 ± 11.8	—	—
$k_{-2}/M^{-1}\ s^{-1}$	65.8 ± 1.2	65.7 ± 0.98	—	—
K_{COM}	9.44 ± 0.4	9.45 ± 0.3	9.25 ± 0.3	9.18 ± 0.2

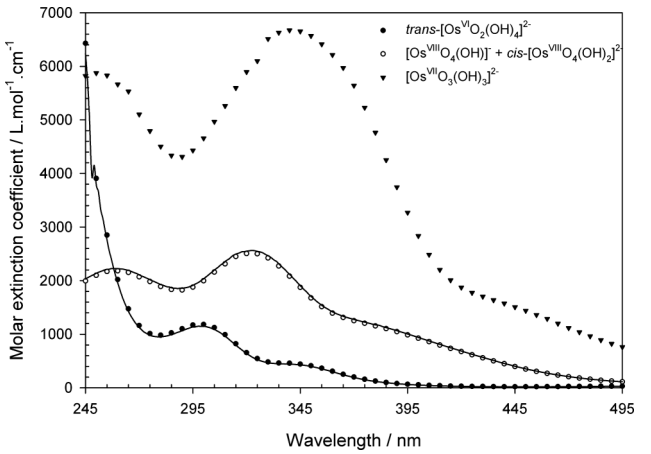

Fig. 6 Symbols = calculated molar extinction spectra for ($[Os^{VIII}O_4(OH)]^-$ + *cis*-$[Os^{VIII}O_4(OH)_2]^{2-}$), *trans*-$[Os^{VI}O_2(OH)_4]^{2-}$ and $[Os^{VII}O_3(OH)_3]^{2-}$. Solid lines = experimental molar extinction spectra.

the possibility that both stereoisomers are present. Unfortunately, numerous attempts to obtain suitable crystals for single crystal X-ray diffraction failed to date, thus direct structural support for the $[Os^{VII}O_3(OH)_3]^{2-}$ complex anion is lacking at present.

Lastly, preliminary EPR (at 298 K) and ^{189}Os NMR (at 292 K and 14.1 T) measurements yielded no further evidence for the $[Os^{VII}O_3(OH)_3]^{2-}$ complex anion. In both cases it is thought that fast relaxation (electronic and nuclear respectively) could be responsible for the lack of observed resonance signals.

Conclusion

In conclusion, the Os^{VIII} and Os^{VI} mole fraction and mole ratio titration data are only consistent with a comproportionation reaction between the *cis*-$[Os^{VIII}O_4(OH)_2]^{2-}$ and *trans*-$[Os^{VI}O_2(OH)_4]^{2-}$ species in a 1 : 1 ratio to form a postulated $[Os^{VII}O_3(OH)_3]^{2-}$ complex anion with an equilibrium constant, K_{COM}, of 9.3 ± 0.3 in a 2.0 M NaOH matrix at 298.1 K. The comproportionation forward, k_{+2}, and reverse, k_{-2}, reaction rate constants of $620.9 \pm 14.6\ M^{-1}\ s^{-1}$ and $65.7 \pm 1.2\ M^{-1}\ s^{-1}$, respectively, were calculated from the kinetic investigation of Os^{VIII} reduction with aliphatic alcohols (MeOH and EtOH) in a 2.0 M NaOH matrix at 298.1 K. The ratio of k_{+2} and k_{-2} agrees quantitatively with K_{COM} and satisfies the principle of detailed balance. Moreover, for the first time it was possible to calculate the molar extinction coefficient spectrum (245–495 nm) of the postulated $[Os^{VII}O_3(OH)_3]^{2-}$ complex anion using the equilibrium and the kinetic data. The model that best fitted the kinetic data support previous findings[4,11–20] that the reduction of Os^{VIII} to Os^{VI} is a one step, two-electron transfer process. Additionally, it was found that the $[Os^{VII}O_3(OH)_3]^{2-}$ species does

not react with MeOH or EtOH. However, the formation of the $[Os^{VII}O_3(OH)_3]^{2-}$ complex anion during the reduction of Os^{VIII} with aliphatic alcohols significantly impedes the overall rate of conversion of $[Os^{VIII}O_4(OH)]^-$ and *cis*-$[Os^{VIII}O_4(OH)_2]^{2-}$ to the *trans*-$[Os^{VI}O_2(OH)_4]^{2-}$ species. In this context care should be taken when interpreting previously reported kinetic studies[4,11–21] that did not account for the formation of an Os^{VII} species, at high enough hydroxide concentration (>0.1 M NaOH), during the reduction of Os^{VIII} in basic media.

Notes and references

1 (*a*) K. B. Sharpless, W. Amberg, Y. L. Bennani, G. A. Crispino, J. Hartung, K.-S. Jeong, H.-L. Kwong, K. Morikawa, Z.-M. Wang, D. Xu and X.-L. Zhang, *J. Org. Chem.*, 1992, **57**, 2768 and references cited therein; (*b*) G. A. Crispino, K.-S. Jeong, H. C. Kolb, Z.-M. Wang, D. Xu and K. B. Sharpless, *J. Org. Chem.*, 1993, **58**, 3785; (*c*) H. B. Henbest, W. R. Jackson and B. C. G. Robb, *J. Chem. Soc. B*, 1966, 803; (*d*) K. A. Jørgensen and R. Hoffmann, *J. Am. Chem. Soc.*, 1986, **108**, 1867; (*e*) E. N. Jacobsen, I. Marko, M. B. France, J. S. Svendsen and K. B. Sharpless, *J. Am. Chem. Soc.*, 1989, **111**, 737; (*f*) J. S. M. Wai, I. Marko, J. S. Svendsen, M. G. Finn, E. N. Jacobsen and K. B. Sharpless, *J. Am. Chem. Soc.*, 1989, **111**, 1123; (*g*) E. J. Corey, M. C. Noe and S. Sarshar, *J. Am. Chem. Soc.*, 1993, **115**, 3828; (*h*) T. Göbel and K. B. Sharpless, *Angew. Chem., Int. Ed. Engl.*, 1993, **32**, 1329.

2 P. Norrby, H. C. Kolb and K. B. Sharpless, *Organometallics*, 1994, **13**, 344.

3 A. J. Delmonte, J. Haller, K. N. Houk, K. B. Sharpless, D. A. Singleton, T. Strassner and A. A. Thomas, *J. Am. Chem. Soc.*, 1997, **119**, 9907.

4 A. Dehestani, W. H. Lam, D. A. Hrovat, E. R. Davidson, W. T. Borden and J. M. Mayer, *J. Am. Chem. Soc.*, 2005, **127**, 3423.

5 (*a*) A. J. DelMonte, J. Haller and K. N. Houk, *J. Am. Chem. Soc.*, 1997, **119**, 9907; (*b*) E. J. Corey, M. C. Noe and M. J. Grogan, *Tetrahedron Lett.*, 1996, **37**, 4899; (*c*) Y. D. Wu, Y. Wang and K. N. Houk, *J. Org. Chem.*, 1992, **57**, 1362; (*d*) J Haller, T Strassner and K N. Houk, *J. Am. Chem. Soc.*, 1997, **119**, 8031; (*e*) W. A. Nugent and J. M. Mayer, *Metal–Ligand Multiple Bonds*, Wiley, New York, 1988.

6 Z. XinHui, W. KeTai and F. Ran, *Sci. China, Ser. B: Chem.*, 2008, **51**, 19.

7 K. B. Sharpless, A. Y. Teranishi and J. E. Bäckvall, *J. Am. Chem. Soc.*, 1977, **99**, 3120.

8 R. I. Edwards, W. A. M. te Riele and G. J. Bernfield, in *Gmelin Handbook of Inorganic Chemistry, Suppl. vol. A1*, ed. J. K. Acres and K. Swars, Springer Verlag, Berlin, 1986.

9 G. Schmuckler and B. Limoni-Relis, *Sep. Sci. Technol.*, 1995, **30**(3), 337.

10 F. L. Bernardis, R. A. Grant and D. C. Sherrington, *React. Funct. Polym.*, 2005, **65**, 205.

11 P. VeeraSomaiah, K. B. Reddy, B. Sethuram and T. Navaneeth Rao, *J. Indian Chem. Soc.*, 1988, **27A**, 876.

12 P. VeeraSomaiah, K. B. Reddy, B. Sethuram and T. Navaneeth Rao, *J. Indian Chem. Soc.*, 1989, **66**, 755.

13 H. S. Singh, S. P. Singh, S. M. Singh, R. K. Singh and A. K. Sisodia, *J. Phys. Chem.*, 1975, **79**(18), 1920.

14 N. P. Singh, V. N. Singh, H. S. Singh and M. P. Singh, *Aust. J. Chem.*, 1970, **23**, 921.

15 V. N. Singh, H. S. Singh and B. B. L. Saxena, *J. Am. Chem. Soc.*, 1969, **91**(10), 2643.

16 H. S. Singh, Oxidation of Organic Compounds with Osmium Tetroxide, in *Organic synthesis by oxidation with metal compounds*, ed. W. J. Mijs and C. R. H. de Jonge, Plenum Press, New York, 1986.

17 N. P. Singh, V. N. Singh and M. P. Singh, *Aust. J. Chem.*, 1968, **21**, 2913.

18 B. Singh, A. K. Singh, M. B. Singh and A. P. Singh, *Tetrahedron*, 1986, **42**, 715.

19 K. K. S. Gupta and B. A. Begum, *Transition Met. Chem.*, 1998, **23**, 295.

20 K. K. S. Gupta and B. A. Begum, *Int. J. Chem. Kinet.*, 1999, **31**(7), 477.

21 W. P. Griffith and M. Suriaatmaja, *Can. J. Chem.*, 2001, **79**, 598–606.

22 I. N. Marov, G. M. Khomushka, V. K. Belyaeva and E. K. Ivanova, *Russ. J. Inorg. Chem.*, 1984, **29**, 146.

23 J. S. Mayell, *I & EC Product Res. Dev.*, 1968, **7**(2), 129.

24 J. E. Bevay, G. Nowogrocki and G. Tridot, *Bull. Soc. Chim. Fr.*, 1967, 2030.

25 W. J. Gerber, K. R. Koch, H. E. Rohwer, E. C. Hosten and T. E. Geswindt, *Talanta*, 2010, **82**(1), 348.

26 J. Kramer and K. R. Koch, *Inorg. Chem.*, 2006, **45**, 7843.

27 J. Kramer and K. R. Koch, *Inorg. Chem.*, 2007, **46**, 7466.

28 W. J. Gerber, P. Murray and K. R. Koch, *Dalton Trans.*, 2008, (31), 4113.

29 (*a*) E. J. Wells, A. D. Jordan, D. S. Alderdice and I. G. Ross, *Aust. J. Chem.*, 1967, **20**, 2315–2322; (*b*) J. L. Roebber, R. N. Wiener and C. A. Russel, *J. Chem. Phys.*, 1974, **60**, 3166–3173.

30 R. D. Sauerbrunn and E. B. Sandell, *J. Am. Chem. Soc.*, 1953, **75**, 3554.

31 M. Meloun, J. Havel and E. Högfeldt, *Computation of Solution Equilibria – A Guide to Methods in Potentiometry, Extraction and Spectrophotometry*, Ellis Horwood, Chichester, 1987.

32 R. L. Burden and J. D. Faires, *Numerical Analysis*, Brooks/Cole Publishing Company, Boston, USA, 6th edn, 1997.

33 J. A. Nelder and R. Mead, *Comput. J.*, 1965, **7**, 308.

34 Z. M. Galbacs, A Zsednai and L. J. Csányi, *Transition Met. Chem.*, 1983, **8**, 328.

35 D. T. Richens, *The Chemistry of Aqua Ions*, John Wiley and Sons, New York, 1997, p 427.

36 W. P. Griffith, in *The Chemistry of the Rarer Platinum Metals (Os, Ru, Ir & Rh)*, Interscience, New York, USA, 1967, ch. 3.

37 K. S. Klausen and F. J. Langmyhr, *Anal. Chim. Acta*, 1963, **28**, 335.

Analytica Chimica Acta 730 (2012) 93–98

Contents lists available at SciVerse ScienceDirect

Analytica Chimica Acta

journal homepage: www.elsevier.com/locate/aca

$^{35}Cl/^{37}Cl$ isotope effects in ^{103}Rh NMR of $[RhCl_n(H_2O)_{6-n}]^{3-n}$ complex anions in hydrochloric acid solution as a unique 'NMR finger-print' for unambiguous speciation

Theodor E. Geswindt, Wilhelmus J. Gerber, D. Jacobus Brand, Klaus R. Koch *

Platinum Group Metals Research Group, Department of Chemistry and Polymer Science, Stellenbosch University, P Bag X1, Matieland, 7602, South Africa

ARTICLE INFO

Article history:
Received 12 July 2011
Received in revised form 30 January 2012
Accepted 3 February 2012
Available online 14 February 2012

Keywords:
^{103}Rh NMR
$^{35}Cl/^{37}Cl$ isotope effects in $[RhCl_n(H_2O)_{6-n}]^{3-n}$ complexes
Direct ^{103}Rh NMR speciation
Isotopologues and isotopomers in NMR

ABSTRACT

A detailed analysis of the $^{35}Cl/^{37}Cl$ isotope effects observed in the 19.11 MHz ^{103}Rh NMR resonances of $[RhCl_n(H_2O)_{6-n}]^{3-n}$ complexes (n = 3–6) in acidic solution at 292.1 K, shows that the 'fine structure' of each ^{103}Rh resonance can be understood in terms of the unique *isotopologue* and in certain instances the *isotopomer* distribution in each complex. These $^{35}Cl/^{37}Cl$ isotope effects in the ^{103}Rh NMR resonance of the $[Rh^{35/37}Cl_6]^{3-}$ species manifest only as a result of the statistically expected $^{35}Cl/^{37}Cl$ isotopologues, whereas for the aquated species such as for example $[Rh^{35/37}Cl_5(H_2O)]^{2-}$, *cis*-$[Rh^{35/37}Cl_4(H_2O)_2]^-$ as well as the *mer*-$[Rh^{35/37}Cl_3(H_2O)_3]$ complexes, additional fine-structure due to the various possible isotopomers within each class of isotopologues, is visible. Of interest is the possibility of the direct identification of stereoisomers *cis*-$[RhCl_4(H_2O)_2]^-$, *trans*-$[RhCl_4(H_2O)_2]^-$, *fac*-$[RhCl_3(H_2O)_3]$ and *mer*-$[RhCl_3(H_2O)_3]$ based on the ^{103}Rh NMR line shape, other than on the basis of their very similar $\delta(^{103}Rh)$ chemical shift. The ^{103}Rh NMR resonance structure thus serves as a novel and unique 'NMR-fingerprint' leading to the unambiguous assignment of $[RhCl_n(H_2O)_{6-n}]^{3-n}$ complexes (n = 3–6), without reliance on accurate $\delta(^{103}Rh)$ chemical shifts.

1. Introduction

South Africa is the world's leading primary producer of the platinum group metals (PGMs, Pt, Pd, Rh, Ru, Ir and Os), contributing more than three quarters of the world's supply of rhodium (>86%) and platinum (>76%), in addition to a significant proportion of the associated metals in 2009 [1]. The strong commercial demand for Rh, used almost exclusively in catalytic applications for automobile exhaust emission control systems as well as in the chemical industry, has resulted in this metal being one of the most expensive, with average prices per troy ounce of Rh ranging between 1592 and 6564 US$ in the years 2006–2009 [1].

In the context of the PGM refining industry, we have been applying methods for chemical speciation [2] to study PGM complexes in aqueous hydrochloric acid solutions as relevant to the separation and recovery of these metals as complex anions, *inter alia* by means of high-resolution ^{195}Pt nuclear magnetic resonance (NMR) spectroscopy [3]. Nuclear magnetic resonance spectroscopy is a powerful tool for *direct* speciation of the kinetically inert $[PtX_n(H_2O)_{6-n}]^{4-n}$ [4], as well as the corresponding hydroxido $[PtX_n(OH)_{6-n}]^{2-}$ (X = Cl^- and Br^-) complex anions [5]. Recently, we developed a novel ^{195}Pt NMR method for the unambiguous speciation of $[PtCl_n(H_2O)_{6-n}]^{4-n}$ (n = 4–6) by exploiting the unique $^{35}Cl/^{37}Cl$ isotope effects visible in the ^{195}Pt NMR resonances obtained at high magnetic fields (14.08 T) in acidic solutions [6]. At high magnetic fields and controlled solution temperature, the ^{195}Pt NMR resonances of $[PtCl_n(H_2O)_{6-n}]^{4-n}$ (n = 4–5) show well resolved 'fine-structure' due the various possible *isotopologues* and *isotopomers* as a result of the natural $^{35}Cl/^{37}Cl$ isotopic distribution unique to each individual Pt^{IV} complex in solution, resulting in an unambiguous ^{195}Pt NMR 'finger-print' for each complex [6].

The nucleus of rhodium naturally occurs only as a single NMR-active isotope ^{103}Rh (I = (1/2)), which has unfortunately a small negative gyromagnetic ratio (γ), and consequently a low resonance frequency Ξ = 3.16 MHz (requiring a special low-frequency NMR probe) relative to ^1H at 100.00 MHz. Moreover the relatively low overall ^{103}Rh NMR receptivity[1] of 0.186, makes routine ^{103}Rh NMR difficult and it is thus not widely practiced. With the more general availability of high magnetic field (>9.04 T) NMR spectrometers with higher sensitivity, ^{103}Rh NMR becomes potentially an attractive tool for speciation of complexes in process and effluent solutions relevant to the PGM refining industry, in which relatively high Rh concentrations may be found, particularly with the aim of developing novel and better separation and recovery methods given high commercial value of rhodium. A survey of the literature

* Corresponding author. Tel.: +27 21 808 3020; fax: +27 21 808 2344.
E-mail address: krk@sun.ac.za (K.R. Koch).

[1] Receptivity of ^{13}C at natural abundance is 1, and ^1H NMR at 5870.

0003-2670/$ – see front matter © 2012 Elsevier B.V. All rights reserved.
doi:10.1016/j.aca.2012.02.009

shows only few NMR studies by directly detected ^{103}Rh NMR, particularly in aqueous solutions. On the other hand, if the Rh atom in a given molecule is bound to a nucleus with a high NMR receptivity, e.g. ^{1}H or ^{31}P, then modern *indirectly* detected NMR methods make the observation of ^{103}Rh spectroscopy more practically useful. The applications of ^{103}Rh NMR in rhodium chemistry have recently been reviewed [7].

Early work involving directly detected ^{103}Rh NMR is limited to the characterization of all ten $[RhCl_{6-x}Br_x]^{3-}$ (x = 0–6) anions [8], as well as some of the possible aquated species $[RhCl_n(H_2O)_{6-n}]^{3-n}$ (n = 0–6) by Mann and Spencer [9], as later confirmed by Sandström *et al.* [10]; nevertheless these studies demonstrate that ^{103}Rh NMR may be a viable tool for examining solutions of relevance to the refining industry, with the potentially useful chemical data being obtainable by this means, exemplified by Glaser and Sandström who used ^{103}Rh NMR to examine the deceptively simple Rh^{III} chemistry in aqueous solutions rich in bromide ions [11]. These authors also examined some octahedral Rh^{III} complexes with sulphur-donor ligands, as well as complexes such as $[Rh(CN)_6]^{3-}$ and $[Rh(SCN)_6]^{3-}$ by ^{103}Rh NMR [12]. The latter study is interesting in that Glaser and Sandström postulate a direct correlation between the $\delta(^{103}Rh)$ chemical shift and the relevant thermodynamic formation constants ($\log\beta_6$) of such complexes. This suggests ^{103}Rh NMR to be a method for the estimation of the formation constants from $\delta(^{103}Rh)$ NMR, a conclusion which in our view, must be treated with some caution at this time. While these studies indicate that ^{103}Rh NMR spectroscopy can be used to identify various complex species such as $[RhCl_n(H_2O)_{6-n}]^{3-n}$ and $[RhBr_n(H_2O)_{6-n}]^{3-n}$ in aqueous solutions by their $\delta(^{103}Rh)$ chemical shift, the relatively high temperature, concentration and matrix dependence of $\delta(^{103}Rh)$ chemical shifts observed in these studies [9–12], makes the unambiguous identification (speciation) of rhodium complexes in such solutions under differing conditions uncertain, and rapid accurate assignments tedious.

We show in this contribution that at high magnetic fields with carefully controlled solution temperatures, the 19.11 MHz ^{103}Rh NMR signals of the series of $[RhCl_n(H_2O)_{6-n}]^{3-n}$ (n = 3–6) complexes in equilibrated hydrochloric acid solutions, are well-resolved into a distinctive 'fine-structure' due to $^{35}Cl/^{37}Cl$ isotopologue and isotopomer effects, resulting in a unique NMR 'finger-print', with which it is possible to uniquely identify all chlorido containing Rh^{III} complexes. By this method the identity of the Rh^{III} complex can readily be obtained from the fine-structure of the ^{103} Rh peaks, without reference to accurate ^{103}Rh NMR chemical shifts. This is potentially a considerable advantage, given the absence of a convenient and universal reference compound for ^{103}Rh NMR [7], resulting in considerable experimental error in measuring $\delta(^{103}Rh)$ chemical shifts, which can vary by as much as ±129 ppm for even the 'simple' $[RhCl_6]^{3-}$ species [10]. Moreover, the relatively small $\delta(^{103}Rh)$ difference of 66 ppm between two Rh^{III} complex isomers such the *trans*-$[RhCl_2(H_2O)_4]^+$ and *cis*-$[RhCl_2(H_2O)_4]^+$ cations, makes it virtually impossible to reliably distinguish between such and other isomers in solution, on the basis of $\delta(^{103}Rh)$ chemical shifts alone. This emphasizes a need for a rapid additional means of unambiguously characterizing $[RhCl_n(H_2O)_{6-n}]^{3-n}$ including possible *cis/trans* and *fac/mer* isomers by means of ^{103}Rh NMR in solution.

2. Experimental

2.1. Preparation of Rh complex solutions

Two solutions of 0.86 M $[RhCl_n(H_2O)_{6-n}]^{3-n}$ (n = 3–6) were prepared by dissolving *ca* 0.9 g of commercially available $RhCl_3{\cdot}nH_2O$ (Johnson Matthey) in 3.5 mL 29% (v/v) $^{2}H_2O/^{1}H_2O$ containing the appropriate quantity of concentrated (32% v/v) HCl: (solution 1 = 6.02 M HCl, 0.868 M Rh; solution 2 = 1.03 M HCl, 0.867 M Rh). These solutions were kept closed at 333 K for a week and thereafter allowed to equilibrate at 292 K for a further 5 days. The total rhodium and chloride concentration of these solutions was determined by means of ICP-OES (SPECTRO Arcos instrument); equipped with a Schott spray chamber and cross-flow nebulizer. The general ICP-OES conditions were: ICP RF power = 1400 W, coolant gas flow = 13.00 L min^{-1}, auxiliary gas flow = 1.00 L min^{-1}, nebulizer gas flow = 0.80 L min^{-1}. The most sensitive rhodium (343.489 nm) and chloride (134.742 nm) wavelengths were used for these determinations. An ULTRASPEC single element rhodium standard (De Bruyn Spectroscopic Solutions; 99.998% purity, 10% v/v HCl) was used for rhodium standardisation, while dried sodium chloride (Sigma–Aldrich; 99.95% purity) was used for the chloride standardisation.

2.2. ^{103}Rh NMR spectroscopy

^{103}Rh NMR spectra at 19.11 MHz were recorded at constant temperature (292.1 K ± 0.1 K) using a three channel Varian INOVA spectrometer (14.1 T magnet corresponding to 600 MHz ^{1}H resonance frequency) with a 10 mm HX Nalorac Z-spec ^{15}N-^{103}Rh (18–61 MHz) broad-band probe. It is important to allow sufficient time for the sample to achieve temperature equilibrium, following which optimal shimming is required. All NMR samples contained *ca* 30% (v/v) D_2O for locking purposes. Since the probe is not equipped for modern gradient shimming, together with the low receptivity of the ^{103}Rh nucleus, optimal shimming was carried out on FID of the D_2O while acquiring a D_2O spectrum in the conventional pulsed mode; with the X channel pre-tuned to ^{103}Rh. Once the best possible shim setting was obtained, the lock channel was used in the conventional mode, and final shimming adjusted for each ^{103}Rh NMR sample. In the absence of a suitable reference compound, chemical shifts (ppm) are reported to Ξ (^{103}Rh) = 3.16 MHz on the TMS scale at 100.000 MHz, as proposed by Goodfellow [13]; the high-frequency positive-shift convention was used [7]. ^{103}Rh spectra were recorded with a spectral width of 19.11 kHz, using a 15.4 μs excitation pulse at maximum practical power in an attempt to ensure approximately homogeneous RF excitation over the entire spectral width, with an acquisition time of 0.5 s and a 1 s pulse delay to ensure sufficient relaxation, under conditions of optimal resolution. A detailed search of the literature yielded no reliable measured estimates of ^{103}Rh T_1 relaxation times, particularly for octahedral Rh^{III} complexes as involved in this work. If the reasonable 'rule of thumb' by Sanders and Hunter (in "Modern NMR Spectroscopy", (2nd edn), Oxford University Press, (1993)) is used which allows for a rough estimate of the rotational correlation time τ_c, (τ_c/ps ≈ M_r where M_r is the relative molar mass of the molecule in question), then for $[RhCl_6]^{3-}$ we estimate a $\tau_c \approx 316$ ps. This means that at the ^{103}Rh resonance frequency of 19.11 MHz at our magnetic field, the condition $\omega_o\tau_c \approx 0.0190$ or $\omega_o\tau_c \ll 1$ is met, suggesting that the extreme narrowing condition for NMR is pertinent. In this region $T_2^* \leq T_2 \leq T_1$, so we can estimate the T_1 for the best resolved peaks of the $[RhCl_6]^{3-}$ species (Fig. 2a) which has a line width of ~2.6 Hz, from which T_2, and thus T_1 of ≈0.12 s results. Thus a pulse repetition rate of 5 × 0.12 s ≈ 0.612 s is adequate to ensure essentially complete relaxation for these Rh complexes. The very good agreement between the experimental and simulated peaks of the isotopologues shown in Fig. 2, attest to this. Typically, due to the low receptivity of the ^{103}Rh nucleus, NMR spectra normally required *ca* 40,000 transients to achieve satisfactory S N^{-1} ratios resulting in total experimental times ≥12 h. In the absence of artificial line-broadening (apodization) of the accumulated FIDs, the typical ^{103}Rh resonance line-widths ($\nu_{½}$ at half peak-height varied

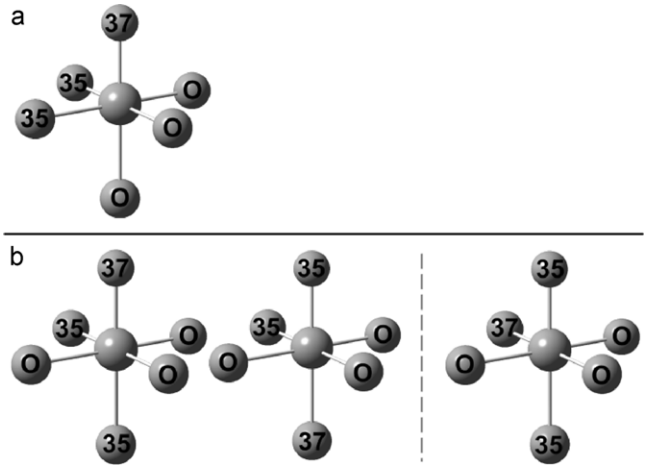

Fig. 1. (a) Isotopologues associated with the *fac*-$[Rh^{35}Cl_2{}^{37}Cl(H_2O)_3]$ species; (b) possible isotopomers associated with the isotopologue of the *mer*-$[Rh^{35}Cl_2{}^{37}Cl(H_2O)_3]$ species where the $^{35}Cl/^{37}Cl$ is coordinated *trans* with respect to water in a 2:1 ratio (35 = ^{35}Cl, 37 = ^{37}Cl, O = H_2O).

from 2.3 to 3.1 Hz at optimal resolution under careful temperature (292.1 ± 0.1 K) control.

SigmaPlot Version 11 (Systat Software Inc.) was used to perform the nonlinear least-squares fits on the ^{103}Rh experimental data. The SigmaPlot curve fitter uses the Marquardt–Levenberg algorithm to find the coefficients (parameters) of the independent variable(s) that give the best fit between the sum of several Lorentzian functions and the experimental data.

3. Results and discussion

At high magnetic fields (14.1 T) and carefully controlled conditions, the high-resolution ^{195}Pt NMR resonance signals of the series of complex anions $[PtCl_n(H_2O)_{6-n}]^{4-n}$ (n = 4–6) are resolved into a secondary structure, due to small chemical-shift differences as a result of both isotopologues and, the possible isotopomers[2] within each set of $[Pt^{35}Cl/^{37}Cl_n(H_2O)_{6-n}]^{4-n}$ isotopologues [6], arising from the natural $^{35/37}Cl$ isotope distribution of the chlorido ligand(s) coordinated to Pt^{IV}. The resulting unique line shapes of the ^{195}Pt NMR resonances for this series of complexes, essentially constitutes an unequivocal $^{35/37}Cl$ isotope resolved 'fingerprint' for the identification of all species in this series, including stereoisomers such as *cis*- and *trans*-$[PtCl_4(H_2O)_2]$, provided at least one chlorido ligand remains bound to the Pt^{IV} complex and exchanges slowly on the NMR time scale.

Rhodium is separated and recovered on a commercial scale in the form of its chlorido $[RhCl_n(H_2O)_{6-n}]^{3-n}$ complex anions in hydrochloric acid, the available species distribution diagram in the literature however suggesting the presence of several species in solution depending on the hydrochloric acid concentration [15,16]. Provided at least one chlorido ligand is bound to Rh^{III}, these complexes can in principle exist as a set of four $^{35/37}Cl$ isotopologues and isotopomers[‡] within each set of isotopologues illustrated for *fac*-$[Rh^{35}Cl_2{}^{37}Cl(H_2O)_3]$ and *mer*-$[Rh^{35}Cl_2{}^{37}Cl(H_2O)_3]$ by way of example, in Fig. 1. In the case of the *fac*-$[Rh^{35}Cl_2{}^{37}Cl(H_2O)_3]$ isotopologue, although *trans* $^{35/37}Cl$-Rh-(OH_2) configurations are possible in a statistical 2:1 ratio, these isotopomers are magnetically equivalent and result in the same chemical shift $\delta(^{103}Rh)$. By contrast for the *mer*-$[Rh^{35}Cl_2{}^{37}Cl(H_2O)_3]$ isotopologue, the isotopomer with a *trans* ^{37}Cl–Rh–(OH_2) configuration is *not* magnetically equivalent to the one with *trans* ^{35}Cl–Rh–(OH_2), which is twice as abundant than the former, resulting in a small chemical shift difference as manifested in the different 'fine-structures' of their respective ^{103}Rh NMR resonances. Similar considerations apply to the corresponding $[RhCl_5(H_2O)]^{2-}$ *cis*-$[RhCl_4(H_2O)_2]^-$ and *trans*-$[RhCl_4(H_2O)_2]^-$ species. Hence ^{103}Rh NMR spectroscopy at high magnetic fields (≥14.1 T) is expected to be useful for the investigation of the species distribution of the $[RhCl_n(H_2O)_{6-n}]^{3-n}$ complex anions in hydrochloric acid, and in particular is likely also to show $^{35/37}Cl$ isotope resolved ^{103}Rh resonances, analogous to the Pt^{IV} complexes [6], referred to above.

As shown in Fig. 2, these expectations are satisfactorily confirmed by the detailed 19.11 MHz ^{103}Rh NMR spectra of several $[RhCl_n(H_2O)_{6-n}]^{3-n}$ complex anions (n = 3–6) at thermodynamic equilibrium at a fixed total Rh^{III} concentration of *ca* 0.87 M, obtained in solutions with 6 M and 1 M hydrochloric acid concentrations respectively. Fig. 2a–f shows the well resolved fine-structure profile for each of the individual ^{103}Rh NMR resonances, recorded at a temperature of 292.1 ± 0.1 K, of the species $[RhCl_6]^{3-}$, $[RhCl_5(H_2O)]^{2-}$ in 6.0 M HCl and *cis*-$[RhCl_4(H_2O)_2]^-$, *trans*-$[RhCl_4(H_2O)_2]^-$, *fac*-$[RhCl_3(H_2O)_3]$ and *mer*-$[RhCl_3(H_2O)_3]$ present in solutions in 1 M hydrochloric acid. The well resolved fine-structure profile of the ^{103}Rh NMR resonance for each species is due to $^{35}Cl/^{37}Cl$ isotope effects. Significantly, the ^{103}Rh resonance of the $[RhCl_6]^{3-}$ anion (Fig. 2a) is resolved only into five of the seven expected $[Rh(^{35/37}Cl)_6]^{3-}$ isotopologues, very similar to what may be observed in the corresponding ^{195}Pt NMR spectrum of the $[Pt(^{35/37}Cl)_6]^{2-}$ complex [3]. In view of the relatively poor receptivity[2] of ^{103}Rh NMR, only five of the seven peaks due to the isotopologues $[Rh(^{35}Cl)_n(^{37}Cl)_r]^{3-}$ (n = 6–2, r = 2–6, $n+r$ = 6), may be experimentally observed within a reasonable ^{103}Rh NMR acquisition time, since the statistically calculated abundance of $[Rh(^{35}Cl)(^{37}Cl)_5]^{3-}$ and $[Rh(^{37}Cl)_6]^{3-}$ isotopologues occur at very low abundances of 0.38 and 0.02% respectively (see Table 1). The relative statistical probability, $P(n)$, for each possible isotopologue in the series of $[Rh^{35/37}Cl_n(H_2O)_{6-n}]^{3-n}$ (n = 3–6) complexes may be calculated at the fractional natural abundance (α) of ^{35}Cl (0.7553) and ^{37}Cl (0.2447) using the binominal probability distribution function[3] for n ^{35}Cl and r ^{37}Cl chlorido ligands ($n+r$ = 6). From a visual inspection of Fig. 2c–f, it can be seen however that the fine-structure of some of the ^{103}Rh resonances, particularly due to the stereoisomer pairs *cis*-$[RhCl_4(H_2O)_2]^-$, *trans*-$[RhCl_4(H_2O)_2]^-$, *fac*-$[RhCl_3(H_2O)_3]$ and *mer*-$[RhCl_3(H_2O)_3]$ respectively differ significantly from a model which takes into account *only* the $^{35}Cl/^{37}Cl$ isotopologue distributions. The experimental ^{103}Rh NMR peak shapes and peak intensity ratios observed, suggest additional *isotopomer* induced fine-structure. The resolved fine-structure of the ^{103}Rh NMR resonances (Fig. 2b–f) can only be accounted for by considering the possible isotopomers[3], within each possible set of isotopologues for the series of 'aquated' complexes $[RhCl_5(H_2O)]^{2-}$, *cis*-$[RhCl_4(H_2O)_2]^-$, *trans*-$[RhCl_4(H_2O)_2]^-$, *fac*-$[RhCl_3(H_2O)_3]$ and *mer*-$[RhCl_3(H_2O)_3]$. The relative statistical probability for each possible isotopomer, $S(n)$, in the series of $[Rh^{35/37}Cl_n(H_2O)_{6-n}]^{3-n}$ (n = 1–5) complexes was deduced as illustrated schematically in Fig. 1; for the *mer*-$[RhCl_3(H_2O)_3]$ species the *trans* $^{35/37}Cl$–Rh–(OH_2) isotopomers are magnetically equivalent, while for the *mer*-$[RhCl_3(H_2O)_3]$ species two sets of magnetically inequivalent isotopomers are possible in a 2:1 statistical ratio (reasonably neglecting any possible $^{17}O/^{18}O$ isotope effects due to the

[2] Isotopomer(s) with respect to whether a ^{35}Cl or ^{37}Cl ligand is *trans* to a coordinated water molecule in the $[M^{IV/III}Cl_n(H_2O)_{6-n}]^{4/3-n}$ complex.

[3] $P(n) = \sum_{n=0}^{n=((n+r)!)/(n!r!)} (\alpha^n_{^{35}Cl}\alpha^r_{^{37}Cl})$.

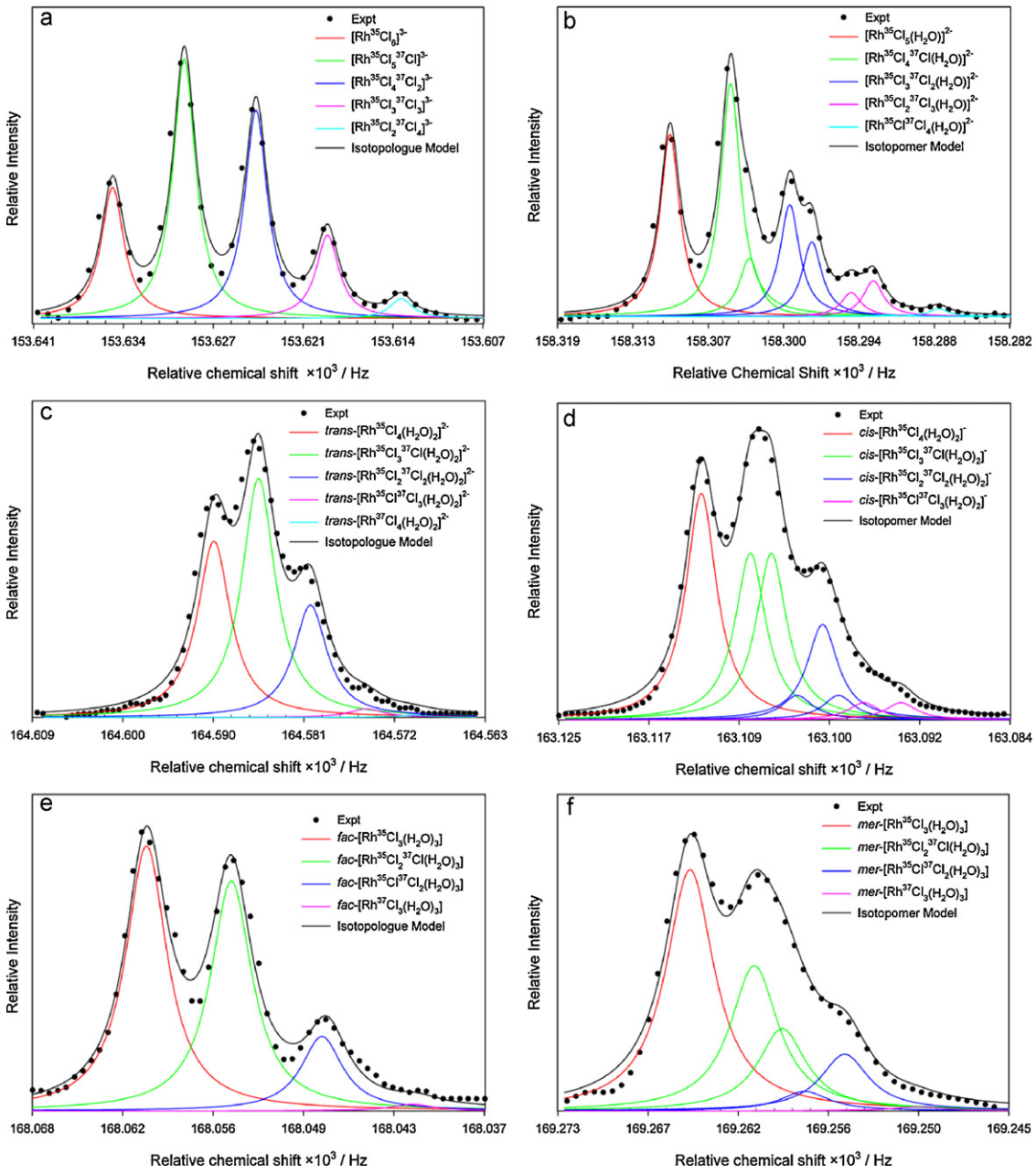

Fig. 2. Experimental ^{103}Rh spectra of $[RhCl_n(H_2O)_{6-n}]^{3-n}$ (n = 3–6) species recorded at 292.1 K (symbols). The least-squares fits (solid lines) between experimental spectra of $[RhCl_6]^{3-}$ (a), *trans*-$[RhCl_4(H_2O)_2]^-$ (c) and *fac*-$[RhCl_3(H_2O)_3]$ (e) and the isotopologue model; the least-squares fits between the experimental spectra and the isotopologue model that includes isotopomers for the $[RhCl_5(H_2O)]^{2-}$, *cis*-$[RhCl_4(H_2O)_2]^-$ and *mer*-$[RhCl_3(H_2O)_3]$ species are denoted by (b), (d) and (f), respectively.

very low natural abundances of these isotopes of oxygen of the coordinated water molecules).

As shown in Fig. 2, the 'simulated' overall ^{103}Rh NMR line-shape obtained from the sum of several Lorentzian peaks of equal half-height peak width (2.64 Hz)[4] and fixed isotope chemical shift spacing per $^{35/37}$Cl isotope, each corresponding to all the possible isotopologues with probability $P(n)$, and the statistically likely but magnetically non-equivalent isotopomers[3] with probability $S(n)$ for each of the complexes listed, leads to an excellent non-linear least-squares fit between the experimental and simulated ^{103}Rh NMR spectra using a 5.33 Hz (~0.279 ppm) shielding ('up-field' isotope shift) per $^{37}Cl^-$ coordinated to the Rh^{III} ion. The essentially quantitative agreement of the experimental line-shape within experimental error with the expected statistical isotopologue and isotopomer distributions are shown in Table 1 for all the $[Rh^{35/37}Cl_n(H_2O)_{6-n}]^{3-n}$ (n = 3–6) considered in this study.

Interestingly, in this context Sadler et al. reported similar resolved $^{35}Cl/^{37}Cl$ isotope effects in the ^{195}Pt NMR spectrum of $[PtCl_6]^{2-}$ complex more than 3 decades ago, at the then highest magnetic field spectrometer generally available [14], although these were erroneously ascribed to $^{35/37}$Cl 'isotopomers'. As is now clear from this study as well as our recent work on the analogous

[4] In the likely event that the $^{35}Cl/^{37}Cl$ quadrupolar relaxation is a dominant contribution to the overall ^{103}Rh relaxation and thus line-width, it might be expected that differing line-width may pertain to differing $[RhCl_n(H_2O)_{6-n}]^{3-n}$ species and their isotopologues. However for the clearly resolved isotopologues peak for the $[RhCl_6]^{3-}$ complex we find a constant line-width leads to the best fit between experimental and simulated peaks. For the other species where the ^{103}Rh isotopologue/isotopomer peaks are less clearly resolved with differing line-widths lead to the good fits as shown in Fig. 1.

Table 1
Comparison of the experimental (Fig. 2a–f) and statistically expected isotopologue and isotopomer distributions for the $[Rh^{35/37}Cl_n(H_2O)_{6-n}]^{3-n}$ (n = 3–6) series of complex anions observable in these solutions.

$^{35/37}$Cl trans to H_2O	Rh^{III} isotopologue	Percent isotopomers		Sum percent of isotopomers to yield isotopologue amount	
		Experimental[a]	Statistical	Experimental[a]	Statistical
	$[Rh^{35}Cl_6]^{3-}$	–	–	18.69 ± 0.3	18.92
	$[Rh^{35}Cl_5{}^{37}Cl]^{3-}$	–	–	36.96 ± 0.2	36.31
	$[Rh^{35}Cl_4{}^{37}Cl_2]^{3-}$	–	–	29.67 ± 0.2	29.03
	$[Rh^{35}Cl_3{}^{37}Cl_3]^{3-}$	–	–	11.86 ± 0.2	12.38
	$[Rh^{35}Cl_2{}^{37}Cl_4]^{3-}$	–	–	2.81 ± 0.2	2.97
	$[Rh^{35}Cl^{37}Cl_5]^{3-}$	–	–	*Not reliably quantifiable*	0.38
	$[Rh^{37}Cl_6]^{3-}$	–	–	*Not reliably quantifiable*	0.02
^{35}Cl	$[Rh^{35}Cl_5(H_2O)]^{2-}$	24.99 ± 0.2	24.97	24.99 ± 0.2	24.97
^{35}Cl	$[Rh^{35}Cl_4{}^{37}Cl(H_2O)]^{2-}$	31.96 ± 0.2	31.94	39.96 ± 0.6	39.93
^{37}Cl		8.00 ± 0.3	7.99		
^{35}Cl	$[Rh^{35}Cl_3{}^{37}Cl_2(H_2O)]^{2-}$	15.33 ± 0.2	15.32	25.56 ± 0.5	25.54
^{37}Cl		10.23 ± 0.2	10.22		
^{35}Cl	$[Rh^{35}Cl_2{}^{37}Cl_3(H_2O)]^{2-}$	3.27 ± 0.1	3.27	8.17 ± 0.4	8.17
^{37}Cl		4.90 ± 0.2	4.9		
^{35}Cl	$[Rh^{35}Cl^{37}Cl_4(H_2O)]^{2-}$	0.26 ± 0.2	0.26	1.31 ± 0.4	1.31
^{37}Cl		1.05 ± 0.1	1.05		
^{37}Cl	$[Rh^{37}Cl_5(H_2O)]^{2-}$	*Not reliably quantifiable*	0.08	*Not reliably quantifiable*	0.08
^{35}Cl, ^{35}Cl	*cis*-$[Rh^{35}Cl_4(H_2O)_2]^{-}$	30.68 ± 0.3	32.96	30.68 ± 0.3	32.96
^{35}Cl, ^{35}Cl	*cis*-$[Rh^{35}Cl_3{}^{37}Cl(H_2O)_2]^{-}$	22.56 ± 0.2	21.08	45.15 ± 0.5	42.16
^{35}Cl, ^{37}Cl		22.59 ± 0.2	21.08		
^{35}Cl, ^{35}Cl	*cis*-$[Rh^{35}Cl_2{}^{37}Cl_2(H_2O)_2]^{-}$	3.30 ± 0.2	3.37	19.15 ± 0.5	20.22
^{35}Cl, ^{37}Cl		12.91 ± 0.3	13.48		
^{37}Cl,^{37}Cl		3.30 ± 0.2	3.37		
^{35}Cl, ^{37}Cl	*cis*-$[Rh^{35}Cl^{37}Cl_3(H_2O)_2]^{-}$	2.31 ± 0.4	2.16	4.62 ± 1.0	4.32
^{37}Cl, ^{37}Cl		2.31 ± 0.4	2.16		
^{37}Cl, ^{37}Cl	*cis*-$[Rh^{37}Cl_4(H_2O)_2]^{-}$	*Not reliably quantifiable*	0.34	*Not reliably quantifiable*	0.34
	trans-$[Rh^{35}Cl_4(H_2O)_2]^{-}$	–	–	32.73 ± 0.5	32.96
	trans-$[Rh^{35}Cl_3{}^{37}Cl(H_2O)_2]^{-}$	–	–	42.40 ± 0.4	42.16
	trans-$[Rh^{35}Cl_2{}^{37}Cl_2(H_2O)_2]^{-}$	–	–	20.85 ± 0.9	20.22
	trans-$[Rh^{35}Cl^{37}Cl_3(H_2O)_2]^{-}$	–	–	3.60 ± 1.0	4.31
	trans-$[Rh^{37}Cl_4(H_2O)_2]^{-}$	–	–	0.42 ± 0.3	0.34
^{35}Cl	*mer*-$[Rh^{35}Cl_3(H_2O)_3]$	43.96 ± 0.9	43.50	43.96 ± 0.9	43.50
^{35}Cl	*mer*-$[Rh^{35}Cl_2{}^{37}Cl(H_2O)_3]$	26.48 ± 1.3	27.82	41.45 ± 2.9	41.73
^{37}Cl		14.97 ± 1.0	13.91		
^{35}Cl	*mer*-$[Rh^{35}Cl^{37}Cl_2(H_2O)_3]$	3.55 ± 0.8	4.45	13.86 ± 2.2	13.35
^{37}Cl		10.31 ± 1.0	8.90		
^{37}Cl	*mer*-$[Rh^{37}Cl_3(H_2O)_3]$	0.72 ± 0.5	1.40	0.72 ± 0.5	1.40
^{35}Cl, ^{35}Cl, ^{35}Cl	*fac*-$[Rh^{35}Cl_3(H_2O)_3]$	–	–	46.02 ± 1.3	43.50
^{35}Cl, ^{35}Cl, ^{37}Cl	*fac*-$[Rh^{35}Cl_2{}^{37}Cl(H_2O)_3]$	–	–	39.91 ± 2.5	41.73
^{35}Cl, ^{37}Cl, ^{37}Cl	*fac*-$[Rh^{35}Cl^{37}Cl_2(H_2O)_3]$	–	–	12.93 ± 1.3	13.35
^{37}Cl, ^{37}Cl, ^{37}Cl	*fac*-$[Rh^{37}Cl_3(H_2O)_3]$	–	–	1.13 ± 0.5	1.42

[a] The isotopologue/isotopomer model was fitted by non-linear least-square analysis to the experimental data from which the 95% confidence interval was estimated. ^{103}Rh NMR spectra of each solution were acquired three separate times, not in succession. For peaks of lower intensity the relative percentage deviation between experimental and fitted resonance intensities naturally is much larger compared to the intense ^{103}Rh peaks. Better agreement can only be obtained at the expense of an unreasonably long ^{103}Rh NMR acquisition time to obtain higher SN^{-1} ratios, although this is superfluous, given the overall good fit of the experimental data without exception.

Pt^{IV} complexes, in general for $[MCl_6]^{2/3-}$ ($M = Pt^{IV}$ or Rh^{III}) species, the resolved fine-structure in the ^{103}Rh (and ^{195}Pt) NMR resonances are only due to the various isotopologues in these complex anions, and no isotopomer effects are resolved for these particular species; to our knowledge no such isotopologues effects have been previously reported for the $[RhCl_6]^{3-}$ complex anion to date.

The isotopomer-induced $^{35/37}$Cl 'fine-structure' effects visible in the ^{103}Rh NMR resonance of the isotopologues $[Rh^{35}Cl_4{}^{37}Cl(H_2O)]^{2-}$ and $[Rh^{35}Cl_3{}^{37}Cl_2(H_2O)]^{2-}$ *etc.*, are due to the possibility of *trans* ^{37}Cl-^{103}Rh-OH_2 and ^{35}Cl-^{103}Rh-OH^2 configurations within these isotopologues. Evidently this additional fine-structure observed in the ^{103}Rh resonances of these complexes arises from small differences in ^{103}Rh shielding of these isotopomer configurations within a given complex. From the least-squares fitting of the experimental line-shapes gives rise to an effective $\Delta(\delta(^{103}Rh))$ of *ca* 0.141 ppm (2.7 Hz) between the *trans*- and *cis*-$[Rh^{35}Cl_4{}^{37}Cl(H_2O)]^{2-}$ isotopomers, depending on whether a ^{37}Cl atom is respectively *trans* or *cis* to the coordinated water molecule. This finding emphasizes the remarkable sensitivity of $\delta(^{103}Rh)$ to very subtle effects on the ^{103}Rh shielding within these complexes, and the necessity of careful temperature control to achieve optimal NMR resolution. While a detailed explanation of the origin of the $^{35/37}$Cl isotope effects must await a full computational (theoretical) investigation, these effects are likely to result from small differences in the vibrational stretching frequencies between the ^{37}Cl-^{103}Rh and ^{35}Cl-^{103}Rh bonds *trans* to the relatively weakly bound coordinated water molecules in these (as well as the corresponding Pt^{IV} [6]) complexes, and is a nice example of the elegant theoretical work by Jameson and Jameson on the 'rovibrational' averaging of nuclear shielding in MX_6-type molecules more than two decades ago [17]. In this context we have recently found in a DFT study that for the series of $[PtX_6]^{2-}$ ($X = F^-$, Cl^-, Br^-, I^-) complexes, the calculated ^{195}Pt NMR shielding of these complexes are extraordinarily sensitive to average Pt-halide bond distances Δ(Pt-Cl); for example the $d(\delta^{195}Pt)/d\Delta(Pt–Cl)$ for the Pt–Cl case is *ca* 183 ppm/picometer [18]. On a more practical level, the $^{35/37}$Cl isotope effects will assist in the establishment of a direct and definitive chemical speciation-distribution diagram for the full series of $[RhCl_n(H_2O)_{6-n}]^{3-n}$ in halide-rich aqueous solutions of interest to the Rh recovery and refining industry,

using ^{103}Rh NMR spectroscopy, something which is currently in progress.

We do not find any observable secondary isotope effects possible due to $^{1/2}$H isotopes associated with the coordinated water molecules, when increasing the $^{2}H_2O$:H_2O ratio from 10 to 30%(v/v) for the $[Rh^{35/37}Cl_n(^{1/2}H_2O)_{6-n}]^{3-n}$ (n = 3–5) complexes; presumably the ^{1}H/^{2}H exchange of water is rapid in solution, resulting in the averaging of any potential (small) isotope effect from this source. Moreover application of ^{1}H-decoupling during acquisition of ^{103}Rh NMR spectra in this study, resulted in significant loss of isotopologue/isotopomer resolution in the recorded ^{103}Rh resonances, presumably due to significant RF absorption of the high ionic-strength aqueous solutions, causing inevitable temperature fluctuations and/or convection currents within the 10 mm sample tube. Considering the significant temperature dependence of the ^{103}Rh NMR chemical shifts reported to be in the range (0.5–3.0 ppm K^{-1})[5] [7–10], and those observed for this series of complex anions (e.g. *ca* 2.0 ppm K^{-1} for $[RhCl_6]^{3-}$), underlines the importance of careful temperature control to at least ±0.1 K when acquiring high resolution NMR spectra; moreover in order to ensure complete thermal equilibrium of the sample in the 10 mm NMR tube, a waiting time of at least 35 min is recommended to achieve satisfactory thermal equilibrium within the sample. We observe a significant deterioration in resolution in the ^{103}Rh NMR resonance signal for $[RhCl_n(H_2O)_{6-n}]^{3-n}$ (n = 3–6) complexes above 300.0 K, very similar to that observed previously in the $[PtCl_n(H_2O)_{6-n}]^{4-n}$ (n = 4–6) complexes [6]. While the reasons for this very high temperature dependence must await a more detailed study of the ^{103}Rh NMR of the complexes described here. *Intra*- and *inter*-molecular ligand exchange ($^{35/37}Cl^-$ or H_2O) is likely to be too slow at temperatures <300 K [15–18], to account for the loss of the isotopologue and isotopomer resolution in the ^{103}Rh NMR resonance structure; in any event such $^{35/37}$Cl isotope effects reported here for the generally kinetically inert Rh^{III} complexes (and elsewhere for the Pt^{IV} complexes) would not be visible under conditions of *fast* chemical exchange on the NMR time scale such as may be expected at higher temperatures (>350 K), as can be confirmed by preliminary temperature dependence NMR experiments. The possibility of variable quadrupolar ^{35}Cl/^{37}Cl relaxation effects for ^{103}Rh in different species as a result of the temperature dependence of this relaxation mechanism is also likely to affect the observed line-widths of the ^{103}Rh resonance at differing temperatures, something in need of more detailed study.[6]

4. Conclusions

The remarkable isotopologue, and for some complexes isotopomer induced fine-structure of the ^{103}Rh NMR resonances (at high magnetic fields) of the series of aquated $[Rh^{35/37}Cl_n(H_2O)_{6-n}]^{3-n}$ (n = 3–6) complex anions in hydrochloric acid solutions constitutes a novel method of direct spectroscopic speciation of $[RhCl_n(H_2O)_{6-n}]^{3-n}$ (n = 3–6) complexes. This is possible without the need for accurate chemical shifts of these species, or the need for the comparison of authentic synthetic complexes many of which are not readily available or even separately synthesizable. Given the large chemical shift range of *ca* 12,000 ppm observed for diverse rhodium complexes to date [7], together with the extreme sensitivity of ^{103}Rh nuclear shielding to numerous effects such solvent, concentration, temperature, pressure and other effects [3], this makes the comparison of chemical shifts subject to considerable uncertainty. The use of $^{35/37}$Cl isotope-resolved ^{103}Rh NMR resonance thus constitutes a significant advance as a convenient and reliable method for the identification of halide containing complexes, provided these are kinetically inert to ligand exchange on the NMR time scale. Particularly noteworthy is the possibility of the unambiguous assignment of stereoisomers such as the *trans*- or *cis*-$[RhCl_4(H_2O)_2]^-$ which differ in chemical shift by only *ca* 76 ± 3 ppm, or the uncharged *fac*-$[RhCl_3(H_2O)_3]$ and *mer*-$[RhCl_3(H_2O)_3]$ isomers differing only by *ca* 63 ± 3 ppm. These can now readily be identified based on their $^{35/37}$Cl isotope induced 'NMR fingerprint', without reference to their accurate ^{103}Rh NMR chemical shifts or the need for a suitable reference compound.

Acknowledgements

Financial support from the University of Stellenbosch, the NRF and Heraeus GmbH, is gratefully acknowledged.

References

[1] D. Jollie, Platinum 2010, Johnson Matthey PLC, Royston, UK, 2010, pp. 44–45 and 58.
[2] D.M. Templeton, F. Ariese, R. Cornelis, L.G. Danielsson, H. Muntau, H.P. van Leeuwen, R. Loinski, Pure Appl. Chem. 72 (2000) 1453–1470.
[3] K.R. Koch, M.R. Burger, J. Kramer, A.N. Westra, Dalton Trans. (2006) 3277–3284.
[4] J. Kramer, K.R. Koch, Inorg. Chem. 45 (2006) 7843–7855.
[5] J. Kramer, K.R. Koch, Inorg. Chem. 46 (2007) 7466–7476.
[6] W.J. Gerber, P. Murray, K.R. Koch, Dalton Trans. 31 (2008) 4113–4117.
[7] J.M. Ernsting, S. Gaemers, C.J. Elsevier, Magn. Res. Chem. 42 (2004) 721–736.
[8] B.E. Mann, C.M. Spencer, Inorg. Chim. Acta 76 (1983) L65–L66.
[9] B.E. Mann, C.M. Spencer, Inorg. Chim. Acta 65 (1982) L57–L66.
[10] C. Carr, J. Glaser, M. Sandström, Inorg. Chim. Acta 131 (1987) L53–L56.
[11] M.C. Read, J. Glaser, M. Sandström, J. Chem. Soc., Dalton Trans. (1992) 233–240.
[12] M.C. Read, J. Glaser, I. Persson, M. Sandström, J. Chem. Soc., Dalton Trans. (1994) 3243–3248.
[13] R.J. Goodfellow, in: R.K. Harris, B.E. Mann (Eds.), NMR and the Periodic Table, Academic Press, London, 1978, p. 244.
[14] I.M. Ismail, S.J.S. Kerrison, P.J. Sadler, J. Chem. Soc., Chem. Commun. (1980) 1175–1176.
[15] E. Benguerel, G.P. Demopoulos, G.B. Harris, Hydrometallurgy 40 (1996) 135–152.
[16] W.J. Gerber, K.R. Koch, H.E. Rohwer, E.C. Hosten, T.E. Geswindt, Talanta 82 (2010) 348–358.
[17] C.J. Jameson, A.K. Jameson, J. Chem. Phys. 85 (1986) 5484–5492.
[18] M.R. Burger, J. Kramer, H. Chermette, K.R. Koch, Magn. Res. Chem. 48 (2010) 38–47.

[5] Higher temperature usually results in down-field shifts (higher δ) or lower shielding (lower σ), so that $d\sigma/dT$ is usually reported as a negative value.
[6] We appreciate this suggestion by one of the reviewers.